Mitteilungen Heft 104

Spatial interpolation of climate data for
hydrological and environmental applications

Spatial interpolation of climate data for hydrological and environmental applications

Von der Fakultät für Bauingenieurwesen und Geodäsie
der Gottfried Wilhelm Leibniz Universität Hannover

zur Erlangung des akademischen Grades
Doktor-Ingenieur
- Dr.-Ing. -

genehmigte Dissertation

von

Dipl.-Ing. **Christian Berndt**
geboren am 12.06.1985 in Rotenburg/Wümme

Hannover, Dezember 2016

Referent: Prof. Dr.-Ing. Uwe Haberlandt
Korreferent: Prof. Dr.-Ing. Erwin Zehe

Tag der Promotion: 02. Dezember 2016

Erklärung

Hiermit versichere ich eidesstattlich, dass ich

1. die Regeln der geltenden Promotionsordnung kenne und eingehalten habe und mit einer Prüfung nach den Bestimmungen der Promotionsordnung einverstanden bin,

2. die Dissertation selbst verfasst habe, keine Textabschnitte von Dritten oder eigener Prüfungsarbeiten ohne Kennzeichnung übernommen und alle von mir benutzten Hilfsmittel und Quellen in meiner Arbeit angegeben habe,

3. Dritten weder unmittelbar noch mittelbar geldwerte Leistungen für Vermittlungstätigkeiten oder für die inhaltliche Ausarbeitung der Dissertation erbracht habe,

4. die vorliegende Dissertation noch nicht als Prüfungsarbeit für eine staatliche oder andere wissenschaftliche Prüfung eingereicht habe,

5. die gleiche oder eine in wesentlichen Teilen ähnliche Arbeit bei keiner anderen Hochschule als Dissertation eingereicht habe und auch keine andere Abhandlung als Dissertation eingereicht habe,

6. damit einverstanden bin, dass die Dissertation auch zum Zwecke der Überprüfung der Einhaltung allgemein geltender wissenschaftlicher Standards genutzt wird, insbesondere auch unter Verwendung elektronischer Datenverarbeitungsprogramme.

Hannover, den 29.09.2016

Christian Berndt

Teile der Arbeit entstammen aus einer Kollaboration, welche bereits unter BERNDT *et al.* (2014) veröffentlicht wurde im Wesentlichen die Ergebnisse des Abschnitts 6.1 beinhaltet. Der von mir geleistete Beitrag umfasst die folgenden Punkte:

1. Datenaufbereitung der Stationsmessungen und Radardaten (Abschnitt 5.3 und 5.4.1),

2. Gestaltung der Kreuzvalidierung unter Verwendung unterschiedlicher Zeitskalen und Stationsdichteszenarien (Abschnitt 5.1 und 5.2),

3. Implementierung von Glättungsmethoden für Radarinformationen (Abschnitt 5.4.2),

4. Variogrammschätzung für alle Interpolationsmethoden (Abschnitt 6.1.1),

5. Anwendung der Interpolationsmethoden Ordinary Kriging, Kriging mit externem Drift und Indikatorkriging mit externem Drift,

6. Auswertung der Ergebnisse,

7. Erstellung aller für diese Dissertation übernommenen Abbildungen und des Texts der Veröffentlichung.

Abstract

Many fields of hydrology, water resources management and environmental sciences require climate information with various temporal resolutions for the modelling of different processes. These data are usually recorded as site-specific point information by weather stations, however many applications need areal data. For instance mean areal rainfall is used for hydrological modelling, while air contaminant transport simulations require time series for unobserved locations. Spatial interpolation techniques are a reliable approach in order to estimate climate information for a specific location from adjacent measurements. The estimation accuracy depends generally on station density, temporal resolution, spatial variation of the regarded variable and the choice of interpolation method.

This work aims at evaluating the influence of several factors on the interpolation performance. Moreover, it investigates whether interpolated data meet the requirements for hydrological and environmental applications. A cross validation analysis of interpolation performance was carried out for different meteorological observations at first, in which various temporal resolutions and station density scenarios were considered. Simple deterministic methods as well as sophisticated geostatistical interpolation approaches were applied and different additional information was taken into account. A special attention was given to the interpolation of rainfall with a high temporal resolution, since this information is the fundamental input for hydrological modelling as well as hydrodynamic simulation of urban stormwater discharge. In particular radar data were tested regarding their potential to provide an additional information for the spatial estimation. Secondly, a validation of interpolated data with respect to urban hydrology and contaminant transport in the atmosphere was conducted. Rainfall time series generated by various interpolation techniques as well as radar data were utilised as the input of an urban stormwater runoff model, while interpolated wind and precipitation time series were used for atmospheric transport simulations.

The cross validation results show that geostatistical techniques are able to provide a better interpolation performance compared to simple deterministic methods. The incorporation of radar data can improve the spatial interpolation of rainfall with a high temporal resolution

(5 min – 360 min), while the consideration of topography is recommended for a lower temporal resolutions of rainfall (1 week – 1 year) and temperature in general. No useful additional information could be found for cloud coverage, sunshine duration as well as wind velocity and direction. The interpolation of relative humidity benefitted from additional temperature data. The influences of temporal resolution, spatial variability and additional information on the interpolation performance appear to be stronger than the corresponding influence of station density.

The validation of rainfall estimation for stormwater runoff purposes resulted in the finding that the incorporation of radar leads to a strong overestimation of rainfall extremes but can help to improve the discharge simulation of single events. A better preprocessing and correction of radar rainfall estimates is needed.

Precipitation as well as wind information time series generated by geostatistical interpolation can be utilised for the simulation of contaminant transport. However, a correction with respect to the annual rainfall sum and the number of hourly time steps with rainfall is required for precipitation. The consideration of radar information could not yield a benefit compared to univariate interpolation for this application.

The applicability of geostatistically interpolated data depends strongly on the actual purpose. The characteristic spatial smoothing of climate data might help for some purposes. However, for some applications, e.g. the analysis of extreme values, the use of interpolated data can be difficult and result in high errors.

Keywords: Precipitation, Climate Data, Geostatistics, Interpolation, Radar, Urban Hydrology, Atmospheric Contaminant Transport

Kurzfassung

Viele Bereiche der Hydrologie, Wasserwirtschaft und Umweltwissenschaften benötigen Klimainformationen mit verschiedenen zeitlichen Auflösungen für die Modellierung diverser Prozesse. Klimainformationen werden in der Regel an Wetterstationen als ortsbezogene Punktmessungen aufgezeichnet, viele Anwendungszwecke benötigen allerdings flächenbezogene Daten. Für hydrologische Modellierungen werden z. B. oft Gebietsmittelwerte des Niederschlags verwendet, während z. B. für die Ausbreitungsrechnung von Schadstoffen in der Luft Zeitreihen für unbeobachtete Punkte erforderlich sind. Räumliche Interpolationsmethoden sind ein bewährter Ansatz, um für diese Punkte Klimainformationen aus benachbarten Stationsmessungen zu schätzen, wobei die Güte der Schätzung im Allgemeinen von der Stationsdichte, der zeitlichen Auflösung, der generellen räumlichen Variabilität der betrachteten Klimainformation und der Wahl der Interpolationsmethode abhängt.

Ziel dieser Arbeit ist es, die Einflüsse auf die Interpolationsgüte zu bewerten und zu ermitteln, ob interpolierte Daten für hydrologische und umweltbezogene Anwendungen geeignet sind. Hierfür erfolgte im ersten Schritt die Durchführung von Kreuzvalidierungen für verschiedene Klimainformationen, wobei unterschiedliche zeitliche Auflösungen und Stationsdichteszenarien berücksichtigt wurden. Es wurden sowohl einfache deterministische als auch komplexe geostatistische Methoden angewandt und unterschiedliche Zusatzinformationen verwendet. Ein besonderer Fokus liegt hier auf der Interpolation von Niederschlag mit hoher zeitlicher Auflösung, da diese Informationen als wesentliche Eingangsdaten für klassische hydrologische Modelle und auch hydrodynamische Stadentwässerungsmodelle benötigt werden. Insbesondere Radarmessungen des Niederschlags wurden bezüglich ihrer Eingnung als Zusatzinformation bei der räumlichen Schätzung geprüft. Im zweiten Schritt erfolgte eine Validierung der Niederschlagsinterpolation für Stadtentwässerungszwecke und die Simulation von Luftschadstoffausbreituntung. Unterschiedlich geschätzte Niederschlagszeitreihen wurden als Input für ein urbanhydrologisches Modell verwendet, während interpolierte Zeitreihen von Wind und Niederschlag Eingang in ein Schadstoffausbreitungsmodell fanden.

Die Kreuzvalidierungen zeigen, dass geostatistische Interpolationsmethoden im Allgemeinen eine bessere Interpolationsgüte liefern als einfache deterministische Ansätze. Die Berücksichtigung von Radardaten kann die räumliche Interpolation von Niederschlag mit hoher zeitlicher Auflösung (5 min – 360 min) verbessern, während eine Berücksichtigung der Topographie für geringe zeitliche Auflösungen des Niederschlags (1 Woche – 1 Jahr) und generell für die Temperaturinterpolation empfohlen wird. Für Windgeschwindigkeit, -richtung, Sonnenscheindauer und Bedeckungsgrad konnte keine nützliche Zusatzinformation gefunden werden, während die Interpolation von relativer Luftfeuchte durch die Berücksitigung von Temperaturinformationen verbessert wird. Generell scheinen zeitliche Auflösung, räumliche Variabilität und die verwendete Zusatzinformation einen größeren Einfluss auf die Interpolationsgüte zu haben als die Stationsdichte.

Die Prüfung interpolierter Zeireihen für Stadtentwässerungszwecke ergab, dass Radardaten keine realistische Wiedergabe der Extremwerte leisten aber eine verbesserte Simulation von Einzelereignissen erreichen können. Im Allgemeinen ist eine bessere Aufbereitung und Fehlerkorrektur der Radarinformationen erforderlich.

Geostatistisch interpolierte Zeitreihen des Niederschlags können für die Simulation von Luftschadstoffausbreitungen verwendet werden, wenn eine Korrektur der Zeitreihen im Bezug auf den mittleren Jahresniederschlag und die Anzahl der Stunden mit Niederschlag erfolgt. Die Berücksichtigung von Radardaten konnte hier keine Verbesserung gegenüber univariater Interpolation liefern.

Die Eignung geostatistisch interpolierte Daten hängt starkt von dem jeweiligen Anwendungsbereich ab. Die charakteristische Glättung der räumlichen Verteilung von Klimainformationen kann für manche Zwecke hilfreich sein. Für bestimmte Anwendungen, z. B. Extremwertanalyse, ist die Nutzung interpolierter Daten allerdings schwierig und mit großen Fehlern verbunden.

Schlagworte: Niederschlag, Klimadaten, Geostatistik, Interpolation, Radar, Stadthydrologie, Ausbreitungsrechnung

Acknowledgements

Contents

Contents

Chapter 1

Introduction

This chapter introduces the topic of this work. Section 1.1 contains a brief overview about the observation of climate variables and their importance for hydrological and environmental applications. The motivation and objectives for the spatial interpolation of climate information are discussed in Sec. 1.2, while an overview regarding the outline of this thesis is presented in Sec. 1.3.

1.1 Observation of climate variables and their importance for hydrological and environmental applications

Climate or weather information, respectively, is usually recorded as site-specific point information by meteorological stations. However, new developments include various remote sensing technologies. The following description contains the most important meteorological variables, explains the corresponding measuring approaches and highlights different purposes for which these data are of importance. The World Meteorological Organization (WMO, 2008) provides a comprehensive summary of all standard methods for the collection of weather and climate information.

The term precipitation (PCP) includes rain, drizzle, fog condensation, snow, hail and various mixed forms of water falling towards the surface of the earth. Rainfall usually refers to liquid water, nevertheless it is used as a synonym for precipitation here. Rainfall or precipitation is generally measured for different temporal resolutions by rain gauges, which are also known as ombrometers or pluviometers. These devices are open cylindric vessels that collect the precipitation volume. In case of daily rainfall measurements, the amount of water is registered

manually and afterwards the vessel is emptied by a person. Daily rain gauges are usually referred as non-recording gauges. Rainfall measurement for fine temporal resolutions requires automatic procedures. Modern recording gauges are based on the weighing principle, i.e. the weight of the water collected by the vessel is constantly measured and the amount of precipitation can be derived for any time period. These devices are characterised by a very fine measuring resolution of 0.01 mm. Another technique is used in tipping bucket rain gauges. Rainfall is led by a funnel to a small bucket that behaves like a seesaw. After a certain amount (usually 0.1 mm), the lever tips and the water is dumped. The tipping signal is recorded electronically and can be used for the calculation of precipitation depth, however the measuring resolution is lower than the one of the gravimetric devices. The spatial distribution of rainfall fields is usually captured via remote sensing, since rain gauge with a sufficient density are not always available. Satellite based rainfall estimation is in particular carried out for regions with sparse ground observations (THIEMIG *et al.*, 2012), while weather radar can provide data with a very high temporal and spatial resolution. Recent advances in capturing spatial rainfall include microwave links (UPTON *et al.*, 2005). Radar and microwave links are generally based on the same principle. A microwave signal is emitted from a source and reflected as well as attenuated by hydrometeors.

Precipitation is the most important input for many hydrological and hydrodynamical applications, since rainfall is the driving force of all runoff processes. Accurate measurements of rainfall are important input data of water balance and rainfall runoff models. In particular for the simulation of urban stormwater discharge and a corresponding optimisation of regulators, rainfall data with a high resolution in space and time is needed (BERNE *et al.*, 2004). In general, long-term statistics of rainfall are required for the design of hydraulic structures. Moreover, groundwater recharge and the availability of water in the vadose zone depend strongly on precipitation. Farming and in particular rain-fed agriculture are influenced by the amount rainfall and its temporal as well as spatial distribution (ROCKSTRÖM *et al.*, 2010). Besides many other purposes, precipitation data are required for the consideration of wet deposition processes in the simulation of contaminant transport in the atmosphere (PRADO-FIEDLER, 1990; GRIMM and LYNCH, 2004).

The term temperature refers here to the air temperature in the atmosphere. It is generally influenced by radiation, the albedo of the earth surface as well as wind and ocean currents. Meteorological temperature data are usually recorded by sun-sheltered thermometers with a height of 2 m above the ground. The air temperature is recorded for a temporal resolution of one hour and then averaged in order to obtain mean temperature data (TAV) for different time scales. Due to the diurnal behaviour of temperature, the maximum (TMA) and minimum

temperature (TMI) are recorded additionally for each day. Temperature variations are in general considered to cause air currents and correspondingly cloud formation, cloud movement as well as precipitation. Besides other purposes, temperature data is required in hydrology for the estimation of potential and actual evaporation (MONTEITH, 1981).

Depending on the temperature, air masses can store a certain amount of water. Often the relative humidity is used to characterise the amount of water dissolved in the air. It is derived from the measurement of actual air temperature in combination with the measurement of temperature in an entirely humid environment, whereas usually a psychrometer is used. The difference between actual and humid air temperature as well as the current saturation vapour pressure is required in order to calculate dew point as well as absolute and relative humidity. Modern sensors, i.e. electric hygrometers, provide an automatic measuring and derivation of all variables. They are either based on measuring changes in electric conductivity of a specific material or detecting the change in capacitance of a thin polymer film (WMO, 2008). Humidity is in general strongly related to other meteorological variables. Assuming a constant absolute humidity, precipitation will occur if the actual air temperature is falling below the corresponding dew point temperature. Furthermore, the water saturation of air is related to the occurrence and the intensity of evapotranspiration.

Cloud coverage (CLD) refers to the percentage of the sky that is obscured by clouds and is usually registered in okta. An okta value of zero represents an entirely clear sky, while an okta value of eight represents an overcast situation. Visual observation of cloudiness is carried out for the main observation times $00{:}00$, $06{:}00$, $12{:}00$ and $18{:}00$ UTC at all synoptical weather stations by a trained person that watches the sky. Automatic measurements are based on photogrammetric methods (SEIZ *et al.*, 2002), but suffer from a general lack of accuracy (WMO, 2008). In addition to coverage, cloud type and height is measured either by visual inspection or automatic lidar and radar techniques. Cloud coverage is directly related to radiation and sunshine duration (SUN). Sunshine duration is usually defined as the time period, in which sun radiation exceeds a certain threshold. Radiation is measured by specific devices, so called pyrheliometers, an a threshold of $120\,\mathrm{W/m^2}$ is recommended by the World Meteorological Organisation (WMO) in order to considerer the effect of diffusive radiation that will also occur if no direct sunshine is present (SONNTAG and BEHRENS, 1992). The theoretical daily maximum sunshine duration depends on latitude, season and the shape of the horizon.

In contrast to all other meteorological variables, which are only characterised by their absolute values, wind information is as a vector which contains velocity (WVE) and direction (WDI).

Wind velocity is usually measured in m/s by an anemometer 10 m above the ground, while the wind direction is observed using a vane. It is given as a category and defines the direction from which the air flow is coming. The German Weather Service (DWD) provides wind data in 36 categories, wherein each category represents a circular segment of $10°$. The data provided for hourly and daily temporal resolutions are generally averaged over the corresponding time periods. Wind affects the movement of clouds and rainfall cells, while it also causes an underestimation of precipitation depth recorded by rain gauges. A strong circulation of air fosters the occurrence and intensity of evaporation, since saturated air volumes over water surfaces are substituted more frequently. Movement of air is generally caused by atmospheric pressure gradients related to temperature differences. Common areas of application for wind data are, for instance, weather forecasts as well as the prediction of airborne pollutant transport.

1.2 Motivation and objectives

Many purposes in hydrology, water resources management and environmental sciences require areal information of climate variables. In particular the modelling of various processes is based on accurate and detailed input data. In contrast to that, accurate measurements of meteorological variables are only available for certain point locations of a more or less dense observation network. The utilisation of remote sensing data is in most cases not an option, since remote sensing techniques are in general based on rather indirect and thus also inaccurate measuring principles. Rainfall observations using weather radar, for instance, can be highly biased due to several error sources (WILSON and BRANDES, 1979). The direct use of these data for hydrological modelling is not recommended (BORGA, 2002).

Spatial interpolation techniques are a possible approach for the estimation of climate information for unobserved locations. LI and HEAP (2014) provide a synopsis of many methods and their features. Some approaches allow the consideration of an additional information related to the primary variable that is to be interpolated. The accuracy of spatial estimation depends on many factors. In general it is assumed that the density of the observation network has a high impact on the interpolation performance. Moreover, the actual spatial variability of the climate information as well as the quality of the additional information are considered to be important. Chapter 2 of this work presents the state of the art regarding the spatial interpolation of meteorological observations. In many case studies, geostatistical interpolation techniques achieved the best interpolation performance.

The main objective of this thesis is the evaluation of interpolation performance achieved by geostatistical approaches for a specific study region in Northern Germany, whereas also simpler methods are taken into account in order to evaluate the benefit of sophisticated techniques. In contrast to other studies, this work tries to provide a complete investigation of all relevant factors influencing the interpolation performance. Several climate variables are evaluated with different temporal data resolutions. Moreover, the interpolation performance is determined for various observation network density scenarios. Multiple additional data are investigated regarding the potential to improve the estimation accuracy, in particular the incorporation of radar information for the interpolation of precipitation with a fine temporal resolution is analysed. Interpolated data is validated using two applications. Rainfall estimations with a temporal resolution of 5 min are used for the simulation of urban stormwater discharge in order to assess whether can be used for the design of urban drainage systems, simulation of flow from past events and the evaluation of combined sewer overflow. Hourly wind and precipitation data are employed for the modelling of contaminant transport in the atmosphere in order to analyse whether spatial interpolation is useful for the generation data for unobserved locations.

1.3 Organisation of the thesis

The thesis is organised as follows. Chapter 2 contains the state of the art regarding the interpolation of different climate variables. The different geostatistical and non-geostatistical interpolation techniques applied for this work are presented and discussed in Ch. 3. Moreover, their performance assessment using different performance criteria is addressed.

The study area and the available data are introduced in Ch. 4, while a special focus is given to the observation networks for the meteorological variables. The design of the cross validation experiments using different temporal resolutions and observation network density scenarios is shown in Ch. 5. Moreover, the data preprocessing techniques that were applied are set out here, wherein in particular radar preprocessing requires a lot of explanation.

Actual cross validation results depending on climate variable, station density and meteorological information are presented and discussed in Ch. 5. The analysis of further issues regarding the influence of station selection and temporal data aggregation as well as a comparison of interpolation performance among all climate information is shown in Ch. 7. The following Ch. 8 and Ch. 9 present two individual case studies, in which interpolated climate information is validated for a specific application purpose. Chapter 8 contains the validation of fine temporal

resolution rainfall estimation for urban hydrological purposes, while Ch. 9 tests whether interpolated wind and precipitation data can be used for simulating the contaminant transport in the atmosphere. The summary, general conclusions and an outlook are presented lastly in Ch. 10.

Chapter 2

Spatial interpolation of climate variables – State of the art

This chapter summarises the current and past developments regarding the interpolation and estimation of spatial climate information. In particular for precipitation, many different regionalisation techniques and data merging methods were proposed over the years. Due to this, the state of the art for interpolation of precipitation is presented in Sec. 2.1, while past research about the interpolation of temperature, cloudiness, sunshine duration humidity and wind information is set out jointly in Sec. 2.2. Less studies addressed the spatial interpolation of other meteorological observations in comparison to rainfall.

2.1 Precipitation

Spatial interpolation of rainfall data has been carried out for a long time until now. First investigations towards this issue were carried out by THIESSEN (1911), who used polygons drawn around the locations of rain gauges on a station network map in order to obtain an estimation of the rainfall distribution. The polygons assign each point in the two-dimensional space the closest rain gauge according to the Euclidean distance. Prior to this development, homogeneous spatial rainfall was simply computed by averaging the recordings of all rain gauges within or in the proximity of the investigation area. A further technique for simple spatial interpolation of rainfall is the inverse-distance approach proposed by SHEPARD (1968). Rainfall estimates for a certain location are calculated using the recordings of four adjacent rain gauges, while the impact of each recording on the estimate is defined according to the inverse of its distance from the location to be estimated. The inverse-distance weight is usually

modified by a constant power or a distance-decay parameter in order to adjust the decrease in relationship with increasing distance. SHEPARD (1968) also suggests that the distance should be raised to the second power, in order to obtain weights that enable a continuous mapping of the regarded point information. Many studies used modified approaches, for instance LU and WONG (2008) proposed an adaptive scheme of inverse-distance weighting. The approach is based on finding the optimal distance-decay parameter for each local point neighbourhood and achieved a better interpolation performance than the standard inverse-distance weighting. These simple univariate interpolation techniques do not allow the hydrologist to take into account other information or special knowledge about the catchment, such as topography. A different approach, as it is described in MANIAK (2010), is the isohyetal approach. The general procedure is to use the location and recorded precipitation depths of each gauge and the knowledge about other factors affecting these precipitation recordings in order to create isohyets, i.e. lines of equal precipitation depth. The precipitation amount at unobserved locations within two isohyets can be obtained by linear interpolation. In general a relatively high rain gauge network density and a lot of manual work is required for the accurate drawing of isohyets. However, the implicit consideration of additional factors like topography can improve the rainfall estimation.

Geostatistical techniques, like kriging as described in CRESSIE (1986), ISAAKS and SRIVAS-TAVA (1990) and CRESSIE (1990), allow the consideration of a spatial correlation among adjacent observations for the estimation of unknown locations. Many studies, for instance the early investigations by PHILLIPS *et al.* (1992) and TABIOS and SALAS (1985), reported that ordinary kriging and other variations can provide a better estimation of rainfall than simple univariate interpolation techniques. Another comparison of kriging with simple algorithms was carried out by DIRKS *et al.* (1998). Inverse-distance weighting and ordinary kriging achieved a better interpolation performance than Thiessen polygons and simple averaging for all temporal resolutions from 1 hour to 1 year. Inverse-distance weighting is preferred due to its simplicity and computational efficiency. Further univariate techniques for the spatial interpolation of precipitation include spline fitting. Two-dimensional thin plate splines can achieve a reasonable performance for the interpolation of daily rainfall recordings, although the short range correlation that is present in the data made the model calibration more difficult (HUTCHINSON, 1998a). The fitting of three-variate splines allows even the incorporation of elevation data, but only a minor improvement was achieved by HUTCHINSON (1998b). A rather theoretical review of several univariate interpolation techniques for rainfall is provided in CREUTIN and OBLED (1982). It is concluded that geostatistical methods are preferable, since they are able to provide a measure of uncertainty. Nevertheless, the better interpolation

performance of ordinary kriging might not always justify the high computational effort that is required. Moreover, in case of repeated interpolations, a method that is calibrated once to the precipitation climate of the study area and does not require a separate estimation of the spatial variability might be the best choice.

Many different interpolation techniques that allowed the incorporation of elevation in the interpolation procedure were developed over time. DALY *et al.* (1994) used a regression approach between rainfall sum and elevation in order to predict monthly and annual precipitation. The proposed method delivered a better performance than the use of kriging based on elevation-detrended data and cokriging. The geostatistical approach kriging with external drift (AHMED and DE MARSILY, 1987) was applied to rainfall sums and compared to other interpolation techniques by GOOVAERTS (2000). The study reported that implementing the elevation as a background information can improve the interpolation performance on a monthly and yearly time scale and that multivariate kriging methods like kriging with external drift, cokriging and simple kriging with varying local means outperform univariate interpolators as well as a linear regression based on elevation. Other geostatistical interpolations considering elevation as additional information were performed by MARTÍNEZ-COB (1996), who concluded that cokriging outperforms ordinary kriging and residual kriging for the spatial interpolation of long-term average annual precipitation and annual reference evapotranspiration for a region in the north of Spain. Multivariate geostatistics, i.e. cokriging, was also applied to average annual precipitation in southern Nevada and southeastern California by HEVESI *et al.* (1992a) and HEVESI *et al.* (1992b). It delivered a better interpolation performance than simple averaging, inverse-distance-weighting, ordinary kriging and linear regression. NALDER and WEIN (1998) compared different methods for the interpolation of mean annual precipitation in the Canadian boreal forest. They propose a technique called 'gradient-plus-inverse-distance squared' that is based on a linear regression and inverse-distance weighting with a power of two and reported that this technique outperforms elevation-detrended kriging, universal kriging and other interpolation approaches. LLOYD (2005) considered cokriging as well as kriging with external drift and other methods in his study about the mapping of monthly precipitation for Great Britain. The application of kriging with external drift resulted in the best interpolation performance from March to December, while ordinary kriging performed best for January and February. DI PIAZZA *et al.* (2011) used ordinary kriging of the residuals from a linear regression between precipitation and elevation in order to fill gaps in monthly time series. Inverse-distance weighting, ordinary kriging, spline fitting, artificial neural networks and several regression techniques performed worse. KYRIAKIDIS *et al.* (2001) proposed the application of geostatistics for mapping mean precipitation using terrain information and other

predictors obtained from the NCEP-NCAR reanalysis product (KALNAY *et al.*, 1996), i.e. specific humidity and horizontal and vertical wind velocities. All predictors were combined and incorporated as additional information in the rainfall interpolation procedure and a significant improvement of estimation accuracy compared to ordinary kriging was observed. TOBIN *et al.* (2011) examined the interpolation of rainfall amounts and mean temperature of different flood events for hydrologic applications in a Swiss Alpine region, while elevation and numerical weather forecast was used as secondary information. Kriging with external drift outperformed nearest neighbour and inverse-distance weighting, in particular when elevation was used as the background information.

In contrast to the aforementioned studies, which analysed mainly the benefit of using elevation as an additional information for long accumulation times and long-term averages of precipitation, the elevation does not always seem to be helpful for shorter time scales. Only few studies that report an improvement for daily or shorter accumulation times are available. CHANG *et al.* (2005) applied a combined interpolation method based on inverse-distance weighting and fuzzy logic for the interpolation of daily rainfall sums. Genetic algorithm was used to estimate the parameters of the fuzzy membership functions, while horizontal distance and elevation were considered as additional information in the fuzzy logic framework. A slight improvement was observed in comparison to Thiessen polygon interpolation and the simple calculation of an arithmetic average. PRUDHOMME and REED (1999) compared two geostatistical methods for the mapping of extreme rainfall in Scotland. A modified residual kriging approach that takes into account the elevation could improve the spatial interpolation of the median of annual maximum daily rainfall in comparison to ordinary kriging. VERWORN and HABERLANDT (2011) applied kriging with external drift to hourly rain gauge data, while they incorporated different additional information. Elevation could hardly improve the spatial estimation compared to ordinary kriging. However, the inclusion of elevation delivered rainfall maps that visually seemed more plausible. LY *et al.* (2011) used different methods for the interpolation of rainfall in a Belgian catchment. Integrating elevation into kriging with external drift and cokriging did not improve the interpolation performance compared to ordinary kriging and inverse-distance weighting. The interpolation of short-duration precipitation taking into account topographical data is addressed by ALLAMANO *et al.* (2009). It was found that the influence of elevation depends strongly on the duration of extreme rainfall, whereas the orographic effect is stronger for longer accumulation times.

Weather radar is widely used for measuring spatial rainfall patterns. The main advantage is that radar measurements have a high resolution in space and time but tend to be strongly biased in general (SEO *et al.*, 1999). A radar device does not measure the precipitation intensity

directly, but rather the reflected energy from hydrometeors at a certain height above the ground. According to WILSON and BRANDES (1979), sources of errors include variations in the relationship between reflected energy and rainfall intensity depending on rainfall type, changes in precipitation particles before reaching the ground, anomalous beam propagation, attenuation as well as clutter. BORGA (2002) used areal rainfall obtained from radar as the input for a conceptual hydrological model of a catchment in South-East-England and concluded that there is a critical importance of the rainfall field obtained from weather radar. Radar data adjusted to rain gauge observations allowed a significantly better streamflow simulation than non-adjusted data. Other studies showed as well that the direct use of uncorrected radar data for hydrological purposes should be avoided (BORGA *et al.*, 2000; SUN *et al.*, 2000). KRAJEWSKI and SMITH (2002) discussed two different approaches for converting the recorded amount of backscattered energy to rainfall intensity. A relationship between reflectivity and rainfall intensity (Z–R–relationship) can either be selected based on the analysis of raindrop size distribution for a specific predominant type of rainfall or calibrated using ground observations like rain gauges. Fitting the radar rainfall intensities to ground observations also accounts for the difference in sampling mechanism of radar and gauge data, i.e. the volumetric radar scans affected by beam blockage, bright band effect, wind drift and other errors are transformed to values as they are actually measured by point observations on the ground. BRANDES (1975) adjusted radar data by calibration factors, which are computed as the average ratio between rain gauge observations and collocated radar measurements. SMITH and KRAJEWSKI (1991) proposed a single spatially uniform adjustment factor for radar data. This technique is called mean field bias correction and was widely applied although the ratio might vary significantly in space according to SEO *et al.* (1999) and SEO and BREIDENBACH (2002). Real-time bias correction of radar data was performed by SEO *et al.* (1999), DINKU *et al.* (2002) and CHUMCHEAN *et al.* (2006), whereas Kalman filtering approaches were used to predict and update the relationship between radar and rain gauge data. CHUMCHEAN *et al.* (2003) presented a method for including a range dependent radar error variance in the calibration procedure. An improvement of approx. 5 % is achieved, when the radar rainfall reliability is considered for the calibration of the Z-R-relationship. RABIEI and HABERLANDT (2015) proposed an adjustment technique based on quantile mapping and reported that radar data quality improved significantly. Further recent developments in radar hydrology include probabilistic rainfall rates. KIRSTETTER *et al.* (2015), for instance, computed probability distributions of precipitation rates instead of deterministic rainfall values using a model quantifying the relation between reflectivity and true rainfall for different precipitation typologies. Other research on radar rainfall uncertainties was carried out by VILLARINI and KRAJEWSKI (2009) as well as VILLARINI *et al.* (2014).

An entirely different way for deriving quantitative precipitation estimates using radar data are geostatistical merging techniques. A merging approach based on cokriging was applied in numerical experiments by KRAJEWSKI (1987), while high quality radar images were used as true rainfall fields. A radar error model and a rain gauge error model was implemented in order to derive daily pseudo radar rainfall fields and daily pseudo rain gauge recordings for a different number of stations. The merged rainfall fields resulting from the cokriging algorithm were compared with true fields in order to assess the accuracy of rainfall estimation. Cokriged rainfall fields were able to provide a slightly better rainfall estimation for all gauge network densities compared to the use of rain gauges only. A similar study was carried out by AZIMI-ZONOOZ *et al*. (1989). The tested cokriging techniques outperformed rainfall estimation by mean field bias correction of radar data and ordinary kriging of rain gauge data. HABERLANDT (2007) used kriging with external drift and indicator kriging with external drift for the interpolation of hourly rain gauge data of a large-scale extreme rainfall event, whereas different drift variables were used. A clear improvement of interpolation performance in comparison to univariate interpolation methods was achieved, wherein Radar was the most valuable additional information followed by daily rainfall sums from a denser network. The use of elevation as further additional information did not improve the quality noticeably. Another study by VERWORN and HABERLANDT (2011) showed the benefit of implementing radar data in kriging with external drift. In particular for convective summer events an improvement to univariate interpolation was observed, whilst radar did not contribute significantly to a better interpolation performance of stratiform winter events. VELASCO-FORERO *et al*. (2009) evaluated ordinary kriging, kriging with an external drift and collocated cokriging in combination with a non-parametric and automatic technique to obtain correlograms from radar images. Kriging with external drift performed best. SCHIEMANN *et al*. (2011) applied the same method and compared it to a different formulation of kriging with external drift that uses an improved approach for estimating the residuals of the radar field that the correlogram computation is based on. An improvement of interpolation accuracy is observed for three test cases consisting of hourly rainfall data.

A further technique to combine radar and rain gauge data is the so called conditional merging approach, which consists of combining an interpolated rain gauge field with rainfall variability information derived from radar data. The method was reported first in EHRET (2003) and is referred as conditional merging by SINCLAIR and PEGRAM (2005). Conditional merging can efficiently reduce the bias and error variance of quantitative precipitation estimates as it was shown in computer experiments by SINCLAIR and PEGRAM (2005). Several merging approaches with different complexity were evaluated for the Walloon region in Belgium by

GOUDENHOOFDT and DELOBBE (2009) using daily rainfall data. They preferred geostatistical merging over univariate rain gauge interpolation and radar data adjustment. Kriging with external drift was the best approach, however conditional merging performed only slightly worse. Furthermore, the effect of station network density on the merging performance was analysed in this study. Geostatistical techniques were more sensitive to the network density than mean field bias correction and other radar data adjustment methods, but also performed best for the lowest station density. A similar study was performed by NANDING *et al*. (2015) for hourly data. Different techniques were compared for a region in England and several rain gauge network densities were analysed. It is reported that kriging with external drift outperforms conditional merging and mean field bias correction for all network configurations. In particular for low network densities a strong improvement to univariate interpolation of gauge data is observed, since radar data based methods allow a better representation of the actual spatial rainfall pattern.

Geostatistical interpolation techniques are generally able to provide an index of estimation uncertainty, i.e. the kriging standard deviation. DELRIEU *et al*. (2014) implemented ordinary kriging and external drift kriging based on hourly radar data for several rainfall events in South France and assessed the estimation accuracy and also uncertainty. A significantly better interpolation performance of KED was obtained for a majority of precipitation events. The incorporation of radar data using kriging with external drift also yielded a much lower uncertainty compared to ordinary kriging. ERDIN *et al*. (2012) addressed the topic of data transformation for rainfall interpolation using geostatistics. They argue that the classical assumptions of geostatistics are not fulfilled by the "skewed and heteroscedastic nature of precipitation" and applied kriging with external drift using different settings of transformations proposed by BOX and COX (1964). Their results indicate that the transformation has only a minor impact on the interpolation performance, however the corresponding estimation uncertainties could be reduced significantly.

Another group of techniques for estimating spatial rainfall distributions is based on copula applications. VOGL *et al*. (2012) used a copula approach for modelling the dependence structure between gauge observations and rainfall derived from radar reflectivity. The proposed technique allows the correction of radar rainfall fields with similar efficiency as it is done by RADOLAN (WEIGEL and WINTERRATH, 2009), the operational system for quantitative radar precipitation estimates operated by the DWD. BÁRDOSSY (2006) proposed an entirely new approach for the spatial analysis, which was later also applied for rainfall interpolation. He used copulas to model the spatial dependence of groundwater parameters. Empirical copulas calculated for different distance classes showed a non-symmetrical spatial dependence for all groundwater parameters.

Non-Gaussian multivariate copulas based on transformed multivariate normal distributions were preferred over Gaussian copulas for modelling the spatial dependence. The actual spatial interpolation is reported in BÁRDOSSY and LI (2008). The cross validation as well as the split sampling analysis showed that Non-Gaussian copulas achieve a slightly better estimation accuracy than Gaussian copulas, ordinary kriging and indicator kriging. Cross validation was also used to validate the confidence intervals of the estimation. The non-Gaussian copula technique delivered a lower uncertainty than indicator kriging, while ordinary kriging delivered the worst result. BÁRDOSSY and PEGRAM (2013) used copula techniques and kriging methods for the spatial interpolation of rainfall sums for one day, five days, one month and one year, while taking into account the elevation as the additional information. The best interpolation results were achieved by using a shifted and smoothed version of the digital elevation model which accounts for the effects of directional advection. The technique based on Gaussian copulas performed well for all temporal resolutions, however a significant reduction of split sampling validation error compared to OK or KED based on the transformed elevation was not detected. The main advantage of applying copulas for the interpolation of rainfall is the improvement of estimation uncertainties as it is shown for rainfall by BÁRDOSSY and PEGRAM (2013) and groundwater quality parameters by BÁRDOSSY and LI (2008).

In regions with few rain gauges and no radar coverage, satellite recordings can be helpful for obtaining rainfall patterns and also quantitative rainfall estimates. THIEMIG *et al.* (2012) evaluated several satellite-based rainfall estimation products by validating them against 205 rain gauge stations over several African river basins. The satellite based estimation algorithms allow a good reproduction of monthly precipitation patterns but tend to be less accurate on a daily time scale. In particular the detection of heavy rainfall events is highly inaccurate. Statistical merging procedures were applied for combining rain gauge and satellite data as well. For instance, LI and SHAO (2010) proposed a nonparametric kernel merging technique for rain gauge and TRMM satellite data. An improvement in comparison to kriging methods was detected for the Australian study area. WOLDEMESKEL *et al.* (2013) used a combination of thin plate smoothed splines and inverse-distance weighting to merge satellite and station data on a monthly time scale. In particular for regions with a sparse station network, an improvement of rainfall estimation was found. CHAPPELL *et al.* (2013) evaluated the suitability of geostatistical methods for combining satellite estimates with rain gauge data for obtaining near real-time daily precipitation fields over Australia. Implementing satellite data in cokriging worsened the overall interpolation performance compared to ordinary kriging of station recordings. However, for some regions in the interior of the Australian continent an improvement was achieved due to the low station density. GRIMES *et al.* (1999) compared satellite data, block kriging, external

drift kriging using satellites and a novel algorithm for areal rainfall estimation in Niger. The newly proposed technique consists of computing areal rainfall as a weighted average value for each satellite pixel with the weights proportional to the inverse of their ordinary kriging estimation variance. An improvement of dekadal rainfall estimates and their spatial distribution was registered. Recently another technique was suggested by VERDIN *et al.* (2015), who implemented a Bayesian kriging approach for merging satellite and ground observations of precipitation and reported an improvement of accuracy on a pentadal time scale compared to residual kriging and the original satellite rainfall estimates.

2.2 Further meteorological data

2.2.1 Temperature

Many of the interpolation algorithms of rainfall were also used for mapping air temperature data over land surfaces. The interpolation of sea surface temperature is another topic and not discussed here. Information about this can be found in REYNOLDS and SMITH (1994), for instance.

The gradient-plus-inverse-distance-squared method (GIDS) taking into account the terrain elevation is also applied to long-term temperature means by NALDER and WEIN (1998). It outperformed nearest neighbor interpolation, regular inverse-distance weighting and several kriging algorithms for a Canadian region dominated by forest vegetation. PRICE *et al.* (2000) compared spline fitting techniques and GIDS for monthly averages of temperature and precipitation for two different Canadian study regions. Spline fitting performed better for 70 of 72 months. Nevertheless, GIDS is easy to implement and can be used as a baseline to compare with more sophisticated methods. Fitting of splines was also applied by JEFFREY *et al.* (2001) in order to create an archive of Australian climate data including daily mean, maximum and minimum temperature. A similar data set was created by HAYLOCK *et al.* (2008) for Europe. Thin plate smoothing splines taking into account elevation were applied for monthly temperature and precipitation averages and daily anomalies were interpolated by kriging. The entire cross validation analysis and comparison with other interpolation methods like nearest neighbor is presented in HOFSTRA *et al.* (2008). Spline fitting was also evaluated for temperature and rainfall in China (HONG *et al.*, 2005) and used for the generation of a Canada-wide data set of daily minimum and maximum temperature as well as precipitation

(HUTCHINSON *et al.*, 2009). DODSON and MARKS (1997) investigated also different approaches for interpolating daily minimum and maximum data. The first technique consisted of converting all temperature recordings according to their elevation to potential sea-level temperatures. Next, inverse distance weighting was applied and actual temperatures were derived via a backtransformation using the digital elevation model of the study area. The second approach is carried out in a similar way, however a constant lapse rate is used instead of equations that involve considerations of air and sea-level pressure. The linear lapse rate method was chosen as the better interpolator.

Ordinary kriging and residual kriging were applied to monthly temperature data for a region in Minnesota, USA, by HOLDAWAY (1996), while two different trend models were considered in the residual kriging approach. A lake effect model that accounts for the influence of Lake Superior with a subsequent kriging of the residuals delivered a better performance than applying ordinary kriging or residual kriging based on a latitude-longitude trend function. Moreover, it is reported that the use of average variograms did not lead to an inferior interpolation performance, although there had been systematic changes in the spatial variability of temperature over the last century. JARVIS and STUART (2001a) and JARVIS and STUART (2001b) found that elevation, northing and the distance to the coast are important predictors of maximum temperature. In case of minimum temperature, the aforementioned predictors as well as an urbanity index can help to improve a regression based interpolation although the strength of relation was highly variable. Interpolation by thin plate spline fitting performed slightly better than trend surfaces as well as inverse-distance weighting or ordinary kriging applied to the residuals of a regression based on the predictors. Sophisticated interpolation methods like ordinary kriging and thin plate splines tend to require fewer covariates for achieving an optimal interpolation performance compared to pure regression. Monthly and annual mean air temperature was mapped by NINYEROLA *et al.* (2007) for the Iberian peninsula using inverse-distance weighting and splines. A general model for the entire study area and local models for single river basins were set up. A multiple regression using logarithmic distances to the coast in combination with residual interpolation by inverse-distance weighting achieved the best interpolation performance. COURAULT and MONESTIEZ (1999) considered circulation patterns in a geostatistical interpolation of daily maximum and minimum temperatures. They conclude that integrating the elevation has a higher impact on the estimation accuracy than atmospheric circulation.

STAHL *et al.* (2006) evaluated various interpolation techniques that are based on temperature gradients caused by elevation differences. The nearest neighbour interpolation carried out in this study, for instance, considered not only the temperature of the closest adjacent station, but also the elevation difference to the estimation point and a specified temperature gradient. Methods

relying on the computation of local lapse rates perform significantly worse for years with a low number of high-elevation observations. Overall, the GIDS method using a linear regression for computing a fixed lapse rate performed best. A similar comparison of interpolation methods was carried out by KURTZMAN and KADMON (1999) for extremes and averages of monthly temperature in Israel, wherein spline interpolation performed best in summer and inverse-distance weighting in winter. Combining multiple regression and spatial techniques improved the prediction performance of extremes only. Another exhaustive analysis of interpolation methods was carried out for the middle Ebro valley in Spain by VICENTE-SERRANO *et al.* (2003). The split sampling validation showed that a regression model considering elevation deduced predictors, latitude and the distance to the Cantabrian sea achieves a better interpolation performance for mean annual temperature than trend surfaces, spline fitting, several kriging approaches and other combined interpolation techniques. Furthermore, it is concluded that the interpolation performance of temperature differs to the one that is obtained for rainfall and that the ranking of interpolation methods depends on the study area. Several techniques need to be implemented in order to select the most appropriate scheme.

Kriging with external drift was applied to mean January air temperature in Scotland by HUD-SON and WACKERNAGEL (1994). The incorporation of topography resulted in a significant improvement of estimation accuracy compared to univariate kriging of station data. CHUNG and YUN (2004) developed an interpolation technique for hourly air temperature in mountain-ous areas that is based on inverse-distance weighting, a lapse rate due to elevation differences and a complex solar irradiation scheme depending on season, land cover, hourly sun position and local topography. The proposed technique creates temperature maps with a higher spatial variability and delivered a better interpolation performance.

2.2.2 Wind

SHOJI (2006) used a spatial and temporal variogram analysis in order to assess wind energy issues in two mountainous regions in central Japan. Most of the spatial variograms did not show clear ranges, but are flat or linearly increasing. This behaviour is explained by the low station density and the snapshot character of the wind measurements that were used. It is concluded that more observations are required, when geostatistics are applied to assess the wind power potential. LUO *et al.* (2008) compared several geostatistical and deterministic interpolation methods for the spatial estimation of daily mean wind velocities in England and Wales. Cok-riging using the elevation outperformed trend surface analysis, inverse-distance weighting, thin plate smoothing splines and also ordinary kriging as well as universal kriging. However,

ordinary kriging performs best if no secondary data is taken into account. Furthermore, it is concluded that all interpolation technique fail to represent the spatial wind velocity pattern in southwest England and Wales and that high values of wind velocity tend to be underestimated due to a lack of high altitude stations. ZLATEV *et al.* (2010) propose a knowledge-assisted kriging algorithm for the spatial information of wind data and applied it to the data set of LUO *et al.* (2008). The study area is divided, such as each subregion shows a coherent spatial behaviour of wind velocity. After the creating real-time automated variograms, the interpolation is performed using ordinary kriging. The novel method did not improve the cross validation error, but allowed a significantly better estimation of the kriging standard deviation.

PALOMINO and MARTÍN (1995) reported a strong correlation between wind speed and elevation for a valley in the south of Spain. They compared the classical inverse-distance weighting of wind information, that was also applied in a study by GOODIN *et al.* (1979), and a wind estimation technique based on the inverse absolute elevation difference for six different stations and concluded that the elevation is an important factor for the local wind estimation in a complex terrain. Local wind conditions, i.e. wind roses, that depend on the topography and nearby obstacles were also inferred by fuzzy systems (GONZÁLEZ DE LA ROSA *et al.*, 2011).

LI *et al.* (2014) used spline fitting in combination with simple kriging of the residuals for the interpolation of wind velocity data in China, whereas elevation and reanalysis data were considered as additional information. The incorporation did not alter the interpolation performance, i.e. a pure spline fitting approach achieved the same estimation accuracy. Wind speed was included by APAYDIN *et al.* (2004) in the comparison of interpolation techniques for the region of the Southeastern Anatolia project in Turkey. Simple kriging and disjunctive kriging delivered a better performance than ordinary kriging, universal kriging, inverse-distance weighting and other techniques. The incorporation of elevation as an additional information in several variations of cokriging could not improve the interpolation performance. VAN ACKERE *et al.* (2015) compared different interpolation techniques, whereas geostatistical interpolation outperformed inverse-distance weighting and other simpler approaches. A simple kriging procedure with a subsequent roughness correction based on land cover was selected for generating maps of wind resources in Flanders, Belgium. YE *et al.* (2015) compared different interpolation techniques for extreme wind velocities over Canada. Geostatistical methods and spline fitting techniques delivered a better interpolation performance than simple techniques like inverse-distance weighting and polynomial interpolation. The consideration of elevation as an additional information in cokriging could not improve the interpolation accuracy significantly.

ŞAHIN and ŞEN (2004) applied inverse-distance weighting and ordinary kriging to hourly wind velocity data. They proposed a trigonometric point cumulative semivariogram concept that is able to consider variations of spatial wind velocity dependence due to different wind directions. They reported an improvement of estimation when kriging weights are calculated based on this novel procedure. The standard semivariogram or correlation function based weighting cannot account for the actual spatial behaviour. CELLURA *et al.* (2008a) compared inverse-distance weighting, ordinary kriging and universal kriging for the mapping of wind information in Sicily and concluded that geostatistical techniques perform better. A neural kriging approach is proposed for the same data set in CELLURA *et al.* (2008b). The large-scale spatial trend of wind fields is estimated using artificial neural networks that are trained using average wind velocities, topography and land cover, while short-scale correlations are considered by residual kriging. An improvement compared to pure kriging approaches was observed. ROBERT *et al.* (2013) proposed general regression neural networks for the spatial interpolation of monthly wind speeds for a complex Alpine topography, while the training was carried out using meteorological observations and terrain features such as convexity, slope, exposure. A significantly better cross validation results was obtained when topography features are incorporated compared to the application of low-dimensional neural networks relying only on elevation and spatial coordinates. Furthermore, it is reported that the performance is lower in summer than in winter due to weaker and more complex relations of wind and topography features. A further technique based on artificial neural networks was applied for a region in the northwest of Turkey by ÖZTOPAL (2006). A different field in which geostatistical methods are employed is the temporal forecasting of wind speed time series. LIU *et al.* (2010), for instance, adopted a Taylor kriging technique and reported that it performs better than autoregressive moving average methods.

Spatial interpolation of wind direction is hardly addressed in the literature. NIELSEN (1999) used an approach based on Bézier polynomials for the interpolation of wind climatologies, i.e. wind roses. However, no case study comparing different interpolation techniques for wind direction was found.

2.2.3 Humidity

In comparison to precipitation and temperature, very few studies address the spatial interpolation of absolute or relative air humidity. Humidity interpolations are often carried out when entire data sets of climate information are generated, whereas the focus is mainly on rainfall and temperature interpolation, respectively. An evaluation of different interpolation techniques

can hardly be found. NGUYEN *et al*. (2015) used two geostatistical techniques for the spatial interpolation of different climate variables in Vietnam. The relative humidity interpolation errors of universal kriging are slightly lower than those of ordinary kriging. Spline fitting was applied by JEFFREY *et al*. (2001) for the interpolation of daily relative humidity recordings. A data set consisting of several variables was created for Australia. A similar data set was constructed for China by LI *et al*. (2014). A combined approach of spline fitting and residual kriging is proposed, whereas elevation and reanalysis data are taken into account as additional information. The incorporation of reanalysis data and the application of simple kriging to residuals leads to a slight improvement of interpolation performance compared to the simple fitting of two-dimensional spline surfaces. APAYDIN *et al*. (2004) evaluated various spatial interpolation techniques for the region of the Southeastern Anatolia project of Turkey, whilst relative humidity was among the meteorological variables that were analysed. Simple cokriging taking into account the elevation performed slightly better than inverse-distance weighting, spline fitting, various univariate kriging and cokriging approaches. A global polynomial interpolation delivered the worst performance.

2.2.4 Sunshine duration and cloud coverage

Sunshine duration and cloud coverage are generally important for the computation of solar radiation and their spatial interpolation is therefore discussed together.

The spatial distribution of sunshine duration over Greece is discussed based on maps by the Hellenic National Meteorologic Service by MATZARAKIS and KATSOULIS (2006). According to them, season-wise and annual sunshine duration can be predicted based on the distance to the nearest coast, land cover, elevation, latitude and longitude. GOODALE *et al*. (1998) compared a polynomial regression approach based on elevation and modified inverse-distance weighting for estimating spatial distributions of average monthly sunshine duration in Ireland. The two methods performed similarly well, however the regression approach needed less computation time. DOLINAR (2006) interpolated station data of sunshine duration for generating a solar energy climatology. The mapping was performed on a mathematical horizon, i.e. annual mean sunshine duration recording were corrected by extrapolating the sunshine duration values on an hourly basis for the time when the measuring site was in shadow due to obstacles on the horizon. Linear regression in combination with residual kriging or inverse-distance weighting is selected for the interpolation, whereas the exact procedure depends on the season and region within Slovenia. In general, the season had a strong impact on the relation between sunshine duration and altitude. RAICHIJK (2012) applied ordinary kriging to monthly mean values in

order to analyse trends in sunshine duration over South America. Two significant trends were found. Temperature decreased in the period from 1961 to 1990 and is increasing from 1990 onwards. JOURNÉE *et al.* (2013) and BERTRAND *et al.* (2013) created daily sunshine duration maps for Belgium and Luxembourg, respectively. Station recordings and satellite estimations of solar radiation were taken into account and kriging with external drift outperformed regression models as well as ordinary kriging. FREI *et al.* (2015) developed a scheme to derive daily and monthly maps of sunshine durations, whereas station data and satellite data were used for a non-contemporaneous combination in Switzerland. Different spatial patterns derived by principal component analysis were used as time invariant additional information together with elevation, latitude and longitude in kriging with external drift. A significant improvement was detected in comparison with no use of satellite information, the best performance was used by direct contemporaneous incorporation though. The proposed non-contemporaneous integration is not limited to the satellite data period but might perform worse in regions with a less complex topography.

Other studies focus on the direct interpolation of solar radiation instead of sunshine duration. ALSAMAMRA *et al.* (2009) applied ordinary kriging and residual kriging for mapping solar radiation over southern Spain. The regression that residual kriging is based on was performed using the elevation and another information derived from the digital elevation model and accounts for shading due to topography. Recently, ANTONANZAS *et al.* (2015) applied inverse-distance weighting, ordinary kriging and universal kriging to solar radiation estimates obtained by a prediction model based on support vector regression machines and genetic algorithm. Ordinary kriging was also applied to parameters of the Angstrom equation (ANGSTROM, 1924) by TIBA (2001) in order to create a data base of solar radiation for northeast Brazil. Point-wise parameters were determined beforehand from collocated observations of sunshine duration and solar radiation. A similar study was conducted by CHELBI *et al.* (2015). Spline interpolation was applied to the parameters here in order to obtain solar radiation maps.

In contrast to solar radiation and sunshine duration, the spatial interpolation of cloud cover has hardly been studied. GARCIA *et al.* (2008) investigated the long-term spatial distribution of cloud coverage by analysing the relation of correlation and spatial distance beween station pairs. Kriging was applied to the data in order to generate cloud cover maps. JEFFREY *et al.* (2001) generated a data set of solar radiation for Australia. They utilised measured radiation in the first place, since it is the most accurate information. In case of no direct data, solar radiation was estimated from sunshine duration. Only if both information are not available, cloud okta data were used.

2.3 Open research questions

In general, there is a lack of climate data with a high resolution in time and space. For rainfall, merging of radar data might help to overcome this problem. In particular for urban hydrological purposes, high-resolution precipitation data is needed (BERNE *et al.*, 2004; EINFALT *et al.*, 1998). According to earlier considerations by SCHILLING (1991), a temporal resolution of 5 min or higher and a spatial resolution of one rain gauge per $1\,km^2$ is required for real-time control purposes and evaluation of specific rainfall events in combination with model calibration. Furthermore, the evaluation of combined sewer overflows requires 5 min data with a spatial resolution of one gauge per $5\,km^2$. In contrast to these urban requirements, many studies focus on the interpolation rainfall for longer accumulation times and only few studies address the issue of rainfall with high temporal resolution, for instance HABERLANDT (2007).

Most previous work focused on improving the interpolation performance for one specific temporal resolution of a certain climate variable. A comparison of interpolation performance for different climate variables is hardly found in the literature. Only few studies evaluate interpolation performance of precipitation and temperature, for instance NALDER and WEIN (1998) and VICENTE-SERRANO *et al.* (2003). A combined geostatistical analysis of all meteorological observations for a mutual study area is only found in APAYDIN *et al.* (2004). Some studies compare the interpolation performance among different station densities (GOUDENHOOFDT and DELOBBE, 2009; YOON *et al.*, 2012; KRAJEWSKI, 1987; NANDING *et al.*, 2015) and even fewer among different time scales (BÁRDOSSY and PEGRAM, 2013; DIRKS *et al.*, 1998), although network density is considered to have a strong impact on the estimation accuracy and the spatial variability of certain climate information depends on the accumulation time. A combined evaluation of all influence factors in order to provide a guidance for the choice of interpolation method depending on study area, climate variable, network configuration, temporal resolution and intended data use is not available.

Another relevant topic for further research is the estimation of rainfall information in sparsely observed regions. Gathering information from alternative data sources as for instance microwave links of telecommunication networks (UPTON *et al.*, 2005; LEIJNSE *et al.*, 2007) or cars using windscreen wiper frequency or optical sensors (HABERLANDT and SESTER, 2010) in combination with few ground observations might improve rainfall estimation in regions with very low rain gauge densities. Moreover, it is still under investigation how the improvement in interpolation performance of precipitation and other climate information improves the modelling of hydrological and other environmental processes.

Chapter 3

Interpolation techniques and their performance assessment

This chapter explains all non-geostatistical and geostatistical interpolation techniques, which were applied in this work. The non-geostatistical techniques are referred as simple interpolation methods (Sec. 3.1) and in contrast to the more sophisticated geostatistical techniques (Sec. 3.2), a quantification of spatial persistence of the regarded climate variable is not considered in the interpolation procedure. All methods described in the following are based on the same principle: The estimate for an unknown location is calculated using a weighted linear combination of a certain number of adjacent measurements, whereas the neighbour selection as well as the calculation of weights depends on the specific interpolation technique.

3.1 Simple interpolation methods

3.1.1 Nearest Neighbour

The nearest neighbor interpolation technique (NN), also known as Thiessen polygon method (THIESSEN, 1911), is a basic approach that is commonly used for the spatial interpolation of precipitation. Each location within the regarded area is simply assigned with the closest available rain gauge measurement. It can be easily applied for the interpolation of other meteorological variables as well.

3.1.2 Inverse-Distance Weighting

Inverse-distance weighting (InvD) allows the consideration of a simple spatial dependency for the interpolation of observed point information (SHEPARD, 1968). In contrast to the more sophisticated geostatistical approaches, it does not require an a priori investigation of spatial variability of the measured values. The estimation of an unobserved location is carried out according to:

$$Z^*(u_0) = \sum_{i=1}^{4} \lambda_i \cdot Z(u_i) \, . \tag{3.1}$$

The estimate Z^* at the location u_0 is calculated as a linear combination of the measurements from four different stations. In each quadrant (north-east, east-south, south-west, west-north), based on u_0, one station is taken into account. The weights λ_i are calculated according to the inverse of the squared distance of the corresponding station from u_0:

$$\lambda_i = \frac{\dfrac{1}{d(u_0,u_i)^2}}{\sum_{i=1}^{4} \dfrac{1}{d(u_0,u_i)^2}} \, , \tag{3.2}$$

with $d(u_0,u_i)$ representing the distance between the locations u_0 and u_i.

3.2 Geostatistical interpolation methods

Kriging, as one of the most important geostatistical methods, originates from the work of the South African mining engineer Danie G. Krige, who analysed the spatial behaviour of gold deposit data (KRIGE, 1951). The corresponding mathematical theory was postulated some years later by MATHERON (1962).

The main assumptions and basic theory of geostatistics are presented at first. Next, the variogram estimation is explained. All geostatistical interpolation techniques that were applied for this study are discussed subsequently.

3.2.1 General assumptions and basic theory

This subsection gives a brief summary of the basic idea and main assumptions used in spatial statistics. For further reading and more details about the mathematical and statistical background, the reader is referred to geostatistical textbooks at this point, for instance GOOVAERTS (1997) and ISAAKS and SRIVASTAVA (1990).

Geostatistics regard spatial data as the result of a hypothetical random process. The random variable theory is the base of geostatistics, it assumes that all measurements are realisations of a random variable characterised by a specific distribution function. A random function is a set of random variables that correspond to all points of the study area, i.e. a random variable exist for each point u within the study area. A regionalised variable is accordingly one specific realisation of the random function.

Theoretically it is possible to describe a random function by an entire set of distribution functions that are individually assigned to each point of the study area and use this to derive local or global averages. However, this is not possible in practice, since only some measurement, i.e. realisations of the random variable at certain locations, are available for the estimation of the distribution function needed for each point within the study area. To overcome this lack of realisations, the random function is estimated jointly from all data points. This requires some statistical hypotheses.

The first hypothesis is the assumption of second order or weak stationarity. The first condition of this hypothesis is, that the expected value of the random function is constant within the study area. Secondly, it presumes that the covariance of two random variables depends only on the distance between these two points and not on the specific point locations. The hypothesis of second order stationarity is often replaced by the intrinsic hypothesis, since it is less restrictive. It also assumes a constant expected value of the random function within the entire domain:

$$E[Z(u+h) - Z(u)] = 0 \ . \tag{3.3}$$

Additionally, it expects that the variance of the increment referring to the two different locations within the random function $Z(u)$ and $Z(u+h)$ depends only on the distance vector h separating them:

$$Var[Z(u+h) - Z(u)] = E[(Z(u+h) - Z(u))^2] = 2\gamma(h) \ . \tag{3.4}$$

The function $\gamma(h)$ is the so called variogram and is discussed in the following section. It only depends on the vector h and not on the locations u and $u + h$.

3.2.2 Variogram estimation

All geostatistical interpolation techniques need information about the spatial persistence of the variable prior to performing any estimations for unknown locations. The investigation is carried out by calculating the empirical variogram and fitting a theoretical model to it. In order to achieve this, the difference in point pair data values is investigated depending on their spatial distance. The empiric semivariogram is estimated in this study as follows:

$$\gamma(h) = \frac{1}{2 \cdot N(h)} \cdot \sum_{i=1}^{N(h)} \left[z(u_i) - z(u_j) \right]^2 \, , \tag{3.5}$$

with $\gamma(h)$ being the variogram value of the regarded distance class h, $N(h)$ representing the number of available point pairs that belonging to h as well as $z(u_i)$ and $z(u_j)$ being measured values of the variable at locations u_i and u_j.

This measure of spatial dependency is widely applied in geostatistics. Due to reasons of simplification, the semivariogram is referred as variogram in many publications and also in the following. In general, there are many other measures to analyse the spatial persistence of point information. Since these measures are less common and not used for the investigations of this study, the reader is referred to geostatistical textbooks like AKIN and SIEMES (1988), ISAAKS and SRIVASTAVA (1990) or GOOVAERTS (1997) here.

Theoretically, a variogram model needs to be fitted for each individual time step if time series are interpolated. Previous research of VERWORN and HABERLANDT (2011) as well as EHRET (2003) showed, that the variogram model has only a small impact on the estimation performance of ordinary kriging (OK) and kriging with external drift (KED), although the distribution of rainfall can be highly dynamic in space and time. VERWORN and HABERLANDT (2011) found also that the use of event specific average variograms delivers an interpolation performance that is similar to those of using an individual variogram for each time step. Due to this, average variograms were used here as well. A standardisation with the spatial variance was carried out for each time step prior to averaging:

$$\gamma_{avg}(h) = \frac{1}{n} \cdot \sum_{t=1}^{n} \frac{\gamma_i(h)}{Var(z_t)} \ . \tag{3.6}$$

In this equation, n is the number of time steps, $\gamma_i(h)$ is the variogram value for distance class h of time step i and $Var_i(x)$ is the variance of observations z_t for time step t.

The exponential variogram model was used for all analyses of rainfall:

$$\gamma_h = c_0 + c \left[1 - exp \left(-\frac{h}{a} \right) \right] \ , \tag{3.7}$$

where a is the range, c the sill and c_0 the nugget effect.

For fine temporal resolution rainfall, two different models were fitted to the experimental variograms. They were averaged separately over all summer and all winter time steps. This separation into summer and winter variogram is considered due to seasonal changes in rainfall type and is in particular relevant for high temporal resolutions. In contrast to that, the interpolation performance for longer rainfall accumulation times and the interpolation performances of all other meteorological observations were analysed using only one isotropic variogram model that was averaged over the entire time. The main advantage of this procedure is that the visual fitting of the theoretical variogram model has to be done only once or twice for each temporal resolution and not for each single time step. All time steps with an average rain gauge rainfall exceeding a certain threshold were taken into account for the calculation of the season-specific experimental variogram. The variogram estimation sections in Ch. 6 contain further details.

Due to the high spatial variability of rainfall for short accumulation times, radar measurements were used for the inference of high temporal resolution rainfall variograms. GERMANN and JOSS (2001) also conducted variogram estimation using radar data and reported that high resolution radar images provide good information about the spatial continuity of precipitation. For longer rainfall accumulation times and all other climate variables, the variograms were estimated based on station measurements as it is the usual procedure in geostatistics.

Two different fitting techniques were applied in order to determine the parameters of the exponential model. The variograms for fine temporal resolution rainfall were fitted visually. On the contrary, an automatic fitting procedure was applied for rainfall of longer accumulation times and all other variables. The R package NLME (PINHEIRO *et al.*, 2016) was utilised for this purpose.

3.2.3 Ordinary Kriging

Ordinary kriging (OK) is the most common and most frequently applied interpolation technique in geostatistics. This approach is classified as an univariate interpolation method, i.e. it only allows the consideration of one data source and no additional information can be taken into account. Here, the station measurements of the regarded climate variable and the regarded time step are the only information used for the spatial interpolation.

The basic idea of OK is similar to the one that simple interpolation methods are based on: An unobserved location is estimated from observations at adjacent points. In contrast to the simple methods, the variogram is used to determine the weights of adjacent measurements taken into account for the interpolation. The estimate Z^* for a certain unknown location u_0 is calculated as a linear combination of n neighbouring measurements Z available for the locations u_i:

$$Z^*(u_0) = \sum_{i=1}^{n} \lambda_i \cdot Z(u_i) \, . \tag{3.8}$$

The weights λ_i are calculated in such way, that the estimate Z_0^* is unbiased

$$E[Z_0^* - Z_0] = 0 \, , \tag{3.9}$$

and that the mean square error is minimal

$$E[Z_0^* - Z_0]^2 = Min \, . \tag{3.10}$$

Due to the unbiasedness constraint (Eq. 3.9), OK is referred as the best linear unbiased estimator (BLUE).

Equation 3.11 results from the assumption of stationarity, i.e. the absence of a spatial trend.

$$E\left[\sum_{i=1}^{n} \lambda_i Z(u_i) - Z_0\right] = \sum_{i=1}^{n} \lambda_i m - m = m\left(\sum_{i=1}^{n} \lambda_i - 1\right) = 0 \tag{3.11}$$

Here, m is the expected value that is constant within the estimation domain. As a consequence of this, the sum of all weights must be one.

The expected vale of the squared error can be expressed with the variogram:

$$E[Z_0^* - Z_0]^2 = Var(Z_0^* - Z_0) = 2 \cdot \sum_{i=1}^{n} \lambda_i \gamma(u_i - u_0) - \sum_{i=1}^{n} \sum_{j=1}^{n} \lambda_i \lambda_j \gamma(u_i - u_j) . \qquad (3.12)$$

In order to minimise the error variance under consideration of the constraints (Eq. 3.9 and Eq. 3.10), a Lagrange multiplier is introduced:

$$\phi = Var(Z_0^* - Z_0) - 2\mu \left(\sum_{i=1}^{n} \lambda_i - 1 \right) . \qquad (3.13)$$

The function $\phi = \phi(\lambda_1, ..., \lambda_n, \mu)$ (Eq. 3.13) is then minimised instead of Eq. 3.12.

The kriging system of $n + 1$ equations can be derived from setting the partial derivatives $\frac{\partial \phi}{\partial \lambda_i}, i = 1, ..., n$ and $\frac{\partial \phi}{\partial \mu}$ to zero:

$$\sum_{j=1}^{n} \lambda_j \gamma(u_i - u_j) + \mu = \gamma(u_i - u_0) \text{ for } i = 1, ..., n \qquad (3.14)$$

$$\sum_{j=1}^{n} \lambda_j = 1 .$$

In matrix form, the kriging system is constituted as follows:

$$\begin{bmatrix} \gamma(u_1 - u_1) & \gamma(u_1 - u_2) & \dots & \gamma(u_1 - u_n) & 1 \\ \gamma(u_2 - u_1) & \gamma(u_2 - u_2) & \dots & \gamma(u_2 - u_n) & 1 \\ \vdots & \vdots & \vdots & \vdots & \vdots \\ \gamma(u_n - u_1) & \gamma(u_n - u_2) & \dots & \gamma(u_n - u_n) & 1 \\ 1 & 1 & \dots & 1 & 0 \end{bmatrix} \cdot \begin{bmatrix} \lambda_1 \\ \lambda_2 \\ \vdots \\ \lambda_n \\ \mu \end{bmatrix} = \begin{bmatrix} \gamma(x_1 - x_0) \\ \gamma(x_2 - x_0) \\ \vdots \\ \gamma(x_n - x_0) \\ 1 \end{bmatrix} . \qquad (3.15)$$

In the case of single point estimations (point kriging), the matrix diagonal is populated by zeros ($\gamma(u_i - u_i) = \gamma(0) = 0$).

By repeatedly solving the kriging system, the weights λ_i can be determined for each point of the interpolation grid. As a final step, the estimates are computed according to Eq. 3.8. The geostatistical software library (GSLIB) provided by DEUTSCH and JOURNEL (1992) was used to carry out all geostatistical computations of this study.

3.2.4 Kriging with External Drift

Kriging with external drift (KED) allows the incorporation of one or more additional variables that are used as background information for the interpolation of the primary variable. Different additional variables were considered in this method for interpolating the meteorological observations (see Ch. 6). The KED method was applied in a same way as in HABERLANDT (2007) and VERWORN and HABERLANDT (2011).

The first part of the intrinsic hypothesis (Eq. 3.3) is not required for KED. Instead it is assumed that the expected value of the random function at location u is linearly related with m additional variables $Y_k(u), k = 1, ..., m$:

$$E[Z(u)|Y_1(u), Y_2(u), ..., Y_m(u)] = b_0 + \sum_{k=1}^{m} b_k Y_k(u) , \tag{3.16}$$

where $b_0 = b_1, ..., b_m$ are unknown constants. The second assumption of the intrinsic hypothesis (Eq. 3.4), that the variance of the increment $Z(u+h) - Z(u)$ of two points depends only on the distance vector h and not on the two locations u and $u+h$, is still valid.

The KED equations are given as follows:

$$\sum_{j=1}^{n} \lambda_j \gamma(u_i - u_j) + \mu_0 + \sum_{k=1}^{m} \mu_k Y_k(u_i) = \gamma(u_i - u_0) \text{ for } i = 1, ..., n \tag{3.17}$$

$$\sum_{j=1}^{n} \lambda_j = 1$$

$$\sum_{j=1}^{n} \lambda_j Y(u_j) = Y(u) ,$$

where n is the number of neighbors, m is the number of additional variables Y_k and μ_k are the m+1 Lagrange multipliers. The m additional variables $Y_k(u)$ must be available for all locations $u_i, 1 = 1, ..., n$ in order to carry out the interpolation. The KED system consists of $m+n+1$ equations and needs to be solved for each point of interpolation grid in order to determine the corresponding weights λ_i and λ_j. The same estimator as for OK (Eq. 3.8) is then used to compute the KED estimate of each unknown point (u_0).

Theoretically, the variogram for KED needs to be estimated from the residuals $Z(u) - m(u)$. This is usually not a simple procedure since neither the residuals nor the trend $m(u)$ is known a priori. As it was also done by HABERLANDT (2007), the experimental variograms for KED were inferred by a simplified approach, i.e. only by using the observations $Z(u)$. DELRIEU *et al.* (2014) compared three different variograms for the merging of rain gauge and radar data using KED. The use of rainfall variograms, as they are required for OK as well, resulted in a similar interpolation performance like the use of residual variograms that were obtained by applying the method of VELASCO-FORERO *et al.* (2009). Only a pure nugget effect variogram resulted in a significant worsening of interpolation performance.

The KED procedure is applied for each time step independently when time series are interpolated. The coefficients $b_0 = b_1, ..., b_m$ of Eq. 3.16 will thus vary in space and time, which allows the consideration of a space-time variable relationship between the primary variable and any additional information.

The GSLIB (DEUTSCH and JOURNEL, 1992) was also used for the KED interpolations of this work. A considerable problem when applying kriging with an external drift for merging of rain gauge and radar data with a high temporal resolution is the frequent occurrence of numerical instabilities in the kriging system (Eq. 3.17). According to DEUTSCH and JOURNEL (1992, p. 67-68) this might happen when the drift variable does not vary smoothly in space, e.g. if many stations have zero precipitation. The number of time steps having these instabilities could be reduced by increasing the number of data points used for the kriging process. In general, 16 neighboring stations were considered in KED for estimating each point value. If the KED system was ill-conditioned or singular, a next attempt was applied that took into account all available stations. In case this was still not successful, the affected time step was interpolated using OK.

3.2.5 Indicator Kriging

Indicator kriging (IK) is commonly used for the spatial interpolation of categorical data, for instance land use or soil types as proposed by BIERKENS and BURROUGH (1993), however the interpolation of continuous variables like rainfall is also possible. Categorical as well as continuous data need to be transformed to binary indicator variables prior to the geostatistical analysis.

In case of categorial data, the observed variable can attain one of n_C different categories. Each category C is transformed to a binary indicator variable I_C:

$$I_C(u) = \begin{cases} 1 \text{ if } u \in C \\ 0 \text{ else} \end{cases} \quad for \ C = 1,...,n_C \ . \tag{3.18}$$

Interpolating continuous data by IK requires the conversion of numerical values to classes. These are defined using a certain number n_α of exceedence thresholds α that must be selected beforehand. The indicator variable I_α of an exceedence threshold is defined by:

$$I_\alpha(u) = \begin{cases} 1 \text{ if } Z(u) \le \alpha \\ 0 \text{ if } Z(u) > \alpha \end{cases} \quad for \ \alpha = 1,...,n_\alpha \ . \tag{3.19}$$

The indicator variable I can be interpreted as the probability of u belonging to a certain category or $Z(u)$ being less than α, respectively:

$$I_C(u) = P[u \in C] \ or \ I_\alpha(u) = P[u \le \alpha] \ . \tag{3.20}$$

In the next step each indicator variable needs to be interpolated using kriging, for instance OK or KED, in order to obtain $P[u \in C]$ or $P[u \le \alpha]$ for all unknown locations:

$$I_C^*(u_0) = \sum_{i=1}^{n} \lambda_i I_C(u_i) \ . \tag{3.21}$$

In case of categorical data, the indicator variable with the highest probability $P[u \in C]$ is taken as the estimate for point u. In case of continuous data, the interpolations for all indicator variables are performed in order to obtain an estimate of the cumulative probability density function (cdf) of $Z(u)$. Thereafter, the estimate of the primary variable $Z(u)$ is calculated by using the so called E-type estimate, which approximates the mean of the cdf (DEUTSCH and JOURNEL, 1992):

$$Z^*(u) = I_{\alpha 0}^*(u)\alpha_0 + \sum_{k=0}^{n_\alpha} (I_{\alpha_{k+1}}^*(u) - I_{\alpha_k}^*(u))\bar{Z}_k \ , \tag{3.22}$$

where $\alpha_k, k = 1,...,n_\alpha$ are the specified thresholds and $a_0 = z_{min}$ as well as $a_K + 1 = z_{max}$ are the minimum and the maximum values of the Z-Range, respectively. $\bar{Z}_k$ denotes the mean value of class k.

The experimental indicator variograms required for the interpolation of all indicator variables were estimated according to:

$$\gamma^*(h) = \frac{1}{2 \cdot N(h)} \sum_{i=1}^{N(h)} \left[I_\alpha(u_i) - I_\alpha(u_j) \right]^2 \, . \tag{3.23}$$

The estimation of experimental indicator variograms is similar to the estimation of standard variograms. Nevertheless, indicator variograms have to be estimated separately for all indicator variables. In case of time series interpolation with indicator kriging, the absolute thresholds α are calculated individually for each time step based on the non-exceedence probabilities of certain predefined quantiles. As the consequence, a set of average indicator variograms for a wide range of predefined absolute thresholds has to be calculated prior to the actual application of IK.

The term IK usually implies that OK is used for the interpolation. In case KED is used, the method is referred as IKED. Here, IK is applied for the interpolation of wind direction categories and IKED for the merging of radar and rain gauge data. An important feature of IKED is the possibility to consider a quasi non-linear relationship between the expected value of the primary variable $E[Z(u)]$ and the additional information $Y(u)$ by the stepwise implicit application of KED for different indicators I_α. Another reason for applying IKED is the linkage of the estimated value to the predefined quantiles. Due to this, severe over- or underestimation, which might be caused by poor radar data quality, is limited. Numerical instabilities can also occur in IKED. Concerned time steps were treated in the same way as in KED. For further information on the application and the theory of IKED, the reader is referred to DEUTSCH and JOURNEL (1992).

For the IKED interpolation of precipitation, relative thresholds from 13 quantiles with non-exceedence probabilities of $p = 0.01, 0.05, 0.1, 0.2, 0.3, 0.4, 0.5, 0.6, 0.7, 0.8, 0.9, 0.95$ and 0.99 are used to calculate absolute thresholds a_k for each time step individually. Thirteen different indicator variables are then interpolated for each time step, based on this. For the interpolation of each variable, the closest indicator variogram is chosen automatically from the five previously inferred ones (see Ch. 6). This means that the indicator variogram is selected, for which the lowest difference between interpolation threshold a_k and inference threshold exists (see also HABERLANDT, 2007).

3.2.6 Conditional Merging

Another method to combine rain gauge and radar data is the conditional merging (CM) approach described by EHRET (2003) and utilised for simulated rainfall fields by SINCLAIR and PEGRAM (2005). Figure 3.1 shows a scheme of the CM procedure. The first step of the conditional merging is to apply OK to the gauge observations (a) in order to obtain the best linear unbiased estimate of rainfall for all grid points (c). Next, radar rainfall values of gauge locations (a) are extracted from the gridded radar data (b) and interpolated by OK as well (d). This is followed by calculating the deviation between interpolated and observed radar rainfall values for each grid point, whereby it gives the value 0 at rain gauge locations (e). Finally, the deviation grid is added to the rain gauge interpolation field from the first step (f). The result is a rainfall field that follows the mean field of the rain-gauge interpolation while simultaneously preserving the rainfall pattern of the gridded radar information (g). A straightforward approach was used for variogram estimation. As mentioned before, variograms for high temporal resolution rainfall interpolation were computed as average variograms for summer time steps and for winter time steps separately, i.e. the same variograms as estimated from radar data for KED and OK before were used here for all interpolations (see Sec. 2.1). In comparison to the other rain gauge radar data merging methods, CM is computationally efficient and robust. Since it only uses OK it is not affected by numerical instabilities.
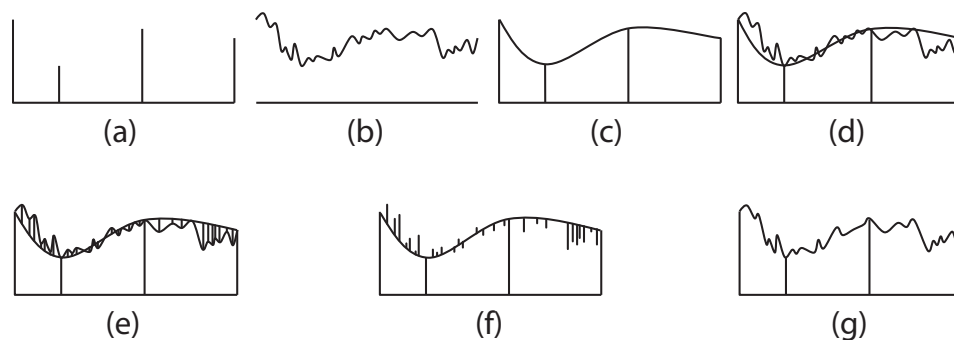

Figure 3.1: Scheme of the conditional merging procedure: (a) Rain gauge observation at discrete points. (b) Radar observation on a regular grid. (c) Interpolation of rain gauge observations by OK. (d) Interpolation of corresponding radar pixel information by OK. (e) Computation of deviation between observed radar grid interpolated radar grid. (f) Addition of deviation grid to the grid of rain gauge interpolation. (g) Resulting rainfall field (SINCLAIR and PEGRAM, 2005).

3.3 Performance evaluation of interpolation techniques

The interpolation performance was assessed by applying "leave-one-out" cross validation. This method is based on a simple principle: A successive estimation of all sampled locations is done by using all other stations while always excluding the sample value at the regarded location. A slightly modified cross validation approach was used for all analyses regarding the observation network density scenarios (see Sec. 4). In order to obtain comparable performance criteria for different station densities, only the stations belonging to the scenario with the lowest station density are considered in calculating the cross validation performance criteria. This approach requires that the set of stations considered in the scenario with the lowest station density is present in all other scenarios as well.

The following performance measures were used to compare estimation Z^* and observation Z for the n locations:

The simple bias criterion

$$Bias = \frac{1}{n} \sum_{i=1}^{n} [Z^*(u_i) - Z(u_i)] \ , \tag{3.24}$$

the root mean squared error normalised with the average of the observations

$$RMSE = \frac{1}{\bar{Z}} \sqrt{\frac{1}{n} \sum_{i=1}^{n} [Z^*(u_i) - Z(u_i)]^2} \tag{3.25}$$

and the RVar coefficient, which indicates the preservation of variance of observed information

$$RVar = \frac{Var[Z^*(u_i)]}{Var[Z(u_i)]} \ . \tag{3.26}$$

In order to avoid the unwanted smoothing effect of rainfall interpolation, an RVar value close to 1 is preferable.

In addition to that, the scaling behaviour of interpolated climate variables is evaluated in Sec. 7.3 using the PBIAS criterion, in which the absolute value of BIAS is standardised with the mean of the observations $\bar{Z}$:

$$PBIAS = \frac{1}{\bar{Z}} \left| \frac{1}{n} \sum_{i=1}^{n} [Z^*(u_i) - Z(u_i)] \right| . \tag{3.27}$$

Moreover, the spatial variability of the meteorological observations was evaluated by calculating the coefficient of variation:

$$CV = \frac{S(Z)}{\bar{Z}} , \tag{3.28}$$

where the sample standard deviation is divided by the mean of the observations. This is not an actual performance criterion but helps to compare the spatial variability among all climate variables (see Sec. 7.2).

3.4 Interpolation of wind data

Wind velocity and direction are provided by the DWD as hourly measurements. These two variables are directly related to each other and therefore a combined approach is used and compared with a standard geostatistical interpolation.

The standard approach implies an individual interpolation of direction and velocity using one ore more of the aforementioned techniques. NN, InvD and OK can be applied for the interpolation of wind velocity. In case of wind direction, only interpolation methods that are suitable for categorical data can be applied. NN can be easily used for this, while InvD and OK do not work here. IK is a variation of OK and was developed in particular for this purpose.

The combined approach that was developed here consists of a transformation of wind direction and absolute wind velocity into a north-south and an east-west component of wind velocity. Any technique that works for continuous data can be applied in the next step for the spatial interpolation of these components. In the last step, the interpolated north-south and west-east velocities are transformed back into absolute wind velocity and direction category.

The transformation of the initial data into velocity components is carried out by the following trigonometrical relations:

$$v_{WE} = v_{abs} sin(\varphi_W) \tag{3.29}$$

$$v_{NS} = v_{abs} cos(\varphi_W) \, .$$

The velocity components of west-east and north-south direction are represented by v_{WE} and v_{NS}, respectively. φ_W is computed from the present wind category. It is defined as the angle between the north direction and the bisectrix of the sector that corresponds with the present category of wind direction.

The back-transformation of velocity components in absolute wind velocity and φ_W is carried out using:

$$v_{abs} = \sqrt{v_{WE}^2 + v_{NS}^2} \tag{3.30}$$

and

$$\varphi_W = \begin{cases} \frac{360}{2\pi} \arctan\left(\frac{v_{WE}}{v_{NS}}\right) & \text{for } v_{WE} \geq 0, \, v_{NS} > 0 \\ \frac{360}{2\pi} \left(\arctan\left(\frac{v_{WE}}{v_{NS}}\right) + 2\pi\right) & \text{for } v_{WE} < 0, \, v_{NS} > 0 \\ \frac{360}{2\pi} \left(\arctan\left(\frac{v_{WE}}{v_{NS}}\right) + \pi\right) & \text{for } v_{NS} < 0 \\ \frac{360}{2\pi} \frac{\pi}{2} & \text{for } v_{WE} > 0, \, v_{NS} = 0 \\ \frac{360}{2\pi} \frac{3\pi}{2} & \text{for } v_{WE} < 0, \, v_{NS} = 0 \end{cases} \, . \tag{3.31}$$

The wind direction category is then directly derived from φ_W.

Chapter 4

Study area and observation networks

This chapter outlines the study area (Sec. 4.1), time period and meteorological data used for the investigation. In particular, the measuring networks for different meteorological variables and their corresponding data availability are presented in Sec. 4.2.

4.1 Study area

The study region is located within the 128 km range of the radar station Hanover in Lower Saxony, North Germany. Figure 4.1 shows the location of the study area. It is identical to the measuring range of the radar device located in Hanover and covers a large area of the German federal state Lower Saxony and the entire city state Bremen. Moreover, small areas of the neighbouring federal states are included.

The northern part of the study area is to be characterised as entirely flat, since it is part of the North German Plain. The Harz Mountains are located in the southeast of the study area and have a maximum elevation of 1141 m.a.s.l. according to the digital elevation model of the German Federal Agency for Cartography and Geodesy (BKG) used in this study. In the south and southwest there are some minor hill ranges, which partly belong to the Weser Uplands. Their elevation does not exceed 500 m a.s.l..

Due to the proximity of the North Sea, a maritime climate is predominant in the northwestern part of the study region. Towards the southeast, the climate is less strong affected by the sea and rather continental. According to the updated Köppen-Geiger climate classification map (PEEL *et al.*, 2007), the study area can be subdivided into two different climate regions: The climate in the north west is temperate, without dry seasons and is characterised by warm summers. The
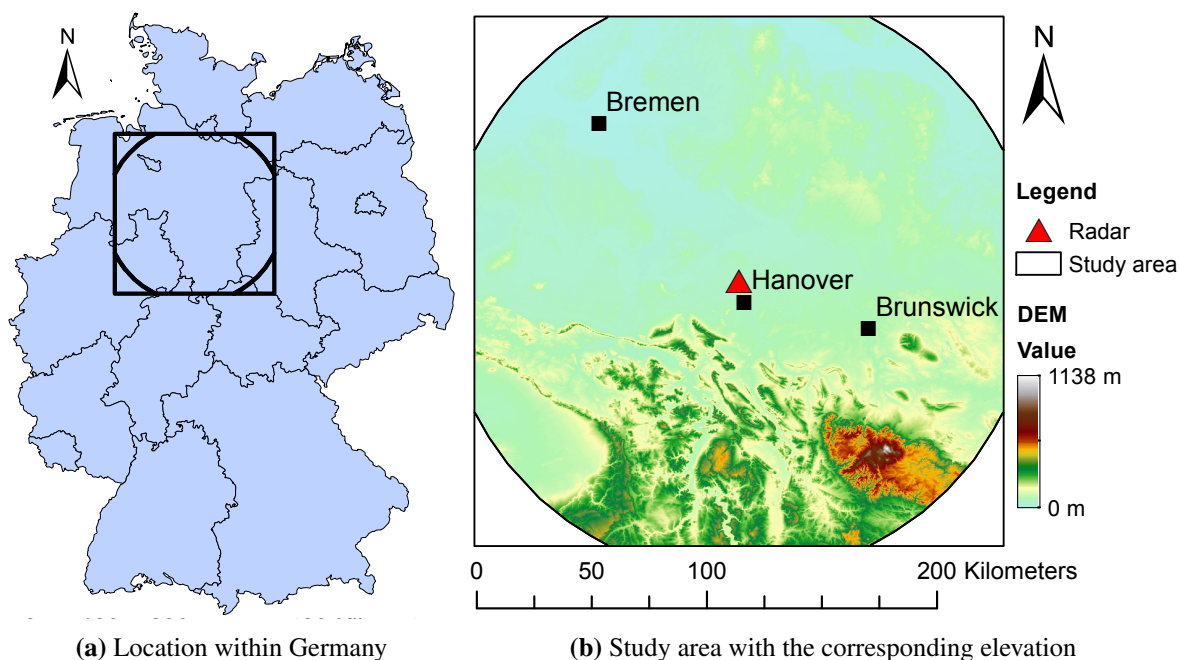
(a) Location within Germany

(b) Study area with the corresponding elevation

Figure 4.1: Study area and its location within Germany

climate in the southeast is colder, does not have any dry season either and warm summers as well.

The air masses which are transported by the prevailing Atlantic westerly winds are in particular in winter and autumn responsible for long-lasting stratiform rainfall events, while summer rainfall is characterised by short and small-scale convective events on the contrary. The average annual precipitation sum varies between 500 mm/yr and 1700 mm/yr, while the highest rainfall amounts occur in the Harz Mountains. Table 4.1 contains minimum and maximum of long-term averages for all meteorological variables considered in this study. The ranges of the variables were determined from the daily station data provided by the German Weather Service (DWD).

Table 4.1: Maximum and minimum value within the study area for long-term averages of all meteorological variables

Variable	Minimum	Maximum
Annual rainfall [mm]	500	1700
Temperature [°C]	3.5	10.0
Relative humidity [%]	73.0	90.0
Daily sunshine duration [h]	3.8	4.8
Wind speed [m/s]	1.5	4.5
Cloud coverage [1/8]	4.0	6.1

4.2 Observation networks and data availability

Weather stations are important devices for the observation of meteorological variables. In Germany, a lot of meteorological observations are carried out by the the German Weather Service (DWD). Different nation-wide measuring networks are operated, i.e. point related weather information is recorded at various locations. This sections gives an overview of the meteorological variables and their corresponding measuring networks for the regarded study area. In addition to the ground based fix weather station data, the DWD also collects weather data using measuring equipment placed on moving ocean vessels, by radiosondes in combination with weather balloons and also using further observation techniques like weather radar, for instance. The website of the German Weather Service (DWD, 2016) contains more information about the recording of climate and weather related information. The observation networks presented here are only related to stationary point measurements, which are recorded close to the ground.

Figure 4.2 and Fig. 4.3 show the number of available station measurements in the time period from 1990 until 2013 for each climate variable analysed in this work. The graphs were created using hourly and daily station data provided by the DWD. Daily and hourly recordings are in general publicly available through Climate Data Center web service (CDC) of the DWD. A station is considered as available for the regarded time step, if the record at the corresponding position in the time series exists and is not marked as missing. The number of data points varies strongly over time and for some variables the number of recording stations is higher than the number of stations that provide daily values. Daily precipitation measurements decreases from more than 500 in the year 1990 to around 200 in the year 2013. The sudden decline visible in the topleft panel occurred in 2007. First hourly rainfall recordings are available in the year 1995. In the period from 2004 until 2008 there was strong increase from 15 to around 100 available rain gauge recordings for the study area.

The number of daily temperature recordings is with approx. 50 stations relatively constant over the regarded time period. However, the number of available hourly recordings is with around 15 stations much lower in the beginning. In the time period from 2002 to 2008, there is a strong increase so that the data of approx. 50 temperature stations are available for the following years too. Minimum and maximum temperature are not displayed separately. These information are only available on the daily time scale and their temporal data availability corresponds to mean daily temperature. The availability of relative humidity recordings behaves generally in a same way. Only minor differences occur for some time steps for daily and hourly data.

(a) Precipitation (Day, Hour)

(b) Temperature (Day, Hour)

(c) Relative humidity (Day, Hour)

(d) Wind velocity (Day, Hour) and direction (Hour)

(e) Sunshine duration (Day, Hour)
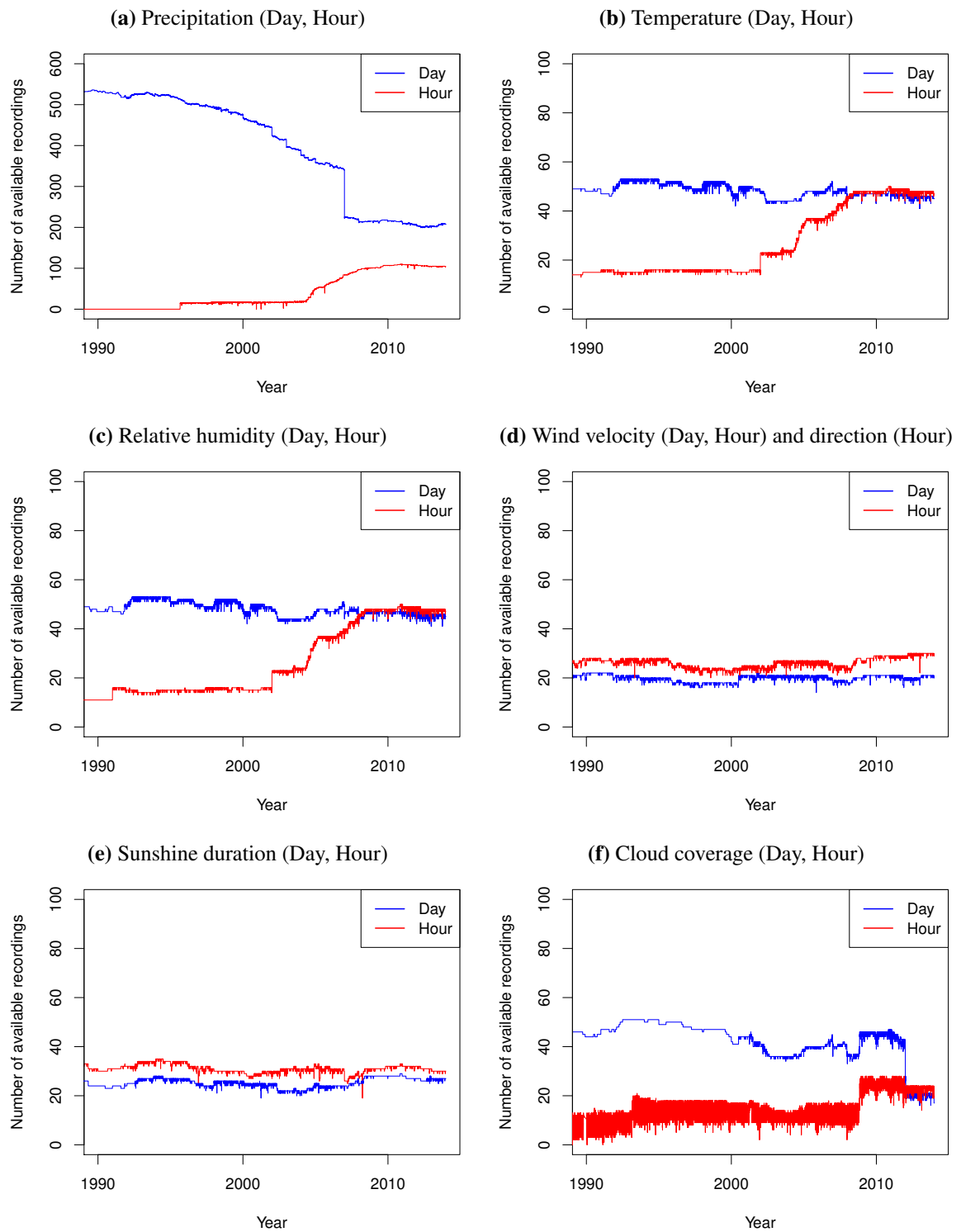
(f) Cloud coverage (Day, Hour)

Figure 4.2: Availability of meteorological measurements for the study area

The number of wind velocity recordings is relatively constant over the regarded time period. Only minor variations occur due to missing values in the available time series. The number of hourly wind direction measurements is identical to the number of hourly wind velocity measurements. The number of daily records (approx. 20 stations) is lower than the number hourly records (approx. 25 stations). This appears to be implausible but supposedly the data preparation by the DWD has not been finished entirely, i.e. some of the hourly stations were not converted to daily time series. The time series were self aggregated by averaging the hourly records from 0:00 UTC to 23:00 UTC. This interval corresponds to the time periods for which daily wind data are provided by the DWD.

The number of available sunshine duration recordings behaves similarly over time as the number of available wind velocity recordings. Here, the number of daily recordings (approx. 20 to 25 stations) is also lower than the number of hourly recordings (approx. 25 to 30 stations). The hourly data was used here as well to derive daily sunshine duration averages.

Generally, there are more daily than hourly cloud coverage measurements. The number of daily cloud coverage observations varies from 35 to 50 in the time period from 1990 until 2012. In 2012 there is a significant drop and only approx. 20 stations are available for the following time steps. The number of hourly recording varies from 10 to 15. In 2008 there is a jump to around 20 to 25 observations. Compared to the other meteorological variables, there are strong short-term variations in the availability of hourly cloud coverage data. The reason for this is, that only some stations are able to observe the cloud coverage during the night. The additional daily cloud coverage observations originate from three manual observations carried out at the standard times 6:00, 12:00 and 18:00 UTC for synoptical observations. The daily cloud coverage value is calculated as the arithmetic mean by the DWD.
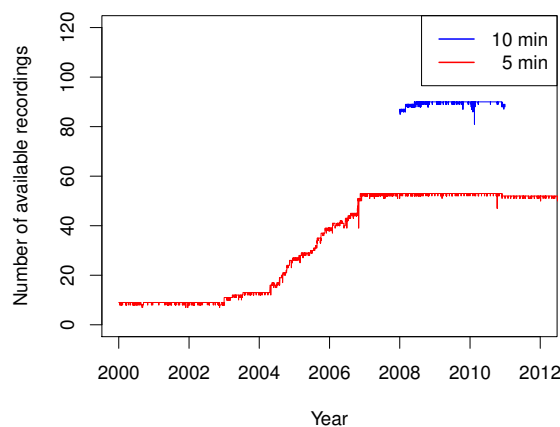

Figure 4.3: Availability of 5 min and 10 min rainfall measurements for the study area

The time period from 2008 to 2013 was used for the cross validation investigations carried out for this work. This time span provided a relative constant number of observations for all meteorological variables except for the cloud coverage recordings. The analysis of cloud coverage interpolation performance was conducted using a shorter investigation time period, i.e. the years 2009, 2010 and 2011.

It is assumed that the DWD can also provide fine temporal resolution rainfall data for all hourly stations. However, the data is not freely available. Due to reasons of data acquisition for different research projects, the time period from 2008 until 2010 was used for the cross validation analysis of fine temporal resolution rainfall. Rainfall accumulations with a temporal resolution of 10 min and 5 min were available for different sets of stations. Figure 4.3 shows the temporal behaviour of the number of available rainfall recordings for the two rain gauge sets.
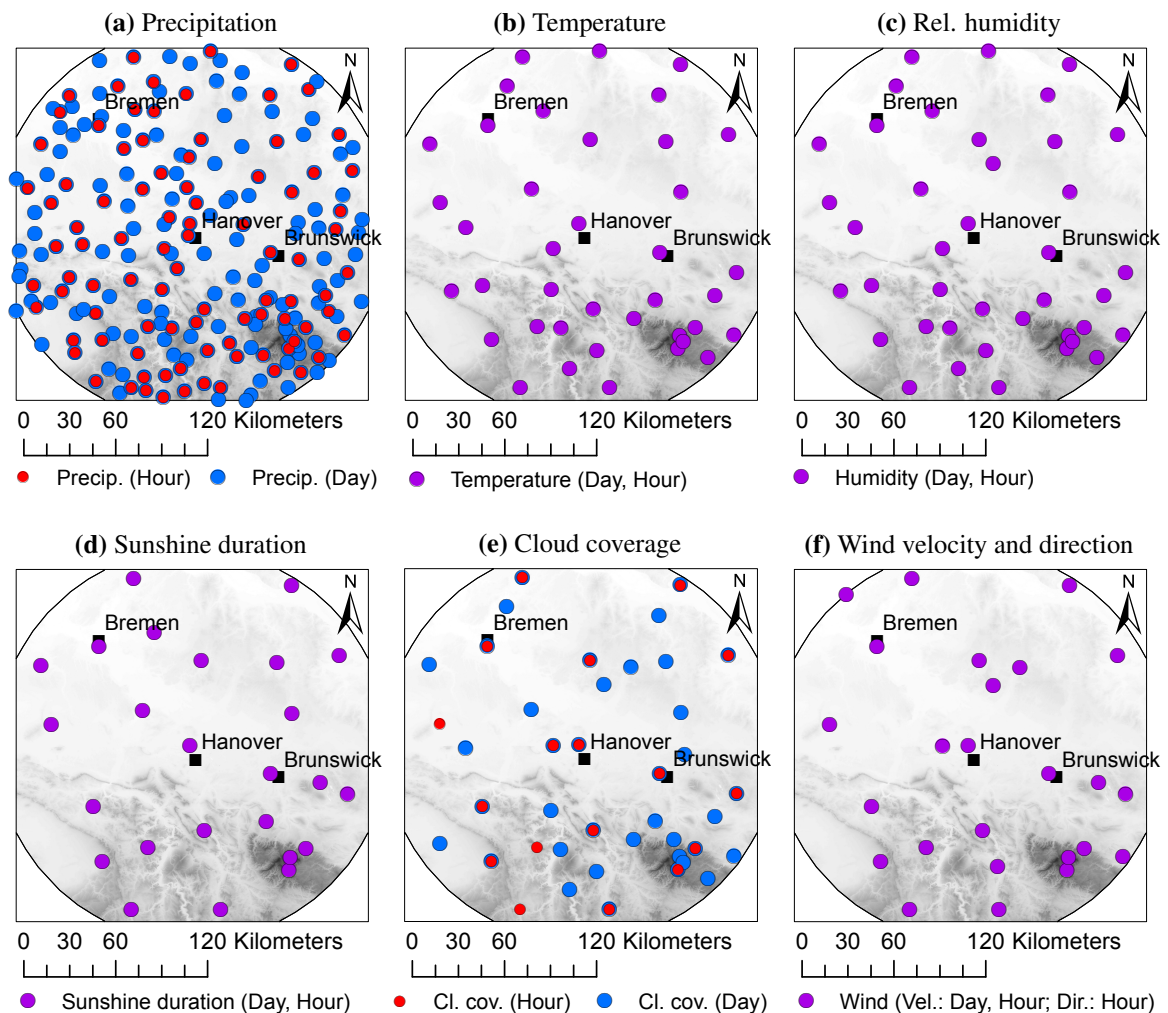
Figure 4.4: Hourly and daily measuring networks of precipitation, temperature, relative humidity, sunshine duration, cloud coverage and wind for the study area
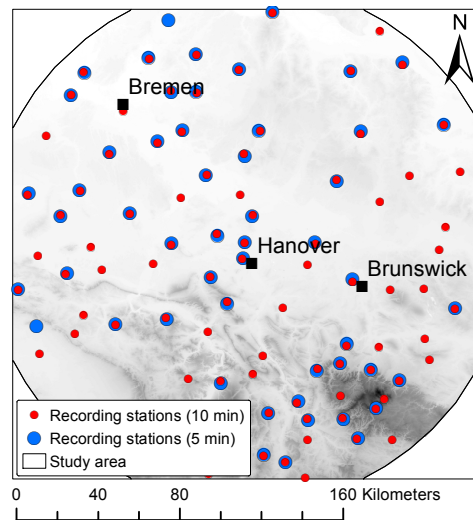
Figure 4.5: Measuring networks of 5 min and 10 min resolution precipitation for the study area

The 5 min rain gauge data is available for the time period from 2000 until 2012, while the the 10 min data is only present for the time period from January 2008 to December 2010. Around 90 time series with a temporal resolution of 10 min are constantly available for the investigation time period. Only some time steps exhibit a much lower number of rainfall observations. The number 5 min rain gauges is increases significantly within the shown time period. Only 8 rain gauges are available in 2000. From 2003 until 2007 there is a constant increase, resulting in 55 available rain gauges for the selected cross validation time period.

Figure 4.4 shows the measuring networks that are used by the DWD to capture the different meteorological variables. The measuring network for the available 5 min and 10 min rain gauge data is shown in 4.5, whereas only stations with time series that cover the entire investigation period are taken into account for 10 min data. Missing recordings for single time steps were considered as acceptable and a certain station was only removed when the general recording period did not cover the years from 2008 to 2010. The measurements of each climate variable are almost equally distributed in space. Only in the Harz Mountains there is a slightly higher local station density for almost all climate variables.

Table 4.2 contains the number of observations for all other meteorological variables and the corresponding investigation time period that was selected for the cross validation analysis. The station density scenarios shown in Sec. 5.2 are selected according to these numbers of available meteorological observations.

Table 4.2: Number of available stations and cross validation time period for all meteorological variables

Climate variable	Abbreviation	Temporal resolution	No. of available observations	Investigation time period
Precipitation	PCP	5 min	55	Jan 2008 - Dec 2010
Precipitation	PCP	10 min	90	Jan 2008 - Dec 2010
Precipitation	PCP	1 h	92	Jan 2008 - Dec 2013
Precipitation	PCP	1 d	202	Jan 2008 - Dec 2013
Mean temperature	TAV	1 h	39	Jan 2008 - Dec 2013
Mean temperature	TAV	1 d	38	Jan 2008 - Dec 2013
Max. temperature	TMA	1 d	38	Jan 2008 - Dec 2013
Min. temperature	TMI	1 d	38	Jan 2008 - Dec 2013
Rel. humidity	HUM	1 h	40	Jan 2008 - Dec 2013
Rel. humidity	HUM	1 d	38	Jan 2008 - Dec 2013
Wind velocity	WVE	1 h	25	Jan 2008 - Dec 2013
Wind direction	WDI	1 h	25	Jan 2008 - Dec 2013
Wind velocity	WVE	1 d	25	Jan 2008 - Dec 2013
Sunshine duration	SUN	1 h	25	Jan 2008 - Dec 2013
Sunshine duration	SUN	1 d	25	Jan 2008 - Dec 2013
Cloud coverage	CLD	1 h	18	Jan 2009 - Dec 2011
Cloud coverage	CLD	1 d	38	Jan 2009 - Dec 2011

Chapter 5

Design of cross validation experiments and data preprocessing

The first part of this chapter (Sec. 5.1 and Sec. 5.2) gives insight into the setup of cross validation experiments. A wide range of temporal resolutions and various station density scenarios were considered in order to investigate their impact on the interpolation performance. Preprocessing of station and radar data is explained in the second part (Sec. 5.3 and Sec. 5.4), while smoothing techniques for radar information and a method to detect time steps with poor radar data are also presented here. Section 5.5 contains a summary of all steps of the cross validation analysis.

5.1 Temporal resolutions

The performance evaluation of spatial interpolation techniques was carried out for various temporal resolutions. The time scales that are considered here are based on the temporal resolution of the observed data. However, coarser temporal resolutions were analysed as well in order to obtain a comparison of interpolation performance among different time scales. The aggregation of measured climate information from the recorded temporal resolution to larger time scales is described in Sec. 5.3.

The investigation of interpolation performance for precipitation with a high temporal resolution was carried out for temporal resolutions from 5 min to 360 min. The 90 rainfall time series with a temporal resolution of 10 min were aggregated to obtain rainfall accumulations for longer intervals. In total, the following temporal resolutions were analysed regarding the performance

of geostatistical interpolation techniques: 5 min, 10 min, 20 min, 30 min, 60 min, 120 min, 240 min und 360 min.

The meteorological observations for hourly and daily time spans described in Sec. 4.2 were treated in a similar way. Daily meteorological observations were converted to longer time scales and as a consequence, temporal resolutions of 1 hour, 1 day, 1 week, 1 month and 1 year were considered in the cross validation investigations. Maximum as well as minimum temperature are not available for the hourly temporal resolution and thus only time scales of 1 hour to 1 year were taken into account.

5.2 Network density scenarios

The network density scenarios were defined according to the number of available stations for the investigation time period (see Sec. 4.2). Table 5.1 shows the network density scenarios that were used for the interpolation performance assessment of each climate variable. In total, seven different network scenarios from 17 up to 200 stations were specified, whereas the presence of a certain scenario depends on the data availability of the corresponding climate variable. All scenarios are only present for rainfall with accumulation times of a day or longer. The cross validation using the same number of stations, i.e. 17 and 24, allows a comparison of interpolation performance among all climate variables at least for the low network density scenarios. The station density scenarios were generally selected in order to obtain interpolation performances for a wide range of observation network densities. Although the station density is assumed to have a major impact on the interpolation performance, only few studies, for instance KRAJEWSKI (1987), GOUDENHOOFDT and DELOBBE (2009) and YOON *et al.* (2012) use different network configurations.

The scenario using 24 stations was not used for the interpolation performance assessment of precipitation with a fine temporal resolution, since this analysis was carried out prior to the analyses of all other meteorological observations. It was published in BERNDT *et al.* (2014). The 24 stations scenario was introduced for the other variables in order to have at least two different station densities for WVE, WDI and SUN, while preserving the initial station density scenarios used for fine temporal resolution rainfall interpolation. Only one network density scenario was analysed for hourly CLD since only 18 measurements with a temporal resolution of 1 h are available for the investigated time period.

Table 5.1: Station density scenarios for interpolation performance evaluation of all climate variables. Scenarios available for the specific meteorological variable are assigned a tick mark.

Variable	Temp. res.	17 St.	24 St.	36 St.	56 St.	70 St.	90 St.	200 St.
PCP	5 min	✓	–	✓	✓	–	–	–
PCP	10 - 360 min	✓	–	✓	✓	✓	✓	–
PCP	1 h	✓	✓	✓	✓	✓	✓	–
PCP	1 d - 1 a	✓	✓	✓	✓	✓	✓	✓
TAV	1 h - 1 a	✓	✓	✓	–	–	–	–
TMA, TMI	1 d - 1 a	✓	✓	✓	–	–	–	–
HUM	1 h - 1 a	✓	✓	✓	–	–	–	–
WVE	1 h - 1 a	✓	✓	–	–	–	–	–
WDI	1 h	✓	✓	–	–	–	–	–
SUN	1 h - 1 a	✓	✓	–	–	–	–	–
CLD	1 h	✓	–	–	–	–	–	–
CLD	1 d - 1 a	✓	✓	✓	–	–	–	–
Stations per 10.000 km^2:		3.58	5.05	7.79	11.78	14.73	18.98	42.08

For each network density scenario, the stations were selected randomly from the total available number of time series for each climate variable. Due to the variability of available stations among the climate variables, the network density scenarios could not be defined in a way that exactly the same stations are used for each meteorological information. In order to achieve a better comparability of interpolation performance among different climate information, the cross validation analysis was based on ten realisations of each network density scenario, i.e. the performance evaluation was carried out for ten different random subsamples that were drawn from the entire set of stations. However, the cross validation analysis of rainfall with a fine temporal resolution was only carried out for a single realisation of each station density scenario. In particular for the application of IKED, the high number of time steps would have resulted in an immense computational effort. Figure 5.1 shows the rain gauges that were considered in each network density scenario. Stations taken into account are marked by solid dots, whereas omitted stations are marked as circles. The scenario consisting of 90 stations is not displayed separately in the figure. It uses the entire set of available rainfall stations.

For each realisation, the random selection of stations is designed in a way that the 17 stations of the lowest network density scenario are present in all other network scenarios as well. The computation of the cross validation performance criteria (Eqs. 3.24, 3.25 and 3.26) only takes into account the observed and estimated values at these 17 locations, although, depending on the network density scenario, more stations might have been used for calculating the estimate. This slightly modified cross validation procedure allows the comparison of
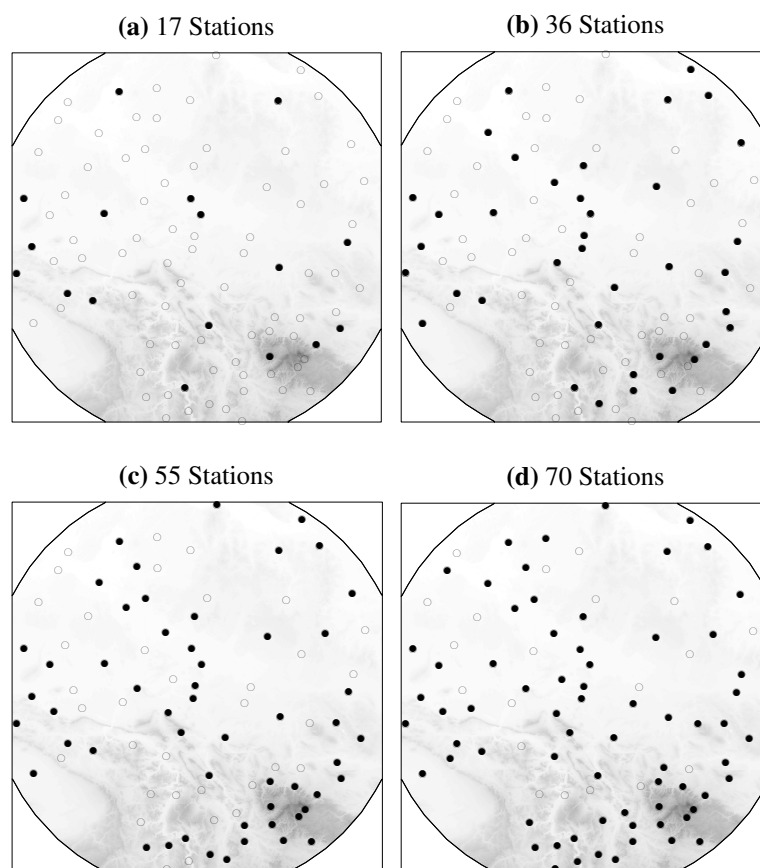
Figure 5.1: Network density scenarios for the interpolation of fine temporal resolution rainfall. Considered stations are marked as solid dots, whereas the full set of rain gauges is marked by circles. The 90 Stations scenario using the entire set is not shown in the figure.

interpolation performances for different density scenarios. Using a different number of stations for calculating the interpolation performance of each network density scenario, i.e. the entire number of stations in the scenario, leads to a variation in the validation sample and derogates the comparability among the density scenarios.

5.3 Preprocessing of station data

The 10 min temporal resolution rain gauge time series provided by the DWD were aggregated to 30 min, 60 min 120 min, 240 min and 360 min rainfall accumulations. These high temporal resolution rainfall sums were then used together with the 5 min data for a comparison with the corresponding radar information and the cross validation procedure. In general there are many different approaches of filling gaps in rainfall time series (COULIBALY and EVORA,

2007; DWARAKISH *et al.*, 2015). Most of the techniques are based on the estimation of rainfall values from spatio-temporal variation patterns. BÁRDOSSY and PEGRAM (2014) compare different infilling techniques and propose a new copula-based method for this task. However, infilling of missing rainfall records was not done here. The geostatistical techniques as well as the simple interpolation methods consider an inconstant number of stations and are able to do the infilling implicitly, considering only a spatial dependency from available neighbouring recordings. Nevertheless, gauges with no observation are not considered for the computation of cross validation criteria for the corresponding time step. The daily rainfall measurements of the DWD were aggregated in the same way to weekly, monthly and yearly rainfall sums. These long-term accumulations were used together with the hourly recordings for the cross validation analyses.

Mean, maximum and minimum daily temperature recordings were averaged for each target temporal resolution and then evaluated separately in the cross validation procedure. The hourly recordings of mean temperature were evaluated together with the mean daily temperature and its corresponding aggregations.

The other meteorological observations were treated accordingly. Daily measurements were averaged to all required target resolutions. The time scale specific averages were then evaluated together with the daily and hourly measurements.

5.4 Radar measurements of rainfall

5.4.1 Preprocessing

Radar data of the C-band instrument at Hanover were provided as raw reflectivities with an azimuth resolution of $1\,°$ and a time discretisation of $5\,min$ (dx-product of the DWD). Accordingly, the data of each time step contained the measurements of 360 radar beam positions, whereas the spatial resolution along each beam was 1 km. The raw reflectivities were transformed into rainfall intensities by a constant Z-R-relationship according to Eq. 5.1.

$$Z = aR^b \, , \tag{5.1}$$

where Z is the reflectivity in $mm^6 m^{-3}$ and R is the rainfall intensity in mm/h. The parameters were set to $a = 256$ and $b = 1.42$ according to the Standard-DWD-relationship (RIEDL, 1986;

SELTMANN, 1997). A simple clutter correction approach was applied as follows. A permitted range of the rainfall sum R_{sum} over the three year period (upper limit R_{max} and lower limit R_{min}) was established according to the information in Tab. 5.2. Radar observation points with a higher or lower rainfall sum were identified as clutter. Additionally, a permitted rainfall duration and permitted dry spell duration is defined. Then, radar observation for a certain point is treated as clutter if the proportion of time steps with rainfall intensity of at least 0.1 mm/h exceeds a threshold of 70 %, or if the percentage of time steps with rainfall intensity of lower than 0.01 mm/h exceeds a threshold of 98 %. These empirically established thresholds were sufficient to provide adequate correction of clutter while not removing to many radar observation points. Blocked radar beams were identified visually and marked as clutter likewise.

Table 5.2: Clutter correction parameters. R_{sum}: Rainfall sum from 2008 to 2010. R_{max}: Maximal allowed rainfall sum. R_{min}: Minimal allowed rainfall sum. $R1_{lim}$: Rainfall threshold for rain. $R0_{lim}$: Rainfall threshold for no rain. $R1_{dur}$: Allowed rain duration. $R0_{dur}$: Allowed no rain duration. D: Rainfall duration and no rainfall duration, respectively.

No.	Criterion	Parameter and corresp. value	
1	$R_{sum} > R_{max}$	R_{max} [mm]	2800
2	$R_{sum} < R_{min}$	R_{min} [mm]	500
3	$D(Ri \geq R1_{lim}) > R1_{dur}$	$R1_{lim}$ [mm]	0.1
		$R1_{dur}$ [%]	0.7
4	$D(Ri < R0_{lim}) > R0_{dur}$	$R0_{lim}$ [mm/h]	0.01
		$R0_{dur}$ [%]	0.98
5	Erroneous beams	Visual inspection	

Thereafter, a coordinate transformation of the radar data was performed. All non-clutter observation points were interpolated on a 1 km × 1 km grid by using inverse-distance weighting. The gridded rainfall intensities in mm/h that were obtained by application of the Z-R-relationship were converted into the corresponding 5 min rainfall depths. A spatial, temporal and spatiotemporal smoothing of the radar data was carried out afterwards (see Sec. 5.4.2). Radar grids for all other temporal resolutions were produced by aggregating the 5 min grids.

To get a first impression of the linear relationship between rain gauge values and corresponding radar data grid points, Pearson's correlation coefficient was calculated and averaged over all stations and time steps for each temporal resolution (Tab. 5.3). As assumed the correlation coefficient decreases with increasing temporal resolution from 0.62 at 6 h resolution to 0.28 at 5 min resolution. This supports the assumption that the benefit of using radar data in combination with rain gauge data might be restricted to lower temporal resolutions.

Table 5.3: Average correlation between radar and rain gauge data for fine temporal resolutions

5 min	10 min	20 min	30 min	60 min	120 min	240 min	360 min
0.28	0.37	0.46	0.51	0.57	0.60	0.62	0.62

5.4.2 Smoothing of radar information

The general intention of using a smoothed radar data grid is the reduction of spatial and temporal mismatches between radar peaks and rain gauge information. Radar measures the by rain drops reflected energy in a specific volume. The size and the vertical location of this domain depend on the distance from the device. In contrast to that, rain gauges provide point related measurements which are located at ground level. Taking into account these different measuring approaches, it is quite obvious that radar data contain a space-time variable bias in comparison to rain gauge data. Considering the advection of precipitation fields, this bias might be larger for higher temporal and spatial resolutions. It is expected that the spatial and temporal smoothing of radar data can improve the interpolation performance of the geostatistical merging methods in particular for high temporal resolutions

The idea of radar data smoothing was also inspired by BÁRDOSSY and PEGRAM (2013). According to them, there is no significant influence of the microtopography on the rainfall sums measured by gauges. However, the prevailing wind direction affects the rainfall sums. Their use of a smoothed and shifted transformation of the elevation improved the interpolation performance for daily to yearly rainfall sums.

In order to evaluate the value of radar data smoothing, seven different techniques were applied on the 5 min radar grids. Afterwards, the data of all other temporal resolutions were produced by aggregating the 5 min radar grids. Tab. 5.4 shows the utilised approaches for smoothing the radar data.

Local spatial smoothing was applied with two different intensities, slight and strong spatial smoothing. For slight smoothing (Method 1) the grid cell values were recalculated by averaging the target cell value and the eight closest neighboring cells. The strong approach (Method 2) consisted of averaging over the 24 adjacent grid cells.

The temporal smoothing was carried out by using a moving average approach that considered the data of 5 time steps and was applied on the 5 min gridded data:

$$P_s(t) = \omega_2 P(t-2) + \omega_1 P(t-1) + \omega_0 P(t) + \omega_1 P(t+1) + \omega_2 P(t+2) \,, \qquad (5.2)$$

where $P_s(t)$ is the smoothed precipitation grid point value for the time step t. $P(t)$ represents the original precipitation grid point value and $P(t \pm j)$, $j = -2, -1, ..., 2$ are the rainfall values of the adjacent time steps. Different weights were chosen, while the sum of all weights is always 1.

These temporal smoothing techniques (Method 3, 4 and 5) do not allow merging of rain gauge and radar data in real-time because future precipitation measurements would be required for this. In order to take into account a scenario where real-time interpolation is theoretically possible, Method 6 was applied (Eq. 5.3). This incorporates only the data of past time steps:

$$P_s(t) = \omega_2 P(t-2) + \omega_1 P(t-1) + \omega_0 P(t) , \tag{5.3}$$

where the weights ω_0, ω_1, ω_2 were selected to 0.7, 0.2 and 0.1, respectively.

Additionally, a spatio-temporal technique (Method 7) was applied as a combination of Method 2 and Method 3. The temporal smoothing was carried out prior to the spatial smoothing.

High frequency signal is generally filtered out by the application of smoothing, i.e. some kind of noise removal is carried out implicitly by these simple and practical approaches. Theoretically, an existing noise could contribute to a possible over- and underestimation. PEGRAM *et al.* (2011) worked on the separation of signal and noise to generate ensembles for uncertainty analyses.

Table 5.4: Smoothing techniques for gridded radar data

Method	Type	Characterisation
1	Spatial	Slight (9 grid cells)
2	Spatial	Stronger (25 grid cells)
3	Temporal	Simple moving average over 5 time steps (central)
4	Temporal	Weighted moving average over 5 time steps (central, $\gamma_0 = 0.4$, $\gamma_1 = 0.2$, $\gamma_2 = 0.1$)
5	Temporal	Weighted moving average over 5 time steps (central, $\gamma_0 = 0.7$, $\gamma_1 = 0.1$, $\gamma_2 = 0.05$)
6	Temporal	Weighted moving average over 3 time steps by only using past data ($\gamma_0 = 0.7$, $\gamma_1 = 0.2$, $\gamma_2 = 0.1$)
7	Spatio-temporal	Simultaneous application of method 2 and method 3

The correlation of rain gauge and radar data for 5 minute values (see Tab. 5.3) improved from 0.28 to 0.41 when Method 7 is applied. This spatio-temporal technique gave the best interpolation performance in the cross validation comparison for KED presented in Sec. 6.3.

5.4.3 Detection of time steps with poor radar data

Radar data quality is of high importance regarding the interpolation performance. A mismatch between radar and rain gauge observations can occurs in particular for high temporal resolutions. In order to assess the impact of radar data quality on the interpolation performance, time steps with poor radar data are detected and removed for the cross validation of high temporal resolution rainfall. Section 6.1 compares the interpolation performance between taking into account poor radar data time steps and omitting these time steps with data mismatches. For longer accumulation times, a mismatch between radar and rain gauge data is usually not a problem. Hence, the cross validation analysis of longer accumulation periods in Sec. 6.2 does not consider radar data quality issues.

A simple approach using two criteria was applied here to filter out time steps with poor radar data quality. First, the standard error between rain gauge values and corresponding radar point information was computed for time steps in which rainfall was detected by rain gauges as well as by the corresponding radar pixels:

$$SE_{PR}(t) = \sqrt{\frac{1}{n} \sum_{i=1}^{n} (R_i(t) - P_i(t))^2} \;\; \forall \, t \; with \sum_{i=1}^{n} P_i > 0 \; and \; \sum_{i=1}^{n} R_i > 0 \, . \qquad (5.4)$$

Here, P is the gauge rainfall, R the radar rainfall and n the number of stations. The time steps in which the standard error exceeds the 98th percentile of the empirical distribution of standard errors were defined as outliers.

In some time steps, an implausible estimation of rainfall by radar occurs, which could not always be detected by the criterion described above. An additional criterion regarding the maximum radar rainfall grid cell was used to detect these time steps. This means that the maximum radar grid rainfall value is determined for each time step without considering a minimum rainfall threshold related to the rain gauge values:

$$R_{max}(t) = \max_{j}[R_j(t)] \;\; \forall \, t \; with \sum_{j=1}^{n} R_j > 0 \, , \qquad (5.5)$$

where j is the number of grid points. Here, the 99th percentile of the empirical distribution of the maximum radar rainfall values is considered to detect those time steps with implausible high rainfall values. The time steps that meet one of these two criteria are treated as poor radar data time steps for further analysis. This detection procedure was applied separately to all temporal resolutions. Tab. 5.5 gives an overview about the number of removed time steps for each temporal resolution. The 98th percentile threshold and 99th percentile threshold were established by manual tests. By this procedure, most time steps with poor radar data and hence a poor interpolation result could be excluded from the cross validation period from 2008 to 2010.

Table 5.5: Detected poor radar data time steps

Temp. resolution [min]	No. of time steps for SE calc.	98th percentile of SE [mm]	No. of detected SE outl.	No. of time steps for radar max. search	99th percentile of radar max. value [mm]	No. of detected radar max. outl.	Total no. of outl.
5	$94,141$	0.42	1768	$286,654$	9.21	2867	3791
10	$49,032$	0.65	981	$143,329$	15.18	1434	1956
20	$27,596$	1.03	552	$71,814$	26.79	719	1009
30	$19,639$	1.30	393	$47,967$	35.03	480	681
60	$10,987$	1.96	220	$24,031$	51.33	241	258
120	6162	2.89	124	$12,051$	69.54	121	190
240	3520	4.62	71	6048	102.03	61	103
360	2540	6.08	51	4045	119.13	41	73

5.5 Procedure of the analyses

This section gives a short summary of the entire cross validation analysis procedure including the data preparation, that was applied in this study. The procedure for fine temporal resolution rainfall differs slightly from the approach that was used for longer accumulation periods of rainfall and for all other meteorological variables.

The approach for rainfall with a fine temporal resolution is summarized as follows:

1. Format transformation of 5 min and 10 min rain gauge data

2. Aggregation of 10 min rain gauge data to all required temporal resolutions

3. Pre-processing of 5 min radar data, including clutter correction (see Sec. 5.4)

4. Smoothing of 5 min radar data grids (see Sec. 5.4.3)

5. Aggregation of smoothed and non-smoothed radar data (5 min temporal resolution) to all required temporal resolutions

6. Estimation of variograms and indicator variograms, separately for summer and winter season

7. Cross validation of OK, KED, IKED and CM for hourly data and a scenario with a medium station density for all smoothing techniques to find out which is the best smoothing method

8. Detection of time steps with poor radar data 5.4.3

9. Cross validation of OK, KED, IKED and CM for all temporal resolutions except 5 min, all available station density scenarios, and the two data quality cases by using the best smoothing technique from step 6

10. Cross validation of OK and CM for 5 min temporal resolution, all available station density scenarios, and the two data quality cases by using the best smoothing technique from step 6

The cross validation of the non-precipitation climate variables and the rainfall accumulations for longer time periods was conducted according to the following procedure:

1. Format transformation of hourly and daily station recordings

2. Computation of weekly, monthly and yearly aggregates from daily station recordings. The sum is used for rainfall and the average for all other meteorological information.

3. Pre-processing of 5 min radar data, including clutter correction (see Sec. 5.4)

4. Smoothing of 5 min radar data grids (see Sec. 5.4.3)

5. Aggregation of smoothed and non-smoothed radar data (5 min temporal resolution) to hourly, daily, weekly and yearly temporal resolutions

6. Preprocessing of the DEM that was obtained from the BKG

7. Estimation of variograms and indicator variograms as average variograms for the entire period of investigation

8. Cross validation of different interpolation methods for all temporal resolutions and station density scenarios, whereas the selection of interpolation methods and additional information depend on the climate variable which was analysed

For each of the climate variables, a different number of interpolation techniques was applied. The selection of the specifically used methods and the corresponding secondary information depends on the regarded meteorological observation. The evaluation of rainfall for longer accumulation periods was conducted using the same radar data smoothing technique as for fine temporal resolutions. The influence of time steps with poor radar data information was not taken into account for the interpolation of longer rainfall accumulations, since the results of the cross validation analyses for high temporal resolution rainfall show, that the radar data quality is less important for temporal resolutions longer than 240 min (see Sec. 6.1.3 and in particular Fig. 6.5). A different variogram model for the summer and the winter period was not used either. It is assumed that the effect caused by the difference in seasonally predominant rainfall type evens out when longer accumulation types are analysed.

Chapter 6

Analysis of interpolation performance

This chapter shows and discusses the cross validation results that were obtained for different temporal resolutions and station density scenarios. In particular rainfall interpolation is discussed in a detailed way, since rainfall is the most important input for hydrological modelling. The rainfall interpolation results are subdivided into two parts. The first part (Sec. 6.1) covers the interpolation of fine temporal resolution rainfall, wherein accumulation times from 5 min to 6 h were analysed. The results shown here are partly published in BERNDT *et al.* (2014). The second part (Sec. 6.2) deals with the interpolation of rainfall with a lower temporal resolution. Here, accumulation times from 1 hour to 1 year were taken into account for the comparison of cross validation performances. The temporal resolution of 1 h is available in both analysis in order to enable a comparison of the cross validation results. The other meteorological observations are only available for time scales of 1 h to 1 a and are discussed from Sec. 6.3 to Sec. 6.7. The simple interpolation techniques NN and InvD are considered for all variables with a temporal resolution from 1 h to 1 a, but not for precipitation with a fine temporal resolution.

In general, only cross validation results are shown and discussed here. Appendix C contains interpolated maps for illustrating the spatial pattern of all meteorological information. A single time step interpolated by the best method according to the cross validation outcome is shown for a selection of temporal resolutions. The wind interpolation was highly influenced by the station situated on the Brocken mountain. The wind velocity maps shown in Fig. C.8 were therefore prepared without taking into account these recordings.

6.1 Precipitation with fine temporal resolution

6.1.1 Spatial variability and persistence

Gridded radar data in different temporal resolutions were utilised for the inference of each experimental variogram. One thousand cells of the 1 km × 1 km radar grid were selected randomly to compute the variogram values for each time step. This number allowed a sufficient estimation of the spatial rainfall structure. After that, the experimental variogram values were averaged for all winter time steps and all summer time steps separately. All time steps with an average radar precipitation higher than 0.1 mm were considered for this estimation of experimental variograms. By the use of this rather low threshold it was ensured that a sufficient number of time steps was taken into account for the estimation of high temporal resolution variograms. Then, a fitting of the theoretical variogram model was carried out visually. Figure 6.1 contains the experimental variograms and fitted theoretical models for the summer and winter period. The corresponding variogram parameters obtained for each temporal resolution and later used for the cross validation analysis are given in Tab. 6.1.

In general, an increase of effective range a_{eff} with increasing temporal resolution was observed for both seasons. The nugget effect c_0 is in summer usually higher than in winter. This might result from the more frequent occurrence of convective rainfall events in summer. Moreover, the variogram range is higher for winter than for summer. This can be explained as well by the difference in predominant rainfall type. Small-scale spatial rainfall structures occur usually a lot more often in the summer period. The experimental variograms for the winter period show

Table 6.1: Parameters of theoretical exponential variogram model used in OK, KED and CM

Temporal res. [min]	Summer			Winter		
	c_0 [-]	c [-]	a_{eff} [km]	c_0 [-]	c [-]	a_{eff} [km]
5	0.25	0.75	30	0.3	0.8	48
10	0.2	0.75	30	0.3	0.8	48
20	0.2	0.82	45	0.1	1	60
30	0.2	0.8	45	0.1	1.1	75
60	0.2	0.8	60	0.1	1.1	90
120	0.2	0.8	75	0.05	1.1	28
240	0.2	0.85	96	0.1	1.1	105
360	0.2	0.9	99	0.05	1.15	105
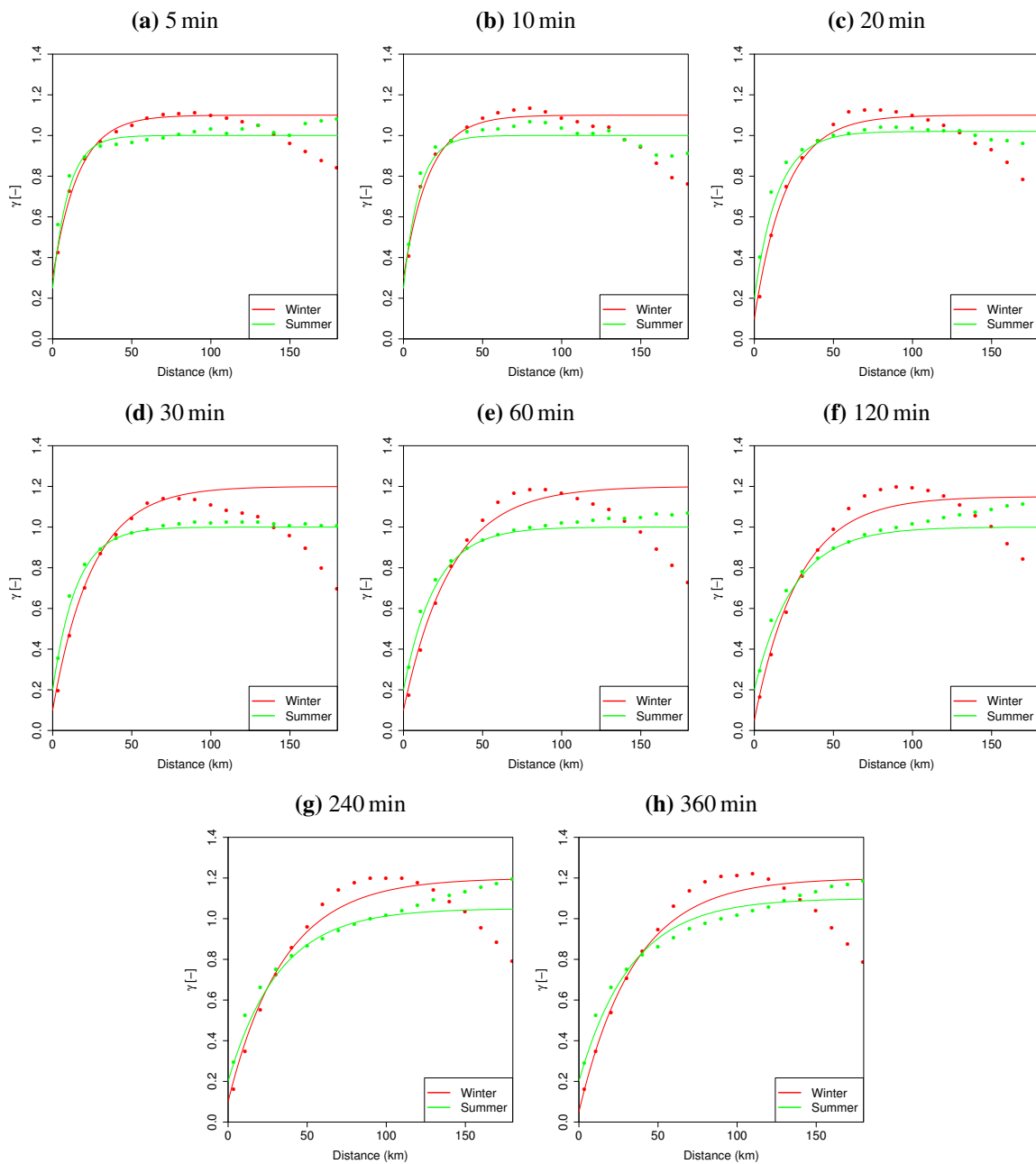
Figure 6.1: Experimental and theoretical variograms of high temporal resolution rainfall for the summer and winter period

a decrease in the variogram value for distances higher than 100 km. It might be possible that this decline is related to the attenuation present in the radar grids from which the experimental variograms were computed. However, this needs to be tested by further analyses. The points of a pair with a high distance are normally located in opposite directions relatively far away from the radar device. Due to the more stratiform character of winter rainfall effects, the effect of

attenuation is generally stronger towards the edge of the radar measuring range and hence the rainfall values of these points are assumed to be quite similar for many time steps. Nevertheless, the variogram estimation using radar data is considered as an appropriate procedure since the spatial structure of high resolution rainfall cannot be captured by rain gauge networks in many cases. The manual fitting focused on the close range, i.e. the low distance classes of the empirical variogram.

The same procedure was used for the inference of indicator variograms. Again, only time steps with significant rainfall are used for the calculation of seasonal averaged experimental variograms. The variograms were estimated separately for each temporal resolution and for five absolute rainfall thresholds τ at 0.1, 0.5, 1.0, 4.0 and 8.0 mm. Altogether 70 indicator variograms were fitted manually. Figure 6.2 and Fig. 6.3 show the theoretical indicator variogram models for summer and winter period, respectively. Each panel contains the theoretical variogram model for the indicator thresholds. The points of the experimental variograms are not shown in order to fit all variograms for the thresholds τ of a certain temporal resolution in a single panel of the figure. The corresponding parameters are displayed in Tab. 6.2.

The fitting of the theoretical indicator variogram models for IKED was as easy and obvious as the fitting of the theoretical variogram models for OK, KED and CM. In general, a decrease in range (a_{eff}) and an increase in relative nugget effect ($c_0/(c_0 + c)$) can be observed with a growing threshold α for most temporal resolutions (see Fig. 6.2, Fig. 6.3 and Tab. 6.2). This shows a weaker spatial persistence of extreme values. For the IKED interpolation, relative thresholds from 13 quantiles with non-exceedence probabilities of p = 0.01, 0.05, 0.1, 0.2, 0.3, 0.4, 0.5, 0.6, 0.7, 0.8, 0.9, 0.95, 0.99 are used to calculate absolute thresholds α_P for each time step. Thirteen different indicator variables are then interpolated for each time step based on the mentioned thresholds. For the interpolation of each variable, the closest indicator variogram is chosen automatically from the five previously inferred ones. This means that the indicator variogram is selected, for which the lowest difference between interpolation threshold α_P and inference threshold τ exists (see also HABERLANDT, 2007).
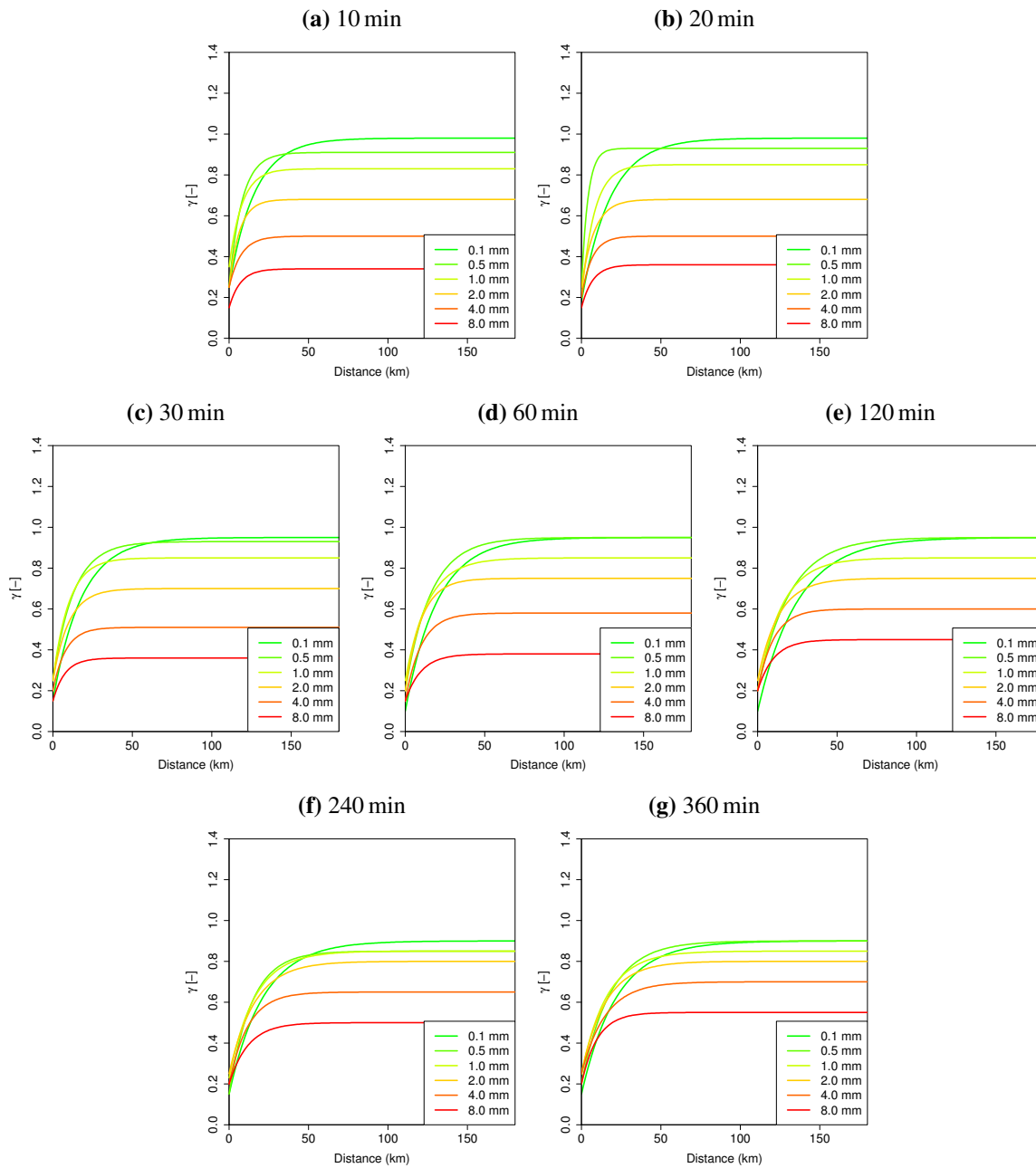
Figure 6.2: Theoretical indicator variograms of high temporal resolution rainfall for the summer period
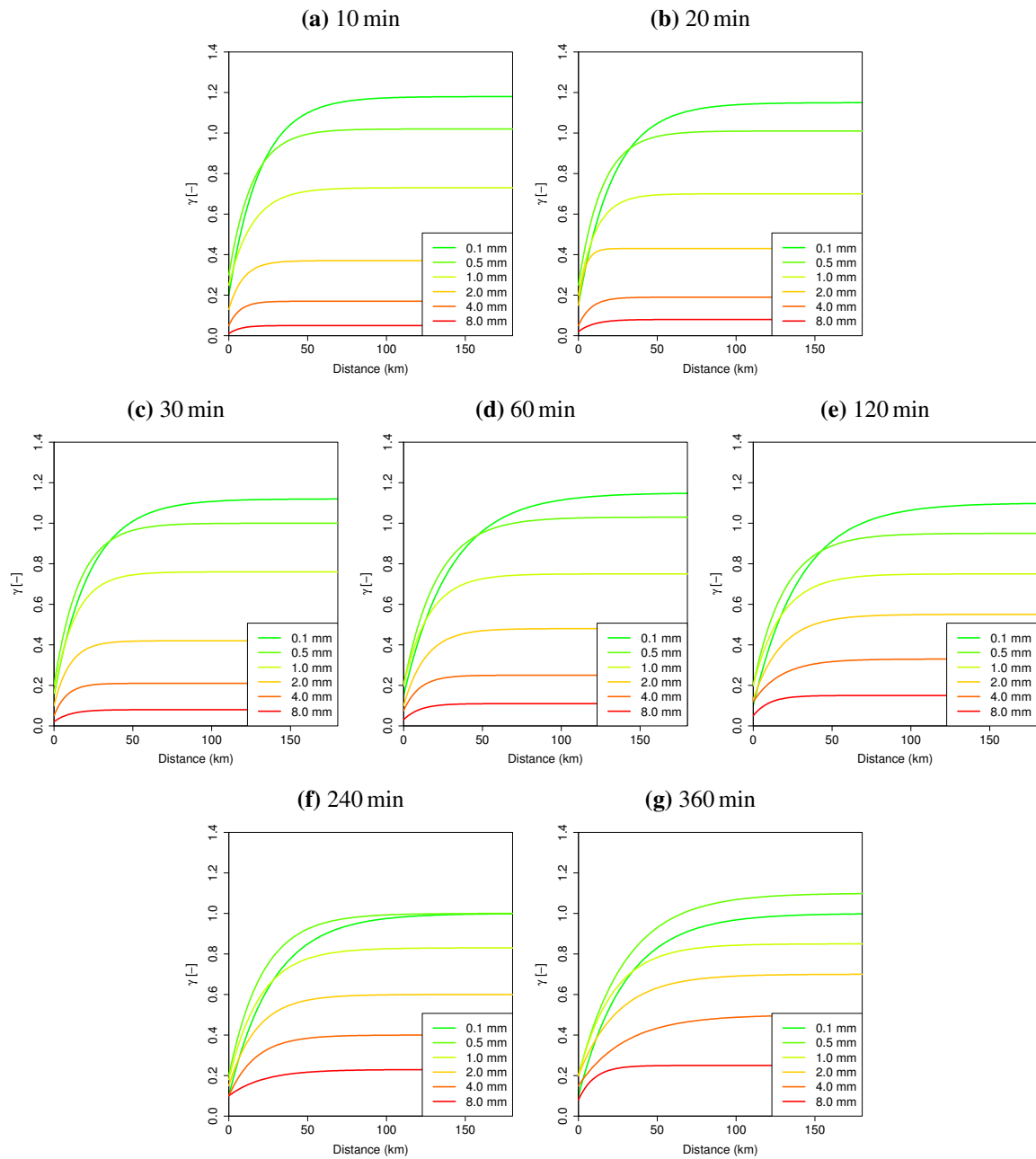
Figure 6.3: Theoretical indicator variograms of high temporal resolution rainfall for the winter period

Table 6.2: Parameters of theoretical exponential variogram models used in IKED for the summer and winter period

α [mm]	Temporal res. [min]	Summer			Winter		
		c_0 [-]	c [-]	a_{eff} [km]	c_0 [-]	c [-]	a_{eff} [km]
0.1	10	0.25	0.73	48	0.20	0.98	60
0.1	20	0.18	0.80	54	0.15	1.00	66
0.1	30	0.15	0.80	54	0.15	0.97	69
0.1	60	0.10	0.85	60	0.15	1.00	90
0.1	120	0.10	0.85	75	0.10	1.00	90
0.1	240	0.15	0.75	64	0.10	0.90	84
0.1	360	0.15	0.75	66	0.10	0.90	90
0.5	10	0.25	0.66	24	0.30	0.72	45
0.5	20	0.25	0.68	12	0.25	0.76	45
0.5	30	0.25	0.68	39	0.20	0.80	48
0.5	60	0.20	0.75	48	0.20	0.83	63
0.5	120	0.20	0.75	60	0.20	0.75	60
0.5	240	0.15	0.70	42	0.20	0.80	64
0.5	360	0.20	0.70	54	0.20	0.90	90
1.0	10	0.35	0.48	24	0.25	0.48	45
1.0	20	0.20	0.65	24	0.20	0.50	33
1.0	30	0.25	0.60	30	0.16	0.60	41
1.0	60	0.25	0.60	42	0.20	0.55	48
1.0	120	0.20	0.65	45	0.20	0.55	54
1.0	240	0.23	0.62	48	0.18	0.65	60
1.0	360	0.25	0.60	48	0.20	0.65	66
2.0	10	0.25	0.43	20	0.13	0.24	27
2.0	20	0.25	0.43	24	0.15	0.28	12
2.0	30	0.25	0.45	30	0.10	0.32	30
2.0	60	0.20	0.55	30	0.10	0.38	42
2.0	120	0.25	0.50	39	0.13	0.42	54
2.0	240	0.25	0.55	48	0.15	0.45	54
2.0	360	0.25	0.55	45	0.20	0.50	75
4.0	10	0.25	0.25	23	0.05	0.12	21
4.0	20	0.20	0.30	20	0.05	0.14	24
4.0	30	0.20	0.31	24	0.05	0.16	24
4.0	60	0.15	0.43	30	0.08	0.18	30
4.0	120	0.20	0.40	30	0.12	0.21	54
4.0	240	0.20	0.45	36	0.10	0.30	51
4.0	360	0.25	0.45	45	0.15	0.35	90
8.0	10	0.15	0.19	21	0.01	0.04	21
8.0	20	0.15	0.21	21	0.02	0.06	30
8.0	30	0.15	0.21	23	0.02	0.06	30
8.0	60	0.15	0.23	30	0.03	0.08	30
8.0	120	0.20	0.25	30	0.05	0.10	30
8.0	240	0.20	0.30	36	0.10	0.13	66
8.0	360	0.20	0.35	30	0.08	0.17	30

6.1.2 Additional information

Observations from weather radar are a common additional information for the spatial estimation of rainfall with a fine temporal resolution. Different studies, for instance HABERLANDT (2007), conclude that weather radar can provide valuable additional information which can improve the accuracy of spatial rainfall estimates. Using the topography as another additional information did not improve the interpolation performance for hourly rainfall recordings, although the DEM can be useful for the interpolation of rainfall for longer accumulation periods. GOOVAERTS (2000), for instance, proved that a DEM can contribute to a better interpolation of monthly and annual rainfall sums. For precipitation with a fine resolution in time, radar was used as the only additional information in this work. The interpolation of rainfall for longer accumulation times that is presented in Sec. 6.2 was carried out using several secondary information, i.e. also the DEM was taken into account.

In order to evaluate the effect of radar data smoothing on the interpolation performance, cross validation was carried out using differently smoothed radar information in the merging process for a temporal resolution of 1 h. The smoothing techniques, that were applied to the radar grids, are explained in Sec. 5.4.2. KED was used to assess the effect of radar data smoothing on the merging performance and all time steps with an average observed station rainfall intensity higher than 1.0 mm/h were considered in the calculation of the performance criteria. Bias, RMSE and RVar (Eq. 3.24 to Eq. 3.26) were averaged over all time steps. The cross validation results are presented for the complete time period from 2008 until 2010 in Tab. 6.3.

Table 6.3: Interpolation performance of KED (Radar) for rainfall using different smoothing techniques on hourly radar grids

Smoothing method	Bias [mm/h]	RMSE [mm/h]	RVar [-]
No radar data use (OK)	0.097	1.075	0.258
Original radar data	0.047	1.025	0.752
1	0.034	0.953	0.673
2	0.025	0.921	0.609
3	0.045	0.992	0.783
4	0.045	1.005	0.768
5	0.046	1.016	0.760
6	0.046	1.005	0.776
7	0.026	0.892	0.649

Generally, smoothing of radar data improved the merging quality. At least a slight improvement in merging performance can be observed for all of the proposed spatial and temporal techniques. Using only spatial smoothing, the 25 cell approach (Method 2) gave the best result with an RMSE of 0.921 mm/h. Method 3 (simple moving average) was the best temporal smoothing approach with a RMSE value of 0.992 mm/h, which is only slightly lower than the RMSE value for using the original radar data (1.025 mm/h). Temporal smoothing resulted in general in a similar preservation of observation variance as when original radar data were used, while the spatial techniques showed a decline in the preservation of variance RVar. Although the reduction of observation variance for Method 2 (RVar = 0.609) was higher than for Method 1 (0.673), Method 2 is regarded here as superior since the RMSE measure is considered more important for the interpolation performance. Overall, the spatio-temporal smoothing approach, Method 7, shows the best results. It gives the lowest estimation error with a RMSE of 0.892 mm/h and was applied for further investigations in this study. This includes not only fine temporal resolution rainfall but also the evaluation of interpolation performance for longer accumulation periods (Sec. 6.2).

In Fig. 6.4, Bias and Standard Error are compared for the use of non-smoothed radar data vs. the use of radar data smoothed by Method 7. Each dot represents one hourly time step. It can be seen that smoothing did not improve the merging performance consistently for all time steps, although the average error decreased. A particular improvement was detected for steps with a high overestimation of rainfall by radar. It is assumed that this is based on the reduction of rainfall peaks in the gridded data. It is also plausible that the improvement was higher for summer than for winter, albeit the evaluations regarding the season are not shown here.
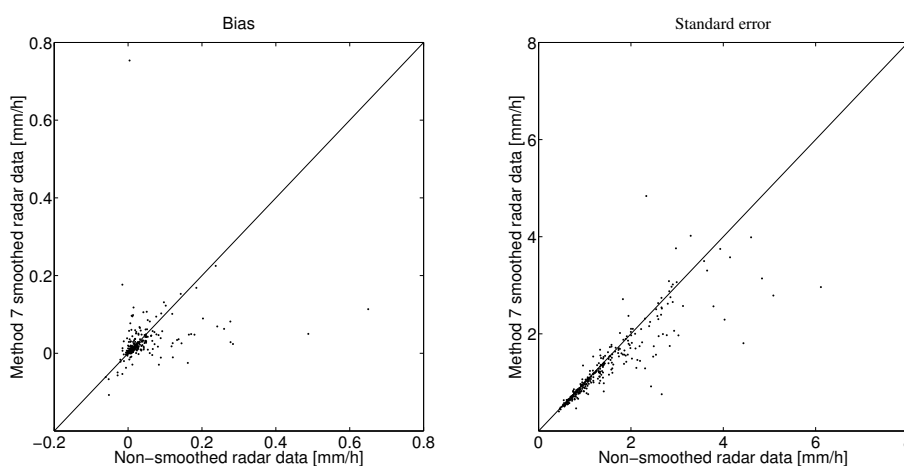
Figure 6.4: Scatter plots of Bias and SE obtained from KED cross validation for hourly rainfall data using radar data smoothed by the Method 7 vs. using original radar data.

Table 6.4: Number of time steps considered in interpolation performance evaluation and corresponding 95th percentile trimming limit (Case A: Considering all time steps for which radar data are available, Case B: Considering all time steps excluding outliers)

Temporal res. [min]	Case A		Case B	
	No. of time steps	95th pctl. [mm]	No. of time steps	95th pctl. [mm]
5	6015	0.070	5829	0.067
10	2884	0.139	2806	0.129
20	1562	0.263	1518	0.243
30	1091	0.385	1060	0.354
60	593	0.729	577	0.668
120	326	1.361	317	1.204
240	183	2.497	178	2.198
360	131	3.427	127	3.019

The following cross validation analyses for different temporal resolutions and network densities were carried out using all available time steps with radar data (Case A) and using only the time steps in which radar data provided a reasonable estimation of rainfall (Case B). In the latter case, time steps with poor radar data were identified by the approach described in Sec. 5.4.3 and neglected in the calculations. The results presented in the following consider only time steps with a significant amount of rainfall. In order to decide whether a certain time step is taken into account, the average rain gauge rainfall is calculated for all temporal resolutions considering all 90 stations available for the total time period from 2008 to 2010. Hereafter all time steps with an average rainfall that is equal to zero were removed. Then, absolute rainfall limits were calculated as the 95th percentile of the remaining time steps, whereas this procedure is done separately for (A) and (B). In both cases only the 5 % of time steps that exceed these trimming limits were taken into account for the evaluations (see Tab. 6.4).

6.1.3 Evaluation of interpolation performance

Many case studies, in which geostatistical interpolation techniques have been applied, e.g. GOUDENHOOFDT and DELOBBE (2009) and KRAJEWSKI (1987), conclude that the density of the rain gauge network is of importance regarding the interpolation performance. Furthermore, the spatial structure and dynamics of precipitation depend strongly on the temporal resolution, for instance, the ascertained variogram parameters show an increase of range with reduction of temporal resolution (see Tab. 6.1). Additionally, the correlation between rain gauge

measurement and corresponding radar pixel is higher for low temporal resolutions (see 3.2). Generally, it is assumed that the relative errors of radar rainfall measurements is lower for coarser temporal resolutions. Advection effects and location mismatches between radar and gauge observation domains are reduced with a decrease in temporal resolution.

The RMSE values (Eq. 3.25) representing the interpolation performance are provided in Fig. 6.5. Values of RMSE are plotted on the vertical axis, while the horizontal axes contain the information about temporal resolution and station density. The improvement of interpolation quality relative to OK is illustrated in addition by the surface color. An improvement of merging performance was achieved for all combinations of temporal resolution and station density colored in green, while a decline in performance is marked in red. All absolute RMSE values and all relative differences between each merging method and OK are interpolated linearly in the three-dimensional surface plots. Comparing the merging methods, it is clear that the CM approach performed best for all pairs of temporal data resolution and station density scenario concerning the RMSE criterion. As expected, the absolute values of RMSE are decreasing with decreasing temporal resolution and increasing station density. Using CM, an improvement in comparison to OK is achieved for the complete range of station densities and temporal resolutions.

KED performs significantly worse than OK for low station densities with high temporal resolution data. Only for temporal resolutions greater than or equal to 60 min, a consistent improvement over all station density scenarios was achieved considering all time steps including radar data outliers for the evaluation (Case A). After removing these outliers (Case B), a consistent advance in performance is observed for temporal resolutions greater than or equal to 20 min. For 360 min and 100 % station density, a slight decrease of KED merging performance in comparison to OK is detected. This might be explained by the high station density which allowed a good performance of OK in this case. IKED performs relatively well for high temporal resolutions. The difference of RMSE in relation to OK is similar for all combinations of temporal resolution and station density. For combinations of small densities and low temporal resolutions, i.e. from 2 h to 6 h and the corresponding 20 % - 60 % scenarios, the merging performance is considerably lower than the one of KED. The relative improvement of the best approach (CM) in comparison to OK ranges from approx. 8 % to approx. 30 % for Case A, and from approx. 10 % to approx. 33 % for Case B. Moreover, it appears that CM and IKED are less sensitive than KED regarding the influence of the station density. In particular, the interpolation performance of KED for high temporal resolutions decreases much more from using 90 Stations for the interpolation to using only 17 Stations in comparison to CM and IKED.
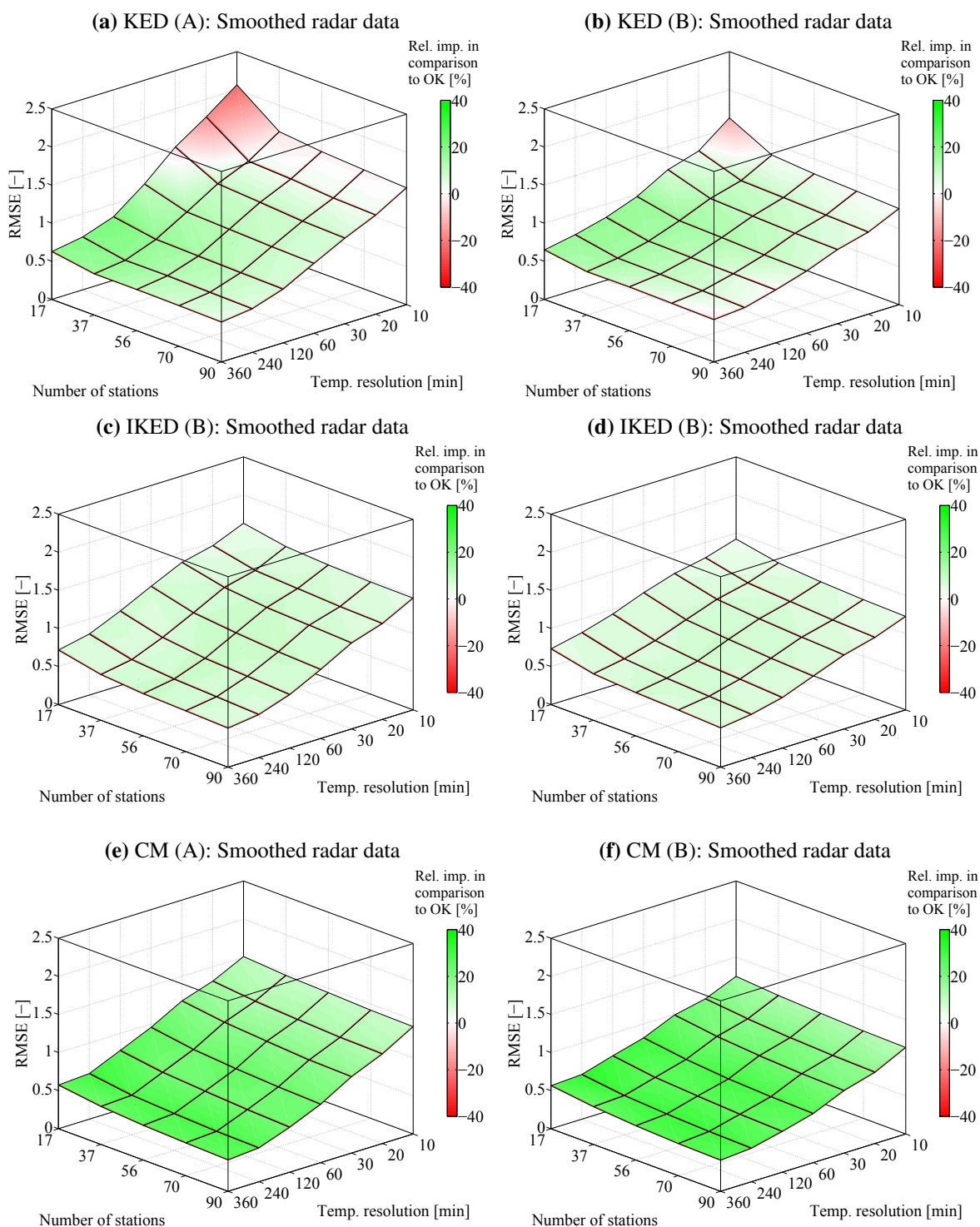
Figure 6.5: Interpolation performance of 10 min to 360 min temporal resolution rainfall using KED (top), IKED (middle) and CM (bottom) in comparison with OK for all network density scenarios. The results are displayed separately for using all time steps (Case A, left) and discarding time steps with poor radar data quality (Case B, right).

Table 6.5: Average interpolation performance (Bias, RMSE, RVar) over all station density scenarios for each temporal resolution

Case	Method	Criterion	Temporal resolution [min]							
			5	10	20	30	60	120	240	360
A	OK	Bias [mm]	0.003	0.006	0.017	0.023	0.049	0.077	0.120	0.119
		RMSE [-]	1.876	1.594	1.409	1.300	1.085	0.861	0.695	0.621
		RVar [-]	0.091	0.165	0.191	0.200	0.232	0.260	0.259	0.256
	KED	Bias [mm]	–	0.014	0.026	0.026	0.030	0.012	0.005	−0.038
		RMSE [-]	–	1.683	1.428	1.232	0.982	0.744	0.607	0.552
		RVar [-]	–	0.578	0.640	0.611	0.594	0.531	0.470	0.479
	IKED	Bias [mm]	–	−0.036	−0.041	−0.046	−0.046	−0.057	−0.078	−0.131
		RMSE [-]	–	1.518	1.327	1.214	1.004	0.803	0.650	0.582
		RVar [-]	–	0.122	0.149	0.163	0.197	0.219	0.219	0.217
	CM	Bias [mm]	0.005	0.008	0.017	0.025	0.034	0.043	0.038	0.025
		RMSE [-]	1.591	1.450	1.228	1.070	0.839	0.665	0.500	0.473
		RVar [-]	0.444	0.486	0.611	0.655	0.709	0.699	0.716	0.743
B	OK	Bias [mm]	0.002	0.006	0.012	0.017	0.028	0.049	0.066	0.055
		RMSE [-]	1.497	1.350	1.218	1.128	0.981	0.811	0.703	0.625
		RVar [-]	0.094	0.176	0.197	0.210	0.235	0.264	0.260	0.250
	KED	Bias [mm]	–	0.007	0.012	0.014	0.013	0.016	0.064	0.017
		RMSE [-]	–	1.366	1.149	1.036	0.863	0.729	0.630	0.582
		RVar [-]	–	0.498	0.527	0.528	0.502	0.482	0.486	0.452
	IKED	Bias [mm]	–	−0.033	−0.038	−0.039	−0.047	−0.061	−0.071	−0.118
		RMSE [-]	–	1.295	1.157	1.061	0.918	0.765	0.659	0.593
		RVar [-]	–	0.126	0.153	0.171	0.197	0.217	0.221	0.216
	CM	Bias [mm]	0.004	0.003	0.005	0.008	0.005	−0.003	0.025	0.017
		RMSE [-]	1.275	1.181	0.992	0.885	0.709	0.602	0.495	0.467
		RVar [-]	0.458	0.432	0.510	0.548	0.585	0.577	0.696	0.690

In general, the benefit of incorporating radar data in the interpolation procedure increases with decreasing temporal resolution, as can be observed in Fig. 6.5. Especially for KED, there is also a growth of radar data value with decreasing station density for temporal resolutions lower than 60 min. Mean interpolation performances for all temporal resolutions are provided in Tab. 6.5. The values of RMSE, RVar and Bias are averaged over all station density scenarios. The Bias is used as control criterion to test the implicit unbiasedness of the geostatistical methods. It is similarly low for all merging methods. In terms of preservation of the observation variance, CM outperforms all other techniques for most temporal resolutions and station density scenarios as well. Only for the lowest station density scenario and highest temporal resolution, KED performs better than CM. The variance preservation of IKED and OK is much lower, whereas OK even outperforms IKED in most cases. As a consequence, the rainfall fields interpolated by OK and IKED show a much smoother distribution than those of KED and CM.
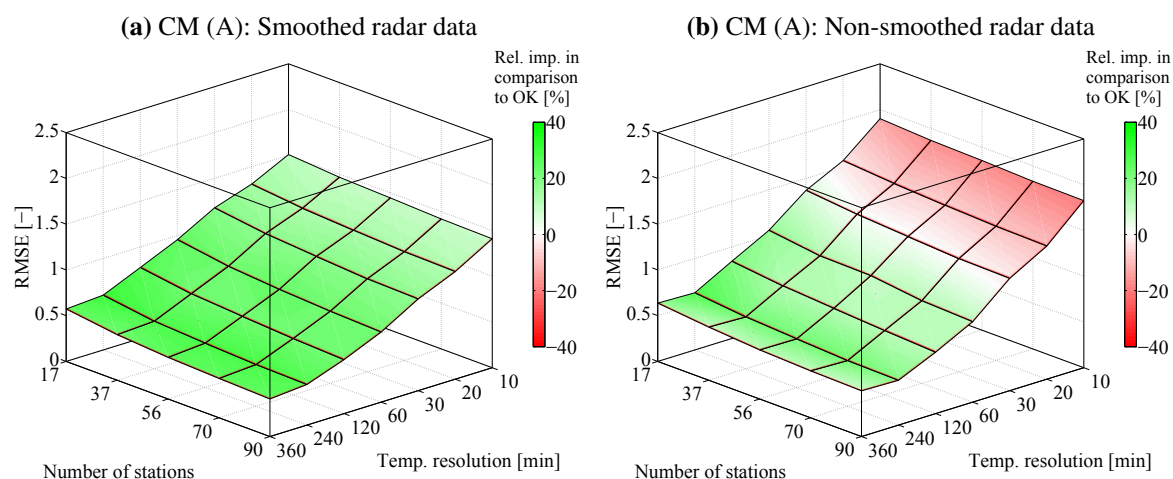
Figure 6.6: Interpolation performance of 10 min to 360 min temporal resolution rainfall using CM in comparison
with OK for different network density scenarios. The results are compared for the use of smoothed
(left) and non-smoothed radar data (right).

In order to highlight the importance of radar data smoothing, the cross validation calculations
for CM were carried out using non-smoothed radar data as well. The results for different
temporal resolutions and station density scenarios are shown in Fig. 6.6. Again, Case A
and Case B are displayed. It is obviously shown that CM performs significantly worse when
non-smoothed radar data are used. In particular for high temporal resolutions a significant
weaker interpolation performance in comparison to OK is evident. In this case a benefit of
using radar data as additional information is only given for temporal resolutions lower than
30 min (Case A) and 10 min (Case B, not shown). Accordingly, radar data smoothing is in
particular important for the merging of high temporal resolution data. As stated before, radar
measuring errors are expected to be higher for fine temporal resolutions due to the mismatch
of station based point observation at ground level and radar reflectivity captured for a volume
with a certain height above the ground. It is assumed that radar data smoothing can compensate
for temporal and spatial mismatches of rainfall peaks to a certain extent.

The cross validation of 5 min rainfall was only performed using CM and OK. CM provided the
best interpolation performance among the tested methods and OK is the univariate standard of
comparison. Figure 6.7 contains the performance using smoothed and non-smoothed radar data.
Again, Case A and Case B are displayed in order to allow an assessment of radar data quality
impact. The colour scheme is selected exactly in the same way as in Figs. 6.6 and 6.5, i.e.
the color of the CM bar gives information about the improvement in comparison to OK. The
application of CM with smoothed radar data delivers also for 5 min rainfall a better interpolation
performance than OK, while CM using non-smoothed radar grids performs worse.
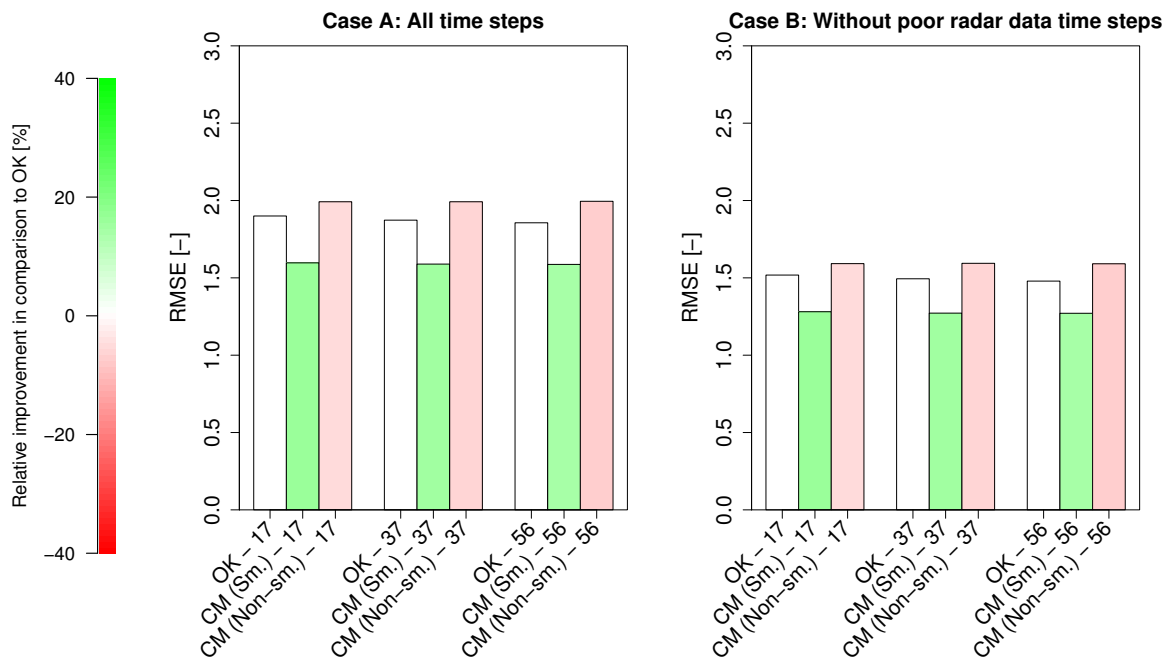
Figure 6.7: Interpolation performance of 5 min temporal resolution rainfall using CM in comparison with OK for different network density scenarios. The results are displayed separately for using all time steps (Case A, left) and discarding time steps with bad radar data quality (Case B, right). The bar color indicates the relative interpolation performance in comparison with OK.

In terms of computation time, CM and KED are preferable compared to IKED. CM needs a double application of OK as well as two simple arithmetical calculations. The KED calculations required a similar amount of computation time. In this study the number of indicator variables for IKED was selected to 13. Accordingly, the required computation time is 13 times higher than those of KED.

Overall, CM using smoothed radar information provided the best solution for the spatial interpolation of rainfall with a high resolution in time. The application of KED fails in particular for very fine temporal resolutions and low station densities. However for accumulation times longer than 30 min, a reasonable interpolation performance could be achieved. IKED delivers a better performance than OK for all combinations of network density and temporal resolution, but performs generally worse than CM.

6.2 Precipitation for longer accumulation times

6.2.1 Spatial variability and persistence

In contrast to fine temporal resolution rainfall, the variograms of rainfall with accumulation times from 1 h to 1 a were computed from the corresponding rain gauge data. Figure 6.8 shows the experimental variograms with the fitted theoretical models for different temporal resolutions. A separate variogram estimation for summer and winter season was not carried out, since the difference in prevailing rainfall type is considered as less relevant when larger accumulation time periods are investigated. Again, the estimation of experimental variograms took into account all time steps with an average precipitation higher than 0.1 mm. Table 6.6 contains variogram parameters of the exponential model fitted to the exponential variogram of each temporal resolution. An automatic fitting procedure was applied, in which the maximum value of the partial sill c was restricted to 1.5.

The variograms look quite similar to those that were inferred for rainfall with fine temporal resolution. In general there is a decrease of the nugget c_0 with increasing temporal resolution. Except for the annual time scale, the values of c_0 are always higher than the nugget effect shown for fine temporal resolution rainfall in Tab. 6.1. This is explained by the data source used for variogram inference here. The 200 rain gauges have a lower spatial density than the 1000 points randomly sampled from radar data for the inference of fine temporal resolution variograms. The results show a relation of time scale and variogram range as well: The lower the temporal resolution of the data, the lower the effective range a_{eff} of the variogram model. The range obtained for the annual temporal resolution is particularly low. This behaviour was not observed for fine temporal resolution rainfall. It could be possible that the steep incline of the variogram value for the annual time scale is caused by local regions with substantially higher rainfall depths (Harz Mountains) interrelated with a comparatively small range of rainfall values for the rest of the study area. Furthermore, the automatic fitting procedure has a strong impact on the resulting variogram parameters.

Table 6.6: Parameters of the exponential variogram model for hourly, daily, weekly, monthly and yearly rainfall

Temporal resolution	c_0 [-]	c [-]	a_{eff} [m]
Hour	0.53	1.50	259,915
Day	0.40	1.50	186,280
Week	0.34	1.50	176,863
Month	0.30	1.11	88,965
Year	0.10	0.91	16,211
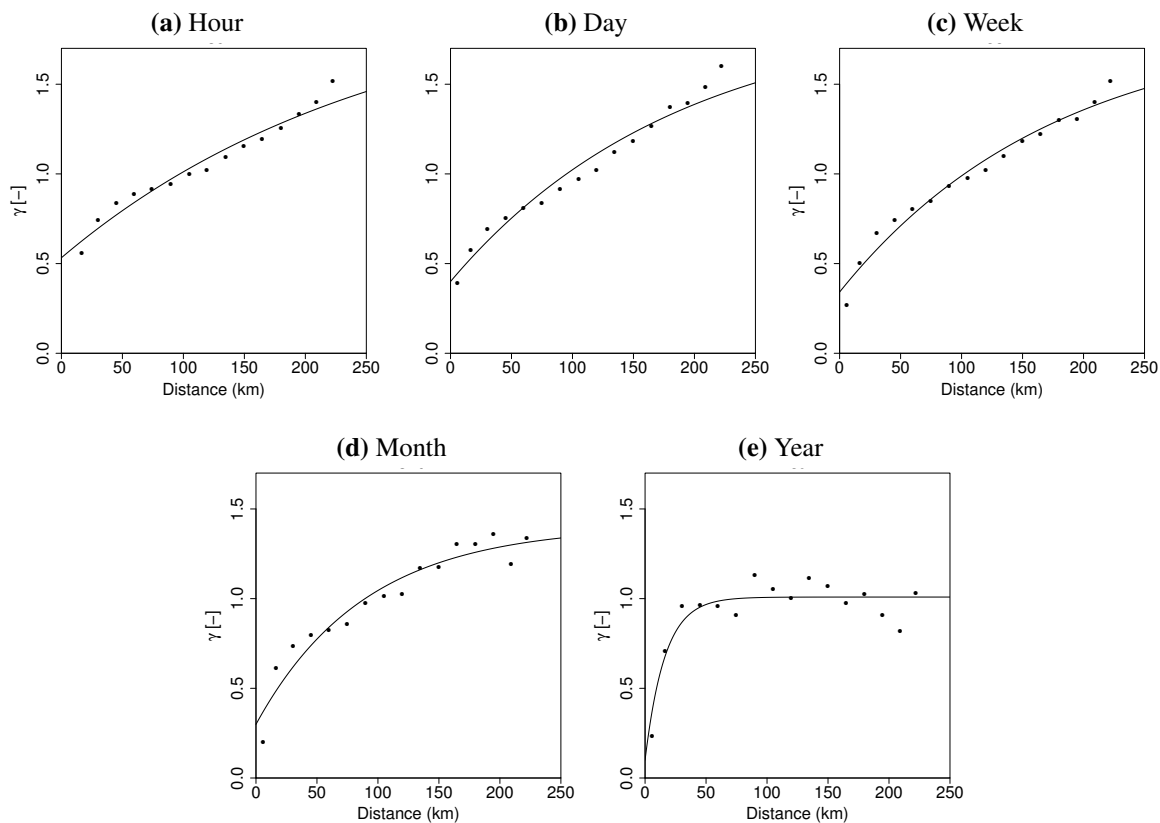
Figure 6.8: Experimental and theoretical average variograms of hourly, daily, weekly, monthly and yearly rainfall

6.2.2 Additional information

Radar information was also aggregated for longer time periods and considered in KED and CM. HABERLANDT (2007) showed that the interpolation performance of hourly rain gauge data is improved when radar is used as an additional information in KED. However, due to errors in radar data and also the absence of a thorough attenuation correction, it is expected that the benefit of using radar data as an additional information might be restricted to certain accumulation times. This is supported by the time scale specific Pearson correlation that was computed for each step between gauge rainfall values and the corresponding radar measurements. The values in Tab. 6.7 are averaged over all available time steps and show that there is almost no correlation for yearly rainfall aggregates.

The same radar information as for the analysis of fine temporal resolution rainfall was used for the cross validations presented here. The same preprocessing techniques, including the spatio-temporal smoothing method, were applied not only to the period from 2008 to 2010, but also to the time period from 2011 to 2013. The clutter identification procedure used for 2008

to 2010 could also provide adequate results for 2011 to 2013. The analysis of using radar for longer accumulation times does not consider different cases of data quality. It is assumed that radar data quality issues are much less important for low temporal resolutions and therefore all available time steps were considered in evaluation of interpolation performance.

In addition to radar data, a digital elevation model was taken into account for the KED interpolations. Different studies, e.g. GOOVAERTS (2000), HEVESI *et al.* (1992a) and HEVESI *et al.* (1992b), reported that the consideration of topographic elevation in geostatistical approaches can improve the interpolation of long-term rainfall accumulations or mean annual rainfall sums. Table 6.7 shows also the average spatial correlation of precipitation sums and the corresponding elevation at rain gauge location for each temporal resolution. The correlation of elevation and precipitation sum increases with a decrease in temporal resolution. It is therefore expected that the benefit of using the DEM in the KED method is also here restricted to the long accumulation periods.

Table 6.7: Spatial correlation between radar and rain gauge time series as well as DEM and rain gauge time series averaged over all available time steps

Temporal resolution	Hour	Day	Week	Month	Year
Correlation Radar [-]	0.194	0.305	0.394	0.280	0.059
Correlation DEM [-]	0.072	0.129	0.237	0.376	0.583

6.2.3 Evaluation of interpolation performance

The cross validation results shown here were computed for all time steps of each temporal resolution in the investigation period. The following figures contain averaged interpolation performances calculated from all time steps with an average rain gauge rainfall higher than 1.0 mm. All available rain gauges were used to compute the time step specific mean rainfall. The time steps that were selected according to the 1.0 mm threshold are the same for all network densities and also for the corresponding realisation of each scenario. The choice of 1.0 mm as the threshold results in a selection of all monthly and yearly time steps. In case of hourly, daily and weekly temporal resolution, not all available time steps are taken into account for the computation of interpolation performance. Table 6.8 contains the number of time steps considered in the performance evaluation of each temporal resolution.

The RMSE interpolation performance of NN and InvD (Eq. 3.25) for longer accumulation times is given in Fig. 6.9. The 3-dimensional plots contain interpolation performances that were averaged from 10 realisations of each network density scenario. Absolute values of the

Table 6.8: Number of time steps considered for the cross validation of precipitation for longer accumulation times

Temporal resolution	Hour	Day	Week	Month	Year
No. of consid. time steps	7804	1318	300	72	6

error are plotted on the vertical axis while the horizontal axes contain the information about temporal resolution and station density. In addition, the surface color illustrates the relative improvement of interpolation quality with respect to OK.

NN performs worse for all combinations of temporal resolution and network density, while the relative difference to OK ranges from -17 % (1 h) to -35 % (1 a). The decline in interpolation quality is less strong for the network density of 200 stations. InvD performs quite similar to OK, i.e. for most network density scenarios and temporal resolutions the interpolation performance is around 1 % to 5 % lower. However, for the 200 stations scenario and for the hourly temporal resolution of the scenarios with 90 and 70 stations InvD performs slightly better than OK. The general behaviour of the increase of interpolation performance with decreasing temporal resolution and increasing network density is also seen for rainfall with longer accumulation times.

Figure 6.10 shows the cross validation results of CM and KED. The elevation as well as radar were used as additional information in KED. Moreover, both additional variables were used simultaneously in multivariate KED. Using the DEM as the only additional information can improve the interpolation performance especially for the annual time scale, whereas the RMSE of KED is around 12 % to 30 % lower than the RMSE of OK. The improvement of
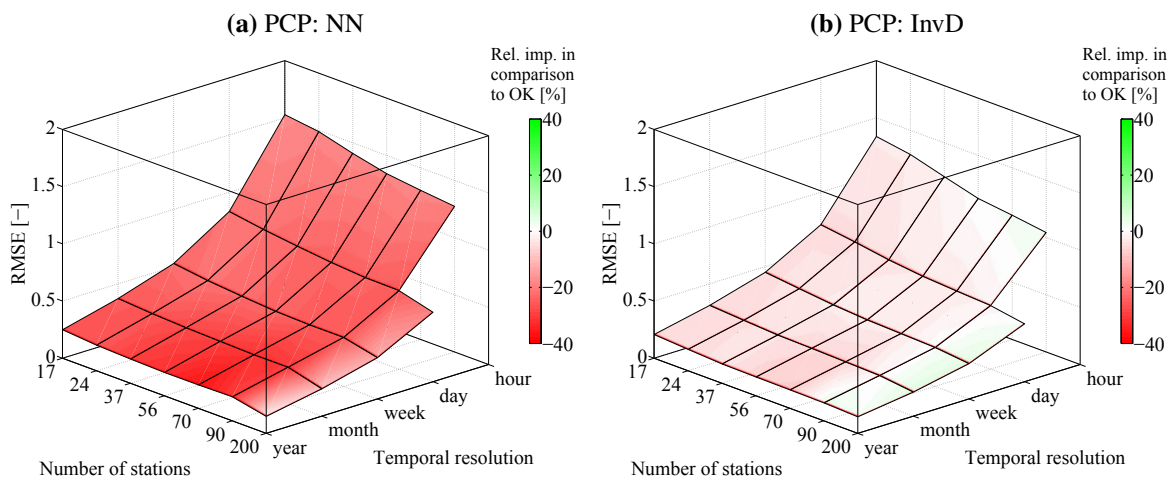
Figure 6.9: Interpolation performance of precipitation using NN and InvD for hourly to yearly time periods and all network density scenarios

monthly interpolation performance is somewhat weaker. It ranges from approximately 5 %
to approximately 12 %. On the weekly time scale there is only a minor benefit of using the
DEM, while on the daily time scale the interpolation performance of KED is already a bit lower
than those of OK for most network densities. Only for the scenario using 200 station and the
scenario using 90 stations a minimal improvement is seen. In case of hourly data, the KED
interpolation performance is approx. 3 % lower for all density scenarios when it is compared to
OK.

The results of KED based on radar data are different. For the annual temporal resolution there
is only a significant improvement of interpolation performance for the scenario consisting of
200 stations. The other annual network densities show either a minor decrease or increase of in-
terpolation performance. The monthly and weekly time scale shows each a slight improvement
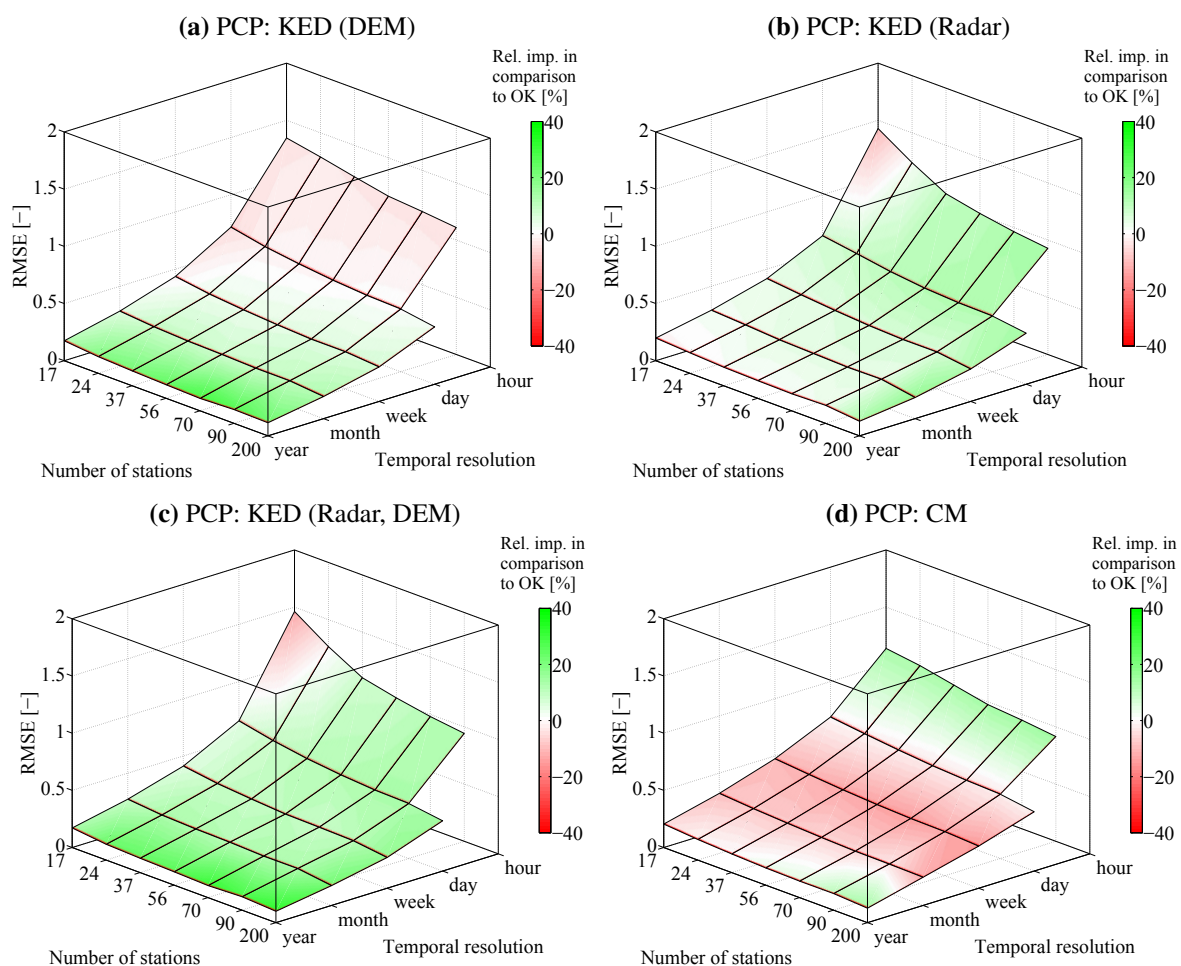
Figure 6.10: Interpolation performance of precipitation using KED (DEM), KED (Radar), KED (Radar, DEM)
and CM for hourly to yearly time periods and all network density scenarios

of around 5 % for all network densities except 200 stations. Here an improvement of around 12 % is achieved. The daily temporal resolution is improved by approx. 6 % (17 stations) to approx. 12 % (200 stations). In case of hourly data, the maximum benefit of using KED with radar can be quantified to 13 % in comparison with OK. However, there is a strong decrease in interpolation performance of approx. 10 % for the network density of 17 stations. An increase of RMSE is also observed for the KED interpolation of rainfall for low station densities (see Fig. 6.5).

KED using both additional information at the same time, DEM and Radar, results in an improvement of interpolation performance compared to OK for almost all combinations of temporal resolutions and network density scenarios. Only for a low station density together with hourly data it performs worse than OK. It can be said that KED using both additional information behaves for low temporal resolutions like KED using the elevation only and for high temporal resolutions like KED using radar only. However, the performance of KED (Radar, DEM) is for the hourly temporal resolution somewhat lower than the interpolation performance of KED (Radar). KED (DEM, Radar) achieves almost the same cross validation result for the daily time scale. In case of weekly and monthly data, KED using both additional information performs even slightly better that using the radar data or the elevation only. The improvement in comparison to OK is approx. 5 % to 18 % for the weekly time scale and approx. 8 % to 21 % for the monthly time scale. The annual interpolation performance of KED (Radar, DEM) and KED (DEM) are approx. the same. Only for 200 stations, KED (Radar, DEM) performs slightly better.

As described before, CM performs the best for fine temporal resolutions. This is also the case for the hourly RMSE values presented in Fig. 6.10 which are approx. 13 % to 14 % lower than those of OK. Also for low station densities an improvement in comparison to OK can be achieved. CM and OK deliver a relatively similar interpolation performance for the daily temporal resolution, i.e. for some station densities CM performs minimal worse. In contrast to KED (Radar), CM performs worse than OK for the weekly, monthly and annual time scale. Only for 90 and 200 stations there is a slightly better interpolation quality of CM. It is assumed that this different behaviour of CM in comparison to KED results from the more direct use of radar data implemented in the CM method. KED uses the radar images in combination with station data to obtain the weights required for calculating the rainfall estimate based on adjacent station recordings. In contrast to that, CM computes a spatial pattern of radar rainfall and adds it directly to the OK estimate.

Another difference of CM and KED (Radar) can be observed from the hourly interpolation per-

formance. The RMSE values of CM are relatively constant over all network density scenarios, while KED (Radar) causes a much higher decline of interpolation quality when less stations are used. This behaviour might also be explained by the difference in the implementation of radar data. The network density scenarios with few stations are not able to capture the skew and non-gaussian spatial distribution of short-time rainfall sums. The more direct use of radar information (CM) can therefore achieve a better performance than the estimation based on a linear combination of neighbouring points, in which radar is only used to determine the weights (KED).

Table 6.9 contains the RMSE, Bias and RVar interpolation performance for all interpolation methods and temporal resolution. The criteria are averaged over all network densities available for the corresponding temporal resolution. Since the Bias criterion is given in mm, the values are increasing with an increase of accumulation time. For low temporal resolutions, the application of geostatistical techniques produces a lower Bias than using simple methods. For hourly and

Table 6.9: Average interpolation performance (Bias, RMSE, RVar) for hourly to annual rainfall over all station density scenarios

Method	Additional information	Criterion	Temporal resolution				
			Hour	Day	Week	Month	Year
NN	–	Bias [mm]	0.006	0.038	0.170	0.694	8.779
		RMSE [-]	1.390	0.742	0.461	0.335	0.217
		RVar [-]	0.955	0.968	0.974	1.051	1.146
InvD	–	Bias [mm]	0.007	0.031	0.136	0.550	6.918
		RMSE [-]	1.181	0.623	0.384	0.273	0.174
		RVar [-]	0.594	0.624	0.619	0.628	0.658
OK	–	Bias [mm]	0.007	0.028	0.121	0.474	5.440
		RMSE [-]	1.178	0.606	0.376	0.263	0.168
		RVar [-]	0.291	0.368	0.373	0.381	0.388
KED	DEM	Bias [mm]	0.008	0.028	0.083	0.284	2.527
		RMSE [-]	1.212	0.612	0.363	0.243	0.133
		RVar [-]	0.327	0.485	0.537	0.611	0.736
KED	Radar	Bias [mm]	0.025	0.058	0.183	0.438	1.554
		RMSE [-]	1.109	0.546	0.357	0.254	0.166
		RVar [-]	0.486	0.609	0.603	0.523	0.464
KED	DEM,Radar	Bias [mm]	0.027	0.059	0.146	0.304	−0.499
		RMSE [-]	1.131	0.546	0.344	0.233	0.129
		RVar [-]	0.529	0.719	0.761	0.769	0.827
CM	Radar	Bias [mm]	0.028	0.081	0.234	0.259	−0.563
		RMSE [-]	1.019	0.615	0.420	0.279	0.164
		RVar [-]	0.607	0.771	0.948	0.902	0.609

daily rainfall accumulations, the Bias of radar based methods is somewhat higher compared to no radar data use. OK shows a lower preservation of the observed variance in comparison to KED using the DEM for low temporal resolutions and in comparison to KED and especially CM incorporating radar data for high temporal resolutions. The smoothing effect of OK is also stronger than the one of InvD, since 12 neighbouring stations are used to calculate the rainfall estimates. InvD uses only four adjacent rain gauges, the closest in each quadrant starting from the location of the estimate. NN preserves the variance in general very well, but delivers the worst interpolation performance according to the other criteria.

It can be summarised that CM performs best for hourly data, but does not help for longer accumulation times. In contrast to the findings of GOUDENHOOFDT and DELOBBE (2009), the interpolation performance of CM was not better than the one of OK for daily data. However, it could be confirmed that KED using Radar outperforms OK and CM. The results of GOOVAERTS (2000), that the elevation can improve rainfall interpolation for longer accumulation times, could be confirmed as well. In addition to that, it could be observed that using radar and elevation simultaneously in KED delivers a slightly better interpolation performance for weekly and monthly data than using the DEM only. EHRET (2003) ranked CM as the best merging technique for rain gauge and radar data with 10 min temporal resolution. Different criteria were used to assess the interpolation performance, however an improvement of RMSE in comparison to OK was not achieved in contrast to the findings here (see Sec. 6.1.3).

6.3 Temperature

6.3.1 Spatial variability and persistence

Figure 6.11 contains the experimental variograms and fitted theoretical variogram models for mean temperature. The experimental variograms were computed using the station recordings of each time step. In contrast to the rainfall variograms no threshold was used, i.e. all available time steps were used and subsequently averaged in order to compute the experimental variogram. The same automatic fitting procedure as for rainfall with longer accumulation times was used, i.e. a maximum value of 1.5 was set as the upper limit of the partial sill c of the exponential model. The corresponding variogram model parameters are shown in Tab. 6.10.

The fitting of the theoretical model is clear and easy for the hourly and daily time scale. However, the spatial persistence of monthly and annual mean temperature is not as obvious.
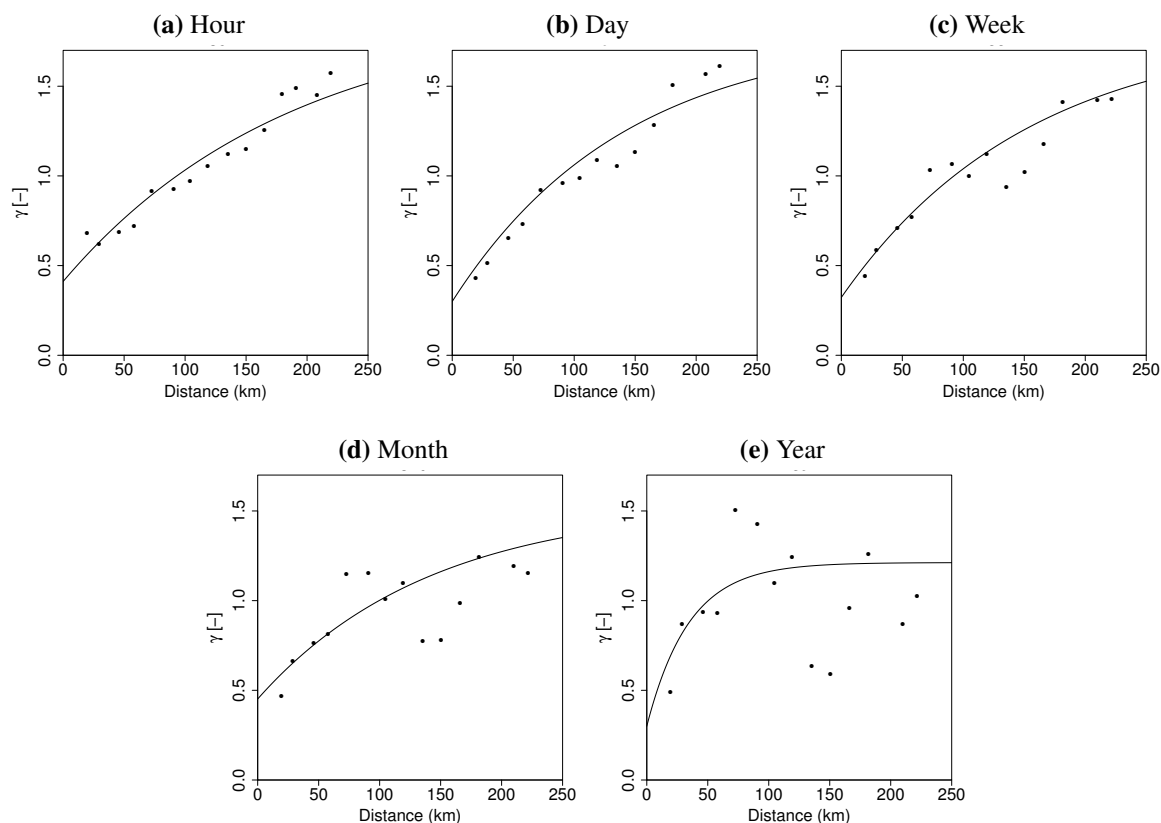
Figure 6.11: Experimental and theoretical average variograms of mean temperature

Although there is a general increase of variogram value with increasing distance, the variogram points scatter heavily around the theoretical model. It has to be concluded that the spatial persistence of annual mean temperature is lower than the spatial persistence of temperature averages for shorter time periods. The range parameter in Tab. 6.10 indicates also a stronger spatial dependency for short aggregation periods. In contrast to rainfall, there is no clear influence of the temporal resolution on the nugget effect c_0. The lower parameter values of the partial sill c for monthly and annual data might result from the automatic fitting in combination with the non-distinct behaviour of the experimental variogram.

Table 6.10: Parameters of the exponential variogram model for mean temperature

Temporal resolution	c_0 [-]	c [-]	a_{eff} [m]
Hour	0.41	1.50	187,094
Day	0.30	1.50	141,143
Week	0.32	1.50	153,716
Month	0.45	1.09	141,324
Year	0.30	0.91	34,559

The variograms obtained for maximum temperature and minimum temperature are shown in Appx. A.1. In general there is a strong similarity to the variograms of mean temperature, i.e. the spatial persistence is also much stronger for short time scales. For minimum temperature the nugget effect c_0 tends to be slightly higher compared to maximum and mean temperature. A somewhat lower interpolation performance is expected due to this.

6.3.2 Additional information

Air temperature and also air pressure are in general strongly connected to terrain altitude. A comparison of different interpolation methods for temperature on a daily time scale was carried out by STAHL *et al*. (2006). An interpolation technique based on a linear regression with a DEM (GIDS) could achieve the best estimation performance. The elevation is also used in this work as an additional information for the interpolation of mean, maximum and minimum temperature. Table 6.11 contains the spatial correlation of all temperature variables with the elevation for all time scales. A strong negative correlation is present in particular for low temporal resolutions.

Other meteorological observations were also tested as additional variables for the interpolation of temperature data. KED requires the additional information to be available for all station locations and the point that is to be estimated. Due to the different measuring networks and data availability, all tested meteorological observations were interpolated on a $1\,\mathrm{km} \times 1\,\mathrm{km}$ grid. For each station, the KED algorithm uses accordingly the value of the collocated point of the interpolation grid. For each meteorological variable tested, the maximum number of stations presented in 4.2 was used for the spatial interpolation of the grids that were used subsequently in the KED interpolation of temperature. The following Sec. 6.3.3 contains more details about the tested meteorological variables and the associated interpolation method for grid preparation.

Table 6.11: Spatial correlation between DEM and temperature time series, averaged for each time scale over all available time steps

Variable	Hour	Day	Week	Month	Year
TAV	-0.669	-0.781	-0.868	-0.909	-0.949
TMA	–	-0.738	-0.844	-0.890	-0.933
TMI	–	-0.571	-0.722	-0.800	-0.883

6.3.3 Evaluation of interpolation performance

Figure 6.12 presents the cross validation results for interpolation using NN and InvD. The results are displayed individually for mean, maximum and minimum temperature. The cross validation was computed for all time steps of each temporal resolution in the investigation period and averaged in order to determine the mean interpolation performance for each combination of temporal resolution and network density. All available time steps were used for the performance evaluation. The problem of many time steps having only zero rainfall recordings does not occur with temperature data.

The evaluations show that NN performs worse than OK for all temporal resolutions and network densities. The decrease in performance compared to OK ranges from 13 % to 50 % for mean temperature, from 23 % to 62 % for maximum temperature and from 10 % to 28 % for minimum temperature. InvD performs only slightly worse than OK for most combination of temporal resolution and station density, while the maximum decrease of interpolation performance is around 6 %. For monthly values there is an improvement of approx. 5 % when 24 stations are used. In case of temperature maxima, the interpolation quality decreases by 5 % to 12 %. InvD outperforms OK for most combinations of temporal resolution and network density in case of temperature minima. The maximum relative improvement is approx. 10 %. For hourly data there is a slight decrease in interpolation performance of around 3 %.

The cross validation results of KED using the elevation and KED using interpolated grids of relative humidity are shown in Fig. 6.13. The humidity grids were interpolated using OK. KED achieves for both secondary variables a really good interpolation performance. The estimation quality of mean temperature improves by almost 30 % for hourly data to almost 70 % for yearly averages when the DEM is used. In case of relative humidity as the additional information, the improvement ranges from 8 % to 23 %. Similar results are achieved for maximum temperature. KED (DEM) improves the interpolation performance by approx. 34 % to 63 % and KED (HUM) by approx. 8 % to 16 %. The interpolation performance of minimum temperature is generally a bit lower than the performance of mean and maximum temperature. The improvements range from 8 % to 32 % and 8 % to 20 % for KED (DEM) and KED (HUM), respectively.

Generally, the effect of network density on the interpolation performance is hardly visible in the plots. Only for minimum temperature, there is a significant decrease when the network density is reduced from 37 to 17 stations. The interpolation depends strongly on the temporal resolution, however for some interpolation techniques there is no clear behaviour, i.e. the interpolation performance does not always increase with decreasing temporal resolution, as it happens for
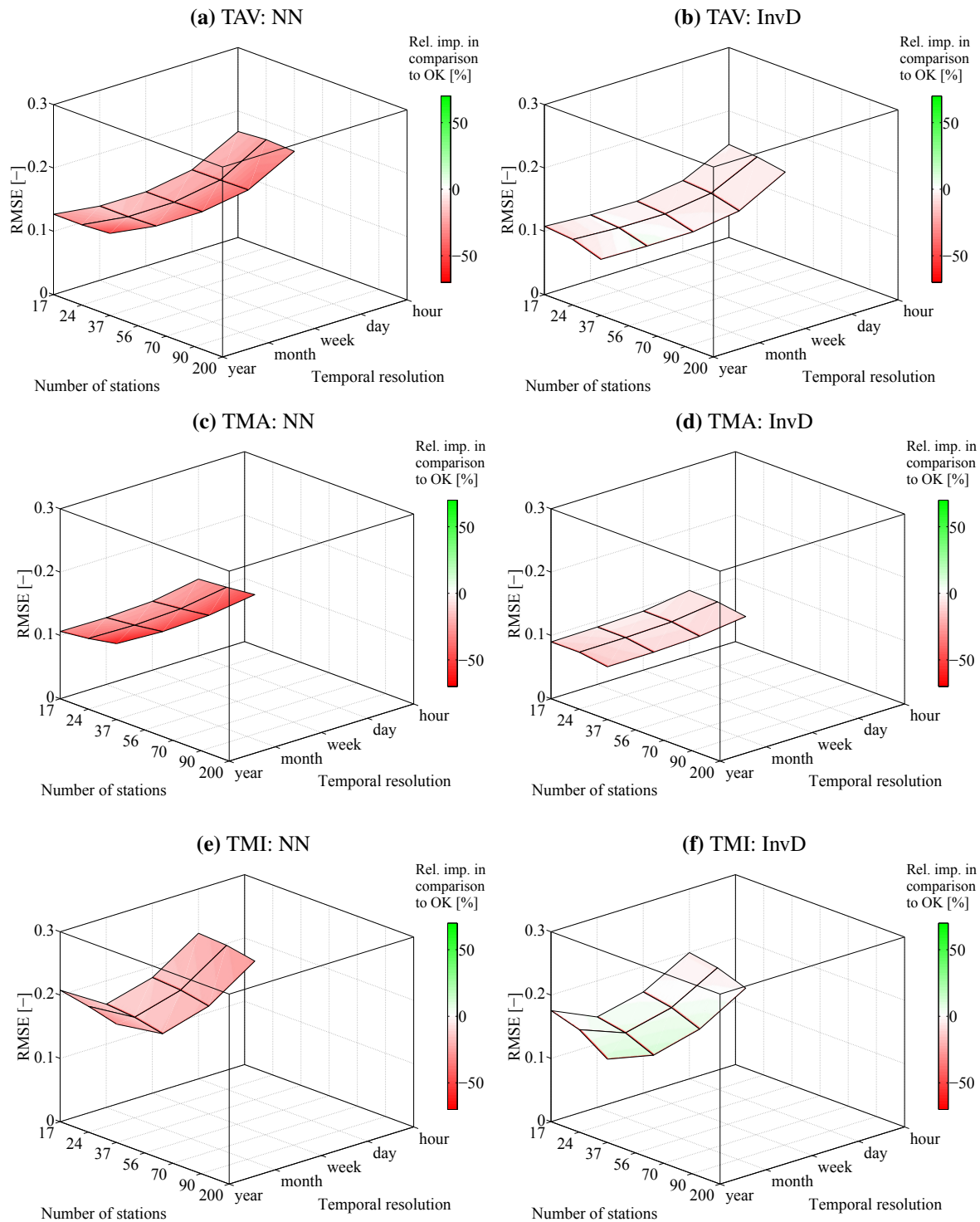
Figure 6.12: Interpolation performance of mean temperature (top), max temperature (middle) and minimum temperature (bottom) using NN and InvD in comparison with OK for hourly to yearly time periods and all network density scenarios

(a) TAV: KED (DEM)

(b) TAV: KED (HUM)

(c) TMA: KED (DEM)

(d) TMA: KED (HUM)

(e) TMI: KED (DEM)

(f) TMI: KED (HUM)
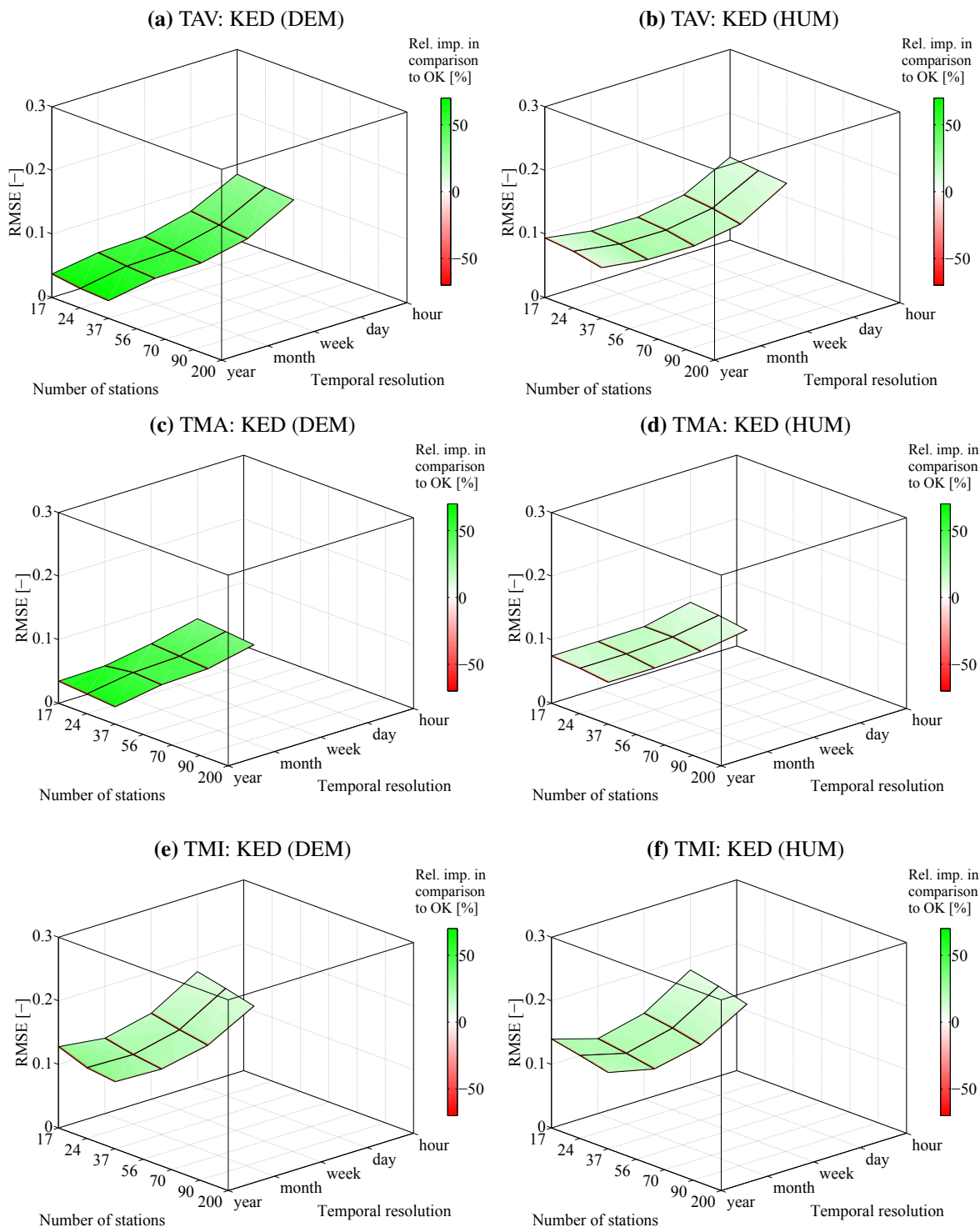
Figure 6.13: Interpolation performance of mean temperature (top), max temperature (middle) and minimum temperature (bottom) using KED (DEM) and KED (Humidity) in comparison with OK for hourly to yearly time periods and all network density scenarios

rainfall. For minimum temperature, the interpolation of annual data scale performs worse than the interpolation on a monthly time scale although there is an increase of performance with decreasing temporal resolution for hourly to monthly data. The same happens for mean annual temperature but the effect is significantly weaker. All univariate interpolation methods and KED (HUM) achieve slightly worse interpolation performances for monthly and annual data. The variogram analysis showed a weaker spatial dependency for these time scales. KED using the elevation allows by far the best interpolation performance and delivers a continuous improvement of RMSE with decreasing temporal resolution. Huge improvements are especially seen for the annual and monthly time scale.

Table 6.12 contains the Bias, RMSE and RVar interpolation performance of mean temperature. The values given for each temporal resolution are averaged over all station densities. Appendix B.1 contains all interpolation performances for maximum and minimum temperature. The Bias of the geostatistical techniques is in general lower than the Bias of NN and InvD. OK delivers always the best interpolation performance in terms of this criterion, however, OK also creates, due to the rather high number of neighbouring stations taken into account, a very smooth surface of the interpolated variable. This is indicated by the lowest preservation of variance expressed by the RVar criterion. InvD and the two KED implementations achieve a similar interpolation performance according to this measure. NN generates a higher variance than the

Table 6.12: Average interpolation performance (Bias, RMSE, RVar) for hourly to annual mean temperature over all station density scenarios

Method	Additional information	Criterion	Temporal resolution				
			Hour	Day	Week	Month	Year
NN	–	Bias [°C]	−0.216	−0.161	−0.175	−0.162	−0.225
		RMSE [-]	0.169	0.130	0.118	0.118	0.128
		RVar [-]	1.063	1.282	1.419	1.394	1.720
InvD	–	Bias [°C]	−0.093	−0.084	−0.095	−0.085	−0.123
		RMSE [-]	0.142	0.106	0.096	0.096	0.100
		RVar [-]	0.616	0.726	0.773	0.753	0.875
OK	–	Bias [°C]	−0.031	0.003	−0.004	0.008	−0.042
		RMSE [-]	0.138	0.103	0.094	0.098	0.095
		RVar [-]	0.349	0.420	0.414	0.361	0.494
KED	DEM	Bias [°C]	0.039	0.027	0.014	0.027	−0.015
		RMSE [-]	0.100	0.063	0.046	0.044	0.032
		RVar [-]	0.583	0.683	0.716	0.684	0.837
KED	HUM	Bias [°C]	0.051	0.037	0.025	0.038	0.000
		RMSE [-]	0.098	0.064	0.051	0.052	0.073
		RVar [-]	0.636	0.701	0.710	0.657	0.559

one present in the observed values. It is assumed that this is caused by the weather station located on the Brocken, the highest peak of the Harz Mountains. This station has by far the highest altitude (1141 m) and two neighboring stations with elevations of around 600 m or less (see Fig. 4.4). I case of NN cross validation, the temperature observation at the Brocken station is taken as the estimate for both stations with a rather low altitude while only the temperature observation of one low altitude station is used as the estimate for the Brocken location. Due to the smoothing effect or the additional information taken into account, this phenomenon is not as severe for the other interpolation techniques.

6.4 Humidity

6.4.1 Spatial variability and persistence

Figure 6.14 shows the experimental variograms and the fitted theoretical models for relative humidity. Again, station data were used and all available time steps were taken into account for the computation of the average variogram. The same automatic fitting procedure as for the variograms shown before was used, i.e. a maximum value of 1.5 was taken as the upper limit of the partial sill c of the exponential model. The corresponding parameters obtained from the fitting procedure are shown in Tab. 6.13.

A clear spatial persistence is present in the recordings of relative humidity. However the variograms tend to have relatively high nugget values, in particular for the temporal resolution of 1 h. The variogram obtained for hourly data has a higher range a_{eff} compared to the variograms for other temporal resolutions. It appears that the mean slope of the variogram is increasing with an expansion of the time interval, i.e. annual relative humidity has a steeper incline of variogram value than hourly relative humidity.

Table 6.13: Parameters of the exponential variogram model for relative humidity

Temporal resolution	c_0 [-]	c [-]	a_{eff} [m]
Hour	0.58	1.50	315,585
Day	0.34	1.18	112,967
Week	0.30	1.10	88,222
Month	0.31	1.11	85,854
Year	0.25	1.50	117,198
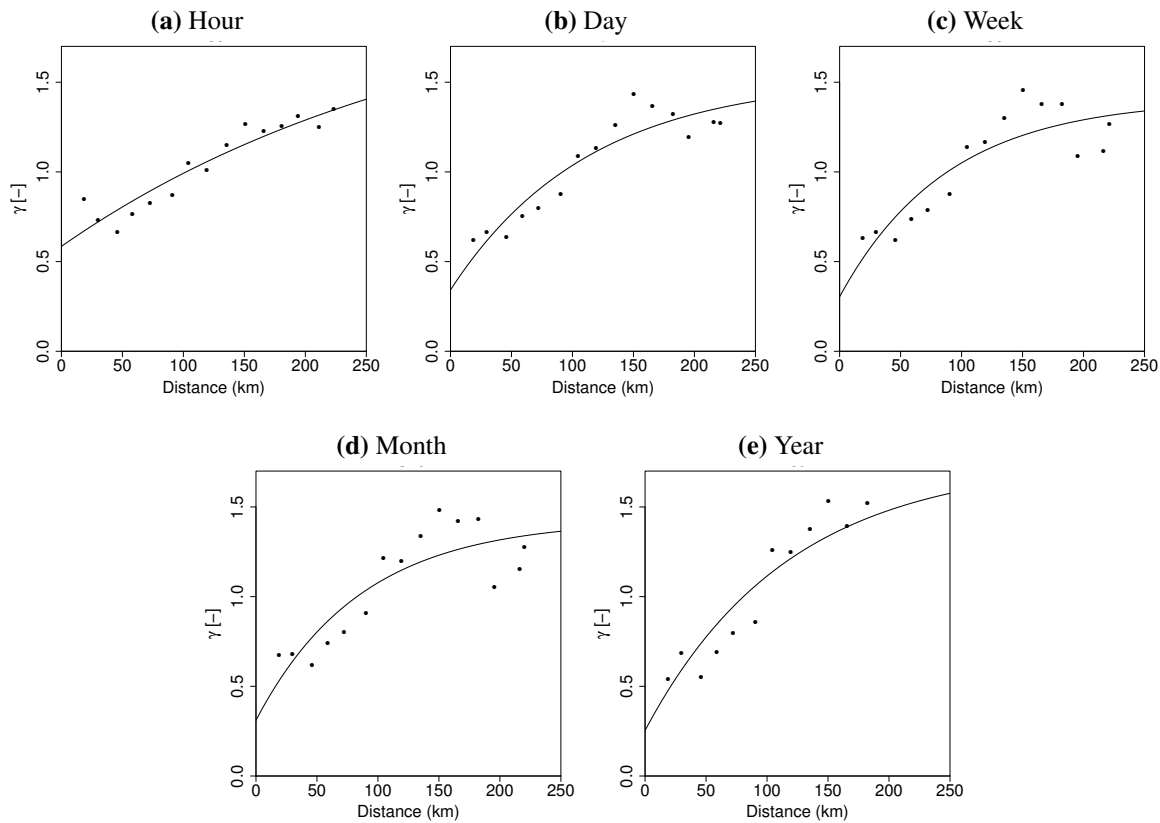
Figure 6.14: Experimental and theoretical average variograms of relative humidity

Due to the high nugget effect of 0.58, a lower interpolation performance of relative humidity on an hourly time scale is expected compared to other temporal resolutions.

6.4.2 Additional information

The relative humidity is defined as the ratio of the actual water vapor present in the air and the maximum water vapor that can be stored without condensation to liquid water. The maximum water vapor depends generally on temperature, i.e. warm air can store more water than cold air. Due to the fact that the temperature correlates negatively with the elevation, it is assumed that there could be also a relation between elevation and relative humidity. Table 6.14 shows the

Table 6.14: Spatial correlation between elevation and relative humidity averaged over all available time steps

Temporal resolution	Hour	Day	Week	Month	Year
Correlation [-]	0.097	0.292	0.356	0.409	0.492

correlation between the two spatial variables. A moderate correlation is seen for low temporal resolutions, while there is almost no spatial correlation for hourly data.

Other meteorological observations were also tested as additional variables for the interpolation of relative humidity. As mentioned before, these variable were interpolated on a $1\,\mathrm{km} \times 1\,\mathrm{km}$ grid prior to the implementation in KED. Due to the relation of temperature and dew point, it is in particular expected that the use of temperature information could deliver an advantage in comparison to univariate interpolation. Moreover, rainfall data were considered as an additional information in KED. The number of rain gauges is significantly higher than the number of stations with humidity recordings and even the entire spatial rainfall distribution from radar is available.

6.4.3 Evaluation of interpolation performance

Figure 6.15 illustrates the RMSE cross validation results obtained for relative humidity using NN and InvD in comparison with OK. The performance criteria were computed for all time steps of each temporal resolution in the period from 2008 to 2013 and averaged in order to determine the mean interpolation performance for each combination of temporal resolution and network density. As for temperature, all available time steps were used for the performance evaluation since there are no time steps with only zero recordings for all stations.

The evaluations show that NN and InvD perform worse than OK for almost all temporal resolutions and network densities. The NN interpolation performance is around 22 % to 40 %
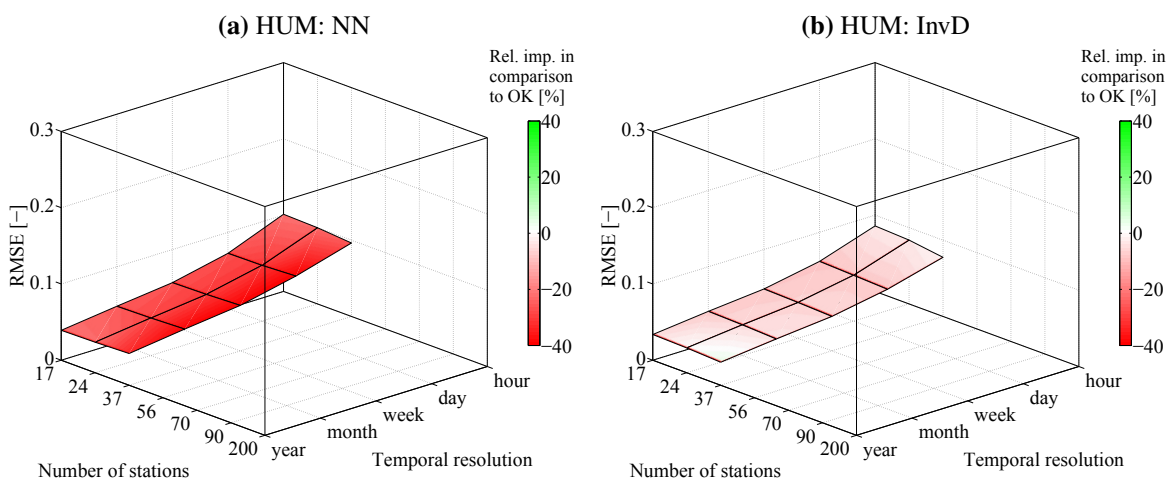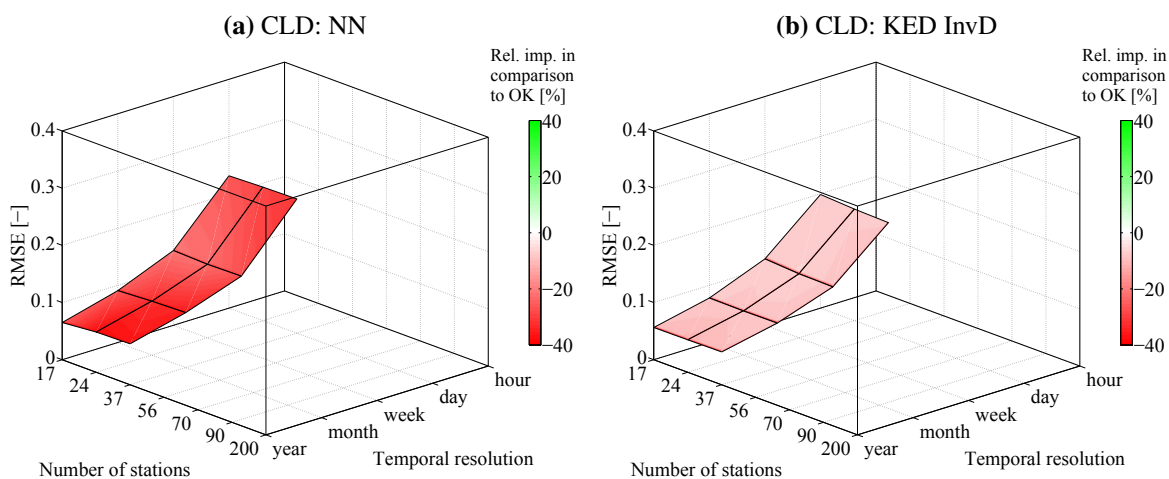

Figure 6.15: Interpolation performance of relative humidity using NN and InvD in comparison with OK for hourly to yearly time periods and all network density scenarios

worse and there is a particular decline for the network density scenario consisting of 37 stations. InvD performs up to 8 % worse than OK. There is only a minor improvement of approx. 3 % for annual data when 37 stations are used.

Cross validation results of KED are shown in Fig. 6.16. The DEM and interpolated grids of temperature and rainfall were used as additional information. Moreover, the number of 5 min time steps with rainfall was computed from each radar grid point for each time step of all temporal resolutions. This information was used as background data in KED as well. OK was applied for the interpolation of rainfall grids, since no interpolation method using either radar or the DEM could achieve a consistent improvement of interpolation performance for all temporal resolutions and network densities (cf. Sec. 6.2.3). The preparation of the temperature grids was carried out using KED, since the incorporation of the DEM could improve the interpolation
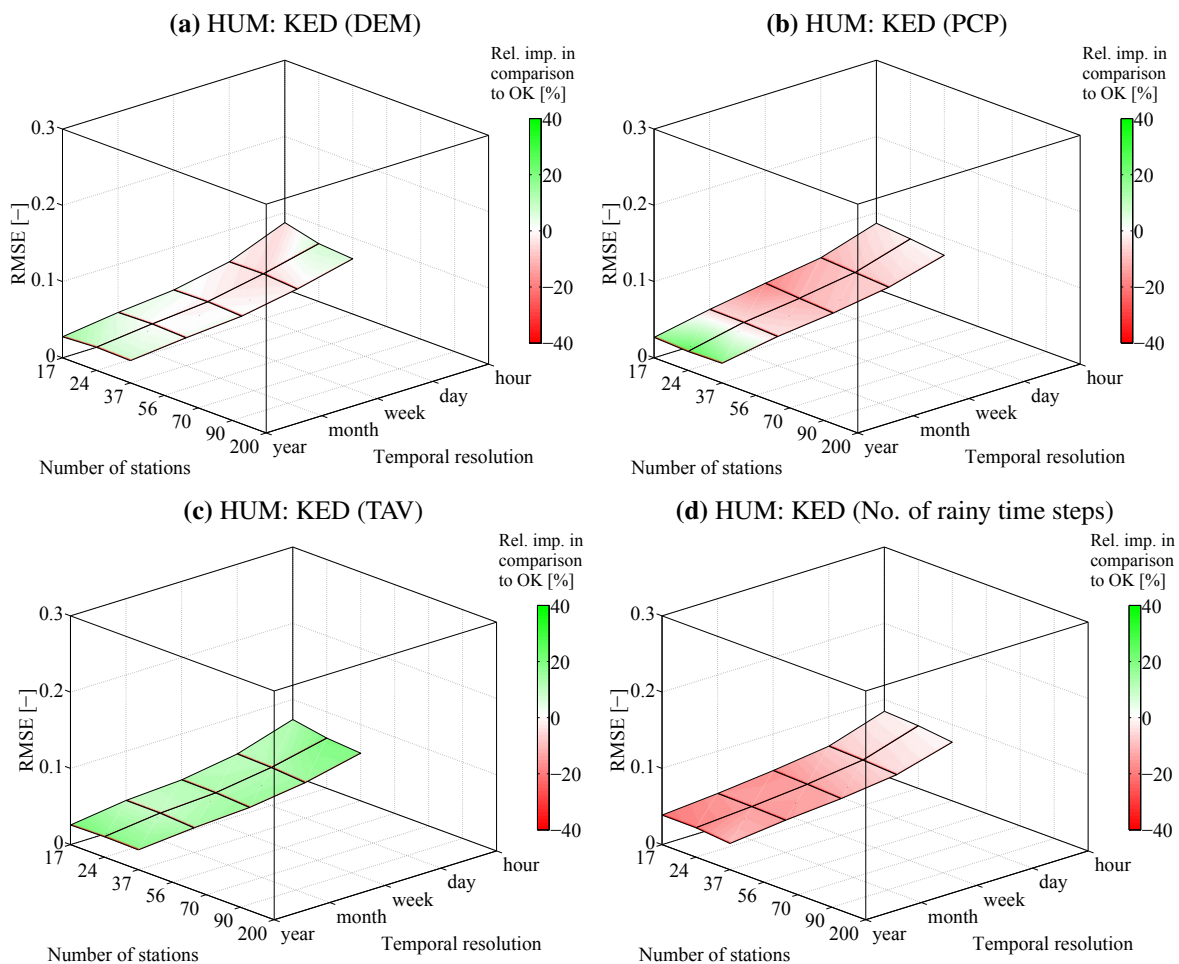
Figure 6.16: Interpolation performance of relative humidity using KED (DEM), KED (PCP), KED (TAV) and KED (Number of wet time steps) in comparison with OK for hourly to yearly time periods and all network density scenarios

performance considerably (cf. 6.3.3) for all combinations of temporal resolutions and network density.

For relative humidity, the interpolation performance of KED using the elevation improves only for some combinations of station density and temporal resolution in comparison to OK. The maximum improvement (approx. 15 %) illustrated by the green color shading in the upper left panel of Fig. 6.16 occurs for annual data using 17 stations. The decline in interpolation performance observed for some combinations of station density and temporal resolution reaches 5 %. The upper right panel of Fig. 6.16 shows that KED using OK interpolated rainfall can improve the interpolation performance only for the annual time scale. An improvement of 18 %

Table 6.15: Average interpolation performance (Bias, RMSE, RVar) for hourly to annual mean relative humidity over all station density scenarios

Method	Additional information	Criterion	Temporal resolution				
			Hour	Day	Week	Month	Year
NN	–	Bias [%]	0.777	0.345	0.345	0.344	0.347
		RMSE [-]	0.099	0.074	0.058	0.050	0.040
		RVar [-]	1.035	1.216	1.295	1.332	1.465
InvD	–	Bias [%]	0.404	0.250	0.251	0.250	0.250
		RMSE [-]	0.082	0.060	0.047	0.040	0.032
		RVar [-]	0.581	0.656	0.668	0.670	0.700
OK	–	Bias [%]	0.193	−0.098	−0.082	−0.084	−0.113
		RMSE [-]	0.081	0.056	0.044	0.038	0.032
		RVar [-]	0.272	0.358	0.352	0.337	0.286
KED	DEM	Bias [%]	0.211	−0.026	−0.021	−0.022	−0.034
		RMSE [-]	0.078	0.057	0.044	0.037	0.029
		RVar [-]	0.641	0.854	0.920	0.973	1.081
KED	PCP	Bias [%]	0.188	−0.066	−0.035	−0.116	−0.139
		RMSE [-]	0.082	0.061	0.049	0.040	0.026
		RVar [-]	0.334	0.633	0.846	0.809	0.914
KED	TAV	Bias [%]	0.066	−0.024	−0.050	−0.072	−0.119
		RMSE [-]	0.067	0.049	0.038	0.034	0.026
		RVar [-]	0.745	0.842	0.925	1.001	1.175
KED	No. of wet time steps	Bias [%]	0.193	−0.083	−0.034	−0.021	−0.107
		RMSE [-]	0.081	0.059	0.050	0.043	0.037
		RVar [-]	0.287	0.495	0.706	0.731	0.844
KED	SUN	Bias [%]	0.171	−0.046	−0.111	−0.165	−0.142
		RMSE [-]	0.082	0.059	0.046	0.039	0.032
		RVar [-]	0.378	0.660	0.746	0.778	0.753
KED	WVE	Bias [%]	0.044	−0.141	−0.164	−0.164	−0.129
		RMSE [-]	0.096	0.069	0.055	0.048	0.040
		RVar [-]	0.708	0.816	0.957	1.054	1.154

to 25 % in comparison to OK is achieved for yearly data, while the interpolation performance declines by around 1 % to 17 % for the other temporal resolutions. KED using temperature grids delivers a consistent improvement of interpolation performance for all temporal resolutions and station density scenarios. The improvement ranges from 9 % to 20 %. The estimation could not be improved by using the number of rainy time steps as an additional information in KED. Besides the additional information displayed in Fig. 6.16, sunshine duration and wind velocity were used in combination with KED. The incorporation of both additional variables could not improve the RMSE interpolation performance in comparison to OK either. The results are shown in Appx. B.2.

An increase of interpolation performance with decreasing temporal resolution is seen for all interpolation techniques. Similar to the interpolation of temperature, the effect of station density on the interpolation performance is hardly seen, i.e. there is only a minimal decrease of interpolation performance when the number of stations is reduced from 37 to 17. Table 6.15 contains the Bias, RMSE and RVar interpolation performance. The values given for each temporal resolution are averaged over all station densities. Also for relative humidity it is seen that the simple interpolation methods NN and InvD generate a higher bias than the geostatistical approaches. OK causes again the highest reduction of variance, while KED using temperature grids achieves a good variance preservation.

6.5 Cloud coverage

6.5.1 Spatial variability and persistence

Figure 6.17 shows the experimental variograms and the fitted theoretical models for cloud coverage. Again, station data were used and all available time steps were taken into account for the computation of average variograms for the daily to annual time scale. The availability of hourly cloud coverage measurements varies much stronger as it is seen in Fig. 4.2. Due to the

Table 6.16: Parameters of the exponential variogram model for cloud coverage

Temporal resolution	c_0 [-]	c [-]	a_{eff} [m]
Hour	0.10	0.97	$33,301$
Day	0.64	1.50	$359,219$
Week	0.62	1.50	$327,490$
Month	0.64	1.50	$318,020$
Year	0.54	1.50	$210,505$
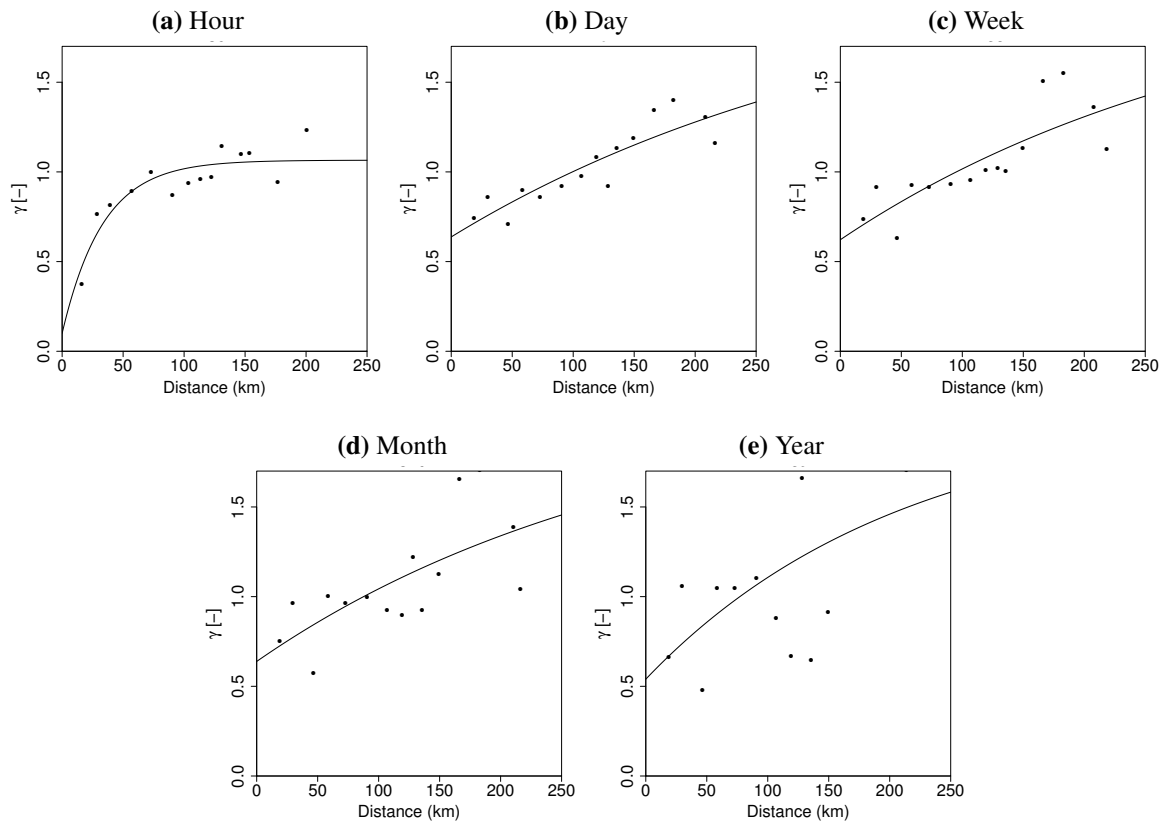
Figure 6.17: Experimental and theoretical average variograms of cloud coverage

high number of missing values usually occurring in the night hours, a threshold of available cloud coverage recordings was established in order to filter out time steps with too few data. Twelve non-missing recordings had to be available for a time step to be taken into account for variogram estimation and cross validation analysis. The same automatic fitting procedure as for the variograms shown before was used, i.e. a maximum value of 1.5 was used as the upper limit of the partial sill c of the exponential model. The corresponding parameters obtained from the fitting procedure are shown in Tab. 6.16.

Similar to temperature, the spatial persistence is more obvious and clear for high temporal resolutions. The fitting of the exponential model is easy for hourly and daily data, while the points of the experimental variogram scatter strongly around the theoretical model for longer time scales. The variogram parameters obtained for the hourly temporal resolution differ significantly from the parameters for other time scales. Nugget effect c_0 and the range a_{eff} are significantly lower. However, this is only caused by the variogram point obtained for the shortest distance class. The variogram behaviour for longer distances is rather similar. The difference in the lowest distance class might be explained by the different number of stations for

hourly data (see Tab. 4.2) and the implication that less point pairs are available for this distance class. When comparing the variogram parameters from daily to annual temporal resolution, it is noticed that there is a decrease of range and nugget effect.

6.5.2 Additional information

Several meteorological observations were tested as additional variables for the interpolation of cloud coverage. As for other climate data, these variables were interpolated on a $1 \, km \times 1 \, km$ grid prior to the implementation in KED. Besides the DEM, interpolated grids of gauge rainfall, sunshine duration and mean temperature were used. In particular sunshine duration is assumed to be related to cloud coverage information. Moreover, radar rainfall and the number of rainy 5 min time steps computed for each radar grid point were used as additional information in KED. The general idea behind the use of rainfall and the amount of wet time steps is, that the occurrence of rainfall is always associated with the occurrence of clouds. Despite the fact that clouds can also occur for dry time steps, it is expected that locations with more rainfall or a higher number of rainy 5 min time steps show higher cloud coverage values as well.

6.5.3 Evaluation of interpolation performance

Figure 6.18 shows the interpolation performance of NN and InvD in comparison with OK for cloud coverage. The performance criteria were computed for all time steps of the daily to annual time scale in the period from 2009 to 2011. For the hourly temporal resolution, only time steps with a sufficient number of available recordings were considered. All performances are averaged over the time steps taken into account in order to determine the mean interpolation performance for each combination of temporal resolution and network density scenario. Table 6.17 contains the number of time steps taken into account for each temporal resolution.

Table 6.17: Number of time steps considered for the cross validation of cloud coverage

Temporal resolution	Hour	Day	Week	Month	Year
No. of consid. time steps	20231	1084	156	36	3

NN and also InvD cannot reach the interpolation performance of OK (see Fig. 6.18). NN performs around 22 % to 36 % percent worse, while InvD shows a decrease of interpolation performance by approx. 5 % to 11 %.
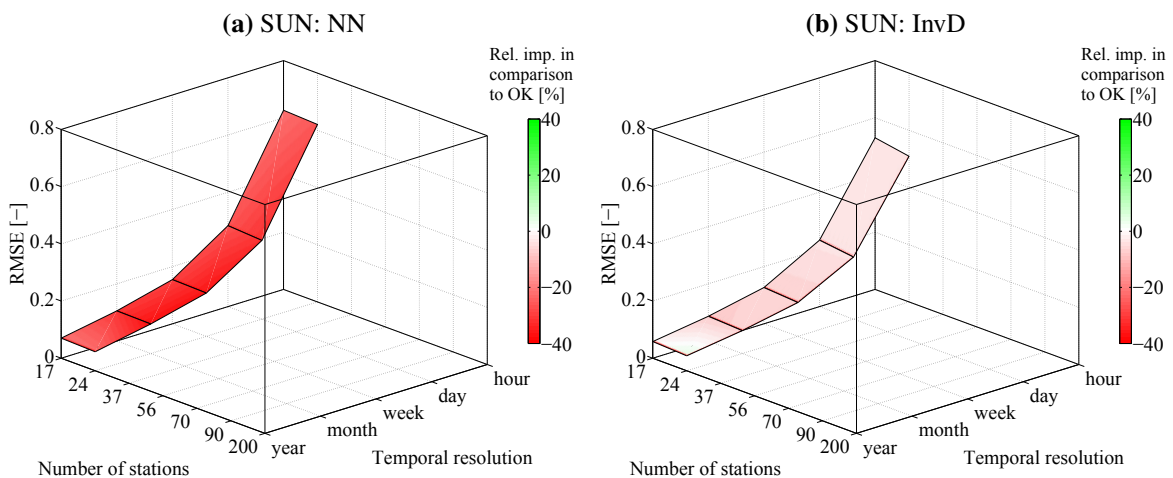
Figure 6.18: Interpolation performance of cloud coverage using NN and InvD in comparison with OK for hourly to yearly time periods and all network density scenarios
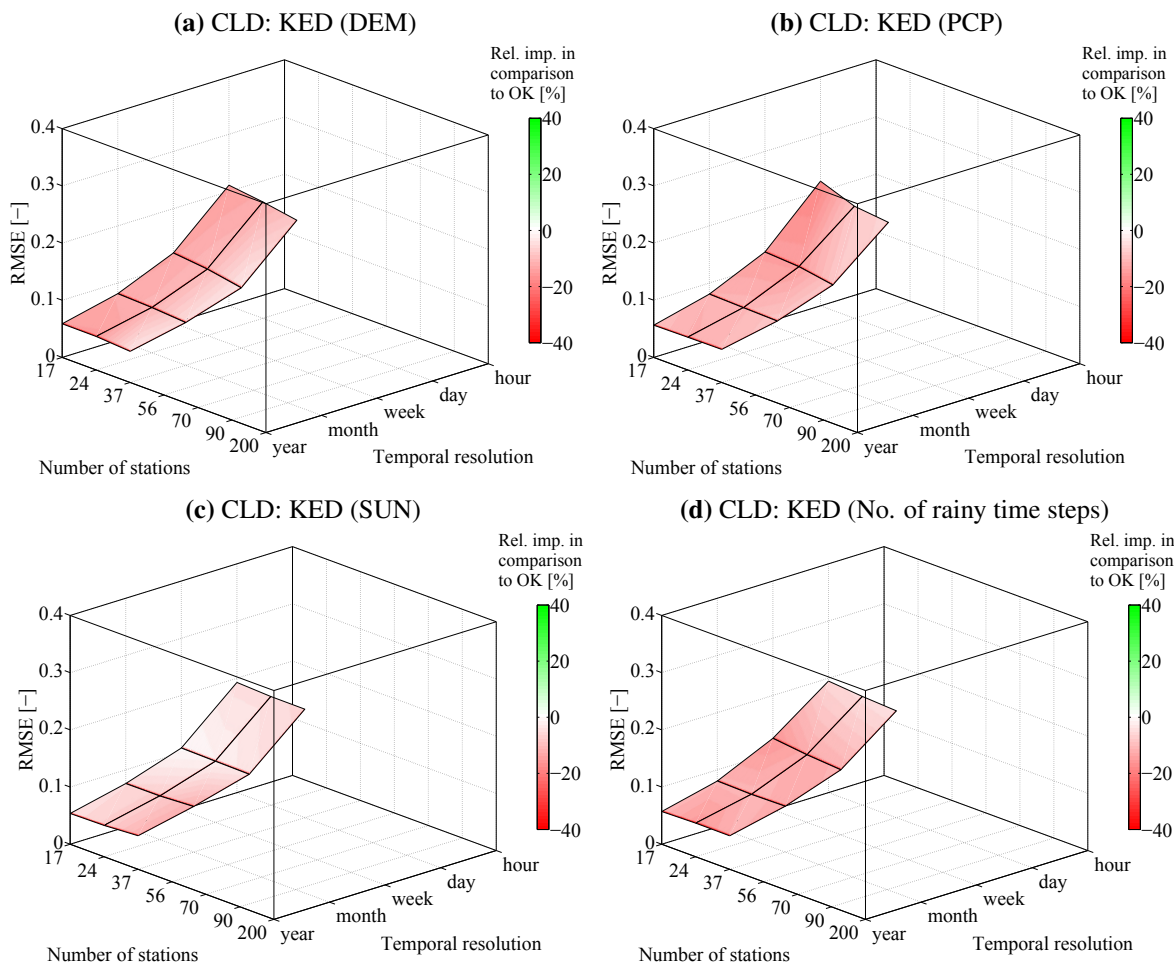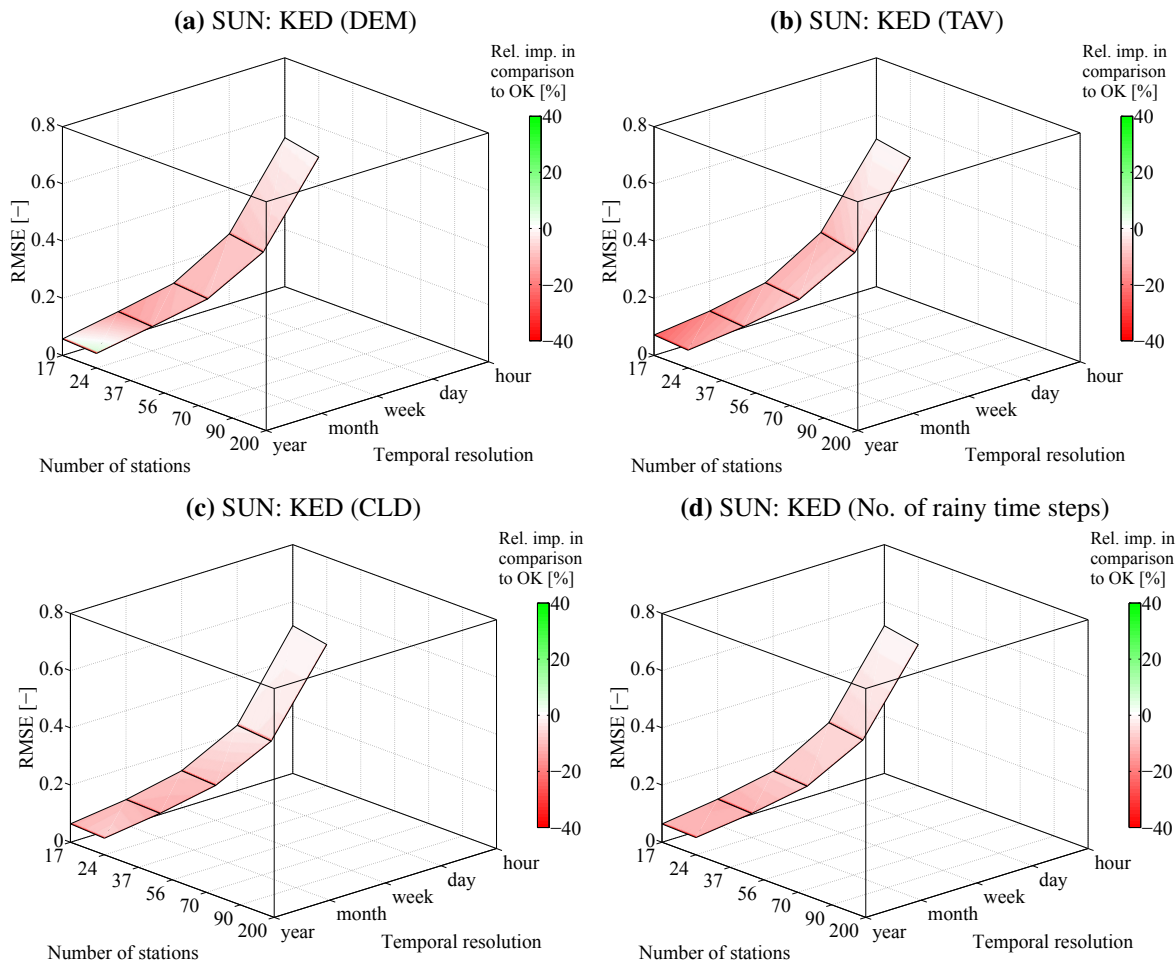

Figure 6.19: Interpolation performance of cloud coverage using KED (DEM), KED (PCP), KED (SUN) and KED (Number of wet time steps) in comparison with OK for all time periods and density scenarios

The interpolation performance of KED in comparison to OK is presented in Fig. 6.19. It is seen that neither for the elevation nor the interpolated rain gauge data an improvement is achieved. Also the use of sunshine duration and the number of wet 5 min time steps result in a decline of interpolation performance for all combinations of temporal resolution and network density. The plots of KED using radar rainfall and mean temperature are shown in Appx. B.3. An improvement is not seen for any of the additional information that was tested. It would be another idea to incorporate remote sensing data of cloud coverage. Different efforts were made, for instance by ROSSOW and SCHIFFER (1991), in order to estimate cloud coverage using weather satellites. However, as far as the author knows, no data product is available for the study region with a sufficient resolution in space and time.

Table 6.18: Average interpolation performance (Bias, RMSE, RVar) for hourly to annual cloud coverage over all station density scenarios

Method	Additional information	Criterion	Temporal resolution				
			Hour	Day	Week	Month	Year
NN	–	Bias [1/8]	0.009	0.043	0.041	0.047	0.048
		RMSE [-]	0.396	0.233	0.130	0.094	0.069
		RVar [-]	0.909	0.990	0.989	1.068	1.092
InvD	–	Bias [1/8]	0.008	0.022	0.038	0.025	0.026
		RMSE [-]	0.338	0.196	0.113	0.078	0.057
		RVar [-]	0.438	0.536	0.532	0.555	0.557
OK	–	Bias [1/8]	0.025	0.020	0.015	0.019	0.018
		RMSE [-]	0.323	0.182	0.106	0.072	0.052
		RVar [-]	0.202	0.245	0.200	0.235	0.248
KED	DEM	Bias [1/8]	0.057	0.016	0.001	0.009	0.008
		RMSE [-]	0.360	0.203	0.115	0.078	0.057
		RVar [-]	0.469	0.567	0.573	0.622	0.647
KED	PCP	Bias [1/8]	0.030	0.029	0.015	0.012	0.005
		RMSE [-]	0.331	0.201	0.118	0.079	0.057
		RVar [-]	0.245	0.445	0.549	0.552	0.613
KED	SUN	Bias [1/8]	0.026	0.014	0.007	0.010	0.010
		RMSE [-]	0.320	0.191	0.107	0.077	0.056
		RVar [-]	0.308	0.548	0.617	0.620	0.606
KED	No.of rainy time steps	Bias [1/8]	0.025	0.019	0.014	0.017	0.004
		RMSE [-]	0.324	0.191	0.119	0.080	0.058
		RVar [-]	0.214	0.339	0.491	0.556	0.590
KED	TAV	Bias [1/8]	0.039	0.009	0.013	0.002	0.002
		RMSE [-]	0.039	0.009	0.013	0.002	0.002
		RVar [-]	0.439	0.525	0.635	0.607	0.564
KED	Radar	Bias [1/8]	0.025	0.024	0.020	0.020	0.013
		RMSE [-]	0.323	0.188	0.119	0.084	0.059
		RVar [-]	0.203	0.291	0.454	0.605	0.527

Bias, RMSE and RVar interpolation performance are shown in Tab. 6.18. The value given for specific temporal resolutions are averaged over all station density scenarios. Geostatistical interpolation techniques deliver a lower bias than NN and InvD in most cases. The smoothing effect of OK causes again a strong reduction of the spatial variance, while only NN can preserve it in its entirety.

6.6 Sunshine duration

6.6.1 Spatial variability and persistence

Figure 6.20 contains the experimental variograms and the fitted theoretical models for sunshine duration. Station data were used, whereas not all available time steps were taken into account for the computation of the average variograms for the hourly to annual time scale. A threshold for the mean of the observations of 0.1 min or 0.1 h was established for the hourly or all other temporal resolutions, respectively. The idea was to leave out time steps with no sunshine at all in order to compute a more accurate variogram and also average interpolation performance for time steps that have a non-uniform spatial distribution of sunshine duration. Mainly the night time steps of the hourly temporal resolution and some hourly time steps that are entirely without sun are removed by this constraint. An identical automatic fitting procedure as for the variograms shown before was used for estimating the parameters of the exponential model. A maximum value of 1.5 was used as the upper limit of the partial sill c in order to allow a stable fitting. The corresponding parameters that were obtained for each temporal resolution are shown in Tab. 6.19.

The spatial persistence of sunshine duration is clear and distinct for rather high temporal resolutions. In case of larger time scales, in particular for the annual scale, there are higher deviations of the experimental points from the theoretical variogram model. A similar behaviour was observed for temperature and cloud coverage, as it was shown before. However, for

Table 6.19: Parameters of the exponential variogram model for sunshine duration

Temporal resolution	c_0 [-]	c [-]	a_{eff} [m]
Hour	0.41	1.50	207,469
Day	0.16	1.50	110,546
Week	0.09	1.50	105,682
Month	0.04	1.50	103,387
Year	0.27	0.91	92,205
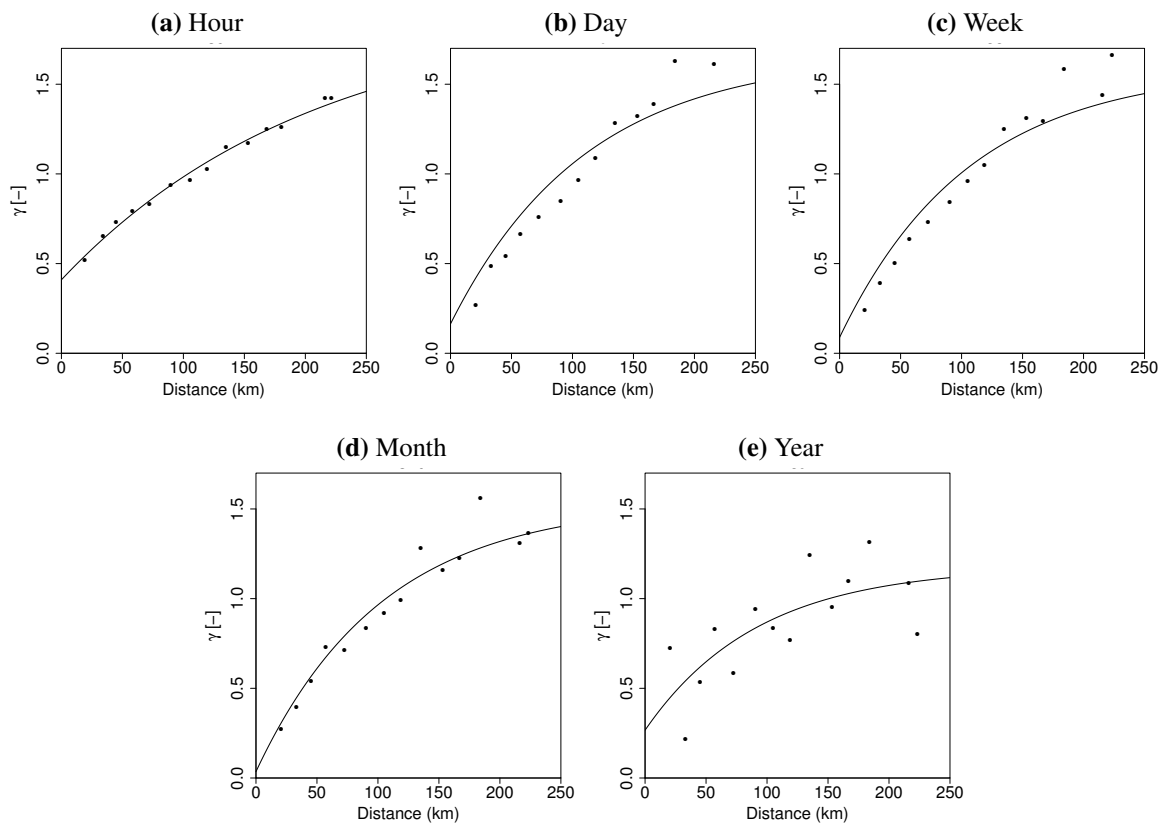
Figure 6.20: Experimental and theoretical average variograms of sunshine duration

sunshine duration, the decrease of spatial persistence with decreasing temporal resolution appears to be less strong. A relatively high nugget effect c_0 is seen for a temporal resolution of 1 h. Daily, weekly and monthly average sunshine durations show in contrast to that really low nugget values, while the nugget value obtained for the annual time scale is again slightly higher. A lower interpolation quality of hourly sunshine duration is expected due to this behaviour.

6.6.2 Additional information

Various other climate variables were tested as additional variables for the interpolation of sunshine duration. As for the interpolation of other climate data, these variables were interpolated on a 1 km × 1 km grid prior to the application of KED using these grids as additional information. The DEM, as well as these grids of gauge rainfall, cloud coverage and mean temperature were tested with regard to a possible benefit for the spatial interpolation of sunshine duration measurements. It is expected that in particular cloud coverage might be able to provide useful additional information. Moreover, radar rainfall and the number of rainy 5 min time

steps computed for each radar grid point were incorporated in KED, since the occurrence of rainfall usually implies the presence of clouds.

6.6.3 Evaluation of interpolation performance

Figure 6.21 shows the interpolation performance of NN and InvD in comparison with OK for sunshine duration. The performance criteria were computed for all time steps where an average sunshine duration of 0.1 min or 0.1 h is exceeded, depending on the temporal data resolution. All interpolation performances are averaged over the time steps that were taken into account in order to determine the mean performance for each combination of temporal resolution and network density scenario. Table 6.20 contains the number of time steps that was taken into account for each temporal resolution.

Table 6.20: Number of time steps considered for the cross validation of sunshine duration

Temporal resolution	Hour	Day	Week	Month	Year
No. of consid. time steps	18759	2014	313	72	6

It is observed that NN as well as InvD cannot reach the interpolation performance of OK. NN performs approx. 21 % to 36 % worse. For InvD, only the scenario with 24 stations shows an increase in interpolation performance of around 5 %. The performance in comparison to OK decreases for all other combinations, whereat the maximum decline is approx. 7 %.
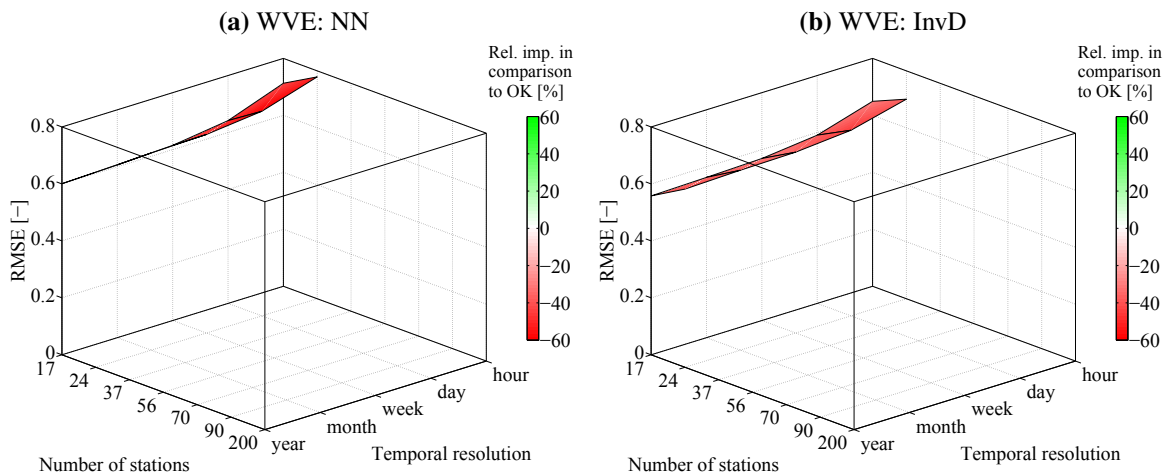

Figure 6.21: Interpolation performance of sunshine duration using NN and InvD in comparison with OK for hourly to yearly time periods and all network density scenarios

(a) SUN: KED (DEM)

(b) SUN: KED (TAV)

(c) SUN: KED (CLD)

(d) SUN: KED (No. of rainy time steps)

Figure 6.22: Interpolation performance of sunshine duration using KED (PCP), KED (TAV), KED (CLD) and KED (Number of wet time steps) in comparison with OK for all time periods and network densities scenarios

The interpolation performance in comparison to OK of KED (PCP), KED (TAV), KED (CLD) and KED using the number of rainy 5 min time steps computed from radar is shown in Fig. 6.22. It is seen that no general improvement is achieved, regardless of the additional information that is used. Only the use of interpolated rain gauge rainfall (PCP) results in a slight improvement of interpolation performance on the annual time scale, i.e. KED performs approx. 1 % to 5 % better. The plots of KED using elevation and radar rainfall are presented in appendix B.4.

Table 6.21 contains Bias, RMSE and RVar interpolation performance. The values given for specific temporal resolutions are averaged over all station density scenarios. OK delivers a lower bias than NN and InvD for all combinations of station density and temporal resolution. No interpolation technique apart from NN achieves a full variance preservation. OK causes again the strongest reduction of the observation variance.

Table 6.21: Average interpolation performance (Bias, RMSE, RVar) for hourly to annual sunshine duration over all station density scenarios

Method	Additional information	Criterion	Temporal resolution				
			Hour	Day	Week	Month	Year
NN	–	Bias [h]	−0.012	−0.038	−0.032	−0.032	−0.032
		RMSE [-]	0.624	0.279	0.153	0.104	0.068
		RVar [-]	0.926	0.941	1.001	1.034	0.930
InvD	–	Bias [h]	−0.004	−0.016	−0.012	−0.012	−0.014
		RMSE [-]	0.520	0.225	0.122	0.083	0.055
		RVar [-]	0.527	0.592	0.627	0.628	0.527
OK	–	Bias [h]	0.001	−0.004	−0.005	−0.005	−0.003
		RMSE [-]	0.505	0.217	0.116	0.078	0.056
		RVar [-]	0.306	0.432	0.479	0.483	0.270
KED	PCP	Bias [h]	0.001	0.024	0.006	−0.001	0.006
		RMSE [-]	0.509	0.234	0.127	0.088	0.054
		RVar [-]	0.315	0.562	0.645	0.677	0.638
KED	TAV	Bias [h]	−0.001	0.002	−0.016	−0.021	−0.014
		RMSE [-]	0.505	0.236	0.126	0.089	0.067
		RVar [-]	0.306	0.633	0.790	0.967	1.112
KED	CLD	Bias [h]	−0.001	0.013	0.001	−0.004	0.011
		RMSE [-]	0.505	0.222	0.126	0.087	0.061
		RVar [-]	0.306	0.687	0.696	0.698	0.615
KED	No. of rainy time steps	Bias [h]	−0.002	0.006	0.000	−0.002	0.006
		RMSE [-]	0.505	0.229	0.124	0.087	0.062
		RVar [-]	0.306	0.508	0.571	0.633	0.418
KED	DEM	Bias [h]	0.005	0.014	−0.012	−0.017	−0.019
		RMSE [-]	0.545	0.245	0.132	0.091	0.068
		RVar [-]	0.439	0.653	0.834	0.947	1.117
KED	Radar	Bias [h]	−0.002	0.003	−0.003	−0.009	−0.004
		RMSE [-]	0.505	0.225	0.123	0.083	0.058
		RVar [-]	0.306	0.475	0.552	0.535	0.299

6.7 Wind

6.7.1 Spatial variability and persistence

Figure 6.23 contains the experimental variograms and the fitted theoretical models for wind velocity. Station data were used for the inference and all available time steps were taken into account for the computation of the average experimental variogram. The same automatic fitting procedure as used for the other variables was used to estimate the parameters of the exponential model. The corresponding parameters obtained for each temporal resolution are shown in Tab. 6.22.

The experimental variograms show an unclear behaviour for lower temporal resolutions and a decent spatial persistence for hourly data. Among all meteorological observations, wind velocity shows the weakest relation between distance and similarity of recorded values. For weekly, monthly and annual data an objective manual fitting of the theoretical model was not possible, since no clear behaviour is seen. The cross validation of wind velocity is carried out
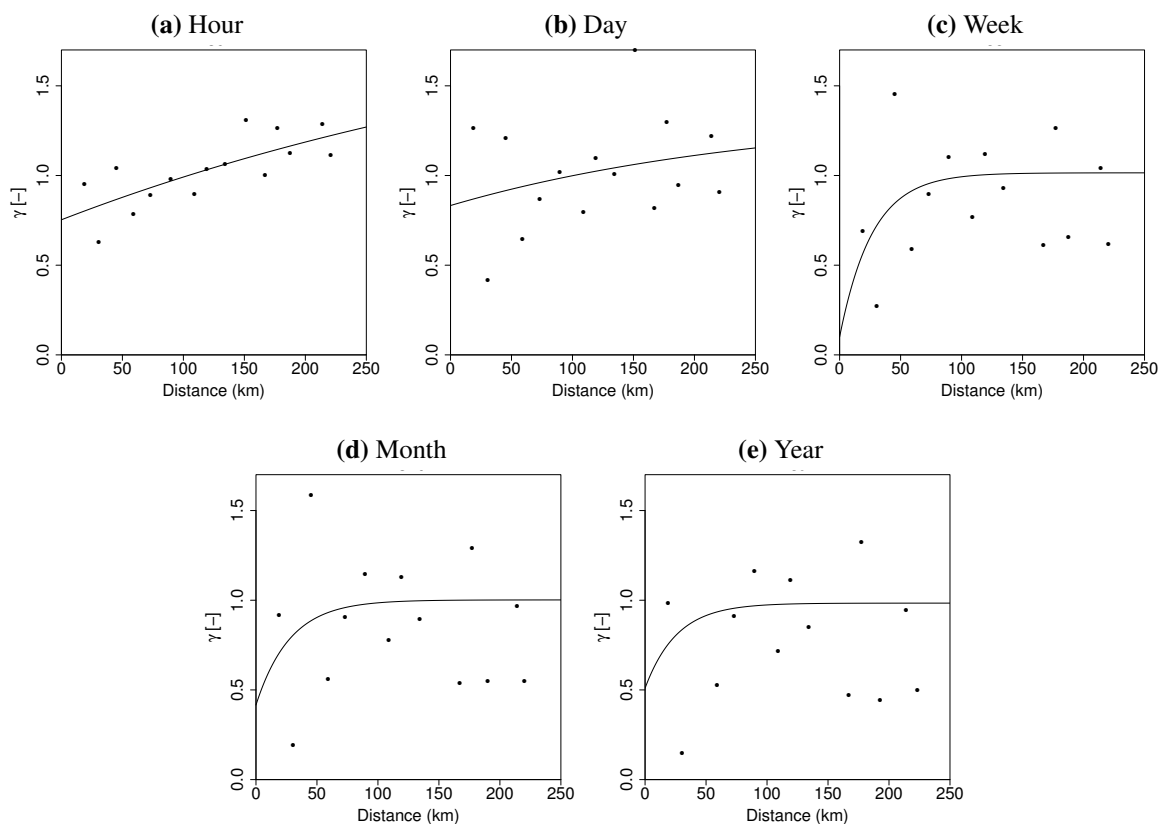
Figure 6.23: Experimental and theoretical average variograms of absolute wind velocity

Table 6.22: Parameters of the exponential variogram model for absolute wind velocity

Temporal resolution	c_0 [-]	c [-]	a_{eff} [m]
Hour	0.75	1.31	500,000
Day	0.83	0.52	258,859
Week	0.10	0.91	26,815
Month	0.42	0.59	27,898
Year	0.51	0.47	26,026

using the obtained variogram parameters regardless of the poor fitting result. Obviously a weak interpolation result is expected due to this.

Figure 6.24 contains the experimental variograms and the fitted theoretical models for the west-east and north-south component of hourly wind velocity, while Tab. 6.23 presents the corresponding parameters. The computation and fitting was conducted in the same manner as for absolute wind velocity. The spatial persistence of north-south velocity as well as west-east velocity seems to be noticeably better than the spatial persistence of absolute velocity. The parameters obtained for west-east and north-south differ considerably. The mismatch is only caused the low value of the first distance class of the experimental variogram for west-east wind velocity.

Table 6.23: Parameters of the exponential variogram model for hourly wind velocity components in west-east and north-south direction

Direction	c_0 [-]	c [-]	a_{eff} [m]
West-East	0.76	0.24	29,499
North-South	0.63	0.52	83,777

(a) Wind velocity W – E   **(b)** Wind velocity N – S
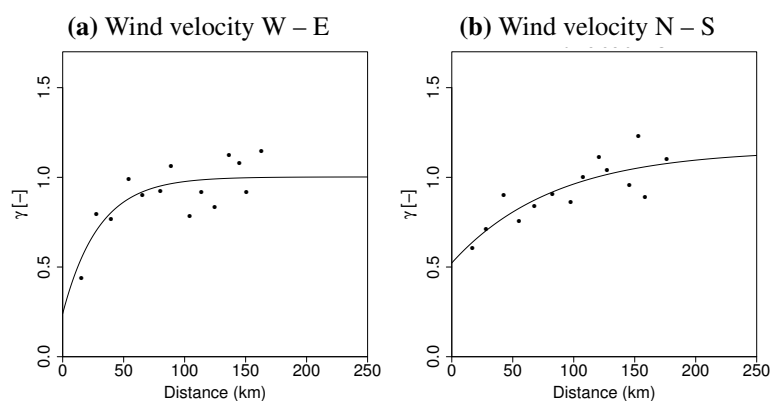
Figure 6.24: Experimental and theoretical average variograms of hourly wind velocity components in west-east and north-south direction

The 36 experimental and theoretical indicator variograms for hourly wind direction and the corresponding parameters are shown in Appx. A.2. Note that the values of the variograms for most directions are significantly lower. This is caused by the fact that the calculation is carried out using zeros and ones only (see Eq. 3.22). Moreover, no standardisation with the variance was applied to indicator variogram values. Generally, there are minor differences in the variograms inferred for different direction categories. Some of them show relatively high variogram values of around 1.0, while others show only maximum values of 0.2.

6.7.2 Additional information

Different additional information was used for the interpolation of wind data. The DEM could help to improve the estimation since exposed terrain locations are expected to have higher wind velocities. Furthermore, coastal regions are assumed to have higher wind velocities due to the lower surface roughness of the terrain. For each point of the interpolation grid, the distance to the coast was computed and used as an additional information in KED.

RUEL *et al.* (1998) carried out laboratory experiments and showed that the wind velocity in complex terrains depends strongly on the microtopography. According to them, hilltops are prone to have high wind velocities for all wind directions, whereas the wind velocity inside a valley depends strongly on the wind direction, the general valley form and other microtopographic factors. Similar results were obtained by NGO and LETCHFORD (2009), who analysed speed-up effects of wind gusts in an experimental study. Hence, it is expected that spatial interpolation using geostatistical approaches might not yield a good interpolation performance.

6.7.3 Evaluation of interpolation performance

Figure 6.25 shows the interpolation performance of NN and InvD in comparison with OK for absolute wind velocity. The performance criteria were computed for all available time steps of the investigation period and are averaged over the time steps that were taken into account in order to determine the mean interpolation performance for each combination of temporal resolution and network density scenario. It is observed that NN as well as InvD perform significantly worse in RMSE interpolation performance compared to OK. The NN interpolation error is around 39 % to 60 % and the InvD error around 29 % to 42 % higher. OK provides a significant advantage compared to these two simple interpolation methods.

The corresponding RMSE interpolation performance for KED is presented in Fig. 6.26. Both additional information, the elevation as well as the distance for each location to the North Sea coast, cannot improve the OK interpolation performance consistently for all temporal resolutions and network densities. KED using the DEM delivers a slightly better interpolation performance for some combinations of station density and temporal resolution. The maximum improvement is approx. 4 %. In general it seems to be implausible that the network density scenario based on 17 stations has a better interpolation performance than the scenario using 24 stations. In particular for NN and InvD, there is a striking difference between the interpolation quality achieved for these two densities. This irregular behaviour is explained by the cross validation setup of this study in combination with the exposedness of the weather station situated

Figure 6.25: Interpolation performance of wind velocity using NN and InvD in comparison with OK for hourly to yearly time periods and all network density scenarios
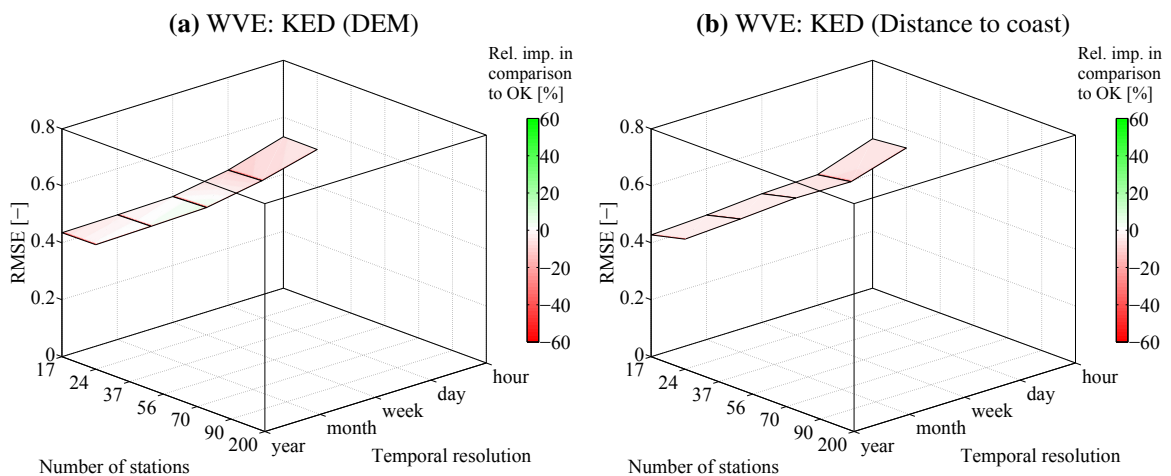
Figure 6.26: Interpolation performance of wind velocity using KED (DEM) and KED (Distance to coast) in comparison with OK for hourly to yearly time periods and all network density scenarios

on the Brocken mountain. The performance evaluation was conducted for ten realisations of each station density scenario, while the stations were selected randomly for the realisations of each scenario. The Brocken station is considered in all ten realisations of the 24 stations scenario and only in seven realisations of the scenario using 17 stations. A significantly higher interpolation error for this particular station causes a reduction of interpolation performance for the concerned realisations and also affects the corresponding average.

Table 6.24 contains Bias, RMSE and RVar interpolation performance. The values given for specific temporal resolutions are averaged over all network densities. The application of OK results in a lower bias compared to other interpolation techniques. With RVar values higher than 1.0, NN and InvD generate an overestimation of the spatial variance. It is assumed that this is phenomenon is also caused by the exposed location of the Brocken station. The observed value of this gauge is used as an estimate for two neighbouring stations in the same way as it happened in the cross validation of temperature data (cf. Sec. 6.3.3). The geostatistical methods, in particular OK, cause a strong smoothing and thus a reduction of estimation variance.

The interpolation of hourly wind data was carried out using two entirely different approaches. It was carried out separately for wind direction and wind velocity (A) and a combined interpolation of direction and velocity was carried out (B). In order to achieve a combined interpolation, wind velocity and wind direction were transformed into north-south and a west-east velocity

Table 6.24: Average interpolation performance (Bias, RMSE, RVar) for hourly to annual wind velocity over all station density scenarios

Method	Additional information	Criterion	Temporal resolution				
			Hour	Day	Week	Month	Year
NN	–	Bias [m/s]	0.330	0.331	0.328	0.329	0.334
		RMSE [m/s]	0.746	0.680	0.656	0.649	0.643
		RVar [-]	1.729	2.120	2.479	2.689	2.792
InvD	–	Bias [m/s]	0.309	0.309	0.308	0.310	0.314
		RMSE [-]	0.675	0.621	0.602	0.597	0.592
		RVar [-]	1.119	1.395	1.630	1.768	1.814
OK	–	Bias [m/s]	0.050	0.043	0.086	0.075	0.068
		RMSE [-]	0.508	0.443	0.456	0.439	0.427
		RVar [-]	0.225	0.204	0.429	0.377	0.332
KED	DEM	Bias [m/s]	−0.193	−0.211	−0.232	−0.231	−0.224
		RMSE [-]	0.531	0.478	0.444	0.439	0.436
		RVar [-]	0.451	0.466	0.499	0.520	0.549
KED	Distance to coast	Bias [m/s]	0.154	0.169	0.177	0.180	0.178
		RMSE [-]	0.530	0.468	0.466	0.452	0.442
		RVar [-]	0.375	0.410	0.576	0.554	0.528

components. These components were interpolated using different methods and subsequently transformed back into direction category and absolute wind velocity. The entire procedure is explained in Sec. 3.4 of this work.

Figure 6.27 presents the results obtained for hourly wind velocity and hourly wind direction. The interpolation of velocity components required for the linked interpolation of absolute wind velocity and wind direction was carried out using NN, InvD and OK. These methods were also used for the direct interpolation of wind velocity, while NN and IK were used for the direct interpolation of wind direction. A lower interpolation performance for wind velocity is seen here as well for the scenario using 24 stations when it is compared to the scenario using 17 stations. This irregular behavior results from the cross validation procedure in combination with the Brocken station, as described before. In terms of wind velocity, there is no significant difference between approach (A) and approach (B). The coupled interpolation does not yield an improvement in comparison to the individual interpolation of wind velocity. As it was also observed in Fig. 6.25, OK provides a significantly better estimation of wind velocity than NN and InvD.

In terms of wind direction, there is almost no difference in interpolation performance between the use of 17 and 24 stations. The coupled interpolation (B) achieves a slightly better performance in combination with InvD and OK for the higher network density and also outperforms the individual interpolation (A). It has to be noted that OK and InvD achieve a quite similar interpolation performance in combination with approach B. A clear advantage of OK as observed for wind velocity is not seen for wind direction. The interpolation of direction using IK fails in
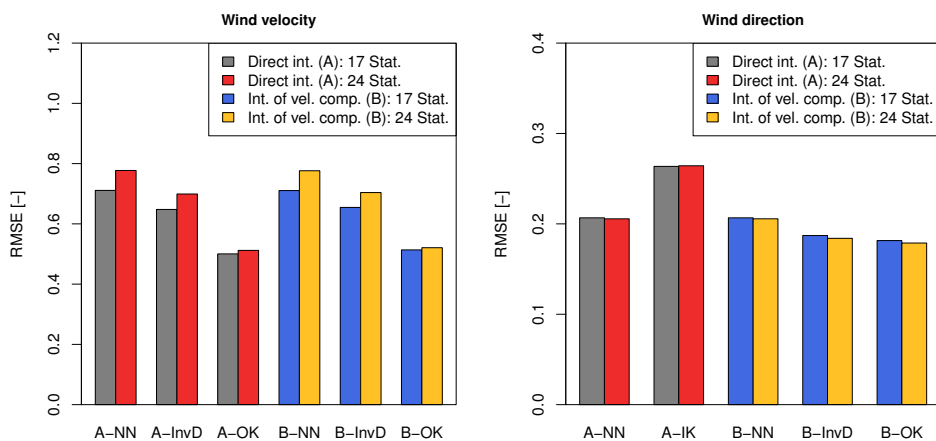
Figure 6.27: Performance of different interpolation methods for hourly wind velocity (left) and hourly wind direction (right) using direct interpolation of velocity and direction (A) and using a transformation approach (B)

Table 6.25: Average interpolation performance (Bias, RMSE, RVar) for hourly wind velocity over all station density scenarios

Criterion	A: Direct		B: Coupled			
	NN	InvD	OK	NN	InvD	OK
Bias [m/s]	0.326	0.305	0.045	0.332	0.135	−0.258
RMSE [-]	0.744	0.674	0.506	0.743	0.679	0.517
RVar [-]	1.733	1.122	0.226	1.726	1.186	0.249

Table 6.26: Average interpolation performance (Bias, RMSE, RVar) for hourly wind direction over all station density scenarios

Criterion	A: Direct		B: Coupled		
	NN	IK	NN	InvD	OK
Bias [$10°$]	3.036	3.655	3.036	2.697	2.612
RMSE [-]	0.206	0.264	0.206	0.186	0.180
RVar [-]	1.334	1.530	1.333	1.219	1.167

terms of estimation accuracy, the performance is worse than the one of NN. In general there is an advantage of using the coupled interpolation approach for wind direction. The performance of OK-B is somewhat better than the interpolation performance of NN-A.

Table 6.25 contains the Bias, RMSE and RVar interpolation performances for all temporal resolutions, in which the values are averaged over the two network density scenarios. The individual approach using OK achieves an RMSE interpolation performance that is marginally better than the RMSE performance of the coupled equivalent. However, the bias of OK-A is significantly lower than the bias of OK-B. The OK interpolations that are carried out for the coupled approach are unbiased in terms of the north-south and west-east velocity components but not necessarily in terms of the absolute wind velocity. OK reduces the variance of the estimated values in a similar way for the individual and the coupled interpolation.

The Bias, RMSE and RVar interpolation performance for hourly wind direction is given in Tab. 6.26 and the values are averaged over the two station density scenarios. Note that the bias criterion is given in $10°$. In general there is a significantly lower bias for the coupled interpolation. The variance of estimated values is higher than the variance of observed values for all interpolation methods, but OK-B causes the lowest increase of spatial variance.

Chapter 7

Further aspects of interpolation performance

This chapter shows and discusses further aspects related to the interpolation performance for different climate variables. Section 7.1 attempts to quantify the effect of the random station selection on the interpolation performance, while Sec. 7.2 delivers a comparison of interpolation performance among all different meteorological observations analysed in this study. Section 7.3 is concerned with the temporal scaling behaviour of climate data interpolations and examines, whether fine temporal resolution interpolations are reliable for obtaining large time scale estimates.

7.1 Effect of station selection on the interpolation performance

This section contains information about the effect of the random selection of stations on the interpolation performance. In order to find out whether the location of the measurement is important, the RMSE cross validation performance obtained for the ten realisations of each density scenario using 17 stations is displayed in box plots. The results of each meteorological variable are presented in a separate figure for all temporal resolutions. The scenario of 17 stations is available for all climate information and allows therefore a thorough comparison among all meteorological information.

Figure 7.1 contains the box plots obtained for the interpolation of 5 min to annual rainfall sums, whereas only selected methods are displayed for each temporal resolution. NN and OK are
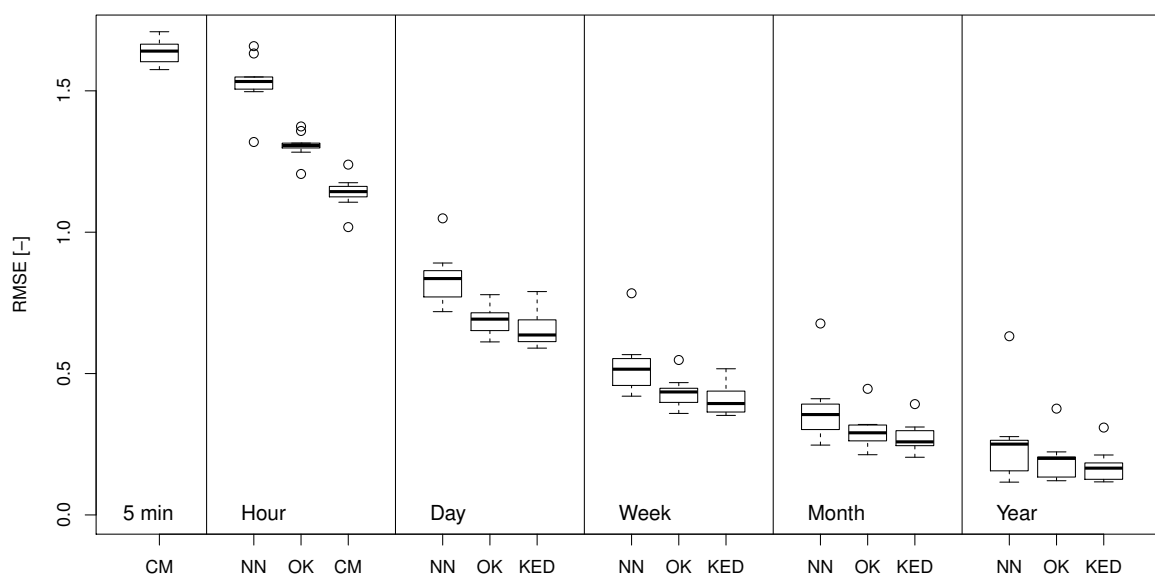
Figure 7.1: Influence of station locations on the interpolation performance of 5 min to annual precipitation sums. The boxes contain each the interpolation performance of NN, OK and KED or CM, depending on the temporal resolution, obtained for the ten different realisations of the network density scenario consisting of 17 stations.

always shown, except for the 5 min temporal resolution. These simple univariate techniques are used as a standard of comparison for the best multivariate approach. NN represents the simplest possible basic interpolation technique, while OK is the basic univariate geostatistical interpolation method. CM is displayed for 5 min and hourly data since it demonstrated the best interpolation performance. For all other temporal resolutions, KED, which uses both elevation and radar data, is shown as the third method. It is generally expected that there is a much stronger variation among the different realisations when NN is used for the spatial interpolation. OK and also the other geostatistical techniques cause a strong smoothing of the interpolated fields and are expected to be influenced less significantly by the random station selection.

There is a significant variation in interpolation performance among the random station selections for each temporal resolution and interpolation method. NN generates a higher variation compared to the geostatistical methods. OK and KED generate a quite similar variation in the error for daily and weekly data. In the case of monthly and annual rainfall sums, KED tends to have a slightly lower variation than OK. In particular one specific realisation causes a high RMSE for the daily, weekly, monthly and annual time scale. It is marked as an outlier for all methods and is explained by the high elevation and the corresponding high amounts of orographic precipitation of the gauge situated on the Brocken mountain. Only one scenario contained this station, since the random selection was drawn from 200 stations in total.
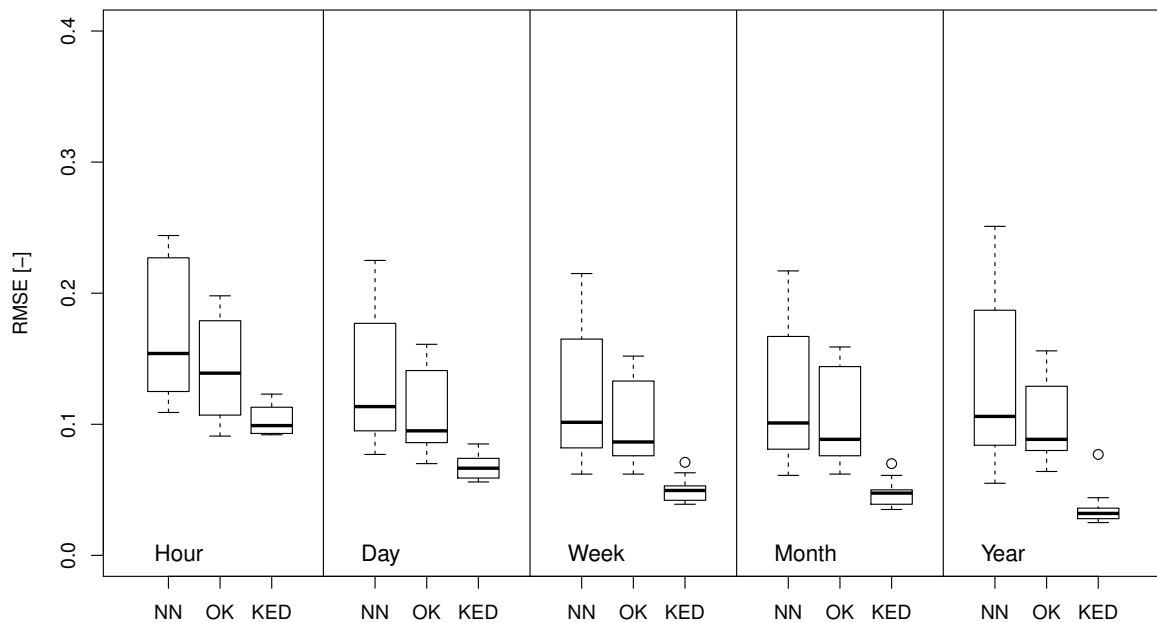
Figure 7.2: Influence of station locations on the interpolation performance of hourly to annual mean temperature. The boxes contain each the interpolation performance of NN, OK and KED obtained for the ten different realisations of the network density scenario consisting of 17 stations.

The variation of temperature interpolation performance is shown in Fig. 7.2, whereas only mean temperature is shown here. Maximum and minimum temperature are displayed in Appx. B.1, since the variations in interpolation performance are quite similar. The KED method presented here used the DEM as the additional information.

The variation in KED interpolation performance is significantly lower than the variation in NN and OK interpolation performance. NN causes the highest variation, while OK generates a medium range of interpolation performances. The distribution of NN and OK interpolation performance appears to be skewed to the right, i.e. a relatively good interpolation performance is achieved for most realisations of each temporal resolution, while some realisations have significantly higher errors. NN and OK do not consider elevation and therefore it is assumed that the weather station on the Brocken mountain, which is not considered in all realisations, causes this behaviour.

Figure 7.3 shows the variation in interpolation performance of relative humidity. It is clearly seen that NN creates the highest variation, while the cross validation of geostatistical techniques, in particular KED using temperature, were able to provide a relatively robust assessment of interpolation quality. A specific reason for the outlier caused by KED for hourly data could not be identified.
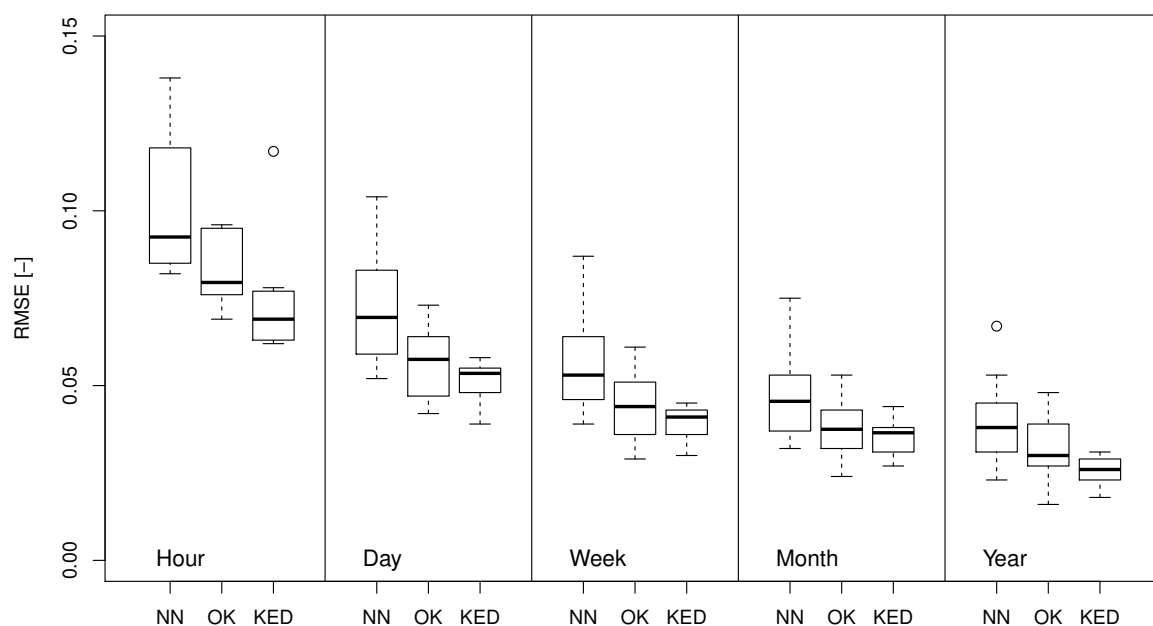
Figure 7.3: Influence of station locations on the interpolation performance of hourly to annual relative humidity. The boxes contain each the interpolation performance of NN, OK and KED obtained for the ten different realisations of the network density scenario consisting of 17 stations.

The results for cloud coverage are shown in Fig. 7.4. The variation is relatively low compared to the meteorological observations shown before. Nevertheless, the application of OK leads to a slightly lower spread of interpolation performances.

The range of sunshine duration interpolation performance is shown in Fig. 7.5. The variations seem to be even lower than those obtained for cloud coverage. It is assumed that the limited number of available stations contributes additionally to the low variations. Random selections were drawn from 25 stations only. Again, OK causes a marginally lower variation of interpolation performance among the ten realisations than NN.

The distribution of wind velocity interpolation performance, seen in Fig. 7.6, is highly skewed for all interpolation methods and temporal resolutions. A relatively poor performance is reached for most realisations, while some random selections, which did not take into account the Brocken station, achieve a much better interpolation quality. The range of interpolation performances is by far the highest, when compared to the other meteorological observations. It is assumed that wind velocity is strongly affected by the local topographic conditions. Realisations that contain only locations with similar local topography achieve therefore the best interpolation performance. A spatial interpolation using the entire set of available stations does not necessarily yield an optimal interpolation quality.
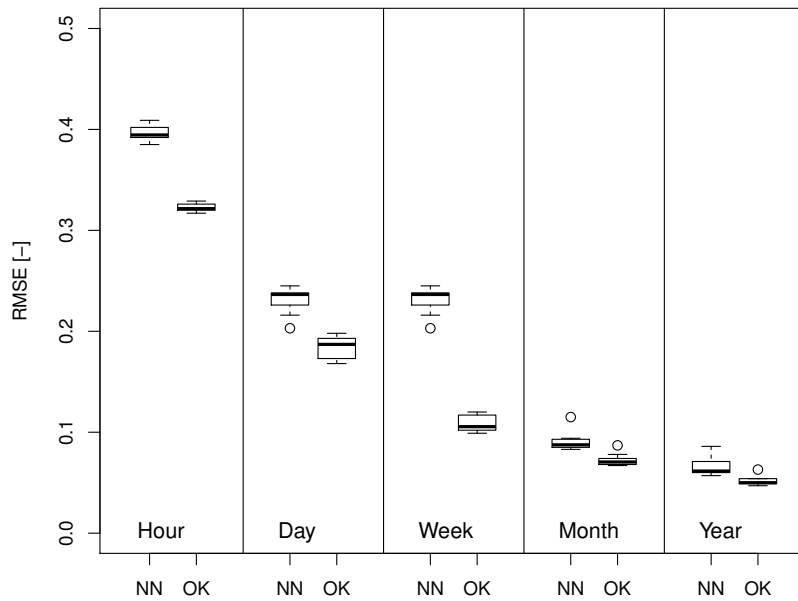
Figure 7.4: Influence of station locations on the interpolation performance of hourly to annual cloud coverage. The boxes contain each the interpolation performance of NN and OK obtained for the ten different realisations of the network density scenario consisting of 17 stations.
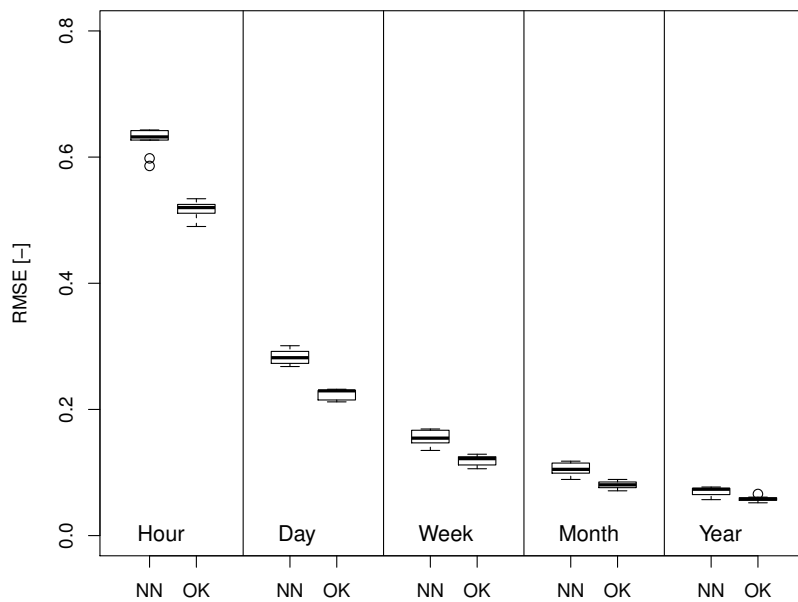
Figure 7.5: Influence of station locations on the interpolation performance of hourly to annual sunshine duration. The boxes contain each the interpolation performance of NN and OK obtained for the ten different realisations of the network density scenario consisting of 17 stations.
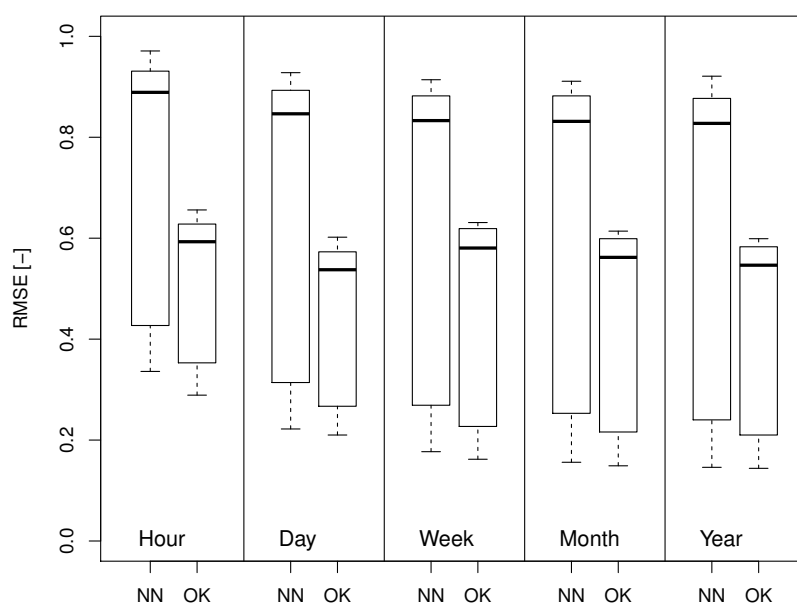
Figure 7.6: Influence of station locations on the interpolation performance of hourly to annual wind velocity. The boxes contain each the interpolation performance of NN and OK that for the ten different realisations of the network density scenario consisting of 17 stations.

Generally, the locations of meteorological measurements have a significant impact on the expected interpolation performance for precipitation, temperature, relative humidity and wind velocity. The variation in interpolation performance can be reduced if geostatistical techniques are applied. In particular KED in combination with appropriate additional information provides significantly lower variation of interpolation performance.

7.2 Interpolation performance compared among all variables

The intercomparison of interpolation performance is carried out for the best interpolation method found in Sec. 6.2 to Sec. 6.7. The results are shown in the upper panel of Fig. 7.7. The panel at the bottom contains the coefficient of variation that was computed for each time step of the different meteorological observations and their temporal resolutions. Note that maximum and minimum temperature are again not available for the hourly time scale. The RMSE performance criterion is used to compare the interpolation performance among the different climate variables. This comparison approach is considered as legitimate, since the RMSE is standardised with the mean of the observations for each climate variable. It is carried out despite the fact that the observation range of sunshine duration, cloud coverage and relative

humidity is limited. The observation ranges are directly linked to the respective variable; for instance the relative humidity cannot be higher than 100 %.
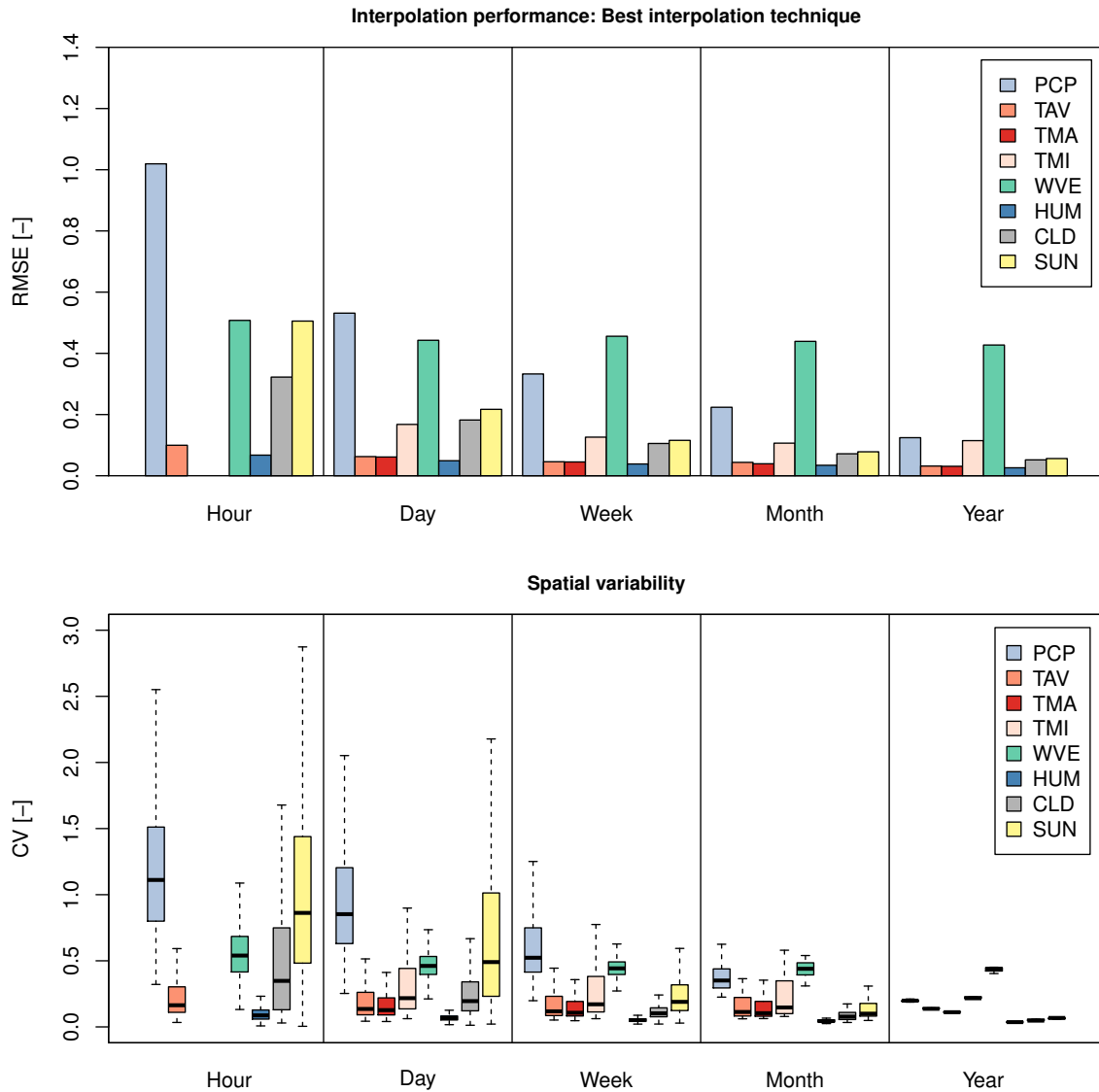
Figure 7.7: RMSE cross validation result for the best interpolation technique (top) and spatial variability (bottom) compared among all climate variables and temporal resolutions

In case of the hourly time scale, the interpolation of precipitation generates the worst result, with an RMSE of approx. 1.0. A good interpolation performance was achieved for relative humidity and mean temperature, i.e. the RMSE is lower than 0.1 for both. Wind velocity, cloud coverage and sunshine duration have a medium interpolation performance.

The interpolation performance of precipitation, sunshine duration and cloud coverage improves significantly when examined at longer time periods. For mean, maximum and minimum

temperature as well as relative humidity, there is a less significant improvement. In contrast to all other variables, the estimation of wind velocity does not improve when longer time periods are interpolated. On the weekly time scale, the interpolation of wind velocity is already a bit worse than the interpolation of precipitation. In terms of yearly performance, the interpolation of wind velocity gives by far the worst result. It is assumed that wind is in general strongly affected by local conditions, in particular by the topography that can cause either shielding or amplification effects, depending on the wind direction. Relative humidity has the lowest interpolation error for all temporal resolutions, whereas the error of the mean and maximum temperature interpolation is slightly higher.

The boxes in the bottom panel of Fig. 7.7 contain each the coefficients of variation that were computed for each time step of the corresponding climate variable and temporal resolution. Outlier time steps are removed to enable a better illustration of the spatial variability. For rainfall, the CV was only computed for time steps that have an observation mean value higher than or equal to 1.0 mm. It is obvious that the interpolation performance is strongly linked to the spatial variability of each climate variable. Moreover, the variation among the time steps decreases significantly with a decrease of temporal resolution.

In general, it is clear that the spatial interpolation of fine temporal resolution rainfall data is the most challenging task. The interpolation performances obtained for 5 min to 30 min accumulation time (see Fig. 6.5 and Fig. 6.7) are even worse than the 1 h performance which is displayed in the upper panel of Fig. 7.7. Rainfall observations with high temporal resolution have a high spatial variability and the expected interpolation error is therefore much higher. The interpolation error of humidity and temperature is in general the lowest. In particular for temperature interpolation, the DEM offers reliable additional information that can improve the cross validation result.

7.3 Temporal scaling behaviour of interpolated data

This section analyses the temporal scaling behaviour of geostatistically interpolated climate variables. As shown from Sec. 6.1 to 6.7, the interpolation performance depends more or less on the temporal data resolution and on the regarded climate variable. It is therefore assumed that aggregating or averaging the outcome of fine temporal resolution interpolations to larger time scales results in an increase of the error. This hypothesis is tested by comparing the original interpolation performance obtained from direct cross validations for each temporal resolution

with the performance which results from aggregating fine temporal resolution interpolations. In total, four different time scales are considered here:

- Day: Direct daily interpolation performance (Original) is compared with aggregated (AGGH) or averaged (AVGH) hourly interpolations

- Week: Direct weekly interpolation performance (Original) is compared with aggregated (AGGH, AGGD) or averaged (AVGH, AVGD) hourly and daily interpolations

- Month: Direct monthly interpolation performance (Original) is compared with aggregated (AGGH, AGGD) or averaged (AVGH, AVGD) hourly and daily interpolations

- Year: Direct yearly interpolation performance (Original) is compared with aggregated (AGGH, AGGD, AGGM) or averaged (AVGH, AVGD, AVGM) hourly, daily and monthly interpolations

Weekly interpolations are not used for aggregations, since entire weeks do not always coincide with a certain month or year. The criteria RMSE and PBIAS are used to assess the interpolation performance. Not all interpolation techniques previously evaluated were taken into account for
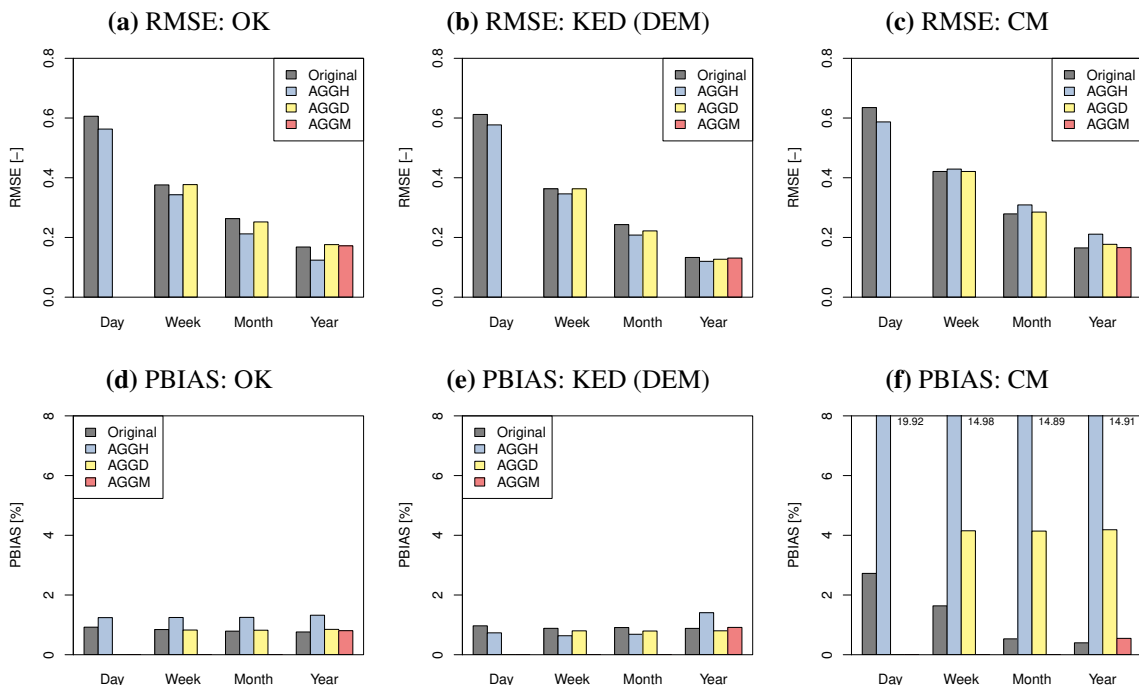
Figure 7.8: RMSE and PBIAS interpolation performance for aggregated fine temporal resolution interpolations of precipitation in comparison with time scale specific interpolation for OK (left), KED using DEM (middle) and CM (right)

(a) RMSE: KED (Radar) **(b)** RMSE: KED (Radar and DEM)

(c) PBIAS: KED (Radar) **(d)** PBIAS: KED (Radar and DEM)
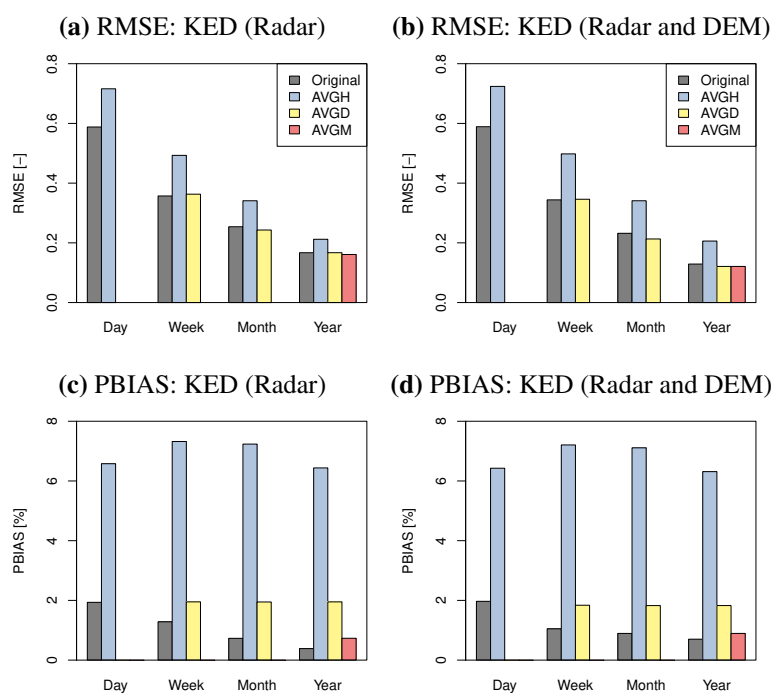
Figure 7.9: RMSE and PBIAS interpolation performance for aggregated fine temporal resolution interpolations of precipitation in comparison with time scale specific interpolation for KED using Radar (left) and KED using Radar and DEM (right)

this analysis. OK and all methods that could provide the best interpolation result for at least one combination of station density and temporal resolution (see Sec. 6.2 to Sec. 6.7) were considered for each variable. Due to the general difference between radar and topography, all methods are shown for the evaluations regarding precipitation.

Figure 7.8 and Fig. 7.9 contain the results for the precipitation evaluations. OK, KED (DEM) and CM are shown in Fig. 7.8, while KED (Radar) and KED (Radar, DEM) are presented in Fig. 7.9. The OK result shows that the RMSE interpolation performance of aggregated fine temporal resolution interpolations is quite similar to the performance obtained by a direct interpolation for the specific time scale. The RMSE interpolation performance of AGGH is a bit better for OK and KED (DEM) and a bit worse for the other interpolation techniques, compared to the direct interpolation. This difference is considered not as significant as the difference in PBIAS that was found. In general, the use of aggregated hourly interpolations to estimate longer time periods increases the PBIAS. Only the daily, weekly and monthly scales of KED (DEM) do not show this behaviour. In particular, the interpolation techniques based on radar data show a strong increase, whereas the PBIAS of CM is significantly higher than the PBIAS of the KED methods. Especially the aggregation of interpolated hourly values show a high error for every target temporal resolution. The PBIAS caused by the aggregation of daily
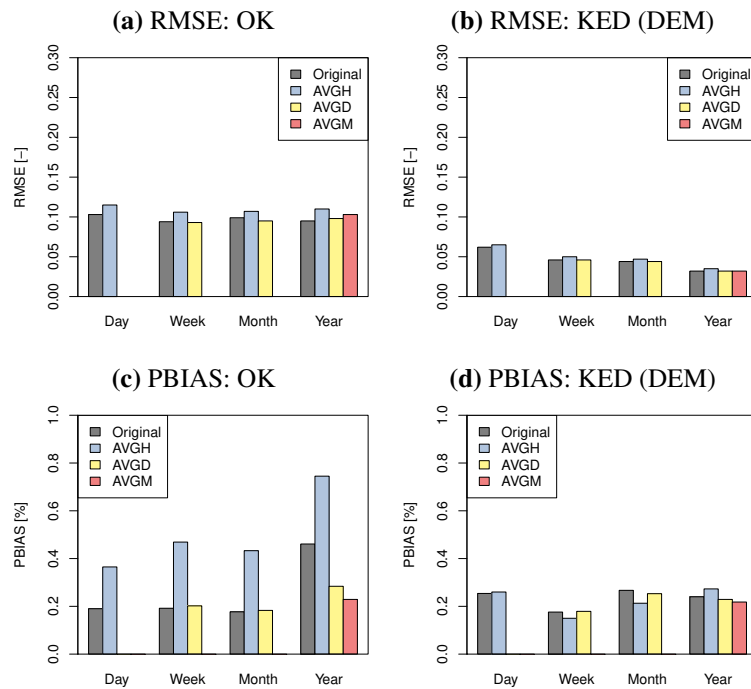
Figure 7.10: RMSE interpolation performance for aggregated fine temporal resolution interpolations of mean temperature in comparison with time scale specific interpolation for OK (left) and KED using the DEM (right)

interpolations is not as high, but still evident, whereas the PBIAS caused by the aggregation of monthly interpolations is quite low.

The results of the mean temperature evaluations are shown in Fig. 7.10. The difference in RMSE for direct interpolation and interpolation of finer temporal resolutions with a subsequent computation of the mean are not significant. Comparing the PBIAS, it is obvious that there are bigger differences. The aggregation of hourly interpolations for OK always results in a higher PBIAS value than the direct interpolation. For the weekly and monthly time scale, there is almost no increase of the AVGD-PBIAS compared to the direct interpolation. Strangely, the averaging of daily and monthly temperature values interpolated with OK results in a lower bias than the corresponding direct OK interpolation. This seems a bit implausible, but generally the range of PBIAS for TAV is with a minimum of 0.2 % and a maximum of 0.8 % quite low. KED (DEM) shows almost the same PBIAS for all aggregated temporal scales.

Figure B.3 and Fig. B.4 in Appx. A.1 contain the results for maximum and minimum temperature, respectively. Note that there are only three time scales shown, since minimum and maximum values of temperature are not available for the hourly time scale. The difference in RMSE between direct interpolation and averaged fine temporal resolution interpolations is
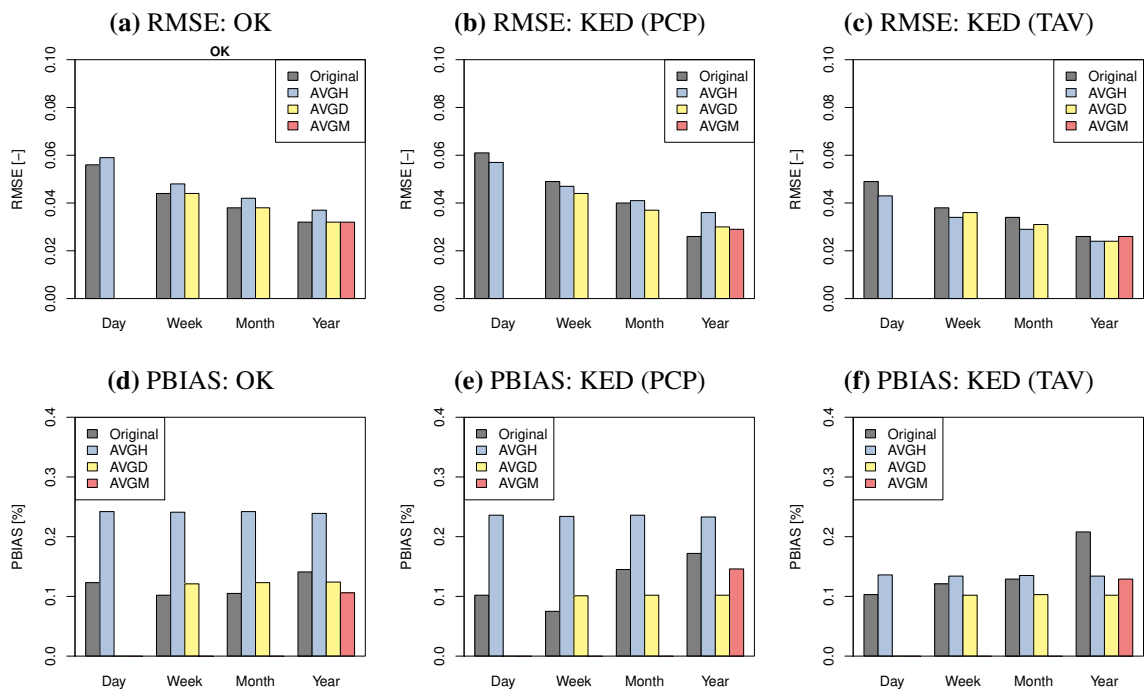
Figure 7.11: RMSE interpolation performance for aggregated fine temporal resolution interpolations of humidity in comparison with time scale specific interpolation for OK (left), KED using precipitation (middle) and KED using mean temperature (right)

very low for the maximum as well as minimum temperature. For minimum temperature there are only slight differences in PBIAS for OK and KED using the DEM. Applying KED with the DEM as additional information for maximum temperature results in a strong similarity of PBIAS values as well, if the time scale specific cross validation results are compared with their corresponding means from fine temporal resolution interpolations. The application of OK for maximum temperature shows a slightly different behaviour for yearly values. Here, AVGD and AVGM give lower PBIAS values than the original interpolation. However, considering the extremely low PBIAS values, these differences are only of minor importance.

The results for relative humidity are shown in Fig. 7.11. Using hourly OK interpolations to compute the mean relative humidity results in slightly higher RMSE values than the direct time scale specific interpolation, however the differences are in general very low. For KED using precipitation grids, the differences in RMSE are also very low. Slight differences do exist for the daily, weekly and monthly time scale and can be recognised in the corresponding panels of Fig. 7.11. The annual RMSE of AVGH is considerably higher than the RMSE obtained from the direct interpolation for the annual time scale and also the RMSE values obtained by AVGD and AVGM. KED using interpolated grids of mean temperature shows a similar RMSE for Original and the fine temporal resolution interpolations for all time scales. The PBIAS

values have a range of 0.09 % to 0.02 % and are thus very low for all interpolation methods. For OK and KED (PCP), there is a considerably higher bias when hourly interpolations are averaged to obtain mean values for coarser temporal resolutions. The PBIAS values of AVGH are approximately 0.22 %, while the PBIAS values of the direct interpolation depend on the temporal resolution. The error is somewhat lower, with a range from 0.09 % to 0.17 %. The PBIAS values of AVGH for KED (DEM) are noticeably lower than those obtained for OK and KED (PCP). This results from the digital elevation model that correlates well with the spatial distribution of the humidity (see Sec. 6.4).

Figure 7.12 shows the results for the cloud coverage cross validations. The RMSE values of the direct time scale specific interpolations are marginally different from the averaged fine temporal resolution interpolations for weekly, monthly and annual time scale. For the daily time scales, the RMSE of the direct interpolation is a bit higher than the RMSE of AVGH, which could be related to the high variability of cloud coverage for fine temporal resolutions. The smoothing effect of OK affects the hourly interpolations more strongly than the daily interpolations and leads to a better estimation of daily cloud coverage values. The PBIAS values are in general very low for all time scales. However, direct interpolation performs significantly better than averaging of hourly interpolations for the computation of daily estimates. On the weekly, monthly and annual scale, AVGH shows again a worse performance. AVGD can almost reach the same accuracy as direct interpolation of weekly and monthly data. In terms of annual values, AVGD and AVDM achieve a marginally better performance than direct interpolation.

The results for sunshine duration are shown in Fig. 7.13. There are no differences between direct interpolation and the estimation based on averaging finer temporal resolution interpolations. The PBIAS values vary within a range of 0.2 % to 0.4 %. The averaging of hourly interpolations causes a slightly better performance on a weekly time scale than the direct interpolation and
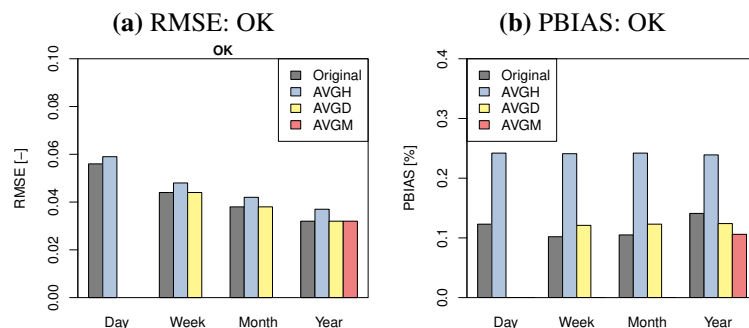
Figure 7.12: RMSE interpolation performance for aggregated fine temporal resolution interpolations of cloud coverage in comparison with time scale specific interpolation for OK
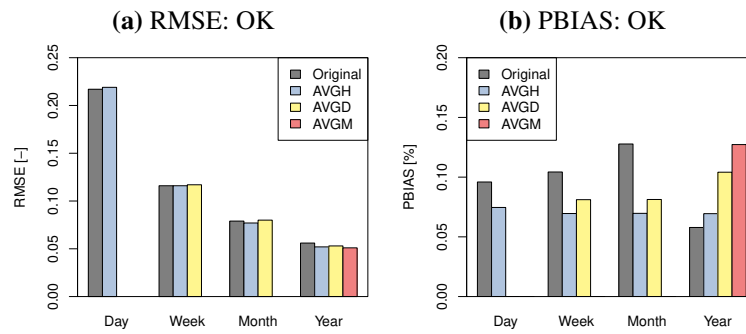
Figure 7.13: RMSE interpolation performance for aggregated fine temporal resolution interpolations of sunshine duration in comparison with time scale specific interpolation for OK
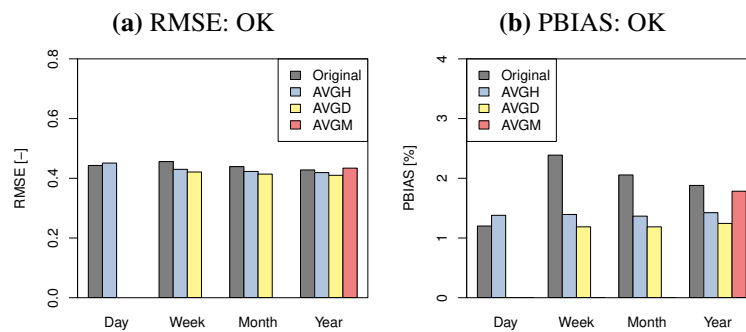
Figure 7.14: RMSE interpolation performance for aggregated fine temporal resolution interpolations of wind velocity in comparison with time scale specific interpolation for OK

AVGD. The performance for the monthly and yearly time scale is a bit worse than the direct interpolation. Figure 7.14 shows the results for the wind velocity interpolations. There is almost no difference in RMSE between direct time scale specific interpolation and interpolation of finer temporal resolutions with a subsequent averaging. The PBIAS for the direct interpolation and the PBIAS for AVGM are a bit higher than those of AVGH and AVGD. The values are varying between 1.0 % and 2.3 %.

It may be concluded that fine temporal resolution interpolations of temperature, cloud coverage, sunshine duration and wind velocity could be used to derive long term estimates of the corresponding variable. The expected interpolation errors are not significantly higher than those that occur if the interpolation is carried out directly for the long-term scale. Long-term estimates of humidity can also be derived from fine temporal resolutions, if KED with the temperature information is used for interpolation. Deducing long-term humidity estimates from hourly interpolations carried out by OK leads to a slightly higher PBIAS and is therefore not recommended. The interpolation of precipitation should be always carried out directly for the respective temporal resolution.

Chapter 8

Application I: Urban hydrological modelling

8.1 Motivation and objectives

Urban hydrological processes are generally characterised by short response times and thus rainfall data with a high resolution in space and time are required for their modelling. NIEM-CZYNOWICZ (1999) states that the rainfall data collected by national meteorological services are often not adequate for urban hydrological applications. Own systems capable of delivering data on a small spatial scale with a fine temporal resolution must be installed. However, the site-specific data collection is quite costly and requires a lot of time until the amount of collected data is sufficient for a meaningful application. Often site-specific data collection is not carried out, for instance no sub-daily rainfall recordings are available within the urban catchments of many towns.

Some past studies focused on resolution requirements for urban hydrology. Theoretical considerations by SCHILLING (1991) suggest, that a temporal resolution of 5 min or higher and a spatial resolution of one rain gauge per $1 \, km^2$ is required for real-time control purposes and evaluation of specific rainfall events in combination with model calibration. BERNE *et al.* (2004) analysed three different urban catchments in combination with variogram analysis of rainfall with a very high temporal and spatial resolution. It is concluded that the minimal required resolution depends strongly on the size of the catchment. Small catchments of approx. 3 ha require a spatio-temporal resolution of 1.5 km/1 min, while for larger catchments of approx. 500 ha a resolution of 3 km/5 min is sufficient. However, recent studies based on

urban hydrodynamic modelling report even higher demands in terms of rainfall data resolution (BRUNI *et al.*, 2015; OCHOA-RODRIGUEZ *et al.*, 2015).

The DWD provides radar data with a temporal resolution of 5 min and a high spatial resolution for the entire area of Germany (cf. Sec. 5.4). According to the literature, this resolution would be sufficient for most applications in many urban catchments. The analyses that are shown in this chapter try to answer the question, whether radar data or rain gauge radar data merging by geostatistics are able to provide a reliable rainfall information for unobserved locations. Three different application purposes were analysed in order to evaluate rainfall data for urban hydrological modelling:

1. Dimensioning of urban drainage systems

2. Simulating the flow behaviour of past events

3. Evaluation of combined sewer overflows in order to assess pollution issues

In terms of the dimensioning task (1), a good representation of extreme rainfall depths has to be fulfilled by the rainfall data. The combined sewer overflow (CSO) evaluation (2) requires in general realistic rainfall amounts and a temporal sequence of storm events which is close to nature. The flow behaviour of past storm events (3) is in particular important for model calibration and real-time operation of system regulators. The actual spatial and temporal distribution of rainfall must be reproduced in the best way by the data product used as the model input for hydrological and hydrodynamical simulations.

8.2 Study area, data and rainfall estimation methods

Figure 8.1 is an image section of Fig. 4.3, whereas only the locations of the 5 min rainfall recordings are shown. Moreover, the locations of three local rain gauges operated by the Brunswick urban drainage works (*Stadtentwässerung Braunschweig*) are displayed. The 5 min stations operated by the DWD as well as radar data are used for quantitative rainfall estimations in the urban catchment of Brunswick, while the local reference gauges are used for a corresponding validation.

The distance from the urban catchment to the nearest DWD station (reference number '10348') is approx. 7 km. Considering this rather close location, two different cases are implemented for the quantitative rainfall estimations: Case A takes into account all DWD stations for rainfall
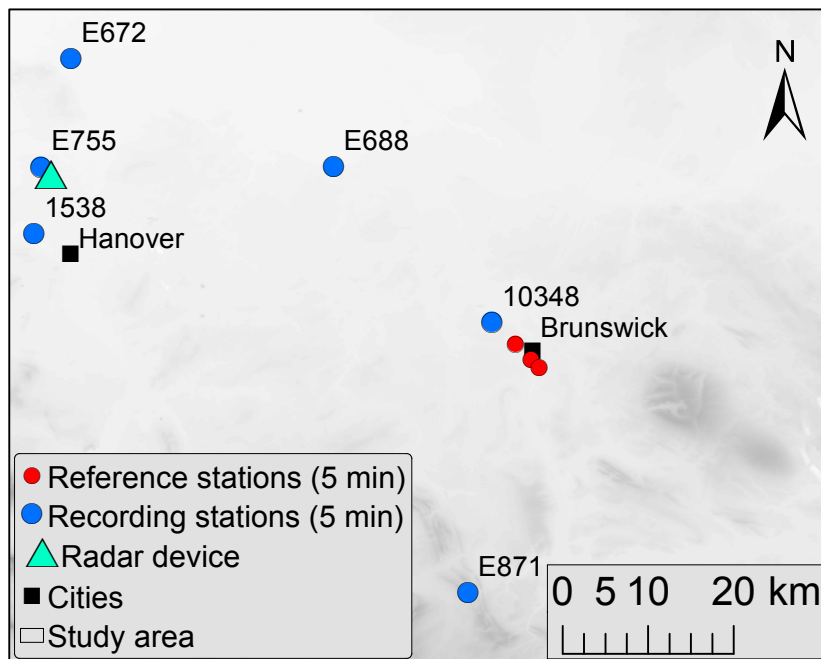
Figure 8.1: Study area for the urban hydrology evaluations of precipitation data

estimation, while station '10348' is omitted for Case B and station 'E688' (distance approx. 35 km) is the closest available rain gauge.

Five different methods for the quantitative estimation of precipitation were applied: NN, OK, Radar, CM and BIASC. NN was applied in the same way as for the cross validation analysis presented in Ch. 6, while a slight modification of OK was used. Due to the strong smoothing effect caused by the rather large search neighbourhood (cf. Sec. 6), only 4 instead of 12 adjacent stations were used for the computation of rainfall estimates according to Eq. 3.8. The radar data were preprocessed as described in Sec. 5.4, however no smoothing and no detection of poor time steps was carried out. CM was applied in the same way as for the cross validation analysis, i.e. 12 neighbouring stations were used and radar data smoothing was performed prior to the merging procedure. BIASC is the radar data correction method proposed by RABIEI and HABERLANDT (2015). This method is referenced as bias correction by the authors and is capable of adjusting the range of radar values to a corresponding range of rain gauge measurements. No cross validation analysis of this technique was performed, nevertheless it is included for the urban hydrological evaluations shown here.

The mutual time periods for which all of the three reference stations and the nearest (Case A) or second nearest DWD station (Case B) delivered precipitation recordings were found to be six and four years, respectively. In particular, the time series of the local reference

gauges contained a lot of asynchronous gaps. For achieving an objective comparison of all rainfall estimation methods, all recordings must be available for a specific time step in order to be taken into account. The available time periods are furthermore also restricted by radar data, which are available from the year 2000 onwards. The time periods of six (A) and four years (B) analysed here are in general too short for a reasonable extreme value analysis that is required for the design of urban drainage structures. Nevertheless, these time periods are investigated in the following regarding their rainfall extremes. It is assumed that this analysis shows tendencies, whether a certain rainfall estimation method will able to provide adequate data if longer recordings are available.

8.3 Validation using urban hydrological simulations

The storm water management model (SWMM, version 5.1) provided by the US Environmental Protection Agency (ROSSMAN, 2015) is used for assessing the estimated rainfall time series regarding their suitability for urban hydrological purposes. It is widely applied in civil and environmental engineering and has been used for various scientific purposes, for instance hydrological impact assessment (JANG *et al.*, 2007) and parameter uncertainty analysis (KLEIDORFER *et al.*, 2009). It allows a continuous as well as an event-based simulation of stormwater quantity and quality issues.

A typical urban drainage area is represented in SWMM using various horizontal subcatchments, while each subcatchment is parameterised by individual data, such as total area, percentage of impervious area, slope, etc. The discharge from each subcatchment is calculated separately, while stormwater flow along with dry weather flow representing domestic and industrial sewage is taken into account. Various hydrological approaches for the consideration of infiltration losses and evaporation are available, a curve number approach and monthly mean values of potential evaporation were selected for this study. The subsequent flow routing across the network of drainage pipes or sewer channels is carried out using the dynamic wave model that approximates the full Saint-Venant equations (ROSSMAN, 2015). Apart from simple conduits, several other elements are available for regulating the simulated flow, for example retention tanks, pumps and weirs. SWMM allows different ponding settings. If ponding is set to 'not allowed', water will be entirely removed when it leaves the drainage system through nodes like maintenance holes or road inlets. If it is set to 'allowed', the flood volume will be stored on the surface and reintroduced into the system when the surcharge of the specific node decreases. The latter option was used for the evaluations of this study, since the elevation differences of

the catchments and thus also the expected surface flows are rather low. The model provides also options for considering percolation, snow accumulation and melting as well as water quality analysis. None of these options was used here for the comparison of rainfall inputs.

Figure 8.2 shows the two urban drainage systems that were implemented in SWMM and used for event-based and continuous rainfall evaluation. The left panel shows the model of the actual urban drainage system of Brunswick. It has a total area of 1733.1 ha, consists of 3855 subcatchments, 6310 nodes as well as 6643 links and was used here for the evaluations regarding dimensioning and flow simulation of past events. Water stage, flow velocity and discharge measurements were continuously available in the time period from 2011 to 2012 for one flow gauge indicated in the map. It is located close to the main outfall of the system and approx. 60 % of the entire water volume, assuming a spatially homogenous rainfall input, passes the conduit where it is installed. Unfortunately the flow records are affected by many gauge failures and data gaps. The right panel of Fig. 8.2 contains the artificial urban system that was used for the continuous CSO evaluation. It is less complex (22 subcatchments, 22 nodes, 20 links), needs less computation time and has a total area of 168.1 m^2. The frequency of combined sewer overflow and corresponding overflow volumes can only be determined via a continuous simulation, which is not possible with the Brunswick model. In order to overcome

(a) Dimensioning, Flow analysis   **(b)** CSO evaluation
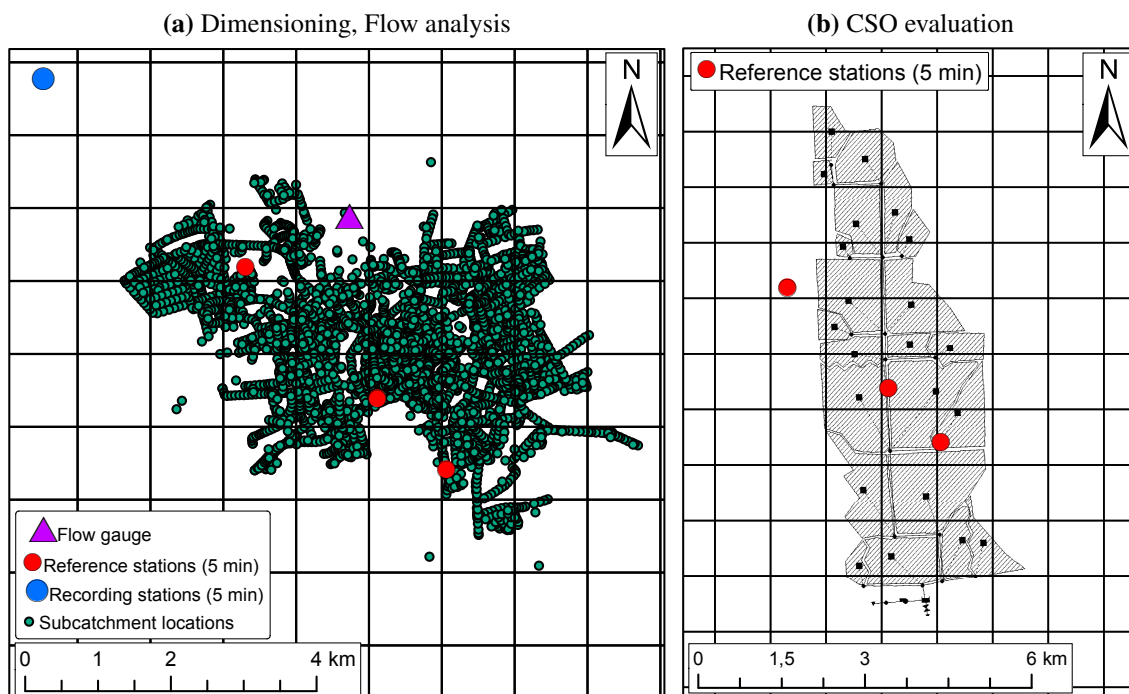
Figure 8.2: SWMM models implemented for the analysis regarding dimensioning of urban drainage systems and past event analysis (left) as well as CSO evaluation (right)

this problem, the artificial system is shifted under the three validation gauges that are available for the Brunswick location. The 1 km × 1 km grid for which radar data was preprocessed and also the interpolations were carried out is displayed additionally in the two figures.

The assessment of estimated precipitation time series for the dimensioning of urban drainage systems was based on extreme value analysis using partial series for different rainfall durations. The computation was carried out according to the German technical guideline DWA-A 531 (2012) that regulates the analysis of intense rainfall depending on return period and duration. However, only extreme events and their corresponding return periods are computed using the suggested procedure. A fitting of a distribution function as proposed for the computation of design rainfall was not performed. The event selection was carried out individually for each estimation method and the reference time series, thus the selected rainfall events are not necessarily the same ones or did not occur at the same time, respectively. Rainfall durations of 10 min, 60 min and 240 min were considered. The rainfall extremes obtained for a duration of 60 min were used as a rainfall input for the urban model in order to assess the effect of rainfall estimation method on different flooding criteria. Theoretically all rainfall durations should be analysed, since rainfall extremes of a short duration might lead to flooding in the upper parts of the urban catchment and extremes of a long duration might causes flooding near the outlets. However, it is assumed that a comparison for a duration of 60 min is able to show whether a certain rainfall estimation method is capable of providing adequate data. The actual internal behaviour of the extreme events was taken as the model input. No transformation into model rainfall, for instance block rain, was carried out as it is often the case when statistical data products of extreme rainfall, for instance KOSTRA (DWD, 2005), are used.

The evaluation of flow analysis for single events was carried out for six cases, that were recorded in the period from 2011 to 2012. The selection was based on the availability of flow and reference rainfall data as well as the performance of the urban model that was obtained. Only events for which the not calibrated urban model delivered a reasonable performance using the three local rain gauges were chosen. Table 8.1 shows the selected events, their corresponding duration as well as the mean rainfall sum of the three reference stations. The measured discharge at the flow gauge location was considered as a reference and the simulated flow using reference stations and estimated rainfall was compared accordingly.

The evaluation of CSO was carried out by a continuous simulation using the less complex artificial model. The entire stormwater and dry weather flow volumes have to pass a retention tank which is located directly before the outlet of the system. The maximum tank outflow is throttled to 0.023 m³/s, which is twice the dry weather flow rate. The capacity of the tank was

Table 8.1: Selected rainfall events for the validation of rainfall time series regarding the analysis of event-specific flow simulation

No.	Start	End	Duration [h:min]	Mean rainfall [mm]
1	26.08.2011 02:30	27.08.2011 19:35	41:05	32.0
2	06.10.2011 14:20	06.10.2011 16:00	01:40	10.2
3	10.10.2011 08:10	11.10.2011 19:35	35:25	38.4
4	18.06.2012 14:15	18.06.2012 15:00	00:45	7.8
5	24.06.2012 16:15	25.06.2012 16:55	24:40	12.1
6	22.12.2012 20:45	23.12.2012 15:20	18:35	27.1

set to $2184\,\mathrm{m}^3$ and complies to the recommendations specified in IMHOFF and IMHOFF (2010), i.e. $20\,\mathrm{m}^3$ storage volume is available per 1 ha of impervious area. In case of no or only slight rainfall, the tank inflow is lower than the outflow and the entire water volume can be routed to a treatment plant, which is not included in the artificial system. The inflow exceeds the outflow and might fill the reservoir completely if heavy rainfall occurs. The excess water volume is then conducted to the receiving water body without prior treatment. Different CSO related criteria for instance the number of overflows were obtained from the urban simulations and compared among reference and rainfall estimation data.

Two different approaches for rainfall input were evaluated, i.e. homogenous single point rainfall input (SP) was compared with the input of the complete rainfall field (CF). In case of SP, the reference station located in the middle (c.f. Fig. 8.2) was used for the reference simulation runs. The simulation run carried out for each rainfall estimation method took the time series of the collocated estimation grid point as the model input. The simulations for CF are based on the entire grid, which means that each subcatchment receives the rainfall estimated for the closest grid point. For the CF reference simulations, the rainfall input is designed in a way that each subcatchment receives the rainfall of one of the three reference stations. The closest gauge is assigned to each subcatchment.

8.4 Results and discussion

8.4.1 Design of urban drainage systems

Figure 8.3 shows the partial series of rainfall extremes that were obtained for durations of $10\,\mathrm{min}$, $60\,\mathrm{min}$ and $240\,\mathrm{min}$ considering the nearest DWD station (A). Note that the return

period is limited to 3 a due to the limited amount of data recordings. The results for the case in which this station is not considered (B) are shown in Fig. D.1 in Appx. D. The results of Case A are discussed here entirely, while for Case B only the differences in comparison to Case A are explained.

Single point rainfall input (SP) and the average of the complete rainfall field input (CF) are displayed at the top and at the bottom, respectively. The results show a strong overestimation of rainfall extremes by radar data for all durations. Some events exceed even a rainfall sum of 50 mm and are thus outside of the visible plot ranges. The main reason for this poor performance is the conversion of radar reflectivity to precipitation intensity by a time-invariant and spatially uniform Z-R relationship. According to EINFALT *et al.* (2004), the selection of corresponding parameters has a strong influence in particular for high rainfall rates. The constant application to a variety of different storm types, drop size distributions and even precipitation types leads to an immense overestimation of extreme values as it is seen here.
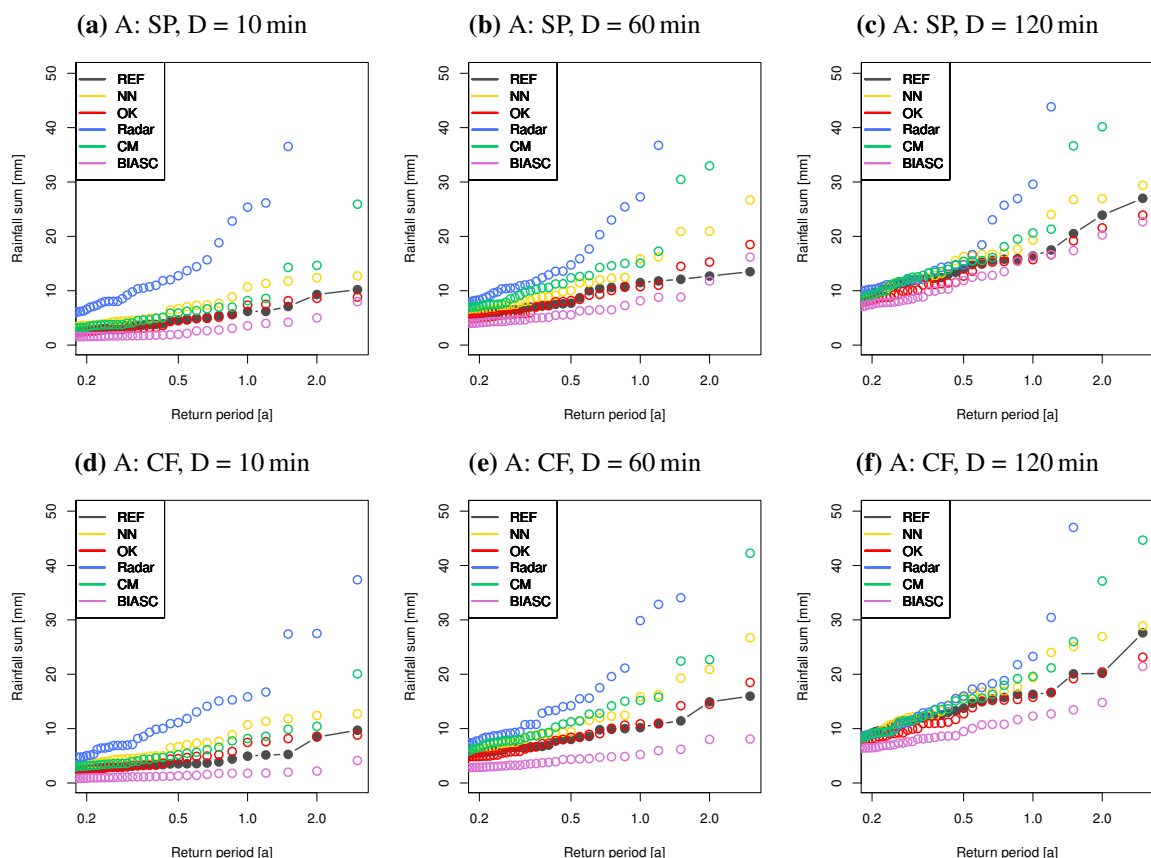
Figure 8.3: Partial series of point rainfall extremes (top) and areal rainfall extremes (bottom) for durations of 10 min, 60 min and 120 min, whereas the closest DWD rain gauge is taken into account for all interpolation methods (Case A)

CM is able to reduce the rainfall peaks of radar data, but strong overestimation is still evident for the higher return periods. Bias correction using quantile-mapping (BIASC) results in an underestimation of rainfall extremes for most durations and return periods, only for a few events with a rather high return periods, a good performance or an overestimation is achieved. The overestimation caused by Radar and CM is reduced when the average of the complete rainfall field is regarded, while the underestimation caused by BIASC even increases. This is explained by the low spatial extent that extreme rainfall events of short durations usually have. Averaging 35 grid points leads to a lower decrease than averaging the three reference gauges. Compared to CM, NN causes a lower overestimation of the reference. However, this has to be regarded as arbitrary since only two specific time series are compared. The case of a low local station density (B) exhibit an underestimation by NN for durations of 60 min and 240 min as it is shown in Appx. D. The smoothing effect of OK leads to lower extremes for Case A and causes therefore the best match, while for the aforementioned durations of Case B an underestimation is generated.

In general it is assumed that the preprocessing technique of radar data has a major impact on the estimation of extreme values. ELDARDIRY *et al.* (2015) used hourly radar grids with a spatial resolution of 4 km 4 km for analysing rainfall extremes in Louisiana. They reported an underestimation of rainfall extremes, which is probably caused by the conditional bias of the radar product that was used. The importance of proper Z-R relationship is also discussed by MARRA and MORIN (2015), who constructed IDF curves by fitting an extreme value distribution function to annual series of radar rainfall extremes. They established an upper threshold for radar values in order to eliminate hail effects and yielded similar curves for rain gauge data and radar information.

The results of the urban hydrological simulations, that were carried out for a duration of 60 min, are shown in Fig. 8.4. The 30 rainfall events with the highest rainfall sums were taken into account for the creation of the boxplots. The total flooding volume, i.e. the amount of water that leaves the drainage system towards the surface was selected as one evaluation criterion. Furthermore, the number of flooded nodes and the duration of flooding were assessed. Note that y-axis data of flooding volume and number of flooded nodes is presented using a logarithmic scale. In contrast to the other methods, only one box is available for NN since the application of this technique did not result in different rainfall time series for the grid points over the urban catchment.

It is clearly visible that the use of radar rainfall results in a significant overestimation of flooding volume and number of flooded nodes. CM is able to reduce this overestimation but is not able

(a) A: Flooding volume **(b)** A: No. of flooded nodes **(c)** A: Flooding duration

(d) B: Flooding volume **(e)** B: No. of flooded nodes **(f)** B: Flooding duration
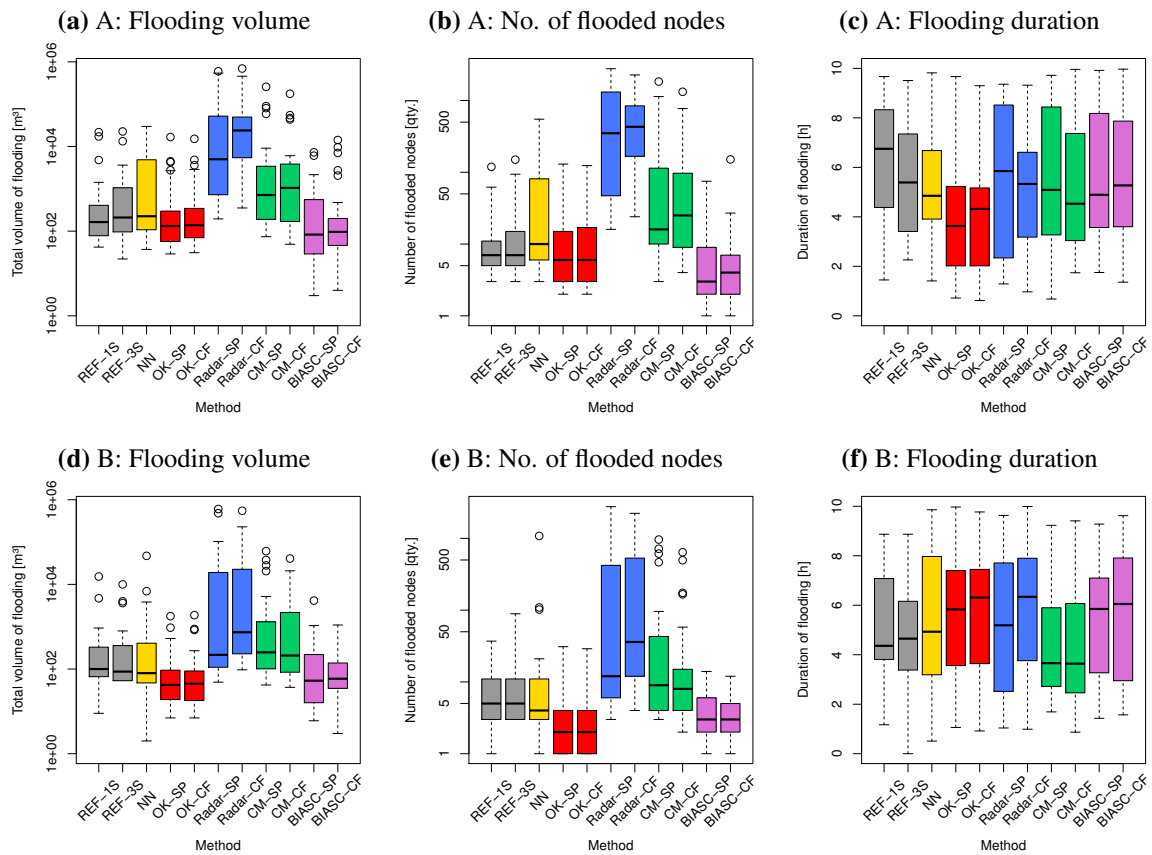
Figure 8.4: Results of urban hydrological modelling using different point rainfall extremes (top) and different spatial rainfall extremes (bottom)

to fit the reference simulations either, while BIASC causes an underestimation of flooding volume and number of flooded nodes. OK and NN seem to deliver the best performance for these two criteria, although in some cases an overestimation by NN and an underestimation by OK is detected. A relatively good performance of OK and NN was also observed in the partial series (cf. Figs. 8.3 and D.1). The flooding duration behaves differently compared to the other criteria. Radar does not cause a strong overestimation as for flooding volume and number of flooded nodes. All methods deliver a relatively similar performance, whereas only OK causes a strong underestimation for Case A. The model input based on the complete rainfall field causes a slightly higher median of flooding volume and number of flooded nodes for each method except OK. This might seem implausible, since averaging of all grid points results in slightly lower rainfall extremes as it as it can be observed in Fig. 8.3. However, the entire spatial extent of the catchment can receive small-scale local rainfall events, whose peaks are not captured by one gauge or pixel, respectively. These events might cause local flooding for some nodes and hence the entire spatial rainfall distribution causes more flooding on average. The rainfall fields

interpolated by OK usually exhibit a smooth and relatively uniform distribution in space and therefore the difference between SP and CF is negligible.

8.4.2 Analysis of single event flow

Figure 8.5 contains the results of the flow analysis of individual events for single point rainfall input and high local station density (Case A). The left panel shows the Nash-Sutcliffe model efficiency coefficient (NSE, NASH and SUTCLIFFE, 1970), while the right panel contains the relative volume error (PBIAS) for the six events that were analysed. The NSE can ranges from $-\infty$ to $+1$, whereas a value close to 1 indicates a good model performance. A positive PBIAS indicates an underestimation of water volume, while negative values result from an overestimation. The last bar of each panel shows the median of the respective criterion over all events.

The general model performance depends strongly on the event, while the reference rain gauge data (grey bar) achieves a NSE performance of around 0.4 to 0.75 and a PBIAS of approx. -30 % to +15 %. Radar data shows a poor NSE performance for some events as it is indicated by the blue bar, which is even cut by the border of the graph and the legend, respectively. This is caused by an immense over- and underestimation of rainfall as it is indicated by the relative volume error. CM delivers a much better performance, since rain gauge data are used for the correction. A negative NSE is only observed for the first event and the median shows that this method outperforms all other estimation techniques. NN as well as OK perform worse than CM, although the nearest station is only 7 km away from the centre of the urban catchment.
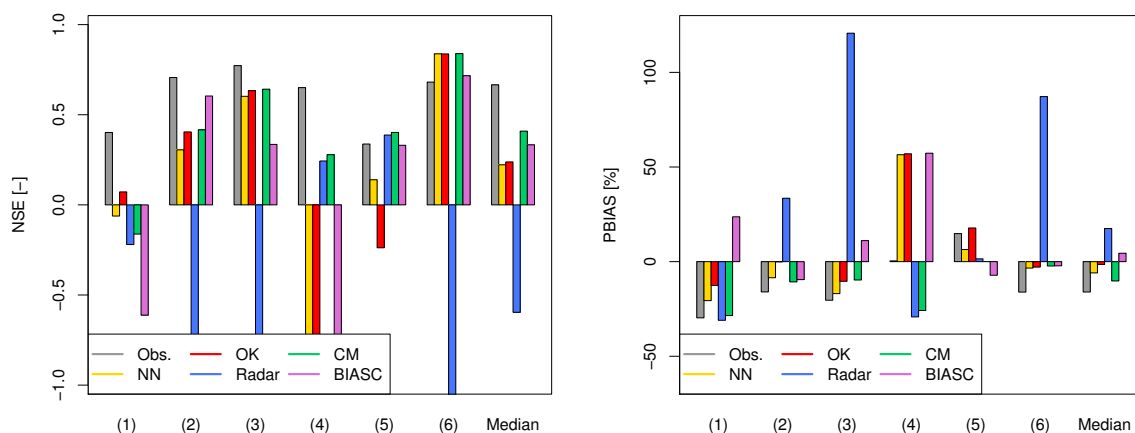
Figure 8.5: NSE (left) and PBIAS (right) for pipe flow at monitoring point Juteweg for six different rainfall events using single point rainfall input considering the closest DWD rain gauge (Case A)
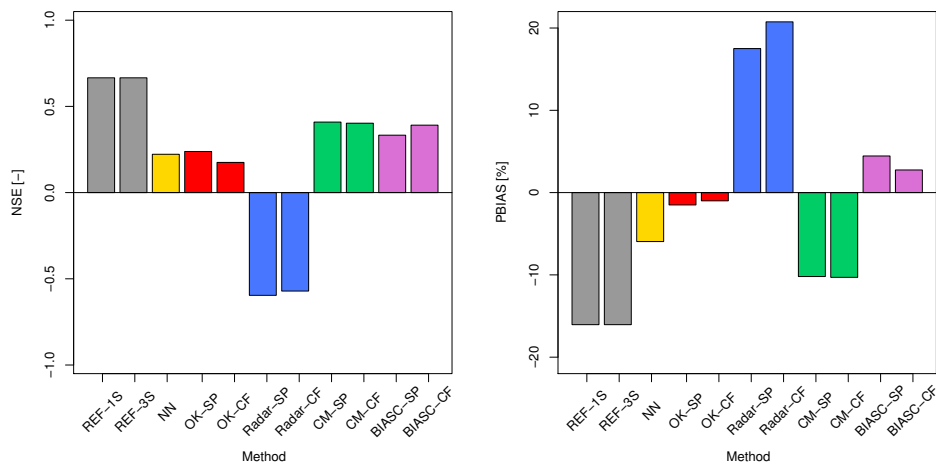
Figure 8.6: Median of NSE (left) and PBIAS (right) obtained from the simulation of six different events using single point rainfall input (SP) and complete rainfall field input (CF) for Case A
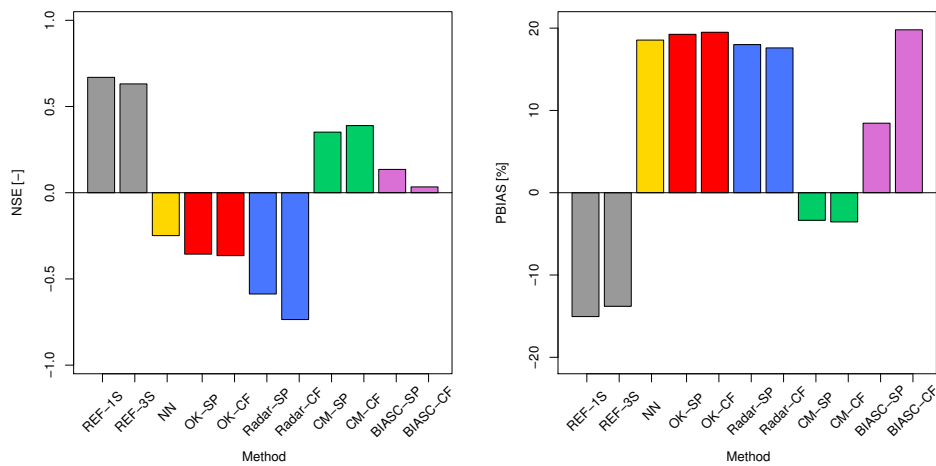
Figure 8.7: Median of NSE (left) and PBIAS (right) obtained from the simulation of six different events using single point rainfall input (SP) and complete rainfall field input (CF) for Case B

BIASC performs almost as well as CM, only for some events a significantly worse model performance was detected. Only radar and CM are able to provide adequate data for the fourth event. The small and convective rainfall cell causing an increase of stormwater flow could not be observed by the DWD network and hence all univariate interpolation methods as well as BIASC show an immense underestimation as it is seen from the PBIAS criterion.

The median of NSE and PBIAS is shown for Case A and Case B in Fig. 8.6 and Fig. 8.7, respectively. Single point rainfall and the complete rainfall field are displayed. It is seen that CM performed best in all cases. The error of NN and OK increases significantly when the local station density is reduced. It results in a much weaker model performance for Case B compared to Case A. The performance obtained for BIASC is also reduced, while CM and Radar are

hardly affected by the distance to the nearest station. Overall, the results indicate that CM can provide valuable information for the simulation of single flow events, if no local rain gauge data are available.

8.4.3 Pollution due to combined sewer overflows

Figure 8.8 shows the results that were obtained for the CSO evalution using a continuous hydrodynamic simulation. The total mixed water overflow volume, the number of overflow events and the average overflow volume per event were selected for the evaluation and are shown in the upper (Case A) and lower panel (Case B). Note that the general variation in CSO volume and number of CSO events results from the different time series lengths used for the simulations. Six years of common data for the three reference stations and the closest DWD station were available for Case A, while only four years of mutual data were available for case B.

NN and OK achieve a good performance in matching the three CSO criteria obtained from the reference simulations. For both local station densities, radar causes a slight underestimation of overflow volume and a stronger underestimation of the number of overflow events, resulting in an overestimation of event-averaged overflow as well. CM leads to an overestimation of total volume and number of events, in particular for Case B. It is assumed that these differences result from a mismatch of radar and rain gauge data for some events. CM takes the OK estimate of a certain pixel and adds a rainfall difference obtained from radar data. In case gauge data indicate rainfall while radar rainfall is zero, the OK estimate from gauge data is used. In the reverse case, the radar error is added although no rainfall was detected by the adjacent stations. Thus, the CM rainfall time series show a higher number of rainy time steps as well as a higher rainfall amounts causing the overestimation of CSO volumes and frequency.

8.5 Conclusions and outlook

So far radar data as well as merging of radar and rain gauge data does not seem promising for the estimation of design rainfall. The application of a simple NN interpolation results in a better representation of extreme rainfall than complex geostatistical algorithms. The main reason for this is the overestimation of rainfall extremes by radar. A better preprocessing of radar data might help to reduce this problem, however an entire correction of radar extremes seems quite

challenging. Better radar technologies, i.e. polarimetric devices, are capable of estimating drop size distribution and precipitation type, which enables the application of a non-uniform Z-R relationship and might help to provide better quantitative precipitation estimates. According to WERNER and STEINERT (2012), these device are installed by the DWD from 2010 onwards. Moreover, the difference between point rainfall extremes and areal rainfall extremes might be a subject of another investigation. Radar provides quite accurate information about the spatial structure of rainfall fields, while quantitative estimations are affected by many errors.

In case of the analysis of single urban runoff events, radar data is able to provide useful information. In particular when small-scale convective events are not detected by rain gauges, radar is the only useful information. In general the application of CM provided the overall best rainfall data for this purpose and is not affected that strongly by the local station density, compared to univariate interpolation. General assertions are quite difficult though. The suitability of radar and also radar rain gauge merging depends strongly on the data quality for

(a) A: Tot. overflow volume   **(b)** A: No. of overflow events   **(c)** A: Average overfl. per event

(d) B: Tot. overflow volume   **(e)** B: No. of overflow events   **(f)** B: Average overfl. per event
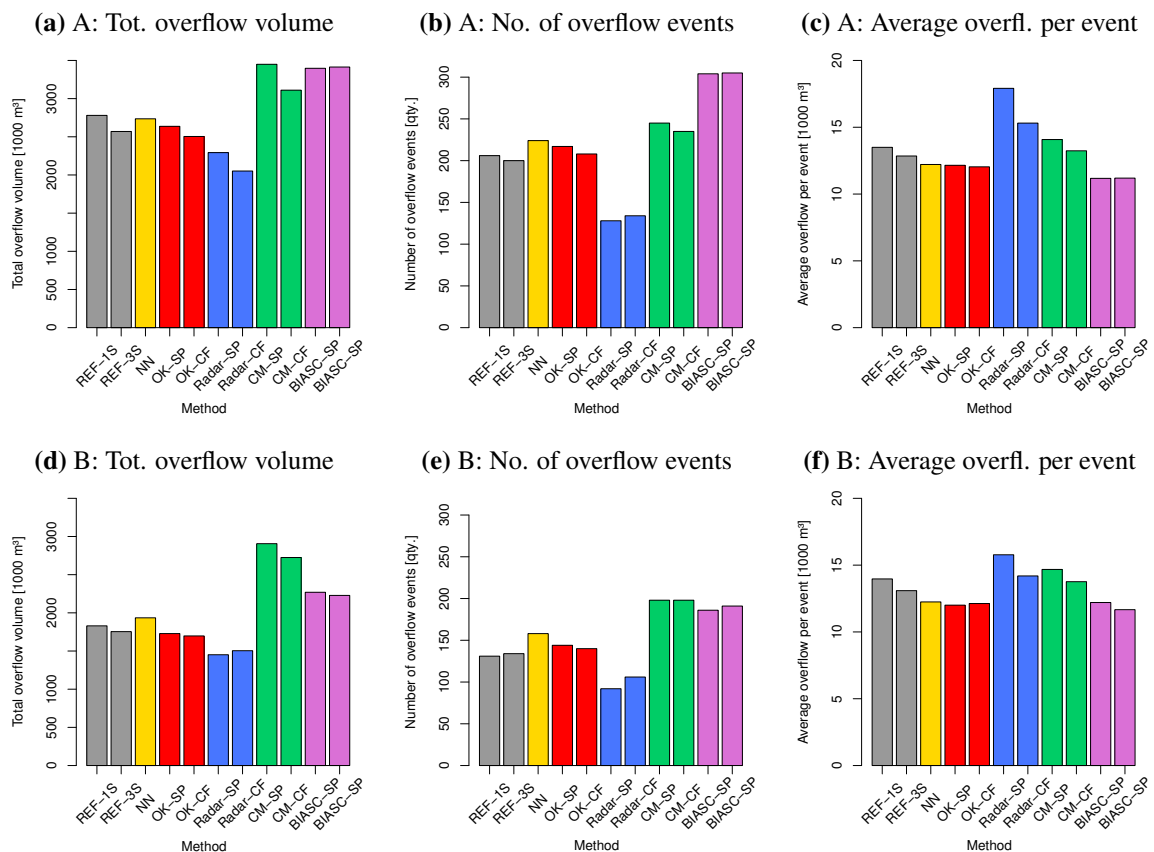
Figure 8.8: Combined sewer overflow volume, number of overflows and average volume per overflow event for single point rainfall input (SP) and complete rainfall field input (CF), whereas the closest DWD rain gauge is considered (top) and not considered (bottom) for the interpolations (bottom)

the regarded flow event. The analysis of CSO issues worked really well using NN and even OK estimated data. It is hard to imagine that an improvement in radar data or radar rain gauge merging can outperform this result.

Chapter 9

Application II: Modelling of atmospheric contaminant transport

9.1 Motivation and objectives

Usually the installation of certain facilities, e.g. factories and power plants, requires an approval by local authorities. In many countries, this approval requires a projection of pollutant immissions to the surrounding region. The German technical regulations for air pollution control (BMU, 2002) appoint the exact requirements to be fulfilled in Germany, while in most cases a transport simulation using a specific model is performed for the verification of compliance.

The contaminant transport simulations are in general based on a time series of hourly wind information, i.e. wind velocity and direction, as well as dispersion class and precipitation. The dispersion class is a measure of atmospheric stability and characterises the air turbulence based on the similarity theory by MONIN and OBUKHOV (1954). A simulation of atmospheric contaminant transport may either consider the processes of wet and dry deposition or only the process of dry deposition, depending on the context of application. Dry deposition refers to the part of the process affected by wind and turbulence only, while wet deposition is caused by the adsorption of pollutant particles by rain droplets.

In general site-specific time series are needed for the simulations. However, this is not possible due to the lack of measurements. The DWD as well as private environmental consultancies offer services for transferring data from locations with similar wind and turbulence statistics, following the technical guideline VDI 3783 (2015). Geostatistical interpolation, as discussed

previously, might be a simpler option for providing data for each location and is tested here regarding its applicability to generate adequate time series for contaminant transport simulations. Due to the fact that precipitation data are not available for most places, contaminant transport simulations are often performed without taking into account wet deposition of pollutants at all. The generation of time series using geostatistical interpolation may help to overcome this problem.

9.2 Study area and interpolation techniques

Figure 9.1 shows the study area for the validation of wind and precipitation data. In contrast to the cross validation analysis, the entire area of the German federal state Lower Saxony was used. Rain gauge as well as wind anemometer locations are displayed in the map. Five validation locations at which precipitation as well as wind velocity and direction recordings were available are marked additionally. The main reason for expanding the study area is, that time series of dispersion class were only available for the five locations. The site-specific turbulence measure was determined for each hour by the DWD based on cloud coverage, wind velocity and day time, whereas the technical guideline VDI 3782 (2015) describes the derivation procedure. In general the DWD is able to provide dispersion class time series for any site, as long as wind and cloud coverage information are available. For this analysis however, only the dispersion class time series at the five selected validation locations were on hand.

The five validation locations represent a wide range of nature and landscape factors. The station Norderney is located on an island in the North Sea, while others ones are located in the interior of the country. The station Braunlage is located in the Harz Mountains at an altitude of 607 m.a.s.l., while the other validation sites are located in the North German Plain. Moreover, the five validation locations possess a different number of adjacent rain gauges or wind anemometers. In particular Norderney has very few neighbouring rainfall recordings. The years 2004 and 2010 were used for the validation of interpolated rainfall and wind. Not all stations displayed in Fig. 9.1 are available due to the variation in network density. Table 9.1 contains the total number of available stations for the study area and the local number of stations near each validation site. All stations within a radius of 90 km around each validation location were utilised.

The direct interpolation of absolute wind velocity and direction category (A) as well as the interpolation of velocity components in north-south direction and west-east direction with a
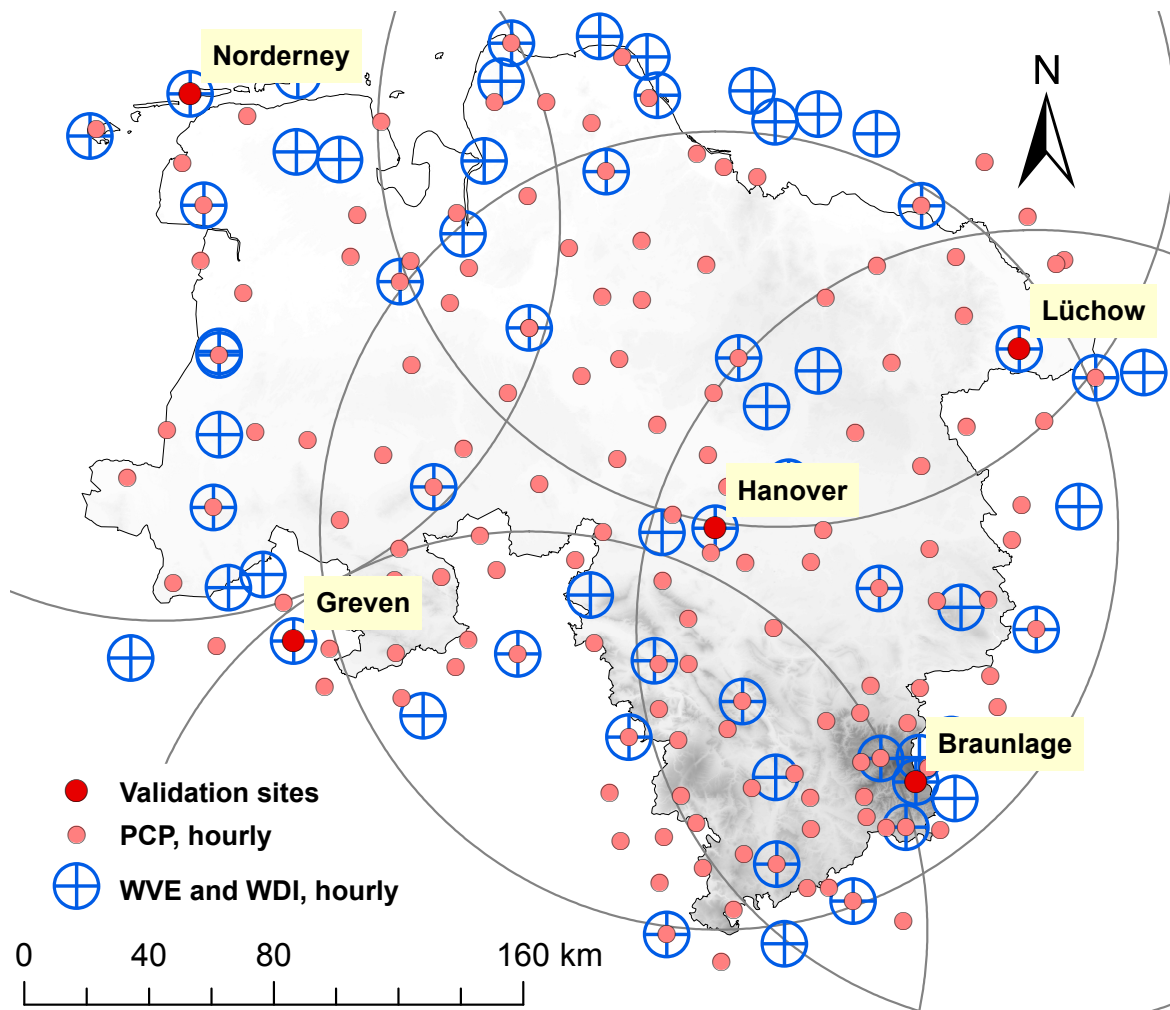
Figure 9.1: Study area for the atmospheric contaminant transport simulations

subsequent transformation into absolute wind velocity and direction category (B) were applied in order to generate time series of wind data. NN and IK were used for the direct interpolation (A), while NN, InvD and OK were used for the interpolation of velocity components (B). The entire procedure is described in Sec. 3.4. For each validation location, the interpolation of wind was performed without considering the reference station. As described in Sec. 6.7, the station on the Brocken mountain is strongly affected by the exposed location and records the highest wind velocity in general. It is quite close to the validation site Braunlage and was therefore omitted for the interpolations.

The geostatistical rainfall interpolation was carried out using the techniques NN, OK, KED (Radar) and CM, while the station of the regarded validation site is again not taken into account. The validation sites Greven and Norderney are outside of the range of the radar device located near Hanover. The radar data of Emden were used for Norderney, while the data of Flechtdorf

Table 9.1: Number of available wind stations and rain gauges for the validation periods regarding contaminant transport. The rows for the five validation locations contain the numbers of available stations within a radius of 90 km from each site, while the total number of stations for the study area is shown in the bottom line.

Location	No. of wind stations		No. of rain gauges	
	2004	2010	2004	2010
Braunlage	11	9	18	44
Greven	9	8	7	25
Hanover	13	11	13	57
Lüchow	9	7	10	24
Norderney	8	7	3	13
Total study area	57	49	79	152

were used for Greven. Radar data preprocessing was carried out in the manner described in Sec. 5.4, only the parameters for clutter correction were changed slightly. Smoothing was included, while no detection and removal of poor radar data time steps was carried out. Moreover, multi-step interpolation techniques were applied for the interpolation of precipitation. These techniques incorporate an indicator interpolation of rainfall occurrence prior to the actual interpolation of rainfall depth. In order to achieve this, precipitation time series are transformed to time series of binary rainfall occurrence indicators and then interpolated using OK. As a result, all points of the interpolation grid are labelled either as dry or wet. The interpolation of rainfall depth is then carried out only for wet grid points, while dry grid points are set to 0 mm. Multi-step interpolation methods (VERWORN and HABERLANDT, 2011) allow a clear delineation between regions with and without rainfall occurrence. They are implemented here since most of the standard geostatistical methods, for instance OK, cause a strong smoothing of interpolated rainfall fields. In this case, where interpolated time series are used as a model input, it leads to an overestimation of the number of wet time steps. In general, rainfall peaks are strongly underestimated and many time steps with no or very few rainfall are overestimated by the OK method.

As discussed previously in Sec. 7.3, there is a high error when the annual rainfall sum is calculated from hourly interpolations. Due to the fact that the amount of wet deposition depends strongly on the annual rainfall sum, two different scenarios are considered in the contaminant transport simulations. In the first scenario, the error of the annual sum is not corrected and the time series are used for the simulations as they are obtained from the geostatistical interpolations. In the second scenario, the interpolated rainfall time series are scaled to the true rainfall sums, i.e. all interpolated hourly time steps are multiplied with a

constant factor in a way that observed annual rainfall sum and annual sum of the hourly rainfall interpolations are identical.

9.3 Validation procedure using contaminant transport simulations

In Germany, simulations of airborne contaminant transport is usually carried out using the reference model AUSTAL2000, which was specifically designed to comply with the regulations set up by the technical regulations for air pollution control (BMU, 2002). The model used here (AUSTAL2000N, Version 2.6) is a variation of this implementation and is able to consider wet deposition processes, which are not implemented in the reference model (UBA and IJ, 2014). It is a Lagrangian model, i.e. it simulates the movement of pollution particles via a random walk process after the transport via advection. A two-dimensional domain must be specified and the emission source of pollutants is usually located in the centre of the area that is covered. A specified grid is used in order to obtain average pollutant concentrations. The vertical discretisation is determined automatically in the model, which delivers the three-dimensional spatial distribution of pollutant concentration for each hourly time step as well as the flux of wet and dry deposition at the ground layer. In general, different emission sources, for instance point-related, line-related and volumes, may be placed within the domain. Three different source types were defined for this analysis:

1. Near-ground point emission source, representing a stable or animal housing

2. Near-ground line emission source, representing a street

3. Point source with a height of 200 m above the ground, representing an industrial chimney

Two validation procedures were set up in order to evaluate whether geostatistical interpolation can provide adequate wind and precipitation data. The two different years and five different locations as well as three different emission source types were used. For each wind and precipitation interpolation method as well as the reference data, all combinations of source type, year and location were simulated, i.e. 30 model runs were prepared. A first set of simulations was carried out to investigate interpolated wind velocity and direction; no wet deposition was considered. The dispersion class data provided by the DWD was used for all runs. A second set of simulations, taking into account wet deposition, was used for analysing interpolated precipitation data, whereas the DWD observations of wind information

and dispersion class were used for all runs. In all cases ammonia (NH_3) was selected as the only pollutant, emitted at a constant rate of 1 g/s by the source. The model contains the substance specific parameters, whereas the conversion of ground layer pollutant concentration to soil pollutant flux is parameterised by the deposition velocity v_d. Pollutant adsorption, desorption and chemical processes due to precipitation are approximated in the model by the rate Λ given in Eq. 9.1.

$$\Lambda = \lambda \left(\frac{R}{R_0} \right)^{\alpha} \tag{9.1}$$

Here, λ is a substance specific rate given in 1/s, R is the actual rainfall intensity, R_0 is 1 mm/h and α is a substance specific exponent. For many pollutants, α is assumed to be 0. Ammoniac was selected however as the pollutant since the substance specific α is 0.6. This represents a strong nonlinear relation between adsorption rate and rainfall intensity, i.e. the entire annual influx of pollutants to the soil due to wet deposition does not only depend on the annual rainfall sum, but also on the frequency of certain rainfall intensities. Assuming constant annual rainfall, a higher amount of wet deposition will result in case of a temporally uniform rainfall rate compared to few rainfall peaks separated by long dry spells.

A nested grid was selected for all simulations, whereas the horizontal domain of investigation represents a 16 km × 16 km square having the emission source located in its centre. Four different spatial discretisations were used. The inner grid close to the emission source has a horizontal resolution of 10 m × 10 m and an extent of 2 km × 2 km. The first underlying grid covers 4 km × 4 km with a spatial discretisation of 20 m × 20 m and is followed by a second one that covers 8 km × 8 km with a spatial discretisation of 40 m × 40 m. The horizontal discretisation of 80 m × 80 m is used for the entire area. This decrease of horizontal spatial resolutions with increasing distance from the emission source is implemented in order to save computation time. This procedure is considered as legitimate, since deposition peaks usually occur close to the pollutant source. The vertical discretisation is selected automatically by the model, i.e. no changes were applied to the default settings. A different roughness length was used for all transport simulations, whereas it is taken automatically from the roughness register for Germany enclosed in the model. In general, the roughness represents the character of the surrounding earth surface and depends strongly on land use. It is required for estimating the logarithmic wind profile for the area under investigation.

The annual spatial distribution of wet or dry deposition influx is compared between the use of observed (reference) and interpolated data of wind and precipitation, respectively. Maxima

of wet or dry deposition m_i are determined for distances of 200 m, 500 m, 2 km and 5 km from the emission source. Equation 9.2 specifies the criterion σ_{MAX}, used to asses deviations of deposition maxima resulting from the use of interpolated time series of wind and precipitation.

$$\sigma_{MAX} = \sqrt{\frac{1}{4} \sum_{i=1}^{4} \left(1 - \frac{m_i^{int}}{m_i^{ref}} \right)^2} \tag{9.2}$$

Moreover, the amount of deposition sd_i was determined for the quadrants ($0\,° - 90\,°$, $90\,° - 180\,°$, $180\,° - 270\,°$, $270\,° - 360\,°$) originating from the location of the emission source. The assessment of directional deposition amounts is based on σ_{SEC} according to Eq. 9.3.

$$\sigma_{SEC} = \sqrt{\frac{1}{4} \sum_{i=1}^{4} \left(1 - \frac{sd_i^{int}}{sd_i^{ref}} \right)^2} \tag{9.3}$$

9.4 Results and discussion

9.4.1 Wind data validation

The results of the evaluation of wind interpolation are shown in Fig. 9.2, wherein σ_{MAX} and σ_{SEC} are averaged over all emission sources and the two time periods for each interpolation method. The two validation criteria were applied to the distribution of dry deposition, since wet deposition of pollutants was not considered in the simulations as discussed before. The individual interpolation of wind velocity and direction (A) delivers a similar result compared to the interpolation of velocity components with a corresponding transformation into absolute velocity and direction (B) in terms of the σ_{MAX} criterion. The application of OK results generally results in in a better performance compared to the other techniques. NN gives the worst result, while InvD is ranked in between. Compared to OK, σ_{MAX} caused by the NN interpolation is approx. 100 % higher. NN-A performs worse than NN-B concerning σ_{SEC}, while OK-A and OK-B are equal. The σ_{SEC} values of NN are around 100 % to 150 % higher than the corresponding σ_{SEC} values of OK.

Figure 9.3 contains a slightly more detailed illustration of the results. σ_{MAX} is plotted against σ_{SEC} and each point represents the results of a transport simulation with a specific interpolation
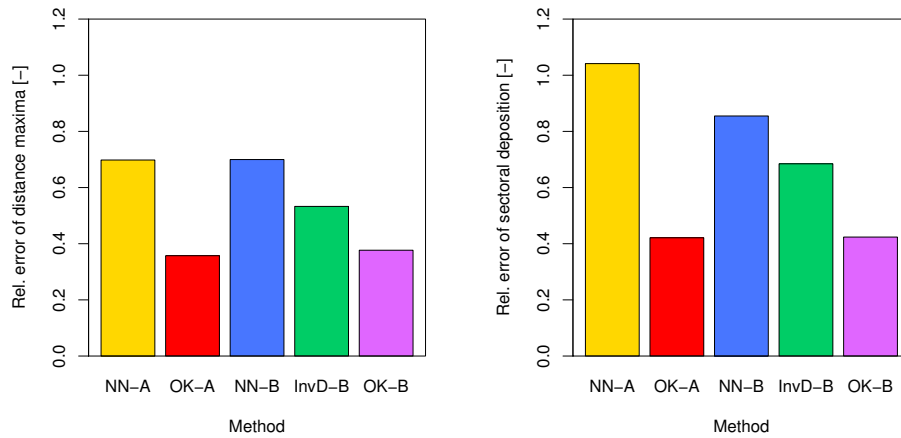
Figure 9.2: Relative error of distance maxima σ_{MAX} (left) and sectoral amounts σ_{SEC} (right) of dry deposition averaged over all emission sources, time periods and stations for each wind data interpolation method
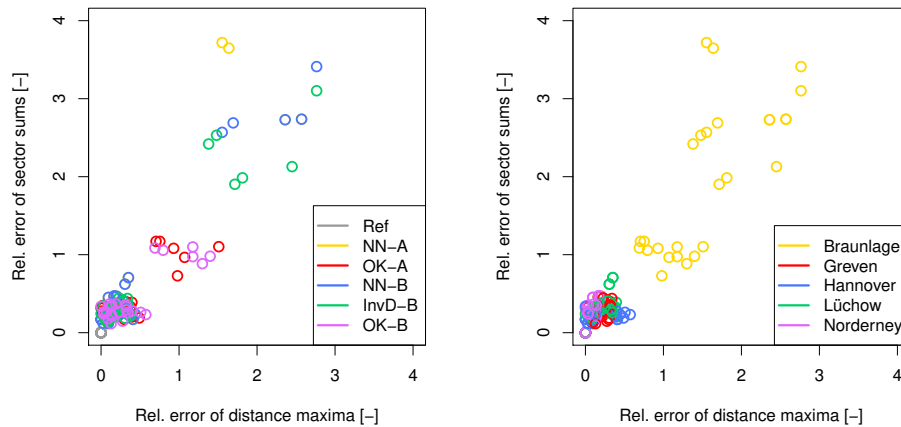
Figure 9.3: Relative error of distance maxima σ_{MAX} vs. relative error of sectoral amounts σ_{SEC} depending on interpolation method (left) and station (right)

method, time period, and emission source type. In the left panel the points are colour-coded regarding the interpolation method, while in the right panel the point color specifies the validation site.

In the left panel, it is seen that some interpolation techniques based on NN and InvD cause a high error in particular for the σ_{MAX} criterion. The right panel shows that only the validation site Braunlage is affected by these high deviations. The two interpolation approaches based on OK achieve a significantly better result than the other techniques for this specific location. If Braunlage is not taken into account for the evaluations, the benefit of OK is less significant compared to InvD and NN but still evident. In this case the OK methods achieve σ_{MAX} and σ_{SEC} values which are approx. 30 % and 20 % lower than the corresponding NN equivalent. It

is assumed that the advantages of InvD and OK are related to the smoothing effect caused by these methods. NN selects the data of one specific wind gauge, whose data might have entirely different characteristics of wind velocity and direction frequencies due to the influence of local topography. In particular OK helps to avoid this problem.

9.4.2 Precipitation data validation

The results for the first scenario of the precipitation evaluations, i.e. no correction of the annual rainfall sum, are shown in Fig. 9.4, wherein the evaluations regarding wet deposition maxima are displayed in the left panel and the evaluations regarding the sectoral amounts of wet deposition in the right. The criteria σ_{MAX} and σ_{SEC} were calculated based on the spatial distribution of wet deposition. Dry deposition was considered in the simulation runs but is not used to determine the values.

KED (Radar) and CM deliver the best result in terms of σ_{MAX}. NN and OK perform slightly worse, while the multi-step techniques cause higher errors. The σ_{SEC} errors are in general somewhat lower than the σ_{MAX} values. NN achieves the best performance here, while the multi-step techniques are able to reduce the high errors of OK, KED (Radar) and CM to a certain extent. The reason for the high errors caused by the geostatistical methods is, that the annual rainfall sum is not met by the hourly interpolations as discussed in Sec. 7.3. The kriging approaches do not cause a significant bias in space for the single hourly time steps but might cause a high temporal bias for time series of individual point location.

Figure 9.5 contains the results of the second scenario. The hourly precipitation time series obtained by spatial interpolation were scaled to the actual annual sums. In practice, the true annual sum is unknown for the validation points. However, the evaluations in Sec. 6.2 proved that the error of spatial interpolation is much lower when large time scales are regarded. Due to this, it is assumed that the annual rainfall may be obtained with a negligible error from a direct interpolation on the annual time scale. CM and MS-KED deliver the best result in terms of σ_{MAX}, while MS-OK and KED perform only slightly worse. NN as well as MS-CM generate the highest deviation of wet deposition maxima. Also for the scaling scenario, the σ_{SEC} values are always lower for the multi-step interpolation techniques compared to their single step equivalents. MS-OK delivers the best performance, while the error of MS-CM is just slightly higher. Considering both criteria, MS-OK and MS-KED achieve the best result. In general, the incorporation of radar data does not achieve an improvement compared to
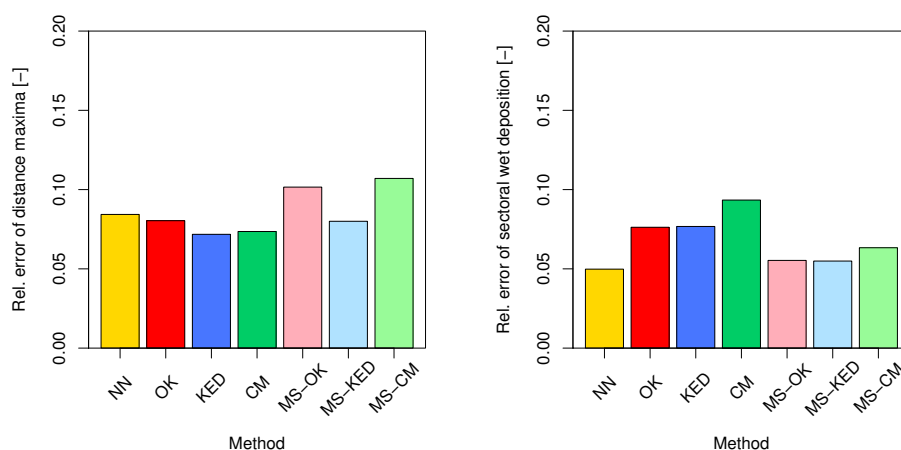
Figure 9.4: Relative error of distance maxima σ_{MAX} (left) and sectoral amounts σ_{SEC} (right) of dry deposition averaged over all emission sources, time periods and stations for each precipitation interpolation method without scaling to annual sums
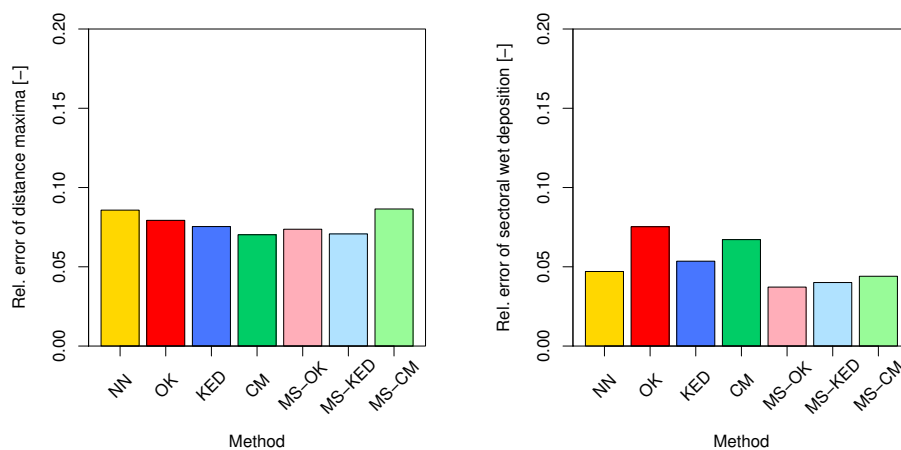
Figure 9.5: Relative error of distance maxima σ_{MAX} (left) and sectoral amounts σ_{SEC} (right) of dry deposition averaged over all emission sources, time periods and stations for each precipitation interpolation method with scaling to annual sums

univariate interpolation by MS-OK. The relative improvement of MS-OK compared to NN is around 15 % for σ_{MAX} and 12 % for σ_{SEC}.

Figure 9.6 and Fig. 9.7 contain a detailed depictions of the results. Figure 9.6 shows σ_{MAX} and σ_{SEC} for the no-scaling scenario (left panel) and the scenario of scaling to annual sums (right panel). The points representing one simulation run for a certain source type, validation site and time period are colour-coded with respect to the interpolation technique. The σ_{SEC} values are generally lower in the right panel, thus scaling to the annual rainfall sum causes a better performance. In both scenarios there are high errors in terms of σ_{MAX} for some simulations.
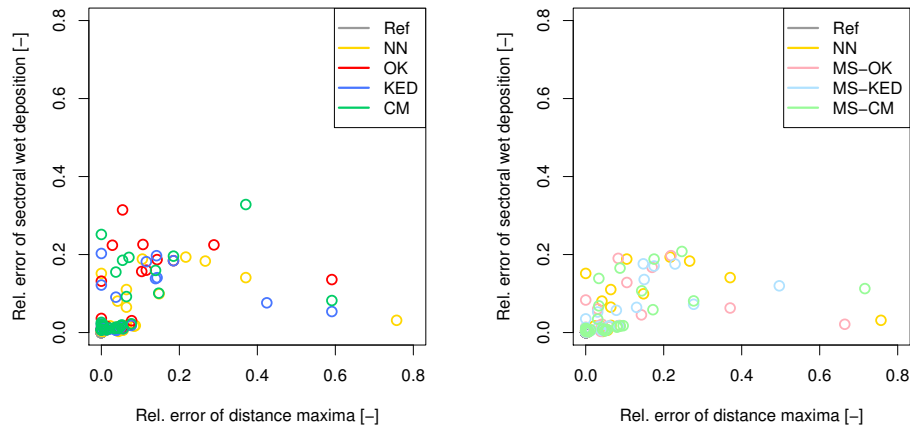
Figure 9.6: Relative error of distance maxima σ_{MAX} vs. relative error of sectoral amounts σ_{SEC} for scaled single-step interpolation methods (left) and scaled multi-step interpolation methods (right)
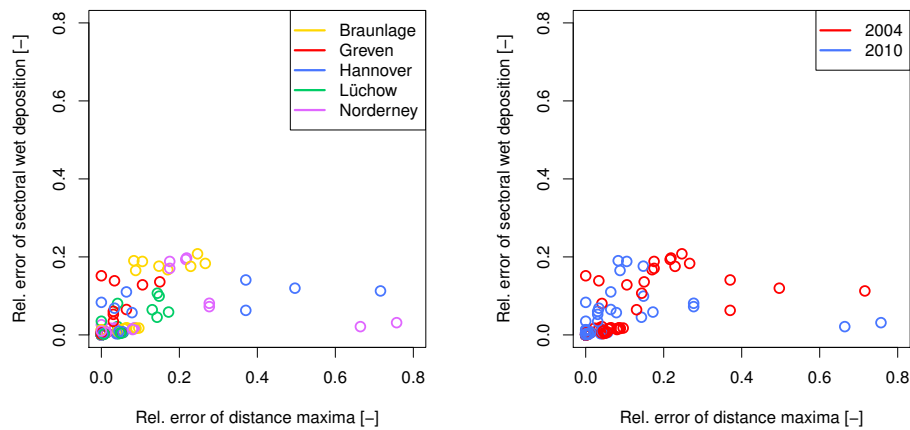
Figure 9.7: Relative error of distance maxima σ_{MAX} vs. relative error of sectoral amounts σ_{SEC} depending on station (left) and year (right) for scaled multi-step interpolation methods

Figure 9.7 shows the results for the scenario in which scaling to the true annual rainfall sum is applied. The points representing individual simulations are colour-coded depending on validation site (left panel) and time period (right panel). It is seen that the σ_{MAX} values belong to the validation sites Norderney and Hanover, whereas the year 2010 is affected for Norderney and the year 2004 for Hanover. In particular Norderney has a lower station density compared to the other validation sites and due to its location on the North Sea, there are in general higher wind velocities. The poor performance for Hanover is in general based on the lower station density in 2004, since only simulations for this time period are affected. Moreover, it is seen that there are some high errors of around 0.2 for the validation site Braunlage. It is assumed that they could be related to the high elevation. Further investigations, which are not shown here,

showed that the annual rainfall sum is strongly underestimated by all interpolation techniques for this location and hence a multiplication with a high factor was carried out for the scaling.

9.5 Conclusions

It may be concluded that the smoothing effect of ordinary kriging helps for the interpolation of wind data. The error of dry deposition caused by either a direct individual interpolation of wind velocity and direction or an interpolation of velocity components with a subsequent transformation to absolute wind velocity and direction is significantly lower when OK is applied. Nevertheless, the error range is still relatively high and the selection of a station with a similar distribution of wind direction and velocity might achieve a better result.

The bias resulting from an aggregation of interpolated hourly rainfall is crucial for considering wet deposition in simulating contaminant transport in the atmosphere. A scaling to the actual annual rainfall sum is required in order to achieve a better performance. Moreover, multi-step interpolation, i.e. an IK interpolation of rainfall occurrence prior to the actual rainfall interpolation, delivers a much better result. These techniques allow a sharp separation of wet and dry regions, which results in a more realistic number of wet hours in the interpolated time series. The incorporation of radar data in CM and KED as well as their corresponding multi-step equivalents is not able to improve the result, although their benefit is clearly seen in the cross validation error statistics.

Chapter 10

Summary, conclusions and outlook

All investigations of this work are briefly summarised in 10.1, while Sec. 10.2 contains a comprehensive synopsis of all conclusions that were drawn. Furthermore, an outlook for future research is presented in Sec. 10.3.

10.1 Summary

This thesis investigated different spatial interpolation techniques regarding their performance for various climate variables observed by weather stations. Simple interpolation techniques (NN, InvD) and more sophisticated geostatistical approaches (OK, IK, KED, IKED, CM) were taken into account, whereas this depends on the specific meteorological variable that is analysed. For each climate variable, different additional information based on topography, other measurements and other factors were used in multivariate interpolation techniques. In particular, radar data were preprocessed in order to improve the spatial interpolation of rainfall. This included smoothing of radar grids and detection of time steps with poor radar data quality.

Cross validation experiments based on different temporal resolutions and station density scenarios were implemented in order to determine the interpolation performance for each climate variable. In all cases OK was selected as the standard of comparison, since it is the univariate interpolation technique that delivers the best interpolation performance in general. The interpolation performance of all other interpolation methods was compared to that and shown for each combination of temporal resolution and network density scenario. Moreover, the interpolation performance was compared among all considered climate variables and different realisations of randomly selected stations. In addition to that, the direct time scale

specific interpolation performance for long time periods was compared with the accumulation or average of fine temporal resolution interpolations.

Time series of precipitation and entire spatial rainfall fields were estimated by various methods and also obtained from radar data for a temporal resolution of 5 min in order to investigate, wether they can provide adequate data for different urban hydrological purposes. The estimated rainfall was used as a model input for two different urban catchments implemented in SWMM. Additionally, hourly time series of interpolated wind data and precipitation were validated for different locations, time periods and interpolation methods using an atmospheric pollutant transport model.

10.2 Conclusions

At first, the conclusions regarding the interpolation of rainfall with a high temporal resolution (5 min to 360 min) are presented. Only radar data were used as an additional information. Generally, it is assumed that the results are valid for regions with similar topography, nevertheless a different behavior might be possible in regions which are predominantly mountainous. Furthermore, the results of this comparison are related to the merging of continuous time series. Combining radar and rain gauge data for a specific event may lead to different findings.

1. Radar data smoothing is strongly recommended for the merging of radar and rain gauge data using geostatistical techniques. The application of CM with non-smoothed radar data led to significantly worse results compared to smoothed data and shows even no benefit at all of using radar data for very high temporal resolutions.

2. In case of 60 min temporal resolution, smoothing improves the merging performance on average. However, a consistent improvement for all hourly time steps is not achieved. A spatio-temporal method is considered as the best approach to smooth the radar grids. The interpolation performance improves with stronger smoothing, but the preservation of the observation variance is reduced. Too strong smoothing is not recommended because this results in a loss of information about the spatial rainfall structure.

3. CM delivered the best interpolation performance. It outperforms KED and IKED for all combinations of station density scenarios and temporal resolution from 5 min to 360 min.

4. An improvement of interpolation performance in comparison to OK was achieved even for radar and rain gauge data with a 5 min temporal resolution. Although the correlation between rain gauge values and the corresponding radar pixels is much lower for high temporal resolutions, the merging process benefitted from the incorporation smoothed radar grids.

5. A detection of time steps with a poor radar data quality can improve the interpolation performance significantly for all methods.

6. The temporal data resolution has a strong impact on the interpolation performance, whereas the network density does not seem as important. In general the interpolation performance decreases with increasing temporal resolution and decreasing station density.

The following conclusions are drawn from the investigation of 5 min rainfall with an urban hydrological model, whereas the rainfall time series were investigated regarding their suitability for different purposes or tasks in urban hydrology.

1. Radar data as preprocessed in this work overestimate rainfall extremes for all durations and can therefore not be used for estimating design rainfall. CM is able to reduce this problem but a significant overestimation is remaining. NN delivered the best representation of rainfall extremes, while OK and a quantile-mapping radar correction technique (BIASC) result in an underestimation.

2. The implementation of radar data and CM interpolated rainfall in an urban hydrological model results in an overestimation of flooding, while OK and BIASC cause an underestimation. NN delivered the best result.

3. The incorporation of radar data is strongly recommended for the analysis of single rainfall events with an urban hydrological model. Some events are not detected by the rain gauge network and CM will provide adequate data for many events if radar data of a sufficient quality are available. Uncorrected radar data should not be used as a model input since strong overestimation or underestimation of rainfall can occur.

4. In case of a high station density, NN and OK interpolated data allow the simulation of most single events with a reasonable performance. However, the model performance decreases strongly if the closest station to the urban catchment is far away.

5. NN and OK achieve a good performance for the analysis of combined sewer overflows using a continuous simulation. Radar underestimates CSO volumes, while CM generates an overestimation.

6. For all urban hydrological simulations, the interpolation method appears to be more important than the difference between the full spatial distribution and single point rainfall as a model input.

In general it is difficult to predict a universal behaviour of radar, since the data quality changes from event to event. Strong overestimation happens for some events and underestimation for others. Errors could be reduced by merging them with rain gauge recordings. Nevertheless, a strong mismatch between gauge and radar information and thus a high error of rainfall estimation might occur.

The following enumeration contains all conclusions from the interpolation of climate information for temporal resolutions of 1 h to 1 a, while different additional information was considered. Also the precipitation interpolations for these time scales are included here.

1. KED using radar as the additional information can improve the interpolation performance of rainfall in comparison to OK particularly for fine temporal resolutions of 1 hour and 1 day. Also for larger accumulation times, a slight improvement was observed. In case of a low station density, it might happen that KED performs worse than OK for high temporal resolutions. KED incorporating the DEM is especially helpful for long time periods but cannot achieve an improvement for high temporal resolutions. When both data sources are used in multivariate KED, a corresponding improvement is achieved for almost all station densities and temporal resolutions. CM delivers the best performance for hourly data but performs worse than OK and KED for temporal resolutions of 1 day or lower.

2. KED using the DEM performs significantly better than OK for temperature data for all temporal resolutions and station densities, while an incorporation of relative humidity could only achieve a slight improvement.

3. KED using temperature grids delivered the best interpolation performance for relative humidity. All combinations of station density and temporal resolution could be improved compared to OK. The incorporation of precipitation grids could only achieve an improvement for the annual time scale. Taking into account the DEM can achieve a minor benefit for some station densities and temporal resolutions.

4. No useful additional information was found for the interpolation of cloud coverage, sunshine duration and wind data. The application of OK resulted in the best interpolation performance for all station densities and temporal resolutions.

5. The simple approaches NN and InvD cannot reach the interpolation performance of OK for most climate variables. Only for precipitation, InvD performs similarly well as OK if a very dense station network is available.

6. The influence of the random station selection on the interpolation performance varies strongly on the climate variable that is interpolated. In particular for wind velocity, a strong impact of the station selection was observed.

7. Moreover, the interpolation performance depends generally on temporal resolution, station density and the specific spatial variability of the climate information. The influences of temporal resolution and spatial variability appear to be higher than the influence of station density.

8. Precipitation with a high temporal resolution shows the highest spatial variability and thus the worst interpolation performance is obtained. For all meteorological variables except wind velocity, the spatial variability decreases with decreasing temporal resolution. The influence of local topography results in a rather poor interpolation performance for wind data, while the best estimation accuracy is achieved for relative humidity and temperature.

9. The calculation of long terms averages or aggregations of fine temporal resolutions is not recommended. A significant increase of Bias might occur in particular for rainfall accumulations when radar is considered.

All results were obtained from the interpolation of continuous time series, i.e. the analysis of single events or short time step sequences might lead to different findings, in particular when radar is taken into account for rainfall interpolation. The study area is characterised by rather few topographic elevations. Especially for wind data it is assumed that the interpolation performance might decrease even further, if a more mountainous area is investigated. The interpolation performances of temperature and relative humidity seem to be rather robust, due to the consideration of DEM and the low spatial variability.

The investigation of time series with a transport model for atmospheric pollutants illustrate, that the spatial interpolation using geostatistics might not be able to reproduce certain characteristics of rainfall time series. In particular the bias of annual rainfall sum caused by the aggregation of hourly interpolations is a problem and needs to be corrected. The main conclusions derived from the transport simulations are summarised as follows:

1. The annual sum of rainfall time series must be corrected in order to achieve good results in simulating the annual spatial distribution of wet deposition.

2. Multi-step interpolation techniques that imply an interpolation of rainfall occurrence by IK are required for obtaining precipitation time series with a realistic fraction of wet and dry time steps, respectively.

3. MS-OK and MS-KED achieve the best result, however the incorporation of radar information in MS-KED could not improve the simulation results

4. When wind data are interpolated, the smoothing effect of OK enables a better simulation of dry deposition compared to NN and InvD.

In general, the benefit of using geostatistical interpolation techniques depends strongly on the purpose for which the data should be used. Due to the smoothing effect, the potential of kriging is rather low for applications in which climate extremes are important.

10.3 Outlook

Overall, it is assumed that a better preprocessing of radar data can improve the interpolation performance of fine temporal resolution rainfall. The development of a more sophisticated strategy taking into account further information in order to classify rainfall events might allow the consideration of a variable Z-R relationship and help to improve radar-based quantitative rainfall estimates and a corresponding merging with ground observations. Furthermore, radar data could be analysed regarding their potential to provide areal information of precipitation extremes. Areal reduction factors could be computed from spatial distributions of rainfall fields, for instance.

The difference in interpolation performance depending on the randomly selected stations suggest that there is a potential for the analysis of network optimisation. The meteorological observation of climate variables provides more valuable information for some sites than for others.

The investigation of rainfall interpolation regarding their potential to provide time series for the simulation of pollutant transport suggests, that there is a need for a technique that is able to optimise the interpolation performance on various time scales. The universal interpolation of

all time scales could allow the generation of data sets that can be used for multiple hydrological and environmental purposes.

It is not clear whether certain hydrological and environmental models are able to take advantage of the improved estimation of climate information. It is assumed that a relatively detailed model structure must be available for the validation of a potential benefit. In particular, the estimation of rainfall with a fine temporal resolution could be tested with an urban model of a catchment with more local reference gauges and conduit flow data.

List of Figures

List of Tables

List of Abbreviations

BIASC	Bias correction
BKG	German Federal Agency for Cartography and Geodesy (*Bundesamt für Kartographie und Geodäsie*)
BLUE	Best linear unbiased estimator
cdf	Cumulative Probability Density Function
CDC	Climate Data Centre (*Meteorological data recorded by the DWD*)
CLD	Cloud Coverage
CM	Conditional Merging
CSO	Combined Sewer Overflow
DEM	Digital Elevation Model
DWD	German Weather Service (*Deutscher Wetterdienst*)
GIDS	Gradient-Plus-Inverse-Distance-Squared Method
GSLIB	Geostatistical Software Library
KED	Kriging with External Drift
HUM	Relative Humidity
IDF	Intensity – Duration – Frequency
IK	Indicator Kriging
IKED	Indicator Kriging with External Drift
InvD	Inverse-Distance Weighting
MS-CM	Multi-Step Conditional Merging
MS-KED	Multi-Step Kriging with External Drift
MS-OK	Multi-Step Ordinary Kriging
NN	Nearest Neighbour
NSE	Nash-Sutcliffe Efficiency
OK	Ordinary Kriging
PCP	Precipitation
QPE	Quantitative Precipitation Estimates
SUN	Sunshine Duration

SWMM	Storm Water Management Model
TAV	Mean Temperature
TMA	Maximum Temperature
TMI	Minimum Temperature
UBA	German Federal Environment Agency (*Umweltbundesamt*)
US-EPA	United States Environmental Protection Agency
WDI	Wind Direction
WMO	World Meteorological Organisation
WVE	Wind Velocity
Z-R	Radar Reflectivity – Rainfall Rate

Bibliography

AHMED, S. and G. DE MARSILY (1987). "Comparison of geostatistical methods for estimating transmissivity using data on transmissivity and specific capacity". In: *Water Resources Research* 23.9, pp. 1717–1737.

AKIN, H. and H. SIEMES (1988). *Praktische Geostatistik - Eine Einführung für den Bergbau und die Geowissenschaften*. Berlin: Springer.

ALLAMANO, P., P. CLAPS, F. LAIO, and C. THEA (2009). "A data-based assessment of the dependence of short-duration precipitation on elevation". In: *Physics and Chemistry of the Earth, Parts A/B/C* 34.10–12, pp. 635–641.

ALSAMAMRA, H., J. A. RUIZ-ARIAS, D. POZO-VÁZQUEZ, and J. TOVAR-PESCADOR (2009). "A comparative study of ordinary and residual kriging techniques for mapping global solar radiation over southern Spain". In: *Agricultural and Forest Meteorology* 149.8, pp. 1343–1357.

ANGSTROM, A. (1924). "Solar and terrestrial radiation. Report to the international commission for solar research on actinometric investigations of solar and atmospheric radiation". In: *Quarterly Journal of the Royal Meteorological Society* 50.210, pp. 121–126.

ANTONANZAS, J., R. URRACA, F. J. MARTINEZ-DE-PISON, and F. ANTONANZAS-TORRES (2015). "Solar irradiation mapping with exogenous data from support vector regression machines estimations". In: *Energy Conversion and Management* 100, pp. 380–390.

APAYDIN, H., F. K. SONMEZ, and Y. E. YILDIRIM (2004). "Spatial interpolation techniques for climate data in the GAP region in Turkey". In: *Climate Research* 28.1, pp. 31–40.

AZIMI-ZONOOZ, A., W. F. KRAJEWSKI, D. S. BOWLES, and D.-J. SEO (1989). "Spatial rainfall estimation by linear and non-linear co-kriging of radar-rainfall and raingage data". In: *Stochastic Hydrology and Hydraulics* 3.1, pp. 51–67.

BÁRDOSSY, A. (2006). "Copula-based geostatistical models for groundwater quality parameters". In: *Water Resources Research* 42.11, W11416.

BÁRDOSSY, A. and J. LI (2008). "Geostatistical interpolation using copulas". In: *Water Resources Research* 44.7, W07412.

BÁRDOSSY, A. and G. PEGRAM (2013). "Interpolation of precipitation under topographic influence at different time scales". In: *Water Resources Research* 49.8, pp. 4545–4565.

BÁRDOSSY, A. and G. PEGRAM (2014). "Infilling missing precipitation records - A comparison of a new copula-based method with other techniques". In: *Journal of Hydrology* 519, Part A, pp. 1162–1170.

BERNDT, C., E. RABIEI, and U. HABERLANDT (2014). "Geostatistical merging of rain gauge and radar data for high temporal resolutions and various station density scenarios". In: *Journal of Hydrology* 508, pp. 88–101.

BERNE, A., G. DELRIEU, J.-D. CREUTIN, and C. OBLED (2004). "Temporal and spatial resolution of rainfall measurements required for urban hydrology". In: *Urban Hydrology* 299.3–4, pp. 166–179.

BERTRAND, C., C. DEMAIN, and M. JOURNÉE (2013). "Estimating daily sunshine duration over Belgium by combination of station and satellite data". In: *Remote Sensing Letters* 4.8, pp. 735–744.

BIERKENS, M. F. P. and P. A. BURROUGH (1993). "The indicator approach to categorical soil data". In: *Journal of Soil Science* 44.2, pp. 361–368.

BMU (2002). *Erste Allgemeine Verwaltungsvorschrift zum Bundes-Immissionsschutzgesetz (Technische Anleitung zur Reinhaltung der Luft - TA Luft)*. Bundesministerium für Umwelt, Naturschutz und Reaktorsicherheit.

BORGA, M. (2002). "Accuracy of radar rainfall estimates for streamflow simulation". In: *Journal of Hydrology* 267.1–2, pp. 26–39.

BORGA, M., E. N. ANAGNOSTOU, and E. FRANK (2000). "On the use of real-time radar rainfall estimates for flood prediction in mountainous basins". In: *Journal of Geophysical Research: Atmospheres (1984–2012)* 105, pp. 2269–2280.

BOX, G. E. P. and D. R. COX (1964). "An analysis of transformations". In: *Journal of the Royal Statistical Society. Series B (Methodological)* 26.2, pp. 211–252.

BRANDES, E. A. (1975). "Optimizing rainfall estimates with the aid of Radar". In: *Journal of Applied Meteorology* 14.7, pp. 1339–1345.

BRUNI, G., R. REINOSO, N. C. VAN DE GIESEN, F. H. L. R. CLEMENS, and J. A. E. TEN VELDHUIS (2015). "On the sensitivity of urban hydrodynamic modelling to rainfall spatial and temporal resolution". In: *Hydrology and Earth System Sciences* 19.2, pp. 691–709.

CELLURA, M., G. CIRRINCIONE, A. MARVUGLIA, and A. MIRAOUI (2008a). "Wind speed spatial estimation for energy planning in Sicily: Introduction and statistical analysis". In: *Renewable Energy* 33.6, pp. 1237–1250.

CELLURA, M., G. CIRRINCIONE, A. MARVUGLIA, and A. MIRAOUI (2008b). "Wind speed spatial estimation for energy planning in Sicily: A neural kriging application". In: *Renewable Energy* 33.6, pp. 1251–1266.

CHANG, C. L., S. L. LO, and S. L. YU (2005). "Applying fuzzy theory and genetic algorithm to interpolate precipitation". In: *Journal of Hydrology* 314.1–4, pp. 92–104.

CHAPPELL, A., L. J. RENZULLO, T. H. RAUPACH, and M. HAYLOCK (2013). "Evaluating geostatistical methods of blending satellite and gauge data to estimate near real-time daily rainfall for Australia". In: *Journal of Hydrology* 493, pp. 105–114.

CHELBI, M., Y. GAGNON, and J. WAEWSAK (2015). "Solar radiation mapping using sunshine duration-based models and interpolation techniques: Application to Tunisia". In: *Energy Conversion and Management* 101, pp. 203–215.

CHUMCHEAN, S., A. SEED, and A. SHARMA (2006). "Correcting of real-time radar rainfall bias using a Kalman filtering approach". In: *Journal of Hydrology* 317.1–2, pp. 123–137.

CHUMCHEAN, S., A. SHARMA, and A. SEED (2003). "Radar rainfall error variance and its impact on radar rainfall calibration". In: *Physics and Chemistry of the Earth, Parts A/B/C* 28.1–3, pp. 27–39.

CHUNG, U. and J. I. YUN (2004). "Solar irradiance-corrected spatial interpolation of hourly temperature in complex terrain". In: *Agricultural and Forest Meteorology* 126.1–2, pp. 129–139.

COULIBALY, P. and N. D. EVORA (2007). "Comparison of neural network methods for infilling missing daily weather records". In: *Journal of Hydrology* 341.1–2, pp. 27–41.

COURAULT, D. and P. MONESTIEZ (1999). "Spatial interpolation of air temperature according to atmospheric circulation patterns in southeast France". In: *International Journal of Climatology* 19.4, pp. 365–378.

CRESSIE, N. (1986). "Kriging nonstationary data". In: *Journal of the American Statistical Association* 81.395, pp. 625–634.

CRESSIE, N. (1990). "The origins of kriging". In: *Mathematical Geology* 22.3, pp. 239–252.

CREUTIN, J. D. and C. OBLED (1982). "Objective analyses and mapping techniques for rainfall fields: An objective comparison". In: *Water Resources Research* 18.2, pp. 413–431.

DALY, C., R. P. NEILSON, and D. L. PHILLIPS (1994). "A statistical-topographic model for mapping climatological precipitation over mountainous terrain". In: *Journal of Applied Meteorology* 33.2, pp. 140–158.

DELRIEU, G., A. WIJBRANS, B. BOUDEVILLAIN, D. FAURE, L. BONNIFAIT, and P.-E. KIRSTETTER (2014). "Geostatistical radar-raingauge merging: A novel method for the quantification of rain estimation accuracy". In: *Advances in Water Resources* 71, pp. 110–124.

DEUTSCH, C. V. and A. G. JOURNEL (1992). *GSLIB: Geostatistical software library and user's guide*. Oxford University Press.

DI PIAZZA, A., F. LO CONTI, L. V. NOTO, F. VIOLA, and G. LA LOGGIA (2011). "Comparative analysis of different techniques for spatial interpolation of rainfall data to create a serially complete monthly time series of precipitation for Sicily, Italy". In: *International Journal of Applied Earth Observation and Geoinformation* 13.3, pp. 396–408.

DINKU, T., E. N. ANAGNOSTOU, and M. BORGA (2002). "Improving radar-based estimation of rainfall over complex terrain". In: *Journal of Applied Meteorology* 41.12, pp. 1163–1178.

DIRKS, K. N., J. E. HAY, C. D. STOW, and D. HARRIS (1998). "High-resolution studies of rainfall on Norfolk Island: Part II: Interpolation of rainfall data". In: *Journal of Hydrology* 208.3–4, pp. 187–193.

DODSON, R. and D. MARKS (1997). "Daily air temperature interpolated at high spatial resolution over a large mountainous region". In: *Climate Research* 8.1, pp. 1–20.

DOLINAR, M. (2006). "Spatial interpolation of sunshine duration in Slovenia". In: *Meteorological Applications* 13.4, pp. 375–384.

DWA-A 531 (2012). *Starkregen in Abhängigkeit von Wiederkehrzeit und Dauer*. Arbeitsblatt der DWA, Hennef.

DWARAKISH, G. S., C. SIVAPRAGASAM, N. MUTTIL, M. C. JESELIA, and S. VISWESHWARAN (2015). "INTERNATIONAL CONFERENCE ON WATER RESOURCES, COASTAL AND OCEAN ENGINEERING (ICWRCOE'15) Infilling of rainfall information using genetic programming". In: *Aquatic Procedia* 4, pp. 1016–1022.

DWD (2005). *KOSTRA-DWD-2000 – Starkniederschlagshöhen für Deutschland (1951-2000)*. Deutscher Wetterdienst, Abteilung Hydrometeorologie, Offenbach am Main.

DWD (2016). *Website of the German Weather Service*. URL: http://www.dwd.de (Retrieved: 04/28/2016).

EHRET, U. (2003). *Rainfall and flood nowcasting in small catchments using weather radar*. 1st ed. Mitteilungen 121. Stuttgart: Eigenverlag des Instituts für Wasserbau der Universitaet Stuttgart.

EINFALT, T., K. ARNBJERG-NIELSEN, C. GOLZ, N.-E. JENSEN, M. QUIRMBACH, G. VAES, and B. VIEUX (2004). "Towards a roadmap for use of radar rainfall data in urban drainage". In: *Journal of Hydrology* 299.3–4, pp. 186–202.

EINFALT, T., V. KREJCI, and W. SCHILLING (1998). "Rainfall data in urban hydrology". In: *Hydroinformatics tools for planning, design, operation and rehabilitation of sewer systems*. Ed. by J. MARSALEK, C. MAKSIMOVIC, E. ZEMAN, and R. PRICE. Dordrecht: Springer Netherlands, pp. 129–168.

ELDARDIRY, H., E. HABIB, and Y. ZHANG (2015). "On the use of radar-based quantitative precipitation estimates for precipitation frequency analysis". In: *Journal of Hydrology* 531, Part 2, pp. 441–453.

ERDIN, R., C. FREI, and H. R. KÜNSCH (2012). "Data transformation and uncertainty in geostatistical combination of radar and rain gauges". In: *Journal of Hydrometeorology* 13.4, pp. 1332–1346.

FREI, C., M. WILLI, R. STÖCKLI, and B. DÜRR (2015). "Spatial analysis of sunshine duration in complex terrain by non-contemporaneous combination of station and satellite data". In: *International Journal of Climatology* 35.15, pp. 4771–4790.

GARCIA, P., A. BENARROCH, and J. M. RIERA (2008). "Spatial distribution of cloud cover". In: *International Journal of Satellite Communications and Networking* 26.2, pp. 141–155.

GERMANN, U. and J. JOSS (2001). "Variograms of radar reflectivity to describe the spatial continuity of alpine precipitation". In: *Journal of Applied Meteorology* 40.6, pp. 1042–1059.

GONZÁLEZ DE LA ROSA, J. J., A. AGÜERA PÉREZ, J. C. PALOMARES SALAS, J. G. RAMIRO LEO, and A. MORENO MUÑOZ (2011). "A novel inference method for local wind conditions using genetic fuzzy systems". In: *Renewable Energy* 36.6, pp. 1747–1753.

GOODALE, C. L., G. D. ABER, and S. V. OLLINGER (1998). "Mapping monthly precipitation, temperature, and solar radiation for Ireland with polynomial regression and a digital elevation model". In: *Climate Research* 10.1, pp. 35–49.

GOODIN, W. R., G. J. MCRA, and J. H. SEINFELD (1979). "A comparison of interpolation methods for sparse data: application to wind and concentration fields". In: *Journal of Applied Meteorology* 18.6, pp. 761–771.

GOOVAERTS, P. (1997). *Geostatistics for natural resources evaluation*. New York: Oxford University Press.

GOOVAERTS, P. (2000). "Geostatistical approaches for incorporating elevation into the spatial interpolation of rainfall". In: *Journal of Hydrology* 228.1, pp. 113–129.

GOUDENHOOFDT, E. and L. DELOBBE (2009). "Evaluation of radar-gauge merging methods for quantitative precipitation estimates". In: *Hydrology and Earth System Sciences* 13.2, pp. 195–203.

GRIMES, D. I. F., E. PARDO-IGÚZQUIZA, and R. BONIFACIO (1999). "Optimal areal rainfall estimation using raingauges and satellite data". In: *Journal of Hydrology* 222.1–4, pp. 93–108.

GRIMM, J. W. and J. A. LYNCH (2004). "Enhanced wet deposition estimates using modeled precipitation inputs". In: *Environmental Monitoring and Assessment* 90.1, pp. 243–268.

HABERLANDT, U. (2007). "Geostatistical interpolation of hourly precipitation from rain gauges and radar for a large-scale extreme rainfall event". In: *Journal of Hydrology* 332.1–2, pp. 144–157.

HABERLANDT, U. and M. SESTER (2010). "Areal rainfall estimation using moving cars as rain gauges - a modelling study". In: *Hydrology and Earth System Sciences* 14.7, pp. 1139–1151.

HAYLOCK, M. R., N. HOFSTRA, A. M. G. KLEIN TANK, E. J. KLOK, P. D. JONES, and M. NEW (2008). "A European daily high-resolution gridded data set of surface temperature and precipitation for 1950–2006". In: *Journal of Geophysical Research: Atmospheres* 113.D20, p. D20119.

HEVESI, J. A., J. D. ISTOK, and A. L. FLINT (1992a). "Precipitation estimation in mountainous terrain using multivariate geostatistics. Part I: Structural analysis". In: *Journal of Applied Meteorology* 31.7, pp. 661–676.

HEVESI, J. A., A. L. FLINT, and J. D. ISTOK (1992b). "Precipitation estimation in mountainous terrain using multivariate geostatistics. Part II: Isohyetal maps". In: *Journal of Applied Meteorology* 31.7, pp. 677–688.

HOFSTRA, N., M. HAYLOCK, M. NEW, P. JONES, and C. FREI (2008). "Comparison of six methods for the interpolation of daily, European climate data". In: *Journal of Geophysical Research: Atmospheres* 113.D21, p. D21110.

HOLDAWAY, M. R. (1996). "Spatial modeling and interpolation of monthly temperature using kriging". In: *Climate Research* 06.3, pp. 215–225.

HONG, Y., H. A. NIX, M. F. HUTCHINSON, and T. H. BOOTH (2005). "Spatial interpolation of monthly mean climate data for China". In: *International Journal of Climatology* 25.10, pp. 1369–1379.

HUDSON, G. and H. WACKERNAGEL (1994). "Mapping temperature using kriging with external drift: Theory and an example from scotland". In: *International Journal of Climatology* 14.1, pp. 77–91.

HUTCHINSON, M. F. (1998a). "Interpolation of rainfall data with thin plate smoothing splines. Part I: Two dimensional smoothing of data with short range correlation". In: *Journal of Geographic Information and Decision Analysis* 2.2, pp. 139–151.

HUTCHINSON, M. F. (1998b). "Interpolation of rainfall data with thin plate smoothing splines. Part II: Analysis of topographic dependence". In: *Journal of Geographic Information and Decision Analysis* 2.2, pp. 152–167.

HUTCHINSON, M. F., D. W. MCKENNEY, K. LAWRENCE, J. H. PEDLAR, R. F. HOPKINSON, E. MILEWSKA, and P. PAPADOPOL (2009). "Development and testing of Canada-wide interpolated spatial models of daily minimum-maximum temperature and precipitation for 1961-2003". In: *Journal of Applied Meteorology and Climatology* 48.4, pp. 725–741.

IMHOFF, K. and K. R. IMHOFF (2010). *Taschenbuch der Stadtentwässerung.* Industrieverlag, Oldenburg.

ISAAKS, E. H. and R. M. SRIVASTAVA (1990). *An introduction to applied geostatistics*. New York: Oxford University Press.

JANG, S., M CHO, J. YOON, Y. YOON, S. KIM, G. KIM, L. KIM, and H. AKSOY (2007). "Using SWMM as a tool for hydrologic impact assessment". In: *Desalination* 212.1, pp. 344–356.

JARVIS, C. H. and N. STUART (2001a). "A comparison among strategies for interpolating maximum and minimum daily air temperatures. Part I: the selection of "guiding" topographic and land cover variables". In: *Journal of Applied Meteorology* 40.6, pp. 1060–1074.

JARVIS, C. H. and N. STUART (2001b). "A comparison among strategies for interpolating maximum and minimum daily air temperatures. Part II: the interaction between number of guiding variables and the type of interpolation method". In: *Journal of Applied Meteorology* 40.6, pp. 1075–1084.

JEFFREY, S. J., J. O. CARTER, K. B. MOODIE, and A. R. BESWICK (2001). "Using spatial interpolation to construct a comprehensive archive of Australian climate data". In: *Environmental Modelling & Software* 16.4, pp. 309–330.

JOURNÉE, M., C. DEMAIN, and C. BERTRAND (2013). "Sunshine duration climate maps of Belgium and Luxembourg based on Meteosat and in-situ observations". In: *Advances in Science and Research* 10.1, pp. 15–19.

KALNAY, E., M. KANAMITSU, R. KISTLER, W. COLLINS, D. DEAVEN, L. GANDIN, M. IREDELL, S. SAHA, G. WHITE, J. WOOLLEN, Y. ZHU, A. LEETMAA, R. REYNOLDS, M. CHELLIAH, W. EBISUZAKI, W. HIGGINS, J. JANOWIAK, K. C. MO, C. ROPELEWSKI, J. WANG, Roy JENNE, and D. JOSEPH (1996). "The NCEP/NCAR 40-year reanalysis project". In: *Bulletin of the American Meteorological Society* 77.3, pp. 437–471.

KIRSTETTER, P.-E., J. J. GOURLEY, Y. HONG, J. ZHANG, S. MOAZAMIGOODARZI, C. LANGSTON, and A. ARTHUR (2015). "Probabilistic precipitation rate estimates with ground-based radar networks". In: *Water Resources Research* 51.3, pp. 1422–1442.

KLEIDORFER, M., A. DELETIC, T. D. FLETCHER, and W. RAUCH (2009). "Impact of input data uncertainties on urban stormwater model parameters". In: *Water Science and Technology* 60.6, pp. 1545–1554.

KRAJEWSKI, W. F. (1987). "Cokriging radar-rainfall and rain gage data". In: *Journal of Geophysical Research: Atmospheres* 92.D8, pp. 9571–9580.

KRAJEWSKI, W. F. and J. A. SMITH (2002). "Radar hydrology: rainfall estimation". In: *Advances in Water Resources* 25.8–12, pp. 1387–1394.

KRIGE, D. G. (1951). "A statistical approach to some basic mine valuation problems on the Witwatersrand". In: *Journal of the Chemical, Metallurgical and Mining Society of South Africa* 52.6, pp. 119–139.

KURTZMAN, D. and R. KADMON (1999). "Mapping of temperature variables in Israel: a comparison of different interpolation methods". In: *Climate Research* 13.1, pp. 33–43.

KYRIAKIDIS, P. C., J. KIM, and N. L. MILLER (2001). "Geostatistical mapping of precipitation from rain gauge data using atmospheric and terrain characteristics". In: *Journal of Applied Meteorology* 40.11, pp. 1855–1877.

LEIJNSE, H., R. UIJLENHOET, and J. N. M. STRICKER (2007). "Rainfall measurement using radio links from cellular communication networks". In: *Water Resources Research* 43.3, W03201.

LI, J. and A. D. HEAP (2014). "Spatial interpolation methods applied in the environmental sciences: A review". In: *Environmental Modelling & Software* 53, pp. 173–189.

LI, M. and Q. SHAO (2010). "An improved statistical approach to merge satellite rainfall estimates and raingauge data". In: *Journal of Hydrology* 385.1–4, pp. 51–64.

LI, T., X. ZHENG, Y. DAI, C. YANG, Z. CHEN, S. ZHANG, G. WU, Z. WANG, C. HUANG, Y. SHEN, and R. LIAO (2014). "Mapping near-surface air temperature, pressure, relative humidity and wind speed over Mainland China with high spatiotemporal resolution". In: *Advances in Atmospheric Sciences* 31.5, pp. 1127–1135.

LIU, H., J. SHI, and E. ERDEM (2010). "Prediction of wind speed time series using modified Taylor Kriging method". In: *Energy* 35.12, pp. 4870–4879.

LLOYD, C. D. (2005). "Assessing the effect of integrating elevation data into the estimation of monthly precipitation in Great Britain". In: *Journal of Hydrology* 308.1–4, pp. 128–150.

LU, G. Y. and D. W. WONG (2008). "An adaptive inverse-distance weighting spatial interpolation technique". In: *Computers & Geosciences* 34.9, pp. 1044–1055.

LUO, W., M. C. TAYLOR, and S. R. PARKER (2008). "A comparison of spatial interpolation methods to estimate continuous wind speed surfaces using irregularly distributed data from England and Wales". In: *International Journal of Climatology* 28.7, pp. 947–959.

LY, S., C. CHARLES, and A. DEGRÉ (2011). "Geostatistical interpolation of daily rainfall at catchment scale: the use of several variogram models in the Ourthe and Ambleve catchments, Belgium". In: *Hydrol. Earth Syst. Sci.* 15.7, pp. 2259–2274.

MANIAK, U. (2010). *Hydrologie und Wasserwirtschaft: Eine Einführung für Ingenieure*. Berlin, Heidelberg: Springer.

MARRA, F. and E. MORIN (2015). "Use of radar {QPE} for the derivation of intensity-duration-frequency curves in a range of climatic regimes". In: *Journal of Hydrology* 531, Part 2, pp. 427–440.

MARTÍNEZ-COB, A. (1996). "Multivariate geostatistical analysis of evapotranspiration and precipitation in mountainous terrain". In: *Journal of Hydrology* 174.1, pp. 19–35.

MATHERON, G. (1962). *Traité de géostatistique appliquée*. Vol. 14. Paris: Éditions Technip.

MATZARAKIS, P. A. and D. V. KATSOULIS (2006). "Sunshine duration hours over the Greek region". In: *Theoretical and Applied Climatology* 83.1, pp. 107–120.

MONIN, A. S. and A. M. OBUKHOV (1954). "Basic laws of turbulent mixing in the surface layer of the atmosphere". In: *Contrib. Geophys. Inst. Acad. Sci. USSR* 151.163, pp. 163–187.

MONTEITH, J. L. (1981). "Evaporation and surface temperature". In: *Quarterly Journal of the Royal Meteorological Society* 107.451, pp. 1–27.

NALDER, I. A. and R. W. WEIN (1998). "Spatial interpolation of climatic normals: test of a new method in the Canadian boreal forest". In: *Agricultural and Forest Meteorology* 92.4, pp. 211–225.

NANDING, N., M. A. RICO-RAMIREZ, and D. HAN (2015). "Comparison of different radar-raingauge rainfall merging techniques". In: *Journal of Hydroinformatics* 17.3, pp. 422–445.

NASH, J. E. and J. V. SUTCLIFFE (1970). "River flow forecasting through conceptual models, Part I – A discussion of principles". In: *Journal of Hydrology* 10.3, pp. 282–290.

NGO, T. T. and C. W. LETCHFORD (2009). "Experimental study of topographic effects on gust wind speed". In: *Journal of Wind Engineering and Industrial Aerodynamics* 97.9–10, pp. 426–438.

NGUYEN, X. T., B. T. NGUYEN, K. P. DO, Q. H. BUI, T. N. T. NGUYEN, V. Q. VUONG, and T. H. LE (2015). "Spatial interpolation of meteorologic variables in Vietnam using the kriging method". In: *Journal of Information Processing Systems* 11.1, pp. 134–147.

NIELSEN, M. (1999). "A method for spatial interpolation of wind climatologies". In: *Wind Energy* 2.3, pp. 151–166.

NIEMCZYNOWICZ, J. (1999). "Urban hydrology and water management – present and future challenges". In: *Urban Water* 1.1, pp. 1–14.

NINYEROLA, M., X. PONS, and J. M. ROURE (2007). "Objective air temperature mapping for the Iberian Peninsula using spatial interpolation and GIS". In: *International Journal of Climatology* 27.9, pp. 1231–1242.

OCHOA-RODRIGUEZ, S., L.-P. WANG, A. GIRES, R. D. PINA, R. REINOSO-RONDINEL, G. BRUNI, A. ICHIBA, S. GAITAN, E. CRISTIANO, J. VAN ASSEL, S. KROLL, D. MURLÀ-TUYLS, B. TISSERAND, D. SCHERTZER, I. TCHIGUIRINSKAIA, C. ONOF, P. WILLEMS, and M.-C. TEN VELDHUIS (2015). "Impact of spatial and temporal resolution of rainfall inputs on urban hydrodynamic modelling outputs: A multi-catchment investigation". In: *Journal of Hydrology* 531, Part 2, pp. 389–407.

ÖZTOPAL, A. (2006). "Artificial neural network approach to spatial estimation of wind velocity data". In: *Energy Conversion and Management* 47.4, pp. 395–406.

PALOMINO, I. and F. MARTÍN (1995). "A simple method for spatial interpolation of the wind in complex terrain". In: *Journal of Applied Meteorology* 34.7, pp. 1678–1693.

PEEL, M. C., B. L. FINLAYSON, and T. A. MCMAHON (2007). "Updated world map of the Köppen-Geiger climate classification". In: *Hydrology and Earth System Sciences* 11.5, pp. 1633–1644.

PEGRAM, G., X. LLORT, and D. SEMPERE-TORRES (2011). "Radar rainfall: Separating signal and noise fields to generate meaningful ensembles". In: *Atmospheric Research* 100.2–3, pp. 226–236.

PHILLIPS, D. L., J. DOLPH, and D. MARKS (1992). "A comparison of geostatistical procedures for spatial analysis of precipitation in mountainous terrain". In: *Agricultural and Forest Meteorology* 58.1, pp. 119–141.

PINHEIRO, J., D. BATES, S. DEBROY, and D. SARKAR (2016). *Package 'nlme'*. Available at: http://cran.r-project.org/web/packages/nlme/nlme.pdf.

PRADO-FIEDLER, R. (1990). "On the relationship between precipitation amount and wet deposition of nitrate and ammonium". In: *Atmospheric Environment. Part A. General Topics* 24.12, pp. 3061–3065.

PRICE, D. T., D. W. MCKENNEY, I. A. NALDER, M. F. HUTCHINSON, and J. L. KESTEVEN (2000). "A comparison of two statistical methods for spatial interpolation of Canadian monthly mean climate data". In: *Agricultural and Forest Meteorology* 101.2–3, pp. 81–94.

PRUDHOMME, C. and D. W. REED (1999). "Mapping extreme rainfall in a mountainous region using geostatistical techniques: a case study in Scotland". In: *International Journal of Climatology* 19.12, pp. 1337–1356.

RABIEI, E. and U. HABERLANDT (2015). "Applying bias correction for merging rain gauge and radar data". In: *Journal of Hydrology* 522, pp. 544–557.

RAICHIJK, C. (2012). "Observed trends in sunshine duration over South America". In: *International Journal of Climatology* 32.5, pp. 669–680.

REYNOLDS, R. W. and T. M. SMITH (1994). "Improved Global Sea Surface Temperature Analyses Using Optimum Interpolation". In: *Journal of Climate* 7.6, pp. 929–948.

RIEDL, J. (1986). "Radar-Flächenniederschlagsmessung". In: *Promet* 2/3, pp. 20–23.

ROBERT, S., L. FORESTI, and M. KANEVSKI (2013). "Spatial prediction of monthly wind speeds in complex terrain with adaptive general regression neural networks". In: *International Journal of Climatology* 33.7, pp. 1793–1804.

ROCKSTRÖM, J., L KARLBERG, S. P. WANI, J. BARRON, N. HATIBU, T. OWEIS, A. BRUGGE-MAN, J. FARAHANI, and Z. QIANG (2010). "Managing water in rainfed agriculture – The need for a paradigm shift". In: *Agricultural Water Management* 97.4, pp. 543–550.

ROSSMAN, L. A. (2015). *Storm Water Management Model User's Manual Version 5.1, Revised September 2015*. U.S. Environmental Protection Agency, National Risk Management Research Laboratory.

ROSSOW, W. B. and R. A. SCHIFFER (1991). "ISCCP Cloud Data Products". In: *Bulletin of the American Meteorological Society* 72.1, pp. 2–20.

RUEL, J.-C., D. PIN, and K. COOPER (1998). "Effect of topography on wind behaviour in a complex terrain". In: *Forestry* 71.3, pp. 261–265.

ŞAHIN, D. A. and Z. ŞEN (2004). "A new spatial prediction model and its application to wind records". In: *Theoretical and Applied Climatology* 79.1, pp. 45–54.

SCHIEMANN, R., R. ERDIN, M. WILLI, C. FREI, M. BERENGUER, and D. SEMPERE-TORRES (2011). "Geostatistical radar-raingauge combination with nonparametric correlograms: methodological considerations and application in Switzerland". In: *Hydrology and Earth System Sciences* 15.5, pp. 1515–1536.

SCHILLING, W. (1991). "Rainfall data for urban hydrology: what do we need?" In: *Atmospheric Research* 27.1, pp. 5–21.

SEIZ, G., E. P. BALTSAVIAS, and A. GRUEN (2002). "Cloud mapping from the ground: Use of photogrammetric methods". In: *Photogrammetric Engineering and Remote Sensing* 68.9, pp. 941–951.

SELTMANN, J. E. E. (1997). "Radarforschung im DWD: Vom Scan zum Produkt". In: *Promet* 26, pp. 32–42.

SEO, D.-J. and J. P. BREIDENBACH (2002). "Real-time correction of spatially nonuniform bias in radar rainfall data using rain gauge measurements". In: *Journal of Hydrometeorology* 3.2, pp. 93–111.

SEO, D.-J., J.P. BREIDENBACH, and E.R. JOHNSON (1999). "Real-time estimation of mean field bias in radar rainfall data". In: *Journal of Hydrology* 223.3–4, pp. 131–147.

SHEPARD, D. (1968). "A two-dimensional interpolation function for irregularly-spaced data". en. In: ACM Press, pp. 517–524.

SHOJI, T. (2006). "Statistical and geostatistical analysis of wind: A case study of direction statistics". In: *Computers & Geosciences* 32.8, pp. 1025–1039.

SINCLAIR, S. and G. PEGRAM (2005). "Combining radar and rain gauge rainfall estimates using conditional merging". en. In: *Atmospheric Science Letters* 6.1, pp. 19–22.

SMITH, J. A. and W. F. KRAJEWSKI (1991). "Estimation of the mean field bias of radar rainfall estimates". In: *Journal of Applied Meteorology* 30.4, pp. 397–412.

SONNTAG, D. and K. BEHRENS (1992). *Ermittlung der Sonnenscheindauer aus pyranometrisch gemessenen Bestrahlungsstärken der Global- und Himmelsstrahlung*. 181st ed. Berichte des Deutschen Wetterdienstes. Offenbach am Main: Selbstverlag des Deutschen Wetterdienstes.

STAHL, K., R. D. MOORE, J. A. FLOYER, M. G. ASPLIN, and I. G. MCKENDRY (2006). "Comparison of approaches for spatial interpolation of daily air temperature in a large

region with complex topography and highly variable station density". In: *Agricultural and Forest Meteorology* 139.3–4, pp. 224–236.

SUN, X., R. G. MEIN, T. D. KEENAN, and J. F. ELLIOTT (2000). "Flood estimation using radar and raingauge data". In: *Journal of Hydrology* 239.1–4, pp. 4–18.

TABIOS, G. Q. and J. D. SALAS (1985). "A comparative analysis of techniques for spatial interpolation of precipitation". In: *JAWRA Journal of the American Water Resources Association* 21.3, pp. 365–380.

THIEMIG, V., R. ROJAS, M. ZAMBRANO-BIGIARINI, V. LEVIZZANI, and A. DE ROO (2012). "Validation of satellite-based precipitation products over sparsely gauged african river basins". In: *Journal of Hydrometeorology* 13.6, pp. 1760–1783.

THIESSEN, A. H. (1911). "Precipitation averages for large areas". In: *Monthly Weather Review* 39.7, pp. 1082–1089.

TIBA, C. (2001). "Solar radiation in the Brazilian Northeast". In: *Renewable Energy* 22.4, pp. 565–578.

TOBIN, C., L. NICOTINA, M. B. PARLANGE, A. BERNE, and A. RINALDO (2011). "Improved interpolation of meteorological forcings for hydrologic applications in a Swiss Alpine region". In: *Journal of Hydrology* 401.1–2, pp. 77–89.

UBA and IJ (2014). *Austal2000N: Programmbeschreibung zur Version 2.6*. Umweltbundesamt and Ingenieurbüro Janicke. Dessau-Roßlau, Überlingen.

UPTON, G. J. G., A. R. HOLT, R. J. CUMMINGS, A. R. RAHIMI, and J. W. F. GODDARD (2005). "Microwave links: The future for urban rainfall measurement?" In: *Atmospheric Research* 77.1–4, pp. 300–312.

VAN ACKERE, S., G. VAN EETVELDE, D. SCHILLEBEECKX, E. PAPA, K. VAN WYNGENE, and L. VANDEVELDE (2015). "Wind resource mapping using landscape roughness and spatial interpolation methods". In: *Energies* 8.8, pp. 8682–8703.

VDI 3782 (2015). *Blatt 6: Bestimmung der Ausbreitungsklasse nach Klug/Manier, Entwurf*. Kommission Reinhaltung der Luft im VDI und DIN - Normenausschuss KRdL, Beuth-Verlag.

VDI 3783 (2015). *Blatt 20: Übertragbarkeitsprüfung meteorologischer Daten zur Anwendung im Rahmen der TA Luft, Entwurf*. Kommission Reinhaltung der Luft im VDI und DIN - Normenausschuss KRdL, Beuth-Verlag.

VELASCO-FORERO, C. A., D. SEMPERE-TORRES, E. F. CASSIRAGA, and J. J. GÓMEZ-HERNÁNDEZ (2009). "A non-parametric automatic blending methodology to estimate rainfall fields from rain gauge and radar data". In: *Advances in Water Resources* 32.7, pp. 986–1002.

VERDIN, A., B. RAJAGOPALAN, W. KLEIBER, and C. FUNK (2015). "A Bayesian kriging approach for blending satellite and ground precipitation observations". In: *Water Resources Research* 51.2, pp. 908–921.

VERWORN, A. and U. HABERLANDT (2011). "Spatial interpolation of hourly rainfall – effect of additional information, variogram inference and storm properties". In: *Hydrology and Earth System Sciences* 15.2, pp. 569–584.

VICENTE-SERRANO, S. M., M. A. SAZ-SÁNCHEZ, and J. M. CUADRAT (2003). "Comparative analysis of interpolation methods in the middle Ebro Valley (Spain): application to annual precipitation and temperature". In: *Climate Research* 24.2, pp. 161–180.

VILLARINI, G. and W. F. KRAJEWSKI (2009). "Empirically based modelling of radar-rainfall uncertainties for a C-band radar at different time-scales". In: *Quarterly Journal of the Royal Meteorological Society* 135.643, pp. 1424–1438.

VILLARINI, G., B.-C. SEO, F. SERINALDI, and W. F. KRAJEWSKI (2014). "Spatial and temporal modeling of radar rainfall uncertainties". In: *Atmospheric Research* 135–136, pp. 91–101.

VOGL, S., P. LAUX, W. QIU, G. MAO, and H. KUNSTMANN (2012). "Copula-based assimilation of radar and gauge information to derive bias-corrected precipitation fields". In: *Hydrology and Earth System Sciences* 16.7, pp. 2311–2328.

WEIGEL, E. and T. WINTERRATH (2009). "Radargestützte Niederschlagsanalyse und -vorhersage (RADOLAN, RADVOR-OP)". In: *Promet* 35, pp. 78–86.

WERNER, M. and J. STEINERT (2012). "New quality assurance algorithms for the DWD polarimetric C-band weather radar network". In: *ERAD2012 – The 7th European Conference On Radar in Meteorology and Hydrology*.

WILSON, J. W. and E. A. BRANDES (1979). "Radar Measurement of Rainfall – A Summary". In: *Bulletin of the American Meteorological Society* 60.9, pp. 1048–1058.

WMO (2008). *Guide to meteorological instruments and methods of observation*. 7th ed. Geneva: World Meteorological Organization.

WOLDEMESKEL, F. M., B. SIVAKUMAR, and A. SHARMA (2013). "Merging gauge and satellite rainfall with specification of associated uncertainty across Australia". In: *Journal of Hydrology* 499, pp. 167–176.

YE, W., H. P. HONG, and J. F. WANG (2015). "Comparison of spatial interpolation methods for extreme wind speeds over Canada". In: *Journal of Computing in Civil Engineering* 29.6, p. 04014095.

YOON, S.-S., A. T. PHUONG, and D.-H. BAE (2012). "Quantitative comparison of the spatial distribution of radar and gauge rainfall data". In: *Journal of Hydrometeorology* 13.6, pp. 1939–1953.

ZLATEV, Z., S. E. MIDDLETON, and G. VERES (2010). "Benchmarking knowledge-assisted kriging for automated spatial interpolation of wind measurements". In: *13th Conference on Information Fusion (FUSION), 2010*, pp. 1–8.

Appendix

A Variograms

A.1 Temperature

Table A.1: Parameters of the exponential variogram model for maximum temperature

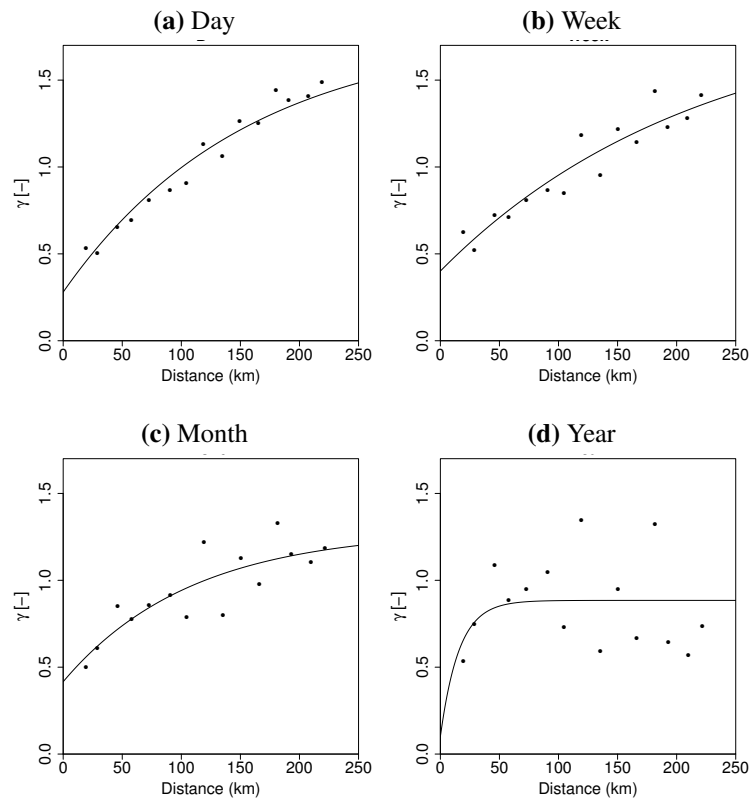| Temporal resolution	c_0 [-]	c [-]	a_{eff} [m]
Day	0.28	1.50	153,950
Week	0.40	1.50	217,790
Month	0.42	0.87	108,203
Year	0.10	0.78	15,758

Figure A.1: Experimental average and theoretical variograms of maximum temperature

Table A.2: Parameters of the exponential variogram model for minimum temperature

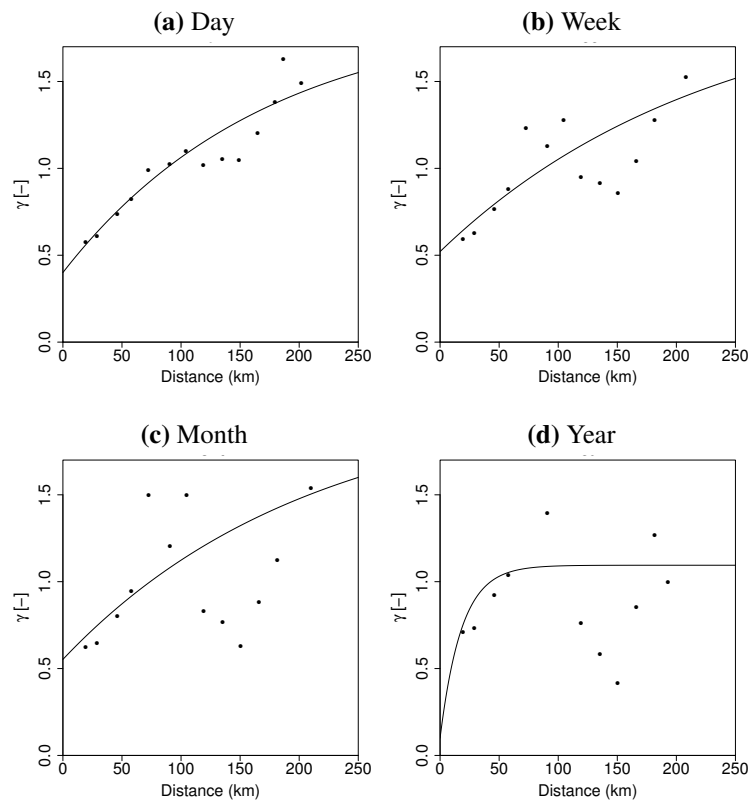| Temporal resolution	c_0 [-]	c [-]	a_{eff} [m]
Day	0.40	1.50	$171,431$
Week	0.52	1.50	$228,708$
Month	0.55	1.50	$208,692$
Year	0.10	0.99	$18,215$

Figure A.2: Experimental average and theoretical variograms of minimum temperature

A.2 Wind direction

Table A.3: Parameters of the exponential indicator variogram model for different wind direction categories of hourly data

| Category	c_0 [-]	c [-]	a_{eff} [m]	Category	c_0 [-]	c [-]	a_{eff} [m]
1	0.16	0.07	440,458	19	0.52	1.39	500,000
2	0.21	0.07	61,982	20	0.57	1.23	500,000
3	0.25	0.09	67,802	21	0.61	0.95	500,000
4	0.28	0.11	73,852	22	0.63	0.76	500,000
5	0.31	0.13	78,180	23	0.61	0.69	500,000
6	0.33	0.14	79,947	24	0.57	0.72	500,000
7	0.35	0.17	89,561	25	0.53	0.77	500,000
8	0.36	0.19	89,762	26	0.49	0.84	500,000
9	0.36	0.24	94,675	27	0.46	0.85	500,000
10	0.39	0.32	145,909	28	0.44	0.82	500,000
11	0.42	0.86	500,000	29	0.42	0.79	500,000
12	0.43	1.10	500,000	30	0.38	0.78	500,000
13	0.47	1.17	500,000	31	0.35	0.66	500,000
14	0.49	0.82	303,504	32	0.33	0.52	500,000
15	0.51	0.85	312,800	33	0.30	0.38	500,000
16	0.51	0.93	351,339	34	0.26	0.15	413,318
17	0.51	1.31	500,000	35	0.19	0.07	500,000
18	0.51	1.36	500,000	36	0.18	0.07	500,000
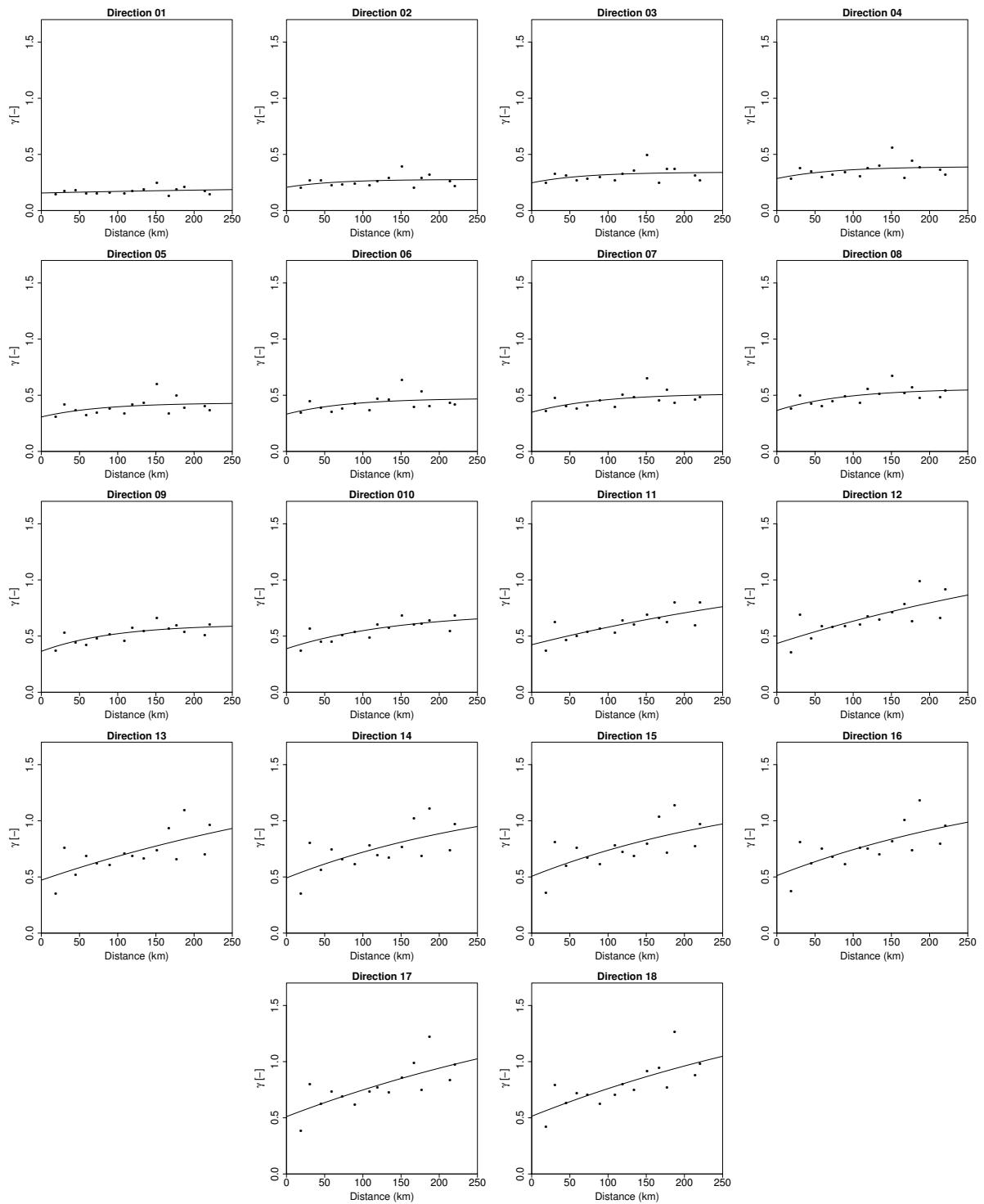
Figure A.3: Experimental and theoretical average indicator variograms of hourly wind direction categories (1-18)
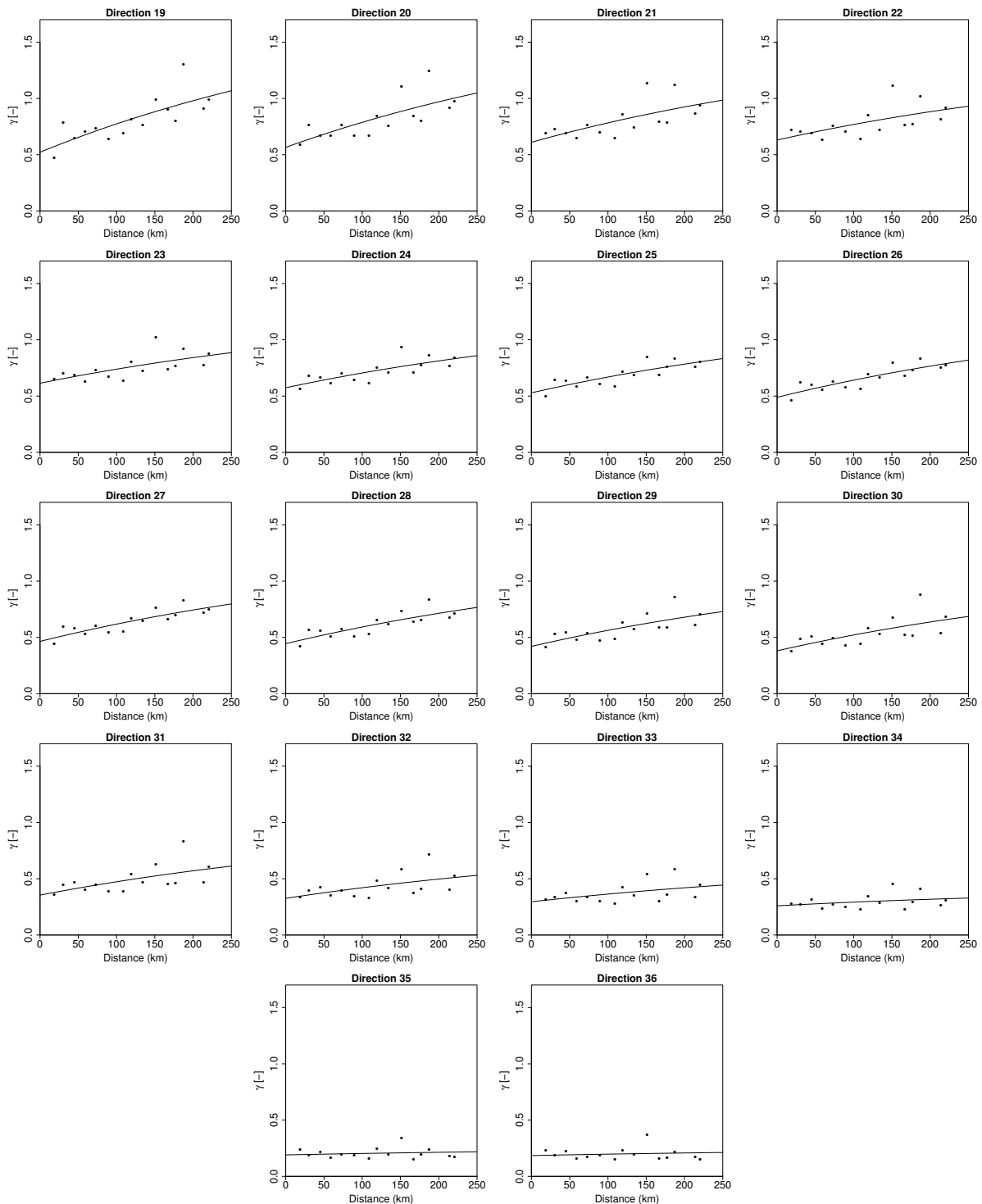
Figure A.4: Experimental and theoretical average indicator variograms of hourly wind direction categories (19-36)

B Interpolation performance

B.1 Temperature

Table B.1: Average interpolation performance (Bias, RMSE, RVar) for hourly to annual maximum temperature over all station densities scenarios

Method	Additional information	Criterion	Temporal resolution			
			Day	Week	Month	Year
NN	–	Bias [°C]	−0.215	−0.218	−0.233	−0.264
		RMSE [-]	0.125	0.114	0.111	0.113
		RVar [-]	1.342	1.540	1.672	1.945
InvD	–	Bias [°C]	−0.106	−0.107	−0.124	−0.138
		RMSE [-]	0.100	0.091	0.088	0.088
		RVar [-]	0.765	0.831	0.888	0.967
OK	–	Bias [°C]	−0.011	−0.005	−0.026	−0.065
		RMSE [-]	0.094	0.086	0.083	0.079
		RVar [-]	0.446	0.408	0.430	0.498
KED	DEM	Bias [°C]	0.044	0.038	0.024	0.005
		RMSE [-]	0.061	0.045	0.039	0.031
		RVar [-]	0.681	0.689	0.713	0.762
KED	HUM	Bias [°C]	0.044	0.043	0.024	0.005
		RMSE [-]	0.069	0.055	0.051	0.044
		RVar [-]	0.686	0.672	0.690	0.699

Table B.2: Average interpolation performance (Bias, RMSE, RVar) for hourly to annual minimum temperature over all station densities scenarios

| Method	Additional information	Criterion	Temporal resolution			
			Day	Week	Month	Year
NN	–	Bias [°C]	−0.025	−0.045	−0.058	−0.135
		RMSE [-]	0.225	0.177	0.157	0.198
		RVar [-]	1.005	1.077	1.125	1.443
InvD	–	Bias [°C]	−0.012	−0.026	−0.037	−0.080
		RMSE [-]	0.189	0.148	0.131	0.156
		RVar [-]	0.566	0.591	0.611	0.766
OK	–	Bias [°C]	0.052	0.043	0.034	−0.015
		RMSE [-]	0.186	0.154	0.139	0.162
		RVar [-]	0.311	0.275	0.276	0.423
KED	HUM	Bias [°C]	0.036	0.022	0.011	−0.025
		RMSE [-]	0.168	0.126	0.110	0.115
		RVar [-]	0.531	0.563	0.599	0.782
KED	HUM	Bias [°C]	0.065	0.053	0.041	0.004
		RMSE [-]	0.161	0.120	0.107	0.113
		RVar [-]	0.536	0.558	0.585	0.693
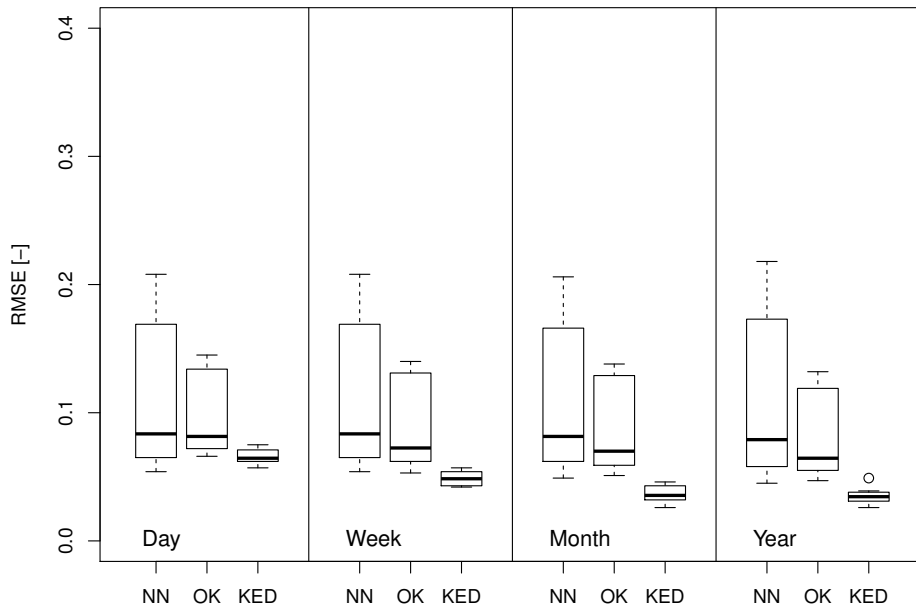
Figure B.1: Influence of station locations on the interpolation performance of daily to annual maximum temperature. The boxes contain each the interpolation performance of NN, OK and KED that was obtained for the ten different realisations of the network density scenario consisting of 17 stations.
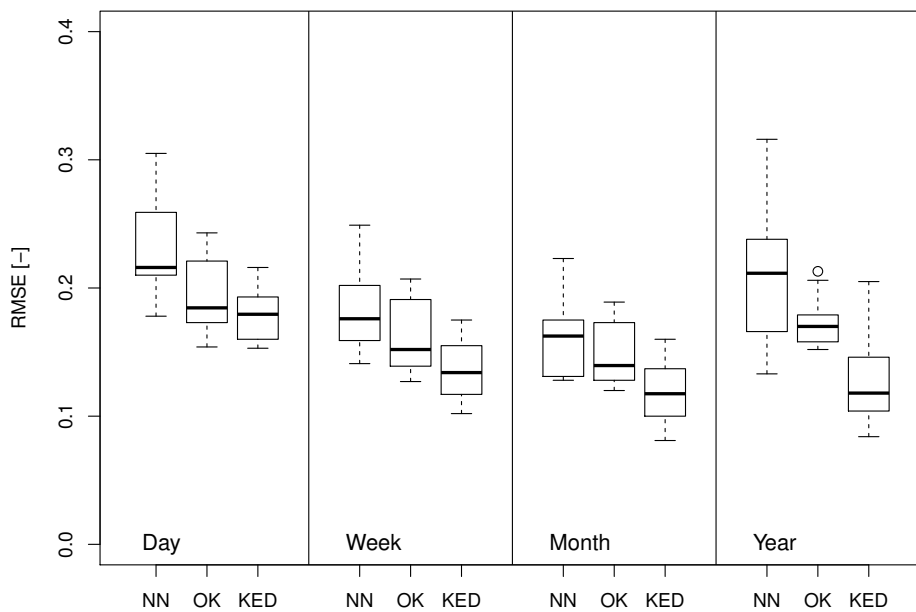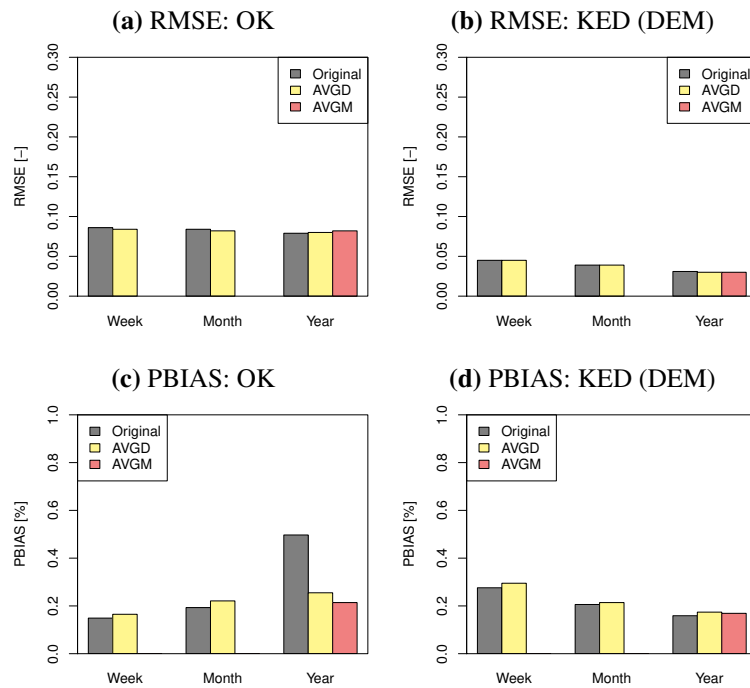

Figure B.2: Influence of station locations on the interpolation performance of daily to annual minimum temperature. The boxes contain each the interpolation performance of NN, OK and KED that was obtained for the ten different realisations of the network density scenario consisting of 17 stations.

Figure B.3: RMSE interpolation performance for aggregated fine temporal resolution interpolations of maximum temperature in comparison with time scale specific interpolation for OK (left) and KED using the DEM (right)
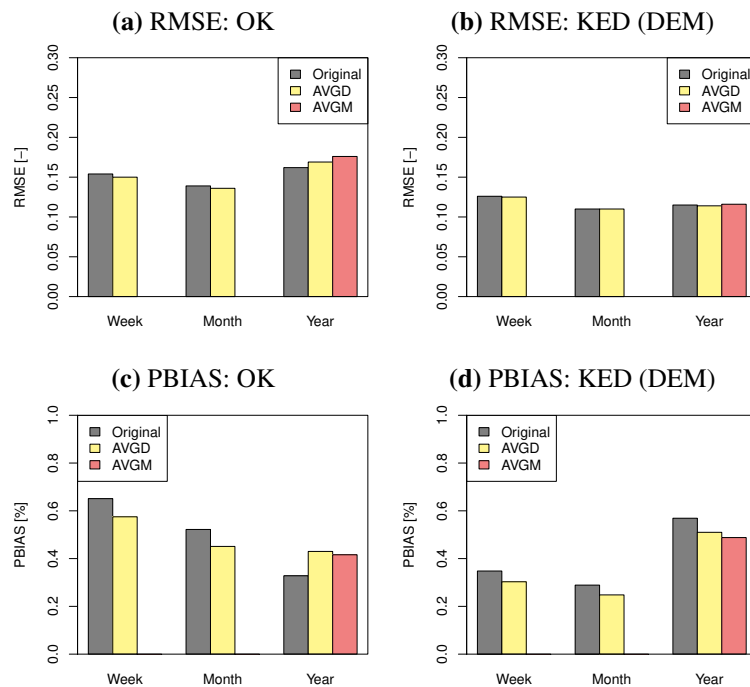

Figure B.4: RMSE interpolation performance for aggregated fine temporal resolution interpolations of minimum temperature in comparison with time scale specific interpolation for OK (left) and KED using the DEM (right)
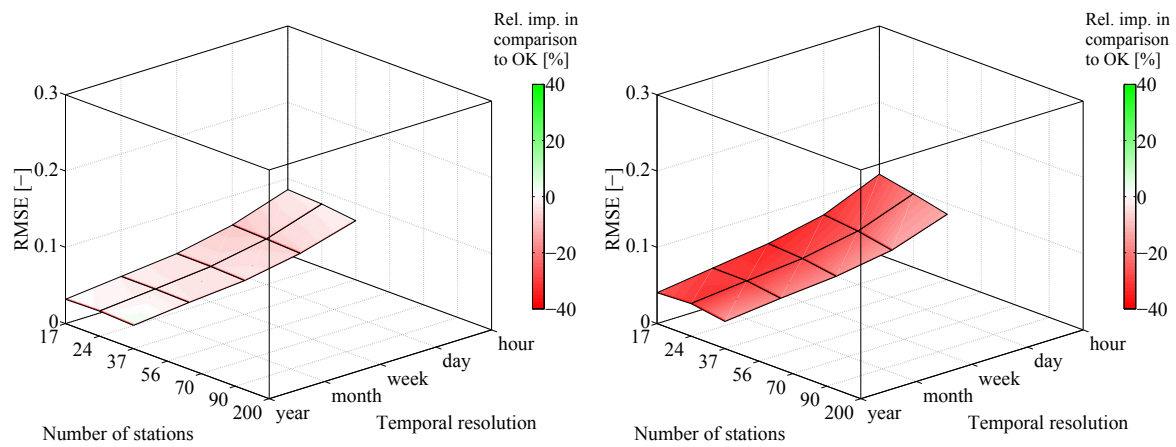
B.2 Humidity

Figure B.5: Interpolation performance of relative humidity using KED (SUN), KED (WVE) in comparison with OK for hourly to yearly time periods and all network density scenarios
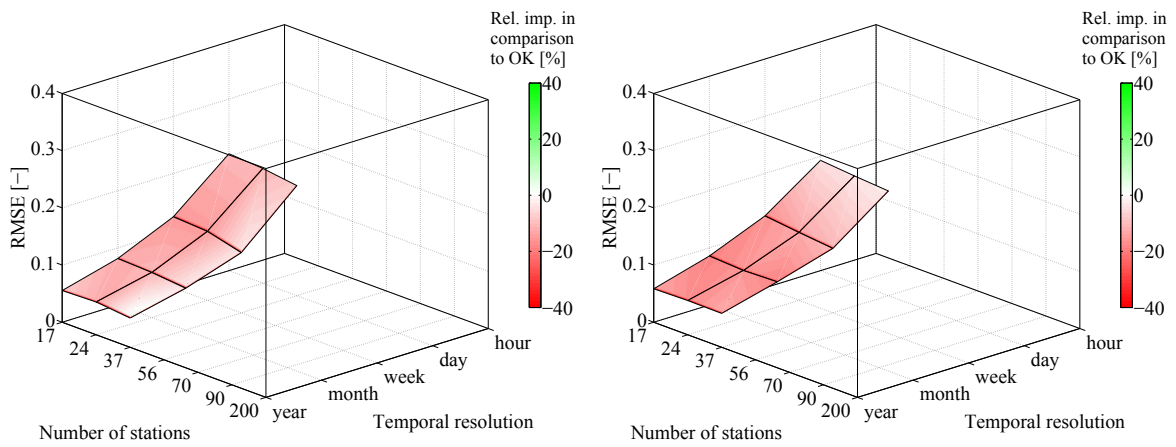
B.3 Cloud coverage

Figure B.6: Interpolation performance of cloud coverage using KED (TAV), KED (Radar) in comparison with OK for hourly to yearly time periods and all network density scenarios
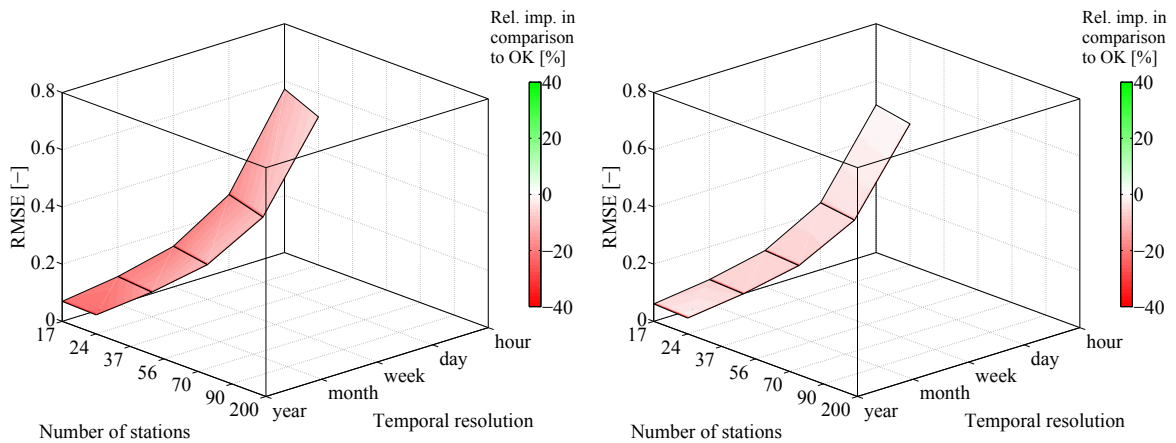
B.4 Sunshine duration

Figure B.7: Interpolation performance of sunshine duration using KED (DEM), KED (Radar) in comparison with OK for hourly to yearly time periods and all network density scenarios

C Maps of interpolated climate variables

Each interpolated map is presented with a different colour range. In each case the lower colour shading cutoff value was defined as the mean value of the corresponding spatial distribution minus three times the standard deviation, while the upper cutoff value is accordingly defined as the mean value plus three times the standard deviation.

The precipitation maps (Fig. C.1)were interpolated with CM (5 min, Hour) as well as KED using elevation and radar (Day, Week, Month, Year). The high temporal resolution maps show more spots without any rainfall, while the spatial distribution of longer temporal resolutions appears to be much smoother. The orographic effect considered by the implementation of the DEM is strongly seen in the monthly and annual interpolations.

All interpolations of temperature (Figs. C.2, C.3 and C.4) as well as relative humidity (Fig. C.5) were interpolated using KED and are dominated by the pattern of the topography. A difference in spatial variability is hardly seen among different time scales.

The spatial distribution of cloud coverage (Fig. C.6), sunshine duration (Fig. C.7) and wind velocity (Fig. C.7) is relatively smooth due to the interpolation by OK. The sharp transitions in the maps of cloud coverage and wind velocity result from the low station density and the high nugget effect of the fitted variogram model (see Tab. 6.16 and Tab. 6.22). The hourly map of sunshine duration shows an entirely uniform spatial distribution, since no sunshine was recorded by any stations. The maps of wind velocity contain single spots with significantly higher values. It is assumed that these spots result from single stations being influenced by the local topography.
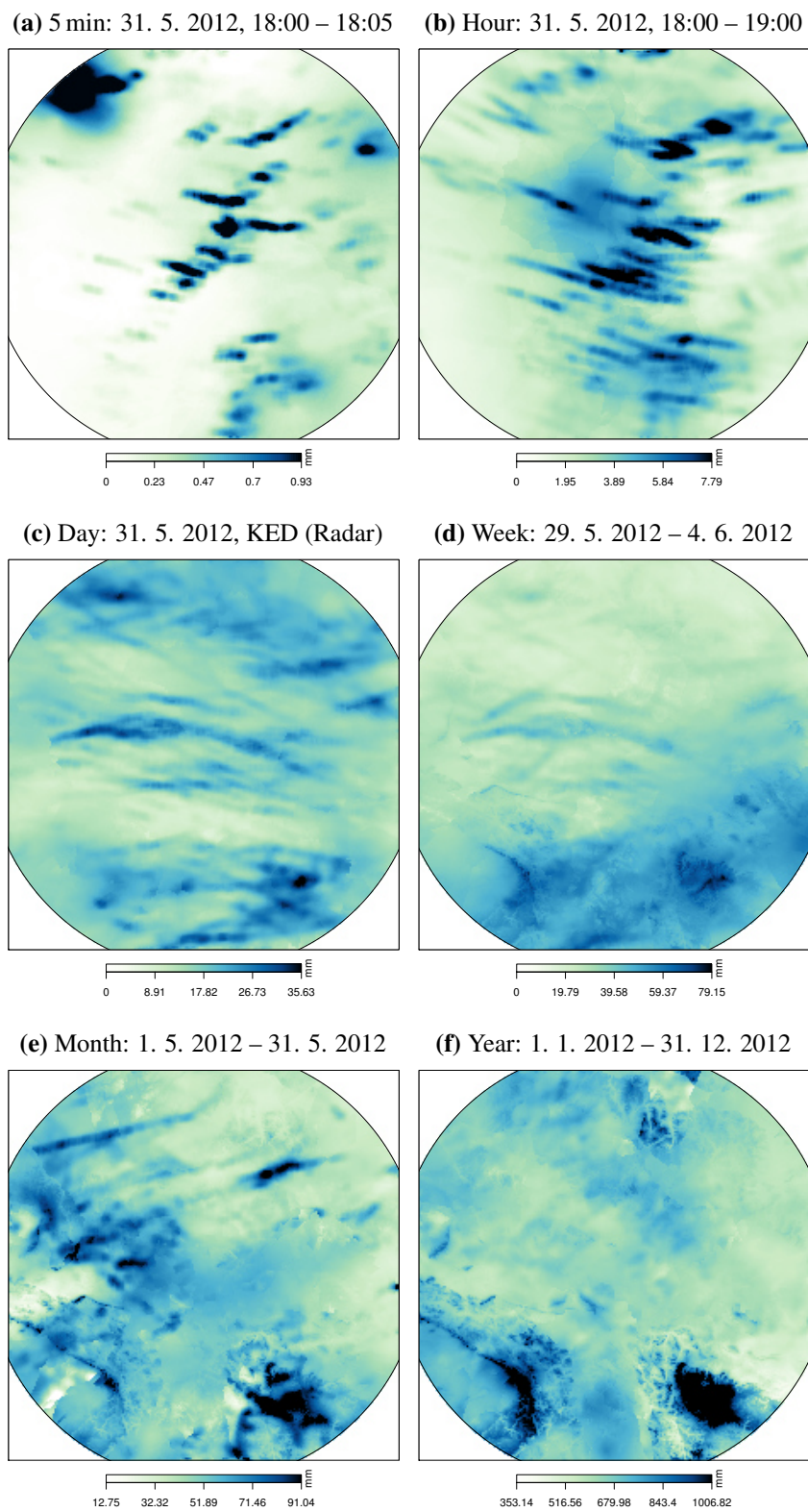
(a) 5 min: 31. 5. 2012, 18:00 – 18:05

(b) Hour: 31. 5. 2012, 18:00 – 19:00

(c) Day: 31. 5. 2012, KED (Radar)

(d) Week: 29. 5. 2012 – 4. 6. 2012

(e) Month: 1. 5. 2012 – 31. 5. 2012

(f) Year: 1. 1. 2012 – 31. 12. 2012

Figure C.1: Interpolated maps of precipitation for a single time step of each temporal resolution. 5 min and hourly data were interpolated by CM, daily data by KED (Radar) and all other temporal resolutions by KED (Radar, DEM)
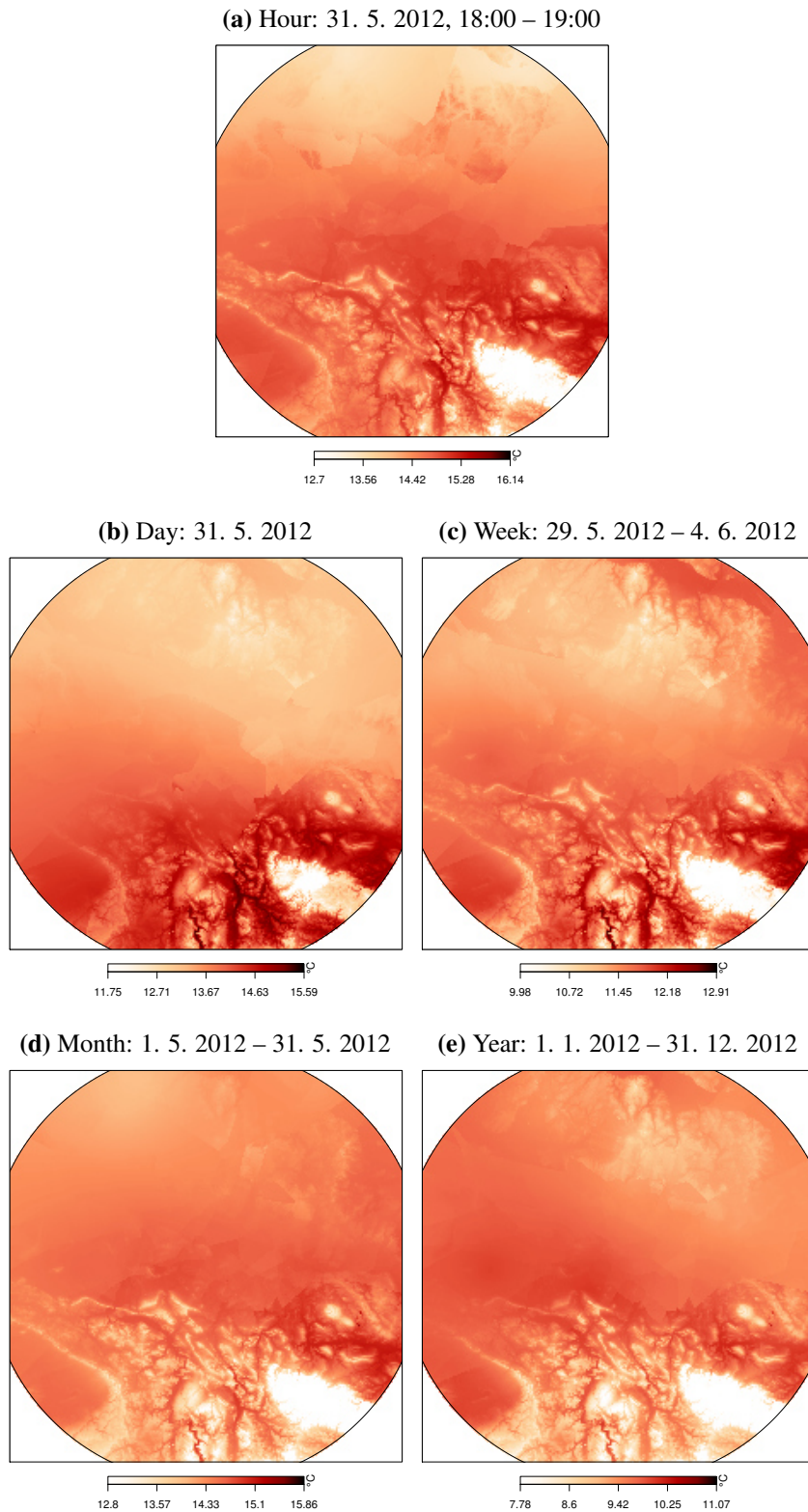
(a) Hour: 31. 5. 2012, 18:00 – 19:00

(b) Day: 31. 5. 2012

(c) Week: 29. 5. 2012 – 4. 6. 2012

(d) Month: 1. 5. 2012 – 31. 5. 2012

(e) Year: 1. 1. 2012 – 31. 12. 2012

Figure C.2: Interpolated maps of mean temperature for a single time step of each temporal resolution. All temporal resolutions were interpolated by KED (DEM).
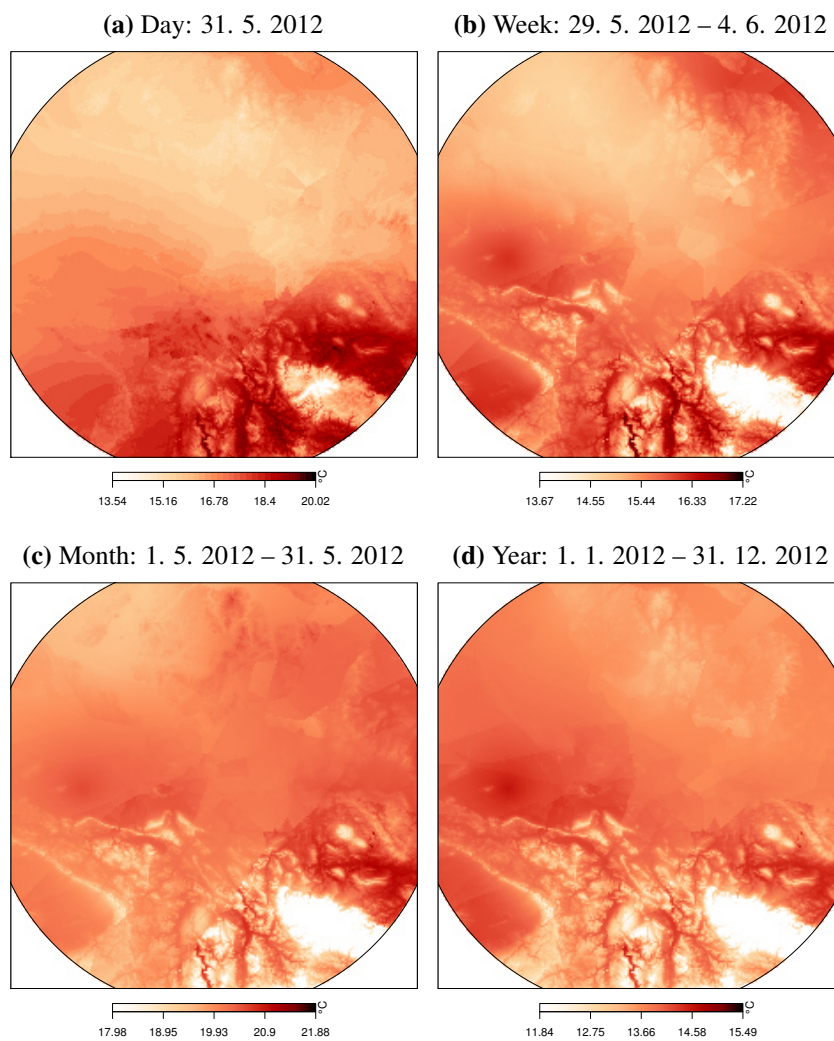
Figure C.3: Interpolated maps of mean maximum temperature for a single time step of each temporal resolution. All temporal resolutions were interpolated by KED (DEM).

(a) Day: 31. 5. 2012

(b) Week: 29. 5. 2012 – 4. 6. 2012

(c) Month: 1. 5. 2012 – 31. 5. 2012

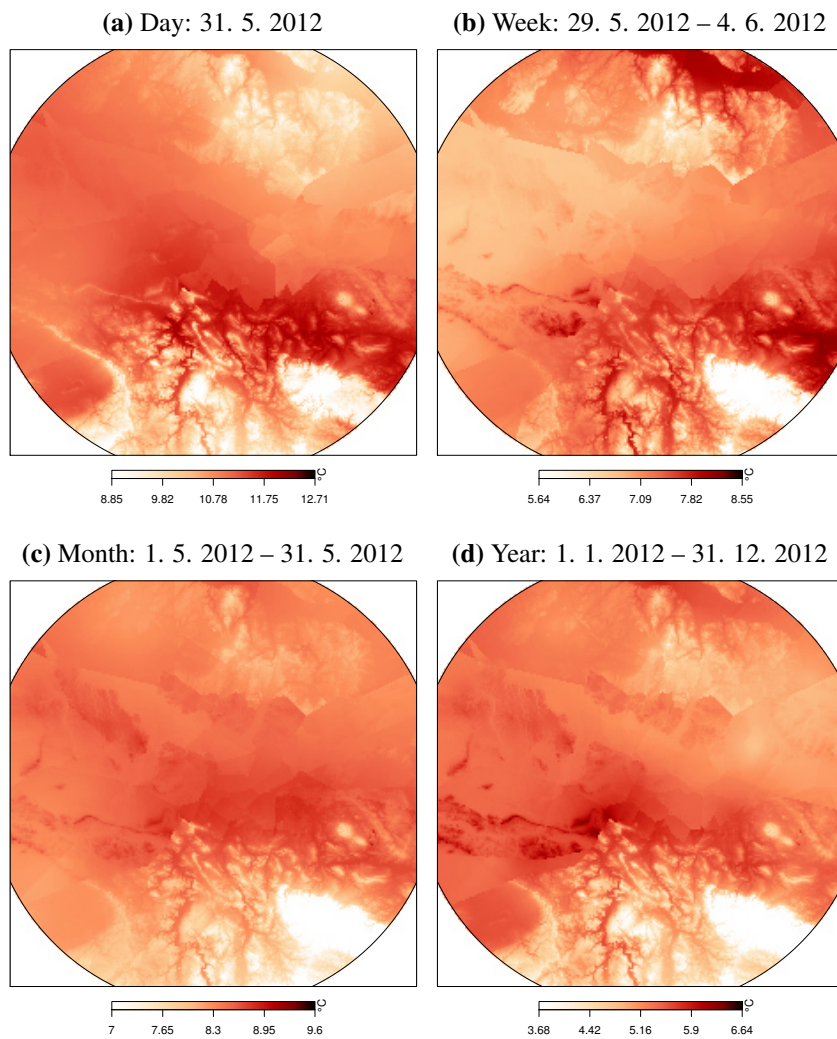**(d)** Year: 1. 1. 2012 – 31. 12. 2012

Figure C.4: Interpolated maps of mean minimum temperature for a single time step of each temporal resolution. All temporal resolutions were interpolated by KED (DEM).
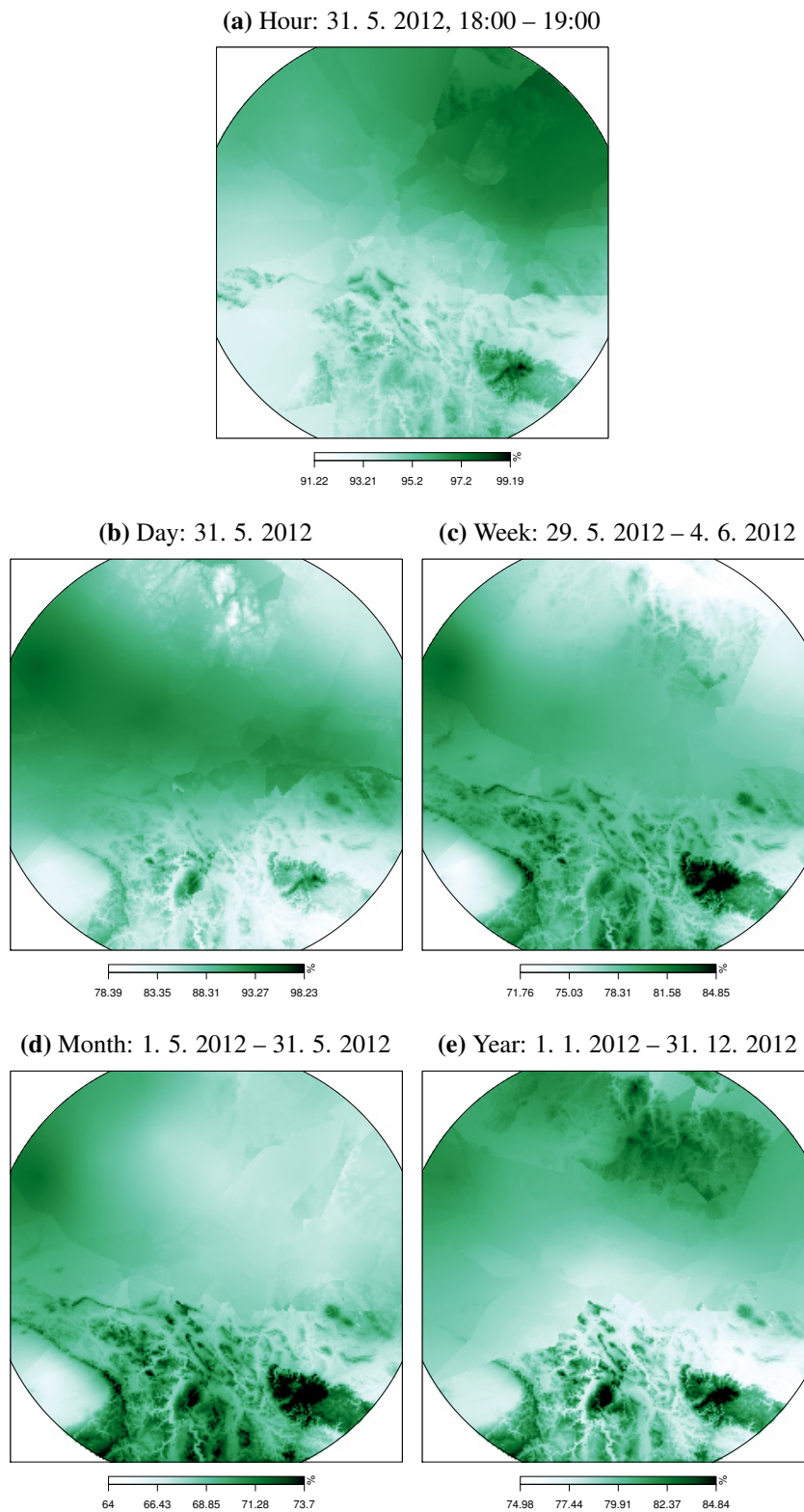
(a) Hour: 31. 5. 2012, 18:00 – 19:00

(b) Day: 31. 5. 2012

(c) Week: 29. 5. 2012 – 4. 6. 2012

(d) Month: 1. 5. 2012 – 31. 5. 2012

(e) Year: 1. 1. 2012 – 31. 12. 2012

Figure C.5: Interpolated maps of relative humidity for a single time step of each temporal resolution. All temporal resolutions were interpolated by KED (TAV).
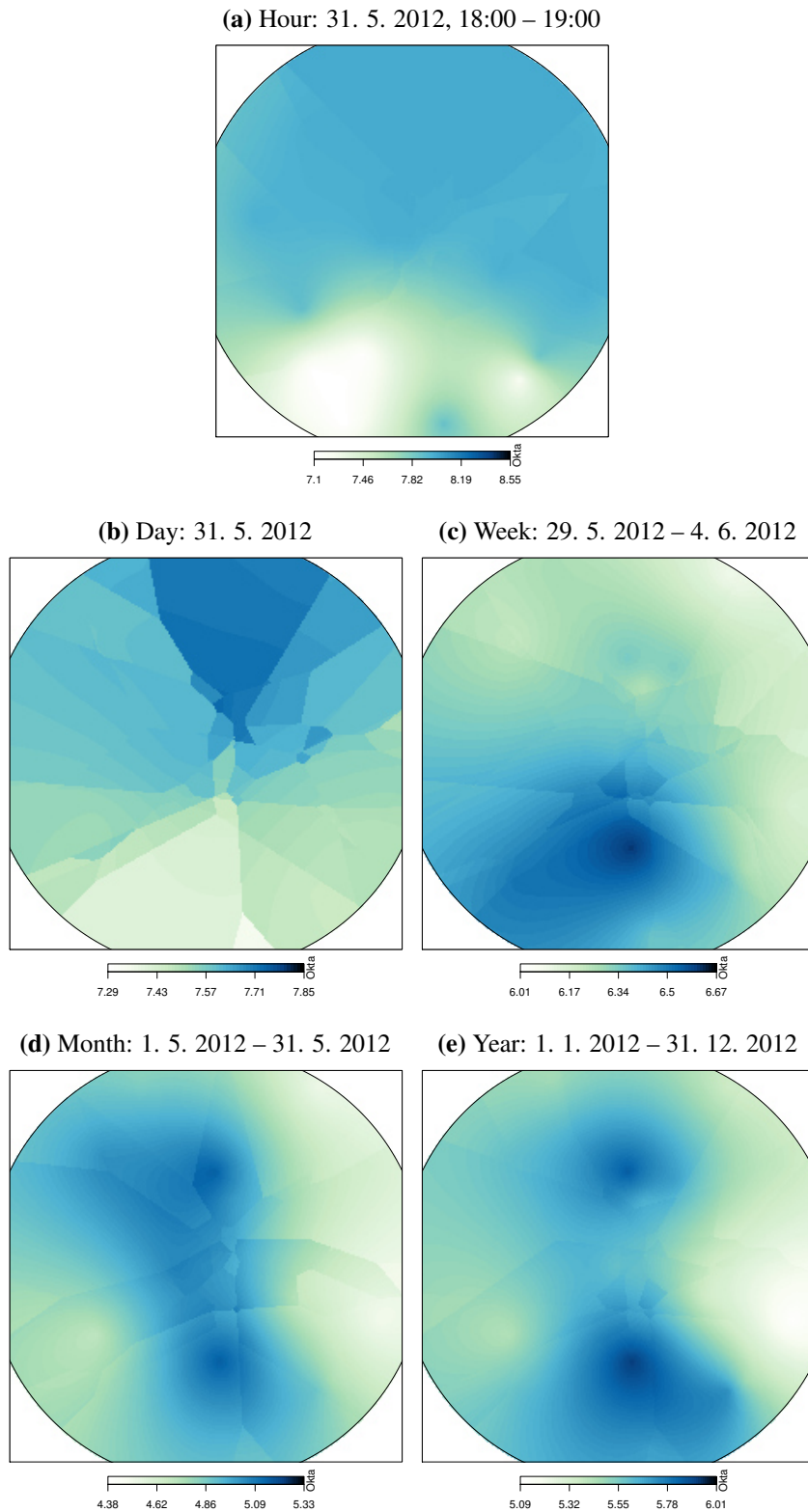
(a) Hour: 31. 5. 2012, 18:00 – 19:00

(b) Day: 31. 5. 2012

(c) Week: 29. 5. 2012 – 4. 6. 2012

(d) Month: 1. 5. 2012 – 31. 5. 2012

(e) Year: 1. 1. 2012 – 31. 12. 2012

Figure C.6: Interpolated maps of cloud coverage for a single time step of each temporal resolution. All temporal resolutions were interpolated by OK.

(a) Hour: 31. 5. 2012, 18:00 – 19:00

(b) Day: 31. 5. 2012

(c) Week: 29. 5. 2012 – 4. 6. 2012

(d) Month: 1. 5. 2012 – 31. 5. 2012

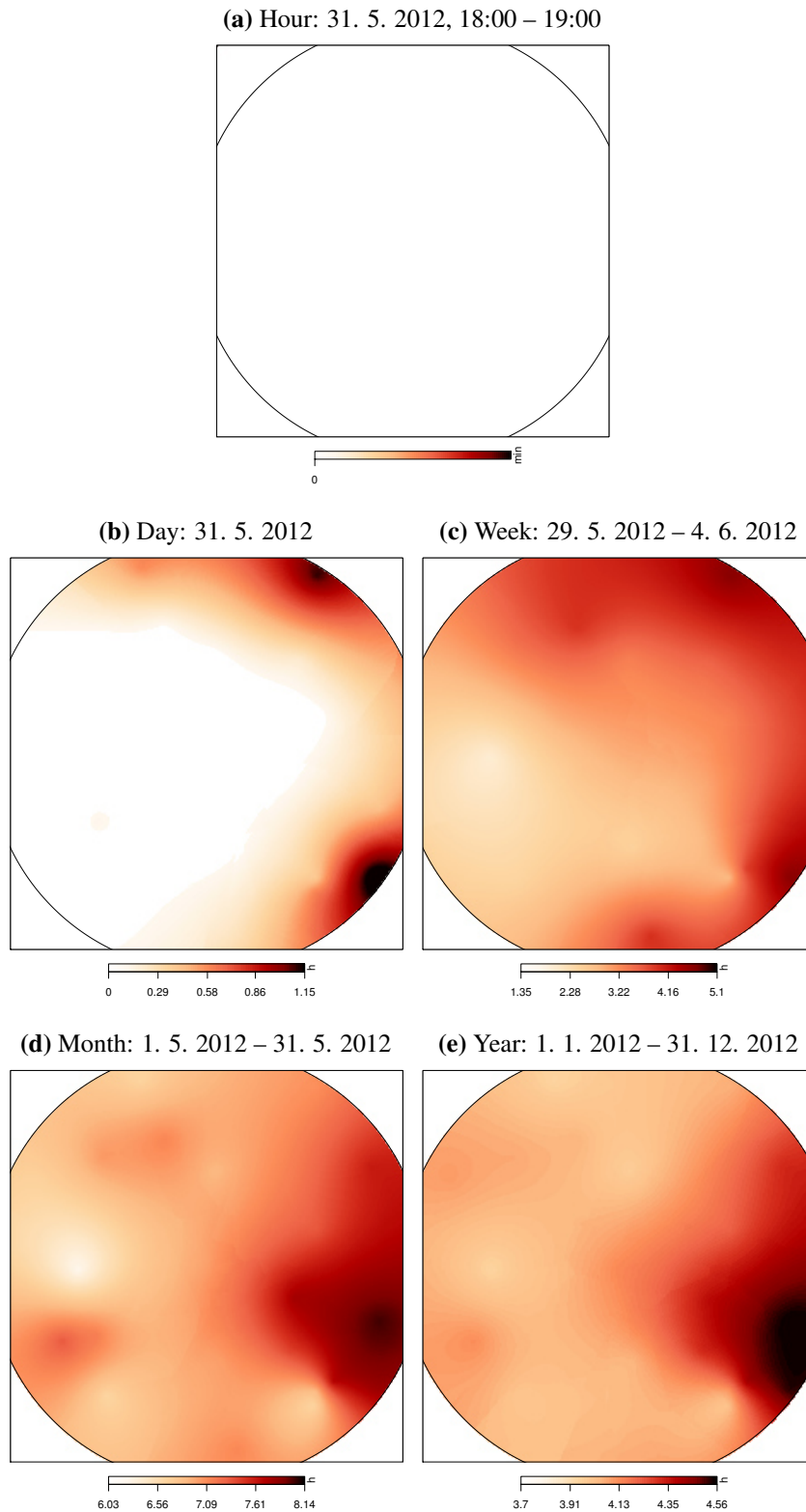**(e)** Year: 1. 1. 2012 – 31. 12. 2012

Figure C.7: Interpolated maps of sunshine duration for a single time step of each temporal resolution. All temporal resolutions were interpolated by OK.

(a) Hour: 31. 5. 2012, 18:00 – 19:00

(b) Day: 31. 5. 2012

(c) Week: 29. 5. 2012 – 4. 6. 2012

(d) Month: 1. 5. 2012 – 31. 5. 2012

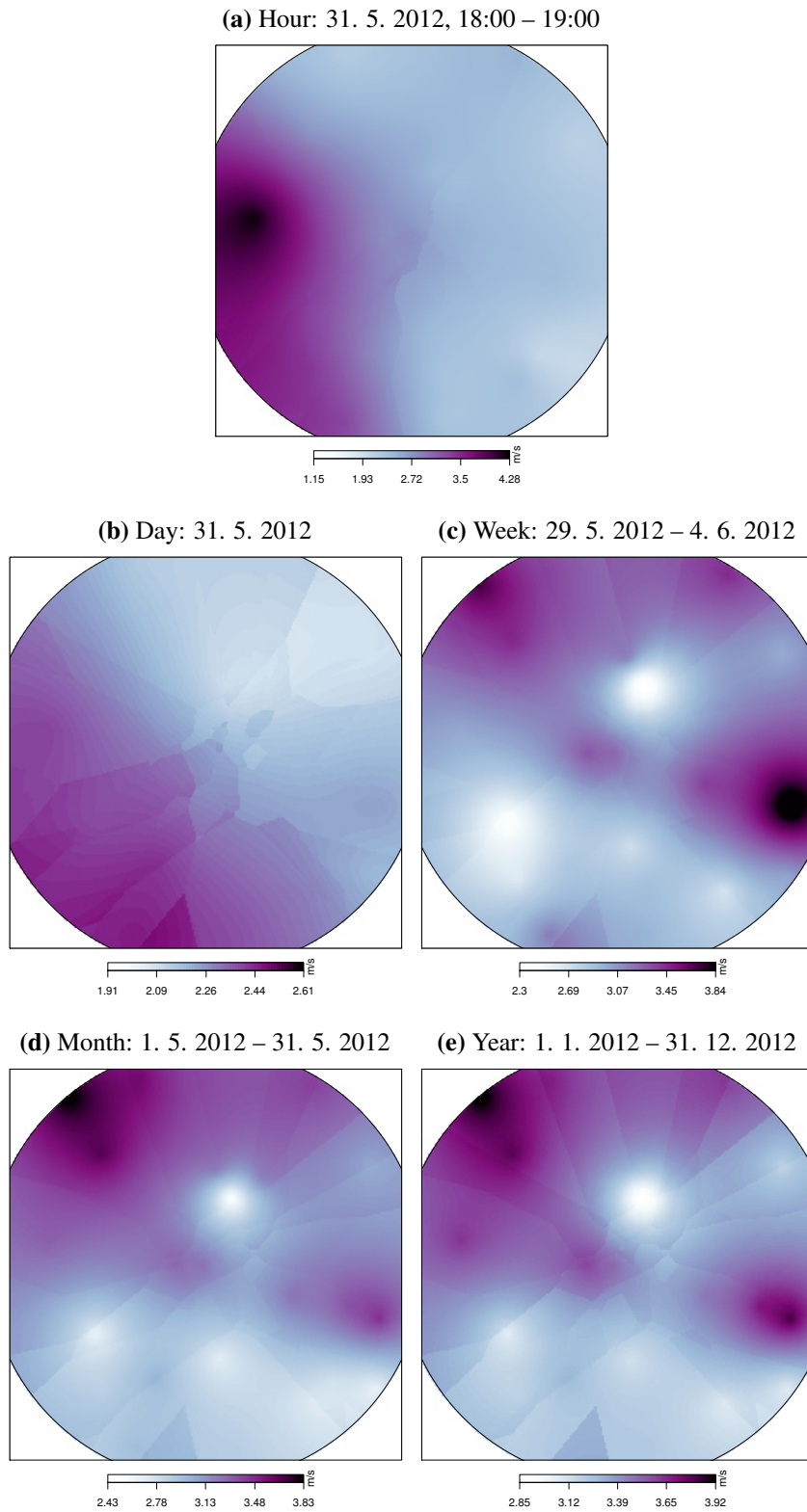**(e)** Year: 1. 1. 2012 – 31. 12. 2012

Figure C.8: Interpolated maps of wind velocity for a single time step of each temporal resolution. All temporal resolutions were interpolated by OK.

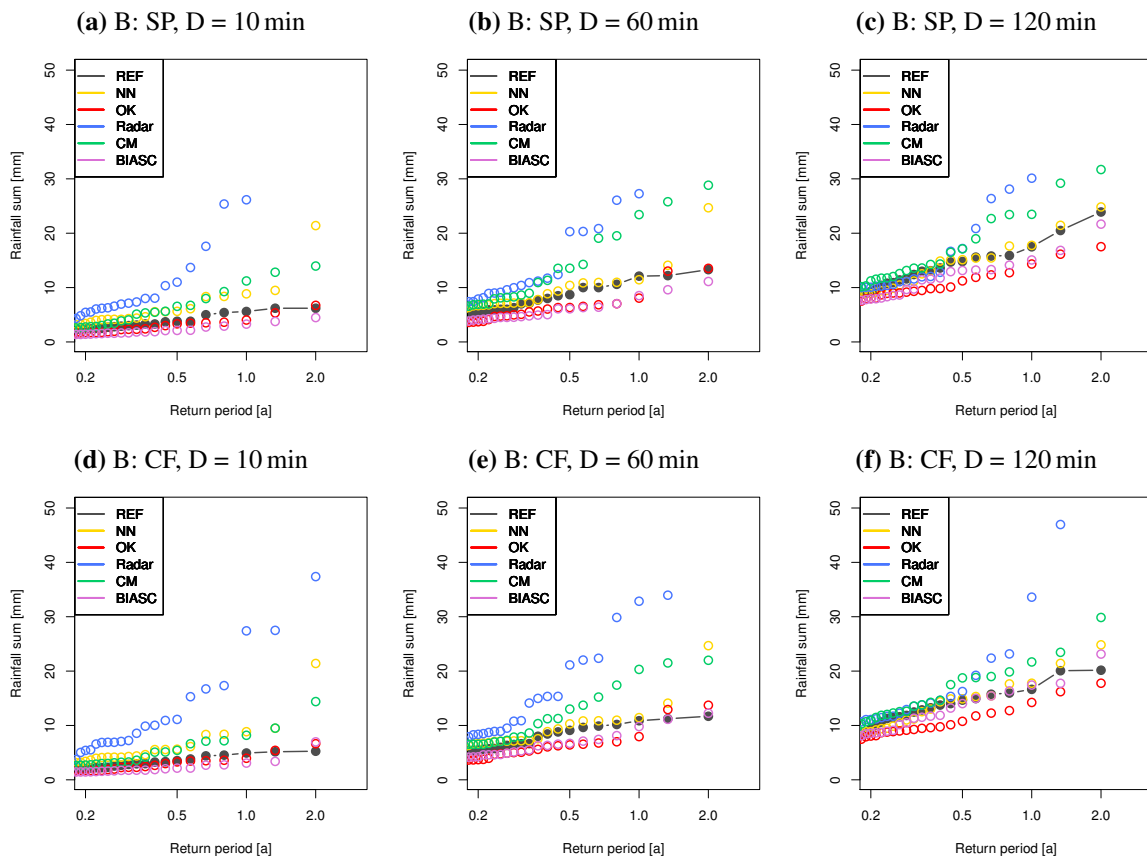# D Partial series of precipitation extremes

Figure D.1: Partial series of point rainfall extremes (top) and areal rainfall extremes (bottom) for durations of 10 min, 60 min and 120 min, whereas the closest DWD rain gauge is not taken into account for all interpolation methods (Case B)